Inertial Vision Pose Estimation Using Non-Linear Observers

Grant Darren Baldwin

October 2009

A thesis submitted for the degree of Doctor of Philosophy
of The Australian National University

Typeset in Times by TEX and LATEX 2ε.

Except where otherwise indicated, this thesis is my own original work.

Grant Darren Baldwin
8 October 2009

Acknowledgements

I would like to start by thanking my supervisors Robert Mahony, Jochen Trumpf and Jonghyuk Kim for their invaluable support, insight, assistance and persistence throughout my PhD experience. Without your confidence and patience the works contained in this thesis would not have come to fruition. Similarly, I would like to thank Tarek Hamel for his support and invaluable insights.

Without mentioning names, so that I can't forget anyone, I extend my thanks to the students and faculty of the College of Engineering and Computer Science. It has been a privilege to work in a such an accessible, collegiate and stimulating environment. You have made it a pleasure to undertake my PhD at the ANU.

I am grateful for financial support received during my PhD from the following sources:

- Australian Postgraduate Award, funded by the Australian Commonwealth Government,
- ANU-NICTA Supplementary Scholarship, funded by National ICT Australia.

Abstract

This thesis considers the problem of obtaining a high quality estimate of pose (position and orientation) from a combination of inertial and vision measurements using low cost sensors. The novelty of this work is in using non-linear observers designed on the Lie group $\mathrm{SE}(3)$. This approach results in robust estimators with strong local and almost-global stability results and straightforward gain tuning.

A range of sensor models and observer designs are investigated, including

- Creating a cascaded pose observer design using component observers for orientation and position, combining pose measurements reconstructed from vision with inertial measurements of angular velocity and linear acceleration.
- Combining inertial measurement of angular and linear velocity with pose measurements reconstructed from vision, and designing an observer using a decomposition of $\mathrm{SE}(3)$ into separate orientation and position components.
- Considering the case where the inertial measurements of angular and linear velocity are corrupted by slowly time varying biases and developing an observer for both pose and velocity measurement bias directly on $\mathrm{SE}(3) \times \mathfrak{se}(3)$.
- Eliminating the need for a pose measurement reconstruction by designing an observer operating directly on the measurements of landmark bearing from a vision sensor. The bearing measurements are combined with unbiased measurements of linear and angular velocity measurements to obtain an observer for pose evolving on $\mathrm{SE}(3)$.

Throughout these works, particular attention is given to designing observers suitable for implementation with multiple independent measurement devices. Care is given to avoid coupling of independent measurement noise processes in estimator dynamics. Further, the final observers proposed are suitable for a multi-rate asynchronous implementation, making timely use of measurements from sensors whose measurement rates may differ by over an order of magnitude.

Contents

List of Figures

List of Tables

Chapter 1

Introduction

Accurate, high-rate estimation of attitude and position is important to many areas of robotics. For example, in the control of autonomous vehicles and the callibration of sensing systems. Such system can usually be modelled as rigid body kinematics and dynamics, where the pose lies naturally in the group of rigid body transformations, the special Euclidean group $\mathrm{SE}(3)$ of dimension four. The problem of pose estimation, and attitude estimation in general, is known to be a highly non-linear problem due to the geometry of rotations in three dimensional space (e.g. Murray et al. 1993). For the estimation of attitude alone, a wide range of techniques have been proposed including Kalman filter variants, particle filters and non-linear observers (Crassidis et al. 2007), each with different merits.

Localization, the process of estimating the position and attitude of an object relative to an operating environment, is thought to occur in humans through a fusion of predictive information from proprioceptive senses, such as the vestibular system in the inner ear, with corrective information from exteroceptive senses, such as sight and hearing. Information from the vestibular system provides an estimate of how our position and attitude have changed, measuring quantities such as angular velocity and acceleration, including gravity, experienced by the head. This information is sufficient for short term state estimation, using an approximate integration of measurements, but, as anyone who has attempted to walk through a room in the dark will notice, does not provide a good long term estimate. Fusing the information from the vestibular with estimates of our surroundings from vision and auditory sensors, and other senses such as touch, provides correction of drift in vestibular estimates.

Similarly, one may estimate the position and attitude, or pose, of a robotic vehicle by fusing the output of multiple sensors. The principal reason for doing this is to combine measurements from disparate sensors with different desirable characteristics, such as a high measurement rate or high accuracy, to obtain a resulting estimate

that combines the desirable properties of several separate sensors. Additionally, multiple independent measurements provide a way of reducing the effects of measurement noise, and fusion may be used to create a composite measurement from sensors each only partially measuring an input or output to a system.

A wide range of sensors, with varying noise and disturbance characteristics, may be used to measure the inputs and outputs of this system, either in full or part. For example, an array of gyrometers measures angular velocity, a Global Positioning System (GPS) device measures attitude and position, and a receiver for an ultrasonic beacon may measure distance from the beacon; a component of position.

A particular sensor combination of recent scientific interest is the combination of an inertial sensor package with a vision sensor, a combination referred to as an inertial-vision sensor system. An inertial sensor package is functionally similar to the human vestibular, providing measurements of angular velocity and linear acceleration, commonly at a very high rate, exceeding 100 Hz, but with undesirable measurement disturbances, especially in low-cost models. A vision sensor, such as a common webcam or digital camera, observes a two dimensional projection of the environment of the vehicle from which, under certain conditions, the pose of the sensor can be calculated. Typically a vision sensor measures at low rates of 30 Hz and below, but with very small, and in particular unbiased, measurement disturbance.

Inertial-vision sensor packages are of scientific interest for several reasons, including the low cost of the sensor combination, the possibility of multi-modal use of vision sensors, and the relationship to human perception. Some techniques for estimation from inertial-vision sensors also support use of other sensors in the place of vision, such as GPS or ultrasonic triangulation.

This thesis considers the problem of obtaining high quality, high rate estimates of attitude and position, or pose, from a combination of inertial and vision measurements using low cost sensors. In particular, it will consider the fusion of high frequency inertial measurements with low frequency vision measurements to obtain a robust, precise and accurate pose estimation updated at the high measurement rate of the inertial sensor.

The appraoch taken it to investigate the use of non-linear observers for pose estimation, with particular emphasis given to designing observers on $\mathrm{SE}(3)$, a mathematical construct encapsulating the natural geometry of the problem. Prior work applying non-linear observers to attitude estimation has notable benefits in their asymptotic sta-

bility proofs and show great promise for future applications (Crassidis et al. 2007). Work presented in this thesis commences by extending work attitude estimation using non-linear observers presented in Mahony et al. (2008).

The research documented considers a range of sensor modalities for both the inertial and vision sensor, and will principally consider the case of onboard sensors. Work includes consideration of both biased and unbiased inertial sensor measurements.

The research documented in this thesis focuses on the design of estimators that are robust to measurement distrubances, have a wide basin of attraction and are simple to implement and tune. These criteria are aimed at being competitve the robustness and accuracy of techniques such as Kalman filtering, while adding additional properties and simplifying their use.

Specifically, this research seeks to produce estimators that are:

- Robust to measurement disturbances, including insensitivity to Gaussian noise and correction of measurement biases.
- Insensitive to initial condition error;
- Capable of being implemented to operate at the rate of the fastest measurement, preferably without requiring regular measurement timing;
- Straightforward to tune, preferably with few scalar gains and demonstrated stability across a wide range of gain values;
- Backed by formal mathematical proof of stability for the continuous time case with no measurement noise.

This thesis includes both simulation and experimental validation of proposed observers, including generation of indigenous experimental data sets.

1.1 Papers and Publications

This thesis includes work contained in the following academic papers

- Cheviron, T.; Hamel, T.; Mahony, R. and Baldwin, G. **Robust Nonlinear Fusion of Inertial and Visual Data for position, velocity and attitude estimation of UAV**. In *Proceedings of the 2007 IEEE International Conference on Robotics and Automation*, Roma, Italy, April 2007. 2010–2016.

- Baldwin, G.; Mahony, R.; Trumpf, J.; Hamel, T. and Cheviron, T. **Complementary filter design on the Special Euclidean group SE(3)**, In *Proceeding of the European Control Conference 2007*, Kos, Greece, July 2007.

- Baldwin, G.; Mahony, R.; Trumpf, J. and Hamel, T. **Complementary Filtering on the Special Euclidean Group**. Submitted to *IEEE Transactions on Robotics*, 2008.

- Baldwin, G.; Mahony, R. and Trumpf, J. **A Nonlinear Observer for 6 DOF Pose Estimation from Inertial and Bearing Measurements**. In *Proceedings of the 2009 IEEE International Conference on Robotics and Automation*, Kobe, Japan, May 2009. 2237–2242.

1.2 Roadmap And Contributions

This thesis comprises seven chapters including this introduction.

- Chapter 2 is a literature review that surveys the body of scientific work on pose estimation, the use of inertial-vision sensors in pose estimation and developments in non-linear observers relevant to pose estimation.

- Chapter 3 describes the systems and protocols used for the collection of experimental data from an inertial-vision system for experimental validation of observers presented in this thesis. Notably, this system, based on a large, 2 m reach, robotic arm includes measurement of ground-truth reference data against which estimates can be compared.

- Chapter 4 presents two approaches to designing a non-linear pose observer by making use of a decompositions that permit independent design of the rotation and position components. The first approach presented comprises independent attitude and position observers, with the attitude estimate used as an input for the position observer for which stability is proven in the presence of an exponentially decaying input disturbance resulting from the cascade. The second and third approaches design the rotation and position estimation components simultaneously but within a single observer by decomposing a Lyapunov function into rotation and translation components.

- Chapter 5 describes the design of an observer for both pose and velocity measurement biases. An almost-global asymptotic and locally exponential Lyapunov stability proof is given together with an extension to the case where velocity measurements are measured in two orthogonal components in different frames of reference with separate bias processes. Implementation issues are addressed including presentation of a sample discrete time algorithm.

- Chapter 6 presents a pose observer that uses projective vision measurements of bearing from the camera to a landmark, instead of vision measurements of pose. This corresponds to a simpler, more direct use of vision measurements without requiring complicated post processing. Again, a Lyapunov stability argument is given, proving local asymptotic stability. Based on work in Chapter 5, the observer is extended to address velocity bias estimation.

- Chapter 7 conclude this thesis, summarising the results of this research.

Experimental data and MATLAB scripts implementing the observers described in this thesis are contained in an attached DVD. Additionally, this thesis contains three appendicies describing the contents of the attached DVD and providing further results not included in the main text.

- Appendix A contains descriptions of the contents of the DVD atttachement to this thesis, including raw and pre-processed data sets from experiment series reported in this thesis.

- Appendix B provides the full proof of a linearisation argument using in Theorem 5.2.1 of Chapter 5.

- Appendix C presents a sample observer for linear velocity from measurements of pose, angular velocity and linear acceleration in the presence of inertial measurement biases. By use of such an observer, one can treat an appropriate inertial sensor as providing measurements of the system velocity, angular and linear. Appendix C also outlines sufficient conditions for ensuring the cascade of a linear velocity estimate into a pose observer is stable.

Chapter 2

Literature Review

In this chapter I will critically review the background literature relevant to the problems considered in this thesis. Section 2.1 reviews historical approaches to the problems of estimating position, attitude and pose. Section 2.2 provides an overview of inertial vision sensor packages and a summary of prior work utilising them for attitude and pose estimation. Finally, Section 2.3 surveys prior work in the use of non-linear observers for the estimation of pose and attitude.

2.1 Pose Estimation

Accurate estimation of the attitude and position of a vehicle is vital to many areas of scientific endeavour, including navigation, robotics and automation. In this section, I present a review of common practices and techniques for the estimation of attitude and position independently, and for their combined estimation as pose.

Position estimation in a static frame of reference is a linear problem which can be tackled by well studied techniques such as Kalman filtering. Attitude estimation is however a highly non-linear problem requiring different techniques. Estimation of both position and attitude by a single estimation system may be simultaneous in a single estimator, or through a cascade of the results from one estimator into another.

2.1.1 Position Estimation

The standard representation for the position of an object in three dimensional space is as a three-vector, $p \in \mathbb{R}^3$. In a non-rotating, inertial, frame, p has the customary kinematics

$$\begin{aligned} \dot{p} &= v \\ \dot{v} &= a \end{aligned} \tag{2.1}$$

where v is linear velocity and a the acceleration, both also three-vectors in $\mathbb{R}^3$. With measurements of p, v or a, or full rank linear combinations thereof, estimating p is then a linear problem.

Estimating position based measurements of p, v or a, or linear combinations thereof, is a self-evidently important problem with applications including navigation, robotics and automation.

2.1.1.1 Asymptotic Observers

One of the simplest methods for defining an estimator for a linear problem is the asymptotic observer (see e.g. Kailath et al. 2000). For the general linear system with state x, input signal u, output y and kinematics

$$\begin{aligned} \dot{x} &= Ax + Bu \\ y &= Cx \end{aligned} \tag{2.2}$$

where A, B and C are known, full rank, matrices, one can define the estimate $\hat{x}$ with kinematics

$$\dot{\hat{x}} = A\hat{x} + Bu + K(y - C\hat{x}) \tag{2.3}$$

from measurements of u and y. By selecting the matrix $K \neq 0$ such that $(A - KC)$ is Hurwitz, one can ensure the estimation error, $\tilde{x} = \hat{x} - x$ will asymptotically converge to zero based on the error kinematics $\dot{\tilde{x}} = (A - KC)\tilde{x}$. Further, the rate of convergence is defined by the eigenvalues of $(A - KC)$. A matrix K can always be selected to ensure $(A - KC)$ is stable provided the system in equation (2.2) is detectable. By application of the pole placement theorem, observability of $\{A, C\}$ is a sufficient condition for detectability (e.g. Polderman and Willems 1998).

Consider a cost function on the state estimate error of the form

$$\mathcal{L} = \tilde{x}^\top P \tilde{x}, \tag{2.4}$$

where P is a symmetric, positive definite matrix. $\mathcal{L}$ is a quadratric cost function measuring the deviation of $\tilde{x}$ from 0. Lyapunov stability theory (e.g. Khalil 2002, Slotine and Lie 1991, Rouche et al. 1977) provides the result that stability of the linear time invariant system $\tilde{x}$ is equivalent to the existence of symmetric positive definite matrix P for any choice of symmetric positive definite matrix Q, such that $-Q = P(A - KC) + (A - KC)^\top P$. Further, Lyapunov stability theory introduces the notion of exponential stability, where the value of a cost function on the state is bounded above by a decaying exponential in time.

Note that as an observer, acting on ideal noise free measurements and unrestricted by innovation energy constraints, it is often possible to make the eigenvalues of $(A - KC)$ arbitrarily large and hence convergence of the error to 0 arbitrarily fast.

Further, consider the case where the input u and measurements y are corrupted by independent additive white Gaussian noise processes, and hence $\hat{x}$ is random variable whose covariance is related to the covariances of u and y. Correspondingly $\tilde{x}$ is also a random variable with the same covariance, and the quadratic cost $\mathcal{L}$ is likewise a random variable with a mean related to the covariance of $\tilde{x}$. Setting the design goal of estimating $\hat{x}$ such that $\tilde{x}$ is zero mean with minimum covariance, minimising the mean of $\mathcal{L}$, one has a Linear Quadratic Gaussian system for which we are attempting to construct a Linear Quadratic Estimator.

2.1.1.2 Linear Kalman Filters

There exists a single optimal estimator for a Linear Quadratic Gaussian system, the Kalman filter (Kalman 1960, Kalman and Bucy 1961). The Kalman filter has been the subject considerable research and many publications over the past 50 years, including analysis and formulations for both discrete and continuous systems. For a detailed analysis see, e.g., Anderson and Moore (1979), Kailath et al. (2000).

Resembling the asymptotic observer for the case of noiseless measurements, equation (2.3), the Kalman filter adds an algorithm for selecting an optimal gain matrix at a given time, $K(t)$, based on solving an algebraic Riccati equation that includes estimating the measurement covariance based on the time history of measurements received so far. The optimal gain $K(t)$ is chose such that the expected value of quadratic cost function is minimised, subject to estimates measurement uncertainty. In the Kalman filter, this is broken down into a predictor and a corrector step at each update. In the predictor step, the covariance and state estimates are propagated based on the input and state dynamics. In the corrector step, the optimal gain computed and innovation terms applied to state and covariance estimates.

Linear Quadratic Gaussian systems form a fundamental and widely studied component of control theory as they model many natural systems, such as position and velocity estimation from noisy inertial measurements, and a simple class of systems that other systems resemble locally. Any continuous non-linear system is approximately linear in a sufficiently small area about its operating point. Further, additive white Gaussian noise is an accurate model of sensor noise process arising from sources such

as transmission of analogue waveforms (e.g. Couch 2001, Proakis and Salehi 2001).

2.1.2 Attitude Estimation

Attitude estimation is an inherently non-linear problem. Unlike the linear problem of position estimation, which occurs on a vector space, attitude estimation occurs on a curved, compact group. Specifically, attitude estimation for objects in three dimensional space occurs on the special orthogonal group $\mathrm{SO}(3)$ of dimension four, a smooth differentiable manifold. The group $\mathrm{SO}(3)$ contains every unique rotation that can be applied to a vector in $\mathbb{R}^3$, including the identity, or rotation by 0 degrees, and the inverse for every rotation. Further, as the angle of rotation passes 180 degrees, the group loops back on itself, giving it its compact property.

Attitude estimation is vitally important for trade, commerce and military applications. In ancient times, the attitude of a ship on the oceans surface was estimated using a magnetic compass and measurements of the stars. Precise estimation of the ships attitude was vital to reaching safe ports and avoiding nautical dangers, especially when out of sight of coastal references. In more recent times, air and spacecraft have extended the need to precise attitude estimation in three dimensions and at high frequency. For aircraft in particular, attitude estimation is vital to their safe operation. Without an accurate estimate of attitude, aircraft risk not only drifting off-course, but loss of control, stalls and crashes.

A number of distinct techniques have been applied to the problem of attitude estimation over the course of the last century, ranging from extensions of linear estimation algorithms to novel non-linear techniques. These techniques have both been driven by and driven the development of accurate and high-performance air and spacecraft, especially autonomous vehicles. Common sensor used in estimation include inertial, magnetic field, vision and Global Positioning System (GPS) sensors.

Crassidis, Markley and Cheng present a comprehensive survey of attitude estimation techniques with particular emphasis on the practicality of each technique in real-world applications (Crassidis et al. 2007). This survey focuses heavily upon Extended Kalman Filter (EKF) based techniques, which have been long established as the workhorse of non-linear estimation (e.g. Allerton and Jia 2005, Armesto et al. 2004, 2008, 2007, Marins et al. 2001, Lefferts et al. 1982, Barshan and Durrant-Whyte 1995, Trawny et al. 2007, Mourikis et al. 2007, Mourikis and Roumeliotis 2007, Bonnabel 2007). The survey also considers newer techniques including unscented filters (e.g.

Julier and Uhlmann 2002a,b, Wan and van der Merwe 2000), particle filters (e.g. Cheng and Crassidis 2004, Gustafsson et al. 2002, van der Merwe et al. 2000), and non-linear observers (e.g. Thienel and Sanner 2003, Thienel 2004, Hamel and Mahony 2006, Mahony et al. 2008, 2005).

Other surveys on the topic of attitude estimation include Lefferts et al. (1982), Allerton and Jia (2005) and Meng et al. (2008).

2.1.2.1 Extended Kalman Filters

The Extended Kalman Filter (EKF) refers to a family of estimators in which non-linear systems are locally approximated by linear quadratic Gaussian systems and their state estimated using the Kalman filter. For a given non-linear system there are many ways of obtaining and maintaining a local linear approximation of the state and input dynamics. Commonly, the local linear estimate will be taken about the current best state estimate using a linearisation chosen for accuracy over an area proportionate to the rate at which the linearisation is updated.

In the problem of attitude estimation, the linearised state is commonly represented using Euler angles (e.g. Craig 1989), Rodrigues parameters (e.g. Murray et al. 1993) or unit quaternions (again, e.g. Murray et al. 1993). Each approach has advantages and disadvantages in terms of the state and input dynamics. In particular, any three dimensional representation of attitude, such as Euler angles and Rodrigues parameters, necessarily has at least one singular point near which state representations must be shifted to avoid singularity.

2.1.2.2 Unscented Kalman Filters

A key performance limitation of an EKF is the region of validity for the linearisation (Julier and Uhlmann 1997). For highly non-linear problems, such as attitude estimation for aircraft, the region of validity of the linearisation of the state dynamics in the update step may be significantly smaller than the movement of the state trajectory over the update time step causing the evolution of the state dynamics to be incorrect and ill-defined. This can be alleviated by raising the rate at which the linearisation is recomputed, a solution that is however limited by available computational resources.

Further, Julier and Uhlmann observe that under the repeated linearisation of the EKF, the state estimates can become statistically biased and inconsistent due to the Taylor series truncation inherent in the linearisation (Julier and Uhlmann 1997). That

is, the state estimate can be incorrect, or biased, and the covariance estimate underestimated, or inconsistent. This combination can cause the filter to diverge.

Julier and Uhlmann propose an alternative in the Unscented Kalman Filter (UKF) (Julier and Uhlmann 1997, Julier et al. 1995). While the EKF handles nonlinear dynamics by linearising the problem about the operating point, the Unscented Kalman Filter (UKF) uses a non-linear transformation of a set of carefully selected points from a Gaussian distribution

The UKF replaces the EKF prediction step, where state and covariance estimates are propagated via linearised system dynamics, with a novel estimation scheme based on the true non-linear trajectory for a set of points characterising the state and covariance distribution, a process called the unscented transformation. A set of point, called sigma points are selected to represent the state and covariance estimate. These points are usually initialised as being along basis directions of the covariance, at a distance of the standard deviation from the mean. For each prediction step, the location of these sigma points is predicted using the true non-linear state dynamics function, and from these predicted sigma points the state and covariance after the time step estimated. Using the true non-linear function of state dynamics rather than a linearisation allows estimation of the state and covariance at up to second order for state and third order for covariance, compared with the first order estimate obtained by the EKF. The corrector step remains the same in the UKF.

Sigma-point based estimators offer several advantages over EKFs. The Unscented transformation is statistically both unbiased and consistent, compared with the biased and inconsistent result obtained using the linearisation to propagate the state and covariance estimates. Additionally, eliminating the need to compute analytic Jacobians for the linearised system dynamics significantly reduces the computational cost of each iteration.

2.1.2.3 Particle Filters

Particle filters have also successfully applied to the attitude estimation problem (e.g. Cheng and Crassidis 2004, Oshman and Carmi 2004a,b). Particle filters form a large class of suboptimal nonlinear estimators based on sequential Monte Carlo simulation in which the state probability density function is approximated using point samples distributed pseudo-randomly according to the prior distribution (Doucet et al. 2001, MacKay 2003). At each iteration of the filter, the particle locations are updated using

drift, diffusion and resampling processes. After estimation, the particles are let 'drift' down gradient directions towards local maxima in the state distribution. To prevent a degenerate case, particles are also 'diffused' using a random walk, and a subset of particles resampled; redistributed pseudo-randomly using the current distribution estimate. Particle filters can differ substantially in the algorithms used for diffusion, drift and resampling point selection, in addition to the number of particles and state representation. Scaling the number of particles used can greatly vary the accuracy and computational efficiency of the filter.

For strongly non-linear and non-Gaussian problems, particle filters can prove superior to conventional nonlinear filters, such as from the Kalman filter family. In particular particle filters are able to estimate multi-modal distributions and, due to the resampling and diffusion processes, are able to cope with local minima.

The two major drawbacks to the particle filter are its inherent suboptimality and computational cost on high dimensional problems. The structure of a particle filter is inherently suboptimal due to the diffusion and resampling processes. As the dimensionality of the problem increases, the number of particles required to approximate the distribution increases with the power of the dimension (Daum and Huang 2003, Oh 1991).

2.1.2.4 Other Solutions to Attitude Estimation

In addition to the application of generic non-linear estimation methods, there have been attempts to develop methods of attitude estimation using the specific properties of the non-linear attitude estimation problem. Of note is the Quaternion Estimator (QueST) (Shuster and Oh 1981), a method based on Wahba's problem (Wahba 1965), which is to find the orthogonal matrix R that minimizes the mean squared error between observations of reference vectors, Z_{y_i}, and estimates of the vector measurements, Rz_i. QueST solves Wahba's problem using a fading memory of previous estimates to smooth process noise. The QueST algorithm includes elements from optimal estimators, such as covariance estimation.

2.1.2.5 Non-Linear Observers

A comparatively recent approach has been the use of an asymptotic observer structure constructed on a non-linear space, in this case $\mathrm{SO}(3)$, to provide estimates of attitude (Thienel and Sanner 2001, 2003, Thienel 2004, Thienel and Sanner 2007, Hamel and

Mahony 2006, Mahony et al. 2008, 2005, Bonnabel et al. 2006b, Vasconcelos et al. 2007).

Non-linear observers offer significant advantages in the simplicity of implementation and tuning, and robustness to measurement noise. As they are often accompanied by global or almost-global stability proofs, many non-linear observers may be initialised with almost any initial conditions and will reconverge after an almost arbitrarily bad noise injection. In addition, many non-linear observers are also locally exponentially convergent, dominating most unbiased measurement noise processes.

The almost-global nature of the stability proofs for non-linear attitude observers is an unavoidable of $\mathrm{SO}(3)$. Due to the compact structure of $\mathrm{SO}(3)$ there necessarily exists an antipodal set in which multiple directions are equi-distant from the goal attitude, such that the vector sum of paths to the goal is zero. Often, this set corresponds to the set of all orientations a rotation of π radians from the goal about any axis. This set necessarily has measure zero.

Many non-linear observers commonly feature a small number of gains, with convergence for a wide range of gains, if not all gains. Even with discrete implementation the range of values for which the observer is convergent can cover several orders of magnitude, significantly simplifying the tuning process.

It is noted by Crassidis et al. (2007) that these newer, non-EKF based approaches have demonstrated several advantages over EKF approaches, particularly as non-linearity, non-Gaussian statistics and poor a-priori state estimates become problematic. In particular, Crassidis et. al. note that although non-linear observers are still in their infancy, these methods show great promise for future applications.

2.1.3 Combined Attitude and Position Estimation

For many applications, including navigation and automation, it is necessary to estimate both the attitude and position of a vehicle. The two may be treated as separate estimation problems, or combined into a single estimation problem, where one estimate is cascaded as input to the other estimator, or where both are estimated simultaneously by a single estimator.

With many practical sensor system, independent estimation is not possible as the system model couples the attitude and position components, such as when measuring linear velocity or acceleration in a body-fixed frame and needing rotate it into an inertial frame. In such a case, an estimate of the rotation from the body-fixed to inertial

frame may be produced by an attitude estimator and used as an input to a position estimator. This sort of two-stage estimation structure is referred to as a cascade system. The stability of the estimate $\hat{p}$ will depend upon the stability of its input, the estimate $\hat{R}$ and upon the ability to estimator p to handle non-Gaussian perturbation in this input. One approach to proving stability in this case is to use theorems on input-to-state stability (Sontag and Wang 1995, Sepulchre et al. 1997).

An alternative is to simultaneously estimate position and attitude using a single estimator. In this case one defines a state vector containing both attitude and position, and defines appropriate state and input dynamics. When used in an extended Kalman filter structure, as in e.g. Kim et al. (2007) or Huster and Rock (2001), this offers the advantage over a cascade solution of organically estimating covariances arising from attitude-position interaction. However, it suffers the notable drawback of being a higher dimensional state space that must be linearised.

Huster and Rock note that for particular sensor configurations, including the monocular camera plus inertial sensor considered in this thesis, an EKF approach exhibits a number of deficiencies. They note substantial error accumulation in the state covariance matrix due to repeated linearisation, leading to biased estimates. Specifically, the EKF does not account for uncertainty in the construction of linearisations arising from uncertainty in state estimates (Huster and Rock 2003).

Other approaches to simultaneous attitude and position estimation include techniques based on the unscented transformation of the unscented Kalman filter (e.g. Huster and Rock 2003), particle filters (e.g. Vernaza and Lee 2006), and other statistical estimators (e.g. Kong 2004).

An area of deficit in the literature until recently has been in the application of non-linear observers to pose estimation, in particular where the observer is posed as a system evolving on the special Euclidean group $\mathrm{SE}(3)$ of dimension four. $\mathrm{SE}(3)$ is a differentiable manifold and Lie group naturally representing the motion of rigid bodies as an attitude and position with corresponding kinematics (see e.g. Murray et al. 1993, Bullo and Lewis 2005). Posing a non-linear observer evolving on $\mathrm{SE}(3)$ allows the design to make use of the natural geometry of the estimation problem. Recent work in this area includes Martin et al. (2004), Bonnabel and Rouchon (2006), Vasconcelos et al. (2007), Martin and Salaün (2008a), Bonnabel et al. (2009a) and this thesis. This area of literature will be examined in detail in Section 2.3.

2.2 Inertial Vision Sensor Systems

Most estimators for attitude and pose, such as the observers and Kalman filter described in Sections 2.1.1 and 2.1.2, feature estimate dynamics that include both measurements of system input and outputs. Using the inputs, the system state is predicted and from comparing the outputs of the true system to those of the estimate, the estimate is corrected.

For a rigid body dynamical system, the inputs to motion are the velocities, forces or accelerations applied and the outputs the attitude and position of the system. Each of these may be measured directly or as some function of the input or output, such as measuring the operating point of a thruster and using that to estimate the forces applied.

A common and widely available sensor package for velocity and acceleration is an IMU, providing measurements of angular velocity and linear acceleration. The cost, availability, accuracy and uniform utility of inertial sensors generally dominates any alternatives such as force estimation from thrust.

For attitude and position common sensors include vision and those based on triangulation from received signals, such as GPS or sonar localisation. Triangulation for received signals requires an operating environment where the signals can be received in a clear and unadulterated manner for optimal accuracy; reflections, noise and delayed transmission can cause considerable error in pose measurements. This means that systems such as satellite based GPS are not always reliable in indoor, urban canyon or other cluttered environments. Vision sensors do not suffer this limitation as their measurements are reliant only on reflected visible light.

Typical vision sensors, such as the standard pinhole camera model, observe a two dimensional projection of the scence in front of the camera. If certain details of the scene are known, such as the position of several objects, the pose of the camera may be calculated using the position of the features corresponding to those objects in the camera image. Using this standard result from computer vision, a camera can be used a sensor for both attitude and position. Additionally, the location of individual features in the projected image, or calculations of visual flow between images may also be used as measurements of the system output in an estimation.

In this thesis, I concentrate on the estimation of pose using the combination of an inertial sensor and a vision sensor. This combination, often referred to as an inertial-vision sensor package, provides measurements of both the inputs and outputs of a

rigid body motion system. An inertial-vision sensor package has several desirable characteristics, including complementary noise spectra between component sensors, the option of pursuing high-rate estimate, the possibility of multi-modal use of the vision sensor and low weight and cost requirements.

The use of inertial-vision sensor packages has been of recent interest to the scientific community, with two workshop (Vincze et al. 2003, Corke et al. 2005) and a tutorial (Dias and Lobo 2008) at recent major international conferences, and with associated journal special issues.

2.2.1 Pose and Attitude Estimation from Inertial Sensors

Inertial sensor packages contain a series of discrete sensors providing measurements of angular velocity, linear acceleration, magnetic field and inclination. A typical inertial sensor package, such as the 3DM-GX1 (Mic 2006b) may contain up to 9, and in some cases more, discrete sensors; 3 each of gyroscopes, accelerometers and magnetomers, one of each aligned to a different cardinal direction, plus other auxilliary sensors.

Using a high quality Inertial Measurement Unit (IMU) pose may be estimated from inertial sensors alone, by direct integration of measurements. This process, known as dead reckoning, has been used for navigation in cases where exteroceptive sensors are unavailable, such as submarines and strategic missiles. This process is used in the original Inertial Navigation Systems (INSs), a technology brought to maturity during the development of nuclear submarines and theatre ballistic missiles in the 1960's. Accurate dead reckoning relies on the use of highly precise, well calibrated and, by necessity, expensive inertial sensors, as integration of noise and bias errors can rapidly accumulate, causing the state estimate to diverge.

In many modern guided munitions and delivery systems, inertial navigation is used as a component of the guidance systems. Modern sensors used in such systems include ring laser gyroscopes and quartz resonance accelerometers. Such sensors are commonly expensive and in some cases their use or export is restricted by legislation. For example, the Joint Direct Attack Munition (JDAM), designed as a cheap guidance system for existing inventories of unguided gravity bombs, and which has an accuracy of 30 m over a course of up to 15 miles on inertial navigation alone, has been priced at US$18,000 per unit, (GlobalSecurity.org 2006, Federation of American Scientists 2008), of which the inertial nagivation system comprises US$6,500 (Sloyan 1999).

For application to small scale Unmanned Aerial Vehicles (UAVs), these cost of

such guidance systems and sensors can easily match or exceed the cost of the aircraft by over an order of magnitude. For example, the functional prototype of the X-4 flyer constructed at The Australian National University (Pounds 2008) carries an estimated price of AU$8,000 sans INS (Pounds 2009), from which mass production would bring considerable cost savings. Further, for a craft under propulsion (other than gravity), the weight and power requirements of such highly accurate sensors can significantly decrease available payload capacity. For these applications, low-cost and light-weight components are required in order to maintain the performance characteristics of the aircraft.

The advent of Micro Electrical Mechanical System (MEMS) has provided cheap and light-weight components for the development of low-coast, light-weight IMU systems for commercial applications. These sensors typically provide high frequency measurements corrupted by Gaussian noise processes and slowly time-varying biases.

For comparison, the bias drift rates of the 3DM-GX1 are quoted as a angular random walk of $3.5^\circ/\sqrt{\text{hour}}$ and in-run acceleration stability of 10 mg (Mic 2006b), compared with $0.125^\circ/\sqrt{\text{hour}}$ and 1 mg for the Honeywell HG1700 (Honeywell 2006) used in some JDAM kits (Business Wire 1995). The off-the-shelf price for a single 3DM-GX1 was US$1,195 in 2004 (Mic 2004) and similar MEMS devices retailing for around US$350 in 1000 piece lots in 2009. All of these are capable of measurement rates of at least 100 Hz.

In devices such as the 3DM-GX1, the sensor quality is insufficient to provide more than a few seconds of reliable dead reckoning due to the accumulation of errors from both noise and bias. To provide a long term stable pose estimate, it is necessary to augment the inertial sensor with an additional exteroceptive sensor.

2.2.2 Pose and Attitude Estimation from Inertial Sensors Augmented with an Additional Exteroceptive Sensor

Augmenting an inertial sensor with an exteroceptive sensor, such as GPS or vision provides a second sensor that can be used in estimation to balance the noise and bias characteristics of the inertial sensor. As previously discussed, a measurement of the system output may be used to form a correction term in an estimator, correcting initial state errors and prediction errors accumulated from integration of system input measurements.

Generally, due to the physics and construction of their measurement devices exte-

roceptive sensors provide low frequency measurements which are corrupted by high frequency noise processes, but stable at low frequencies. In particular, they are free of measurement biases. Typical measurement rates range include up to 30 Hz for most commercial vision sensors, including webcams and video cameras, and up to 20 Hz for GPS sensors (Saripalli et al. 2003, Novatel 2009).

Augmenting an inertial sensor system with such an exteroceptive sensor permits exploitation of the complementary properties of these sensors. That is, one can combine the high frequency inertial measurement, corrupted by low frequency noise, with a low frequency exteroceptive measurement corrupted by high frequency noise, to produce a high frequency estimate with low noise over the entire spectrum.

Applied to linear time invariant systems, this approach is termed complementary filtering (e.g. Brown 1972, Brown and Hwang 1992) and can be represented as the sum of two or more filters, each applied to different signals, where the filters are chosen so that at all frequencies their transfer functions sum to 1 For example, choosing $F_1(s) = \frac{k}{s+k}$, a low pass filter, and $F_2(s) = \frac{s}{s+k}$, a high pass filter, one can form the complimentary filter $\hat{X}(s) = F_1(s)Y_1(s) + F_2(s)Y_2(s)$. If $Y_1(s)$ and $Y_2(s)$ are noise free measurements of the same signal then $\hat{X}(s)$ is a faithful representation of the signal. Moreover, $Y_1(s)$ is low pass filtered while $Y_2(s)$ is high pass filtered. Figure 2.1 illustrates the frequency responses of $F_1(s)$ and $F_2(s)$.

The idea of complementary filtering has been applied to non-linear systems in pose and attitude estimation by a number of authors over the past 40 years, e.g. Brown (1972), Bachmann et al. (1999), Pascoal et al. (2000), Mahony et al. (2008)

As mentioned earlier, in this thesis I concentrate discussion on and provide experimental results for estimation using the combination of an inertial and a vision sensor. However, many of the techniques presented generalise to other sensors, such as GPS, particularly where the vision sensor is solely for pose.

2.2.3 Linear Velocity from Inertial and Exteroceptive Measurements

For many applications, such as those considered in this thesis, it is desirable to measure both angular and linear velocity. In the case of pose estimation based on Lie group techniques, these form a complete element of a vector field over $\mathrm{SE}(3)$, admitting design of a simpler estimator with a greater affinity for the underlying differential geometry.

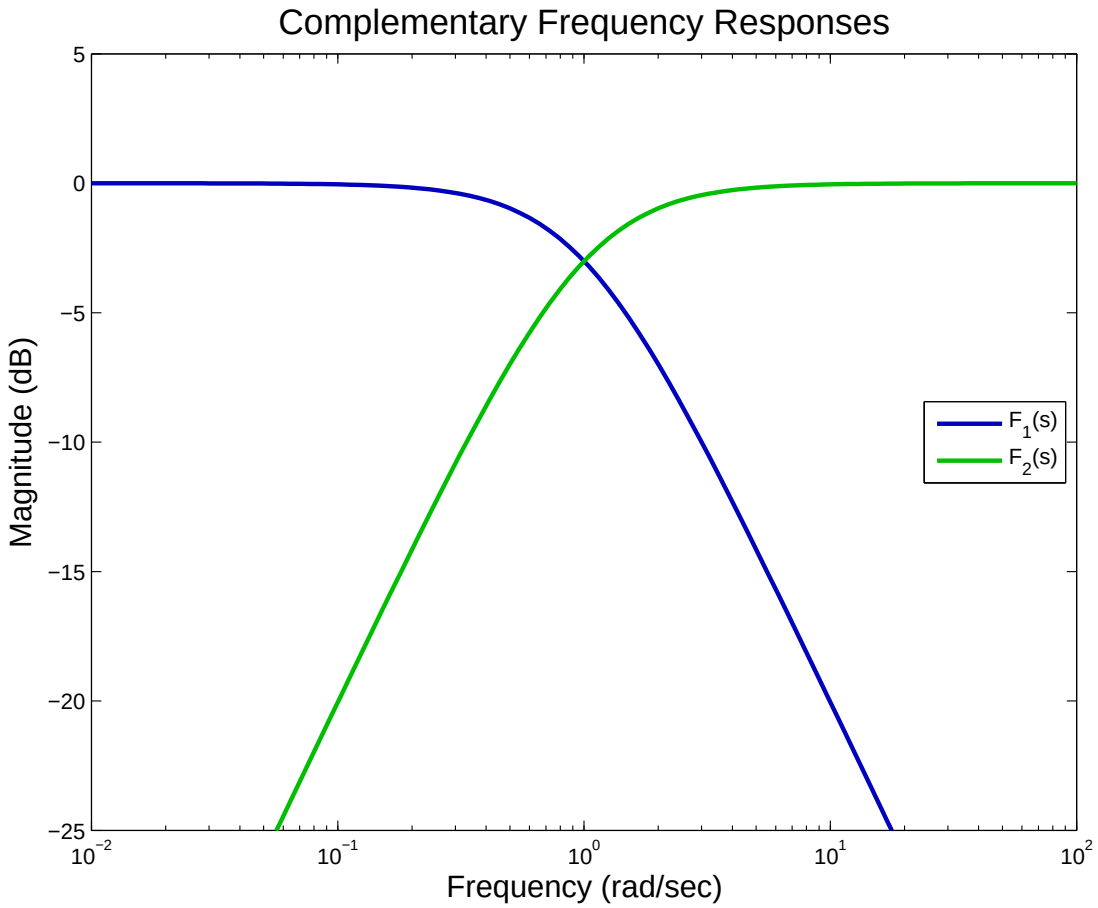

Figure 2.1: Illustration of two functions with complementary frequency responses. At all frequencies, $F_1(s) + F_2(s) = 1$ (0 dB).

Measuring angular velocity is straightforward, using widely available intrinsic sensors; gyrometers. For linear velocity there does not exist a widely available intrinsic sensor, leaving one with more complicated and expensive exteroceptive options such as laser or ultrasonic doppler sensors, or magnetic or visual field derivative sensors. However, instead one may estimate linear velocity using a measurement of position and measurements of linear acceleration obtained from accelerometers commonly co-packaged with gyrometers in inertial measurement units.

Appendix C presents a sample observer for linear velocity from measurements of pose, angular velocity and linear acceleration in the presence of inertial measurement biases. Moreover, it contains an outline of the sufficient conditions for using such an estimate of linear velocity as an input to a pose observer of the types described in this thesis, and ensuring the compositie system arriving from this cascade is stable.

Throughout this thesis, I will commonly assume that linear velocity is available from a inertial-vision sensor package by way of an estimator such as that of Appendix C.

2.2.3.1 Inertial Vision Pose Estimation using Pose Measurements from Vision

As mentioned previously, the pose of single vision sensor can be estimated from each frame using correspondences between observed image coordinates of landmarks and a-priori knowledge of the landmark location.This is a standard result from computer vision, known as the perspective-n-point problem (e.g. Horaud et al. 1989, DeMenthon et al. 2001, DeMenthon and Davis 1992).

In recent literature there have been several investigations of pose estimation using inertial sensors and vision sensors in this modality.

Armesteo et. al. consider pose estimation on $\mathrm{SE}(3)$ for a mobile robotics platform operating a in a cluttered environment (Armesto et al. 2004, 2007, 2008). Using an experimental platform consisting of an inertial and vision sensor package attached to the end of a robotic arm, they estimate pose relative to a specially designed visual target. They compare the performance of extended and unscented Kalman filters and particle filters.

Many authors have considered the problems of attitude (e.g. Mahony et al. 2008) and pose estimation (e.g. Niculescu 2002) from a combination of inertial measurements and direct measurements of attitude or pose, using simulated measurements rather than measurements obtained using a physical sensor such as a vision or GPS

system.

In the field of visual servoing, many authors have considered the problems of control and combined estimation and control for a system with a single camera observing a set of landmarks whose location is known in the inertial frame. When the image features are used to estimate the pose of the camera, this is known as position-based visual servoing and is a well studied problem (e.g. Corke 1994, Wiess 1984).

When the locations of landmarks are not known a-priori, stereo cameras may be used to provide a pose estimate. When the displacement between the cameras is known, pose can be estimated from landmarks observed in both image, using the epipolar geometry of the cameras (e.g. Hartley and Zisserman 2004).

Stereo cameras in combination with inertial sensors have been used in several robotic helicopter projects. Early work from Amidi (Amidi 1996, Amidi et al. 1999) investigates the combination of stereo cameras, GPS and inertial sensors. A team from CSIRO investigated a helicopter platform using stereo vision as the sole exteroceptive sensor (Roberts et al. 2002, Buskey et al. 2003, Corke 2004). In Saripalli et al. (2003), the CSIRO helicopter is compared with other robotic helicopter projects. Saripalli et. al. note that while other helicopters use high performance, high cost avionic grade sensors that can cost more than order of magnitude more than the aircraft, the CSIRO project using considerably cheaper sensors compares favourably, being able to provide good low-bandwidth control.

2.2.3.2 Inertial Vision Pose Estimation using Image Features Directly

Rather than use pose reconstructed from image features in pose estimation, some authors have considered using the image features directly in the estimation process. This approach eliminates a source of approximation error and a significant portion of per-frame computation.

Huster and Rock (Huster and Rock 2001, Huster et al. 2002, Huster and Rock 2003) estimate the position of a moving Autonomous Underwater Vehicle (AUV) relative to a stationary object using inertial measurements of angular velocity and linear acceleration, and the bearing of the stationary object, determined using a single image feature from a monocular camera. Using a modified EKF they estimate position, attitude, inertial measurement biases, linear velocity and external, uncontrolled forces such as ocean currents. They successfully use their estimator in closed-loop experiments performing docking operations using a robotic manipulator from unknown

initial conditions and under simulated output disturbances.

Rehbinder and Ghosh (2003) consider estimation of attitude, position and linear velocity using inertial measurements of angular velocity and linear acceleration, and vision measurements as observations of line features. They propose a nonlinear observer for attitude on $\mathrm{SO}(3)$, proving local convergence, and cascade the resulting estimate into an observer for position and linear velocity.

Vasconcelos et al. (2007) estimate pose on $\mathrm{SE}(3)$ using inertial measurements of angular and linear velocities and vision measurement of the range and bearing of a constellation of landmarks, such as obtained by a laser range finder. They propose a non-linear observer evolving directly on $\mathrm{SE}(3)$ to estimate pose together with linear velocity measurement bias and prove almost-global exponential stability. Recent work from Vasconcelos et. al. consider attitude estimation on $\mathrm{SO}(3)$ in a similar setting, with the addition of bias and noise to angular velocity measurements (Vasconcelos et al. 2008, 2009).

Vik and Fossen (2001) consider full pose estimation from inertial and GPS measurements for a submersible craft. Instead of using measurements of position, attitude from their GPS, they use a tightly coupled architecture utilizing direct measurements of satellite psuedorange and deltarange.

As discussed in Section 2.1.2, the QueST algorithm is a stochastic estimator for attitude estimation from vector measurements.

In contrast to position-based visual servoing mentioned earlier, some authors investigate image-based visual servoing, where control laws are designed to control the motion of observed image features directly, rather than the motion of the camera relative to the landmarks the features correspond to (e.g. Corke 1994, Wiess 1984, Cunha et al. 2007, Guenard et al. 2008, Le Bras et al. 2006).

Considerable research has gone into estimating motion from a sequence vision measurements alone, without inertial measurements. Soatto has considered the application of non-linear estimation techniques to the problem of structure from motion (Soatto et al. 1996), and recently including inertial-aided structure from motion (Jones et al. 2007)

Mourikis and Roumeliotis consider pose estimation for ground vehicle using a camera and IMU in an on-road environment Mourikis and Roumeliotis (2007). They use an EKF technique which estimates not only current position, but also prior camera poses using inter-frame constraints on observed landmarks.

In the related area of Simultaneous Localisation and Mapping (SLAM), practitioners aim to estimate both the pose of a vehicle and the position or pose of landmarks dynamically encountered along a trajectory. Commonly this is achieved by use of a Kalman filter based technique running atop an feature visual extraction and correspondence detection algorithm, using inertial and visual sensors. An excellent review of SLAM techniques is given in Durrant-Whyte and Bailey (2006) and Bailey and Durrant-Whyte (2006). Bekris et al. (2006) presents a good review of the case where SLAM estimation is made from measurements of the bearing to features only.

The use of bearing only measurements in aid of inertial measurements for guidance has been considered in Pachter and Porter (2004).

2.2.4 Multi-rate Sensor Fusion

It is a common practice to design an estimator, especially a deterministic observer, as a continuous time system and yet implement the estimator as a discrete time system on a microprocessor. Generally, strong local convergence properties of the continuous time system, together with a sufficiently small time step, will serve to dominate any additional perturbations from the discrete approximation.

A concern in converting a continuous time system with multiple sensor inputs to discrete implementation is in handling different measurement rates from different sensors. Previously, it was mentioned that common inertial measurement units are capable of measurement rates of 100 Hz and up, and that measurement rates for common exteroceptive sensors were 30 Hz and below.

The simplest approach is to subsample faster measurement rates down to the rate of the slowest measurement and run the estimator at that rate. However, this discards available information that could be used to maintain a higher bandwidth estimate.

Armesto, Tornero and Vincze study multi-rate sensor fusion with relevance to the pose estimation problem, analysing the common techniques of zero, first and higher order holds applied to low rate measurements, assuming synchronicity and periodicity of measurements, in applications including unscented and extended Kalman filters and particle filters Armesto et al. (2004, 2007, 2008).

Alternatively, one may design an estimator such that in the continuous time estimation kinematics there is no multiplicative coupling between measurements from different sensors, and then integrate along the corresponding component as each measurement arrives based on the quasi-linear assumption that locally the kinematics com-

ponents are additive. An example and implementation strategy for this approach will be given in Section 5.3. This approach also offers advantages reducing multiplicative coupling of measurement noise processes, and allows the relaxation of assumptions of measurement synchronicity or periodicity.

In this thesis, this approach will be pursued and termed an asynchronous multi-rate implementation

2.2.4.1 Zero Order Hold versus Impulsive Integration

In an asynchronous multi-rate implementation, kinematics associated with the slowest measurement can be integrated using an impulsive integration, or 'all at once.' For a non-linear system this is the most correct approach as the kinematics are applied when the system is closest to the state in which the measurement was made. Alternatives, such as a zero-order hold, delay some or all of the kinematics causing them to be applied when the system has moved on and they may no longer be in 'the right direction'.

Consider a general non-linear system evolving on a Lie group $\dot{G} = GA$, where G is the current state, such as attitude, and A is an element of vector field, such as angular velocity. Let an estimator from two measurements be given by $\dot{\hat{G}} = \hat{G}(A_y + \alpha)$, where A_y is a measurement of velocity and α is an innovation based on a measurement of G. Further, consider the right invariant error term $\tilde{G} = \hat{G}G^{-1}$ with kinematics $\dot{\tilde{G}} = \tilde{G}\,\mathrm{Ad}_G\,\alpha$.

Consider the discrete zero-order hold implementation

$$\hat{G}_{k+1} = \hat{G}_k \exp(\tau A_{y_k} + \tau\alpha_{k-\kappa}) \tag{2.5}$$

where $\kappa = 0$ when a measurement of G arrives and is incremented on any other iteration. With simple forwards Euler integration, the error dynamics over a period s, between consecutive measurement of G, is given by

$$\tilde{G}_{k+s} = \tilde{G}_k \Pi_{l=k}^{k+s} \mathrm{Ad}_{G_l} \exp(\tau\alpha_k). \tag{2.6}$$

Conversely, using impulsive integration defined as

$$\hat{G}_{k+1} = \hat{G}_k \exp(\tau A_{y_k} + \delta_{k \bmod s} s\tau\alpha_k) \tag{2.7}$$

where s remains the period between measurement of G, and $\delta_{k \bmod s}$ signifies the α term is only included in the dynamics when available. In this case, the error dynamics over

the period s are given by

$$\tilde{G}_{k+s} = \tilde{G}_k \, \mathrm{Ad}_{G_k} \exp(\delta_{k \bmod s} s \tau \alpha_k). \tag{2.8}$$

The latter performs a single impulsive correction, using the innovation α_k in the state closest to that in which it is measured, while the former performs a slow correction, transforming the innovation with the evolving state. This slower integration may introduce additional errors due to the non-linear and non-commutative nature of the state dynamics.

2.3 Non-Linear Pose Observers

Problems such as attitude and pose estimation are examples of non-linear optimisation problems that exhibit strong structure properties that can be represented using differential geometry. Smooth, continuously differentiable surfaces combined with properties such as invariance of cost functions and symmetry provide sufficient structure to support novel optimisation techniques arising as natural extensions of established linear techniques (Absil et al. 2008, e.g.), with a recent workshop (Absil et al. 2007) bringing authors from areas including robotics, computer vision, bioinformatics, data mining and signal processing.

Specific to the problems of attitude and pose estimation, and the estimation of related quantities such as velocity, there have been a number of works proposed over the past twenty years. Early work from Salcudean (1991) proposed an observer for angular velocity using a quaternion representation, with global convergence properties. Vik and Fossen (Vik and Fossen 2001) designed an observer for attitude and positions, using a quaternion representation of attitude and simultaneous attitude and position estimation dynamics.

Rehbinder and Ghosh (2003) propose an observer for pose from a combination of inertial and vision sensors, where the vision measurements are of lines in the camera image corresponding to line features whose position and direction are known a-priori. They identify the line measurements as the implicit outputs of a perspective system and prove local convergence. The problem is re-addressed in a quaternion formulation by Wu et al. (2006).

Recent work from Thienel and Sanner (Thienel and Sanner 2001, 2003, Thienel 2004) proposed a series of observer and control designs for spacecraft attitude from

measurements of attitude and biased measurements of angular velocity, again utilizing the quaternion representation.

Mahony, Hamel and Pflimlin (Mahony et al. 2005, Hamel and Mahony 2006, Mahony et al. 2008) propose observers using the rotation matrix and quaternion representations of attitude, identifying similarities to linear complementary filters. While early work considers measurements of attitude and biased measurements of angular velocity, in later the work the attitude measurement is replaced with a projective measurement in the gravity vector.

Martin and Salaün (Martin and Salaün 2008a,b,d,c, 2007) apply invariant and symmetry-preserving observers, developed by Bonnabel, Martin and Rouchon (Bonnabel et al. 2009a, 2008), to the problem of attitude estimation from inertial measurements.

Vasconcelos, Cunha, Silvestre and Oliveira (Vasconcelos et al. 2007, 2008, 2009) consider the design of observers for pose and attitude from measurements of angular and linear velocity and vector measurements of the bearing and distance to landmarks whose position is known a-priori. Related work in Cunha et al. (2007) and Cunha et al. (2008) considers the visual-servo control problem using purely visual measurements is considered.

In related work, Batista et al. (2007) consider the design of a non-linear observer for a class of systems inlcuding position and velocity estimation in a moving frame of reference.

2.3.1 Perspective Systems

As mentioned previously, Rehbinder and Ghosh (2003) propose an observer for pose from inertial measurements and vision measurements of the perspective image of known line features. They identify the line measurements as the implicit outputs of a perspective system. An implicit output being an output given by an implicit function, in this case $d_i^\top R^\top y_i = 0$, where d_i is the true line and y_i is a normal to the observed line.

The term perspective system is introduce in (Ghosh et al. 1992) and a general perspective system defined in (Ghosh et al. 1994). These papers address the problem of correspondences between line measurements for a camera undergoing unknown rotation and translation.

Several non-linear observers have been proposed based on the perspective system formulation. In early work, Jankovic and Ghosh (1995) develop an observer for range

estimation from vision measurements. In Matveev et al. (2000), a Luenberger-type observer is given for a general system with implicit outputs. Aguiar and Hespanha (2005) proposes a robust observer using a H_∞ approach for the pose of a vehicle using a combination of velocity measurements, pose measurements and implicit output vision measurements. Other pose and attitude observers include Chen and Kano (2002), Hespanha (2002), Abdursul et al. (2004), Aguiar and Hespanha (2006).

2.3.2 Observers from Vector and Bearing Measurements

Another useful modality of vision sensors is where the location of image features are treated as bearing on the sphere $\mathbb{S}^2$ from the camera to a landmark whose position is known. A similar case is where a laser rangefinder is used to obtain vector measurements on $\mathbb{R}^3$ of both the distance and bearing to landmarks. These problems are examples where measurements taken on a homogenous space acted upon by a Lie group (Boothby 2002).

When designing observers for systems based on vector or bearing measurements a number of additional difficulties are presented. Firstly, multiple measurements are required to ensure (almost) global stability as opposed to stability to a subspace, generally three or more such that they collectivelly span $\mathbb{R}^3$. Errors and innovations from each of these measurements then need to be combined in the dynamics of the estimate, complicating stability proofs. Additionally, in the case of bearing measurements the measurement is a linear operation of the system state, causing additional difficulties in obtaining stability proofs.

As describe in Section 2.1.2, Wahba's problem (Wahba 1965) and the QueST algorithm (Shuster and Oh 1981) address the problem of estimating attitude from vector measurements. Recent work on the problem includes Sanyal et al. (2008).

As mentioned earlier, Vasconcelos, Cunha, Silvestre and Oliveira (Vasconcelos et al. 2007, 2008, 2009) consider the design of observers for pose and attitude from inertial and vectorial measurements.

Mahony et al. (2008) consider the problem of attitude and angular velocity measurement bias estimation from inertial and vector measurements in their explicit complementary filter.

Another case where measurements are made on a homogeneous space is when the, scalar, range from a known object to a vehicle is measured. When three or more range measurements are made, well understood techniques for trilateration may be applied

to determine the position of the vehicle, though the attitude can not be instantaneously determined. Alocer et al. (2006a,b) consider the estimation of both attitude and position from range measurements using geometric descent. The work of Vik and Fossen (2001) using pseudo-range measurements from GPS sensors is related to this problem.

2.3.3 Invariant and Symmetry Preserving Observers

A substantial body of work from Rouchon, Martin, Bonnabel, Aghannan and Rudolph concerns systems with smooth state dynamics that are invariant under the action of a local transformation group and the design of observers that make use of this symmetry. This work is especially relevant to the design of observers for quantities evolving on Lie groups, such as pose on $\mathrm{SE}(3)$, where the system dynamics can be naturally expressed as the action of a left (or right) invariant vector field.

Formally, consider the general non-linear system with continuous state dynamics $\dot{x} = \mathrm{f}x$ where $x \in \mathcal{X} \subset \mathbb{R}^n$; for example let $T \in \mathrm{SE}(3)$ be the pose of a vehicle, then $\dot{T} = T\Xi$, where Ξ is an element of a left-invariant vector field over $\mathrm{SE}(3)$ constructed from the angular and linear velocities of the vehicle.

Let G be a local transformation group acting on $\mathcal{X}$, giving $X = \{\varphi_g(x) | \forall g \in G\}$. Then dynamics $\dot{x} = \mathrm{f}(x)$ are said to be $G-$*invariant* if for every $g \in G$, the dynamics are unchanged; i.e. $\dot{X} = \mathrm{f}(X)$ (Olver 1995). In the case of $T \in \mathrm{SE}(3)$, let $G = \mathrm{SE}(3)$ and $\varphi_g(T) = Tg$ such that g corresponds to an arbitrary change of initial condition. Without loss of generality, if $T(0) = I$ then one has that the dynamics $\dot{T} = T\Xi$ evolve symmetrically from any initial condition $\varphi_g(T(0)) = g$.

An output $y = h(x)$, $y \in \mathcal{Y} \subset \mathbb{R}^p$ is defined to be $G-$*equivariant* (Bonnabel et al. 2008) (or $G-$*compatible* (Martin et al. 2004)) if there exists a transformation group ρ_g on $\mathcal{Y}$ such that $h(\varphi_g(x)) = \rho_g(h(x))$. Note this is trivially satisfied when $\mathrm{h}(x)$ is the identity map or when $\mathrm{h}(x)$ is $G-$*invariant*, when $h(\varphi_g(x)) = h(x)$.

An observer $\hat{x} = \hat{f}(\hat{x}, y)$, where $y = h(x)$ is an output of the system x, is then said to be $G-$*invariant* (Aghannan and Rouchon 2002) if and only if for all $g \in G$, and all states $\hat{x}$ and x,

$$\hat{f}(\varphi_g(\hat{x}), \rho_g(y)) = D\varphi_g(\hat{x}) \cdot \hat{f}(\hat{x}, y). \tag{2.9}$$

Additionally, define a pre-observer as an observer such that $\hat{f}(x, h(x)) = f(x)$ for all x, that is an observer for which any trajectory of the true system is a trajectory of the observer.

Further, an invariant output error $E(\hat{x}, y)$ satisfies the condition $E(\varphi_g(\hat{x}), \rho_g(y)) = E(\hat{x}, y)$ for all $\hat{x}$, y and g, and for each $\hat{x}$, $E(\hat{x}, y)$ is a diffeomorphism with $E(\hat{x}, h(\hat{x})) = 0$. For example, consider the error function on $\hat{T} \in \mathrm{SE}(3)$ given by $E(\hat{T}, T) = I - \hat{T}T^{-1}$, which is invariant under the right group action $\varphi_g(T) = Tg$.

Using the invariance of the system kinematics, observer kinematics, and error terms general results applicable to systems on Lie Groups are obtained in Bonnabel et al. (2009a) and Bonnabel et al. (2008), providing a constructive approach to observer design by specification of a form for all $G-$*invariant* pre-observers, and addressing local convergence around trajectories. Extended definitions for systems with inputs are given analogously.

Application of work on invariant and symmetry preserving observers are varied and include inertial navigation systems (Bonnabel and Rouchon 2005, Bonnabel et al. 2006a, Bonnabel and Rouchon 2006, Martin and Salaün 2007, 2008a,b,d,c), control of mechanical systems Martin et al. (2004), chemical plants (Aghannan and Rouchon 2002, 2003, Bonnabel and Rouchon 2005), mechanical systems (Aghannan and Rouchon 2003), oceanography (Auroux and Bonnabel 2008), quantum systems (Bonnabel et al. 2009b), and coordinated motion (Sarlette et al. 2008a,b).

From the work of Martin and Salaün (Martin and Salaün 2007, 2008a,b,d,c), the efficacy and utility of these methods are demonstrated experimentally on the inertial navigation problem, using inertial, gps, magnetic and barometric sensors.

Chapter 3

Experimental Apparatus and Methodology

In this chapter I present a system and protocols for collection of experimental data from an inertial vision system, augmented with ground-truth reference measurements. The experimental system describe was used to obtain data for inertial-vision based algorithms that are described later in this thesis.

The system presented in this chapter consists of a strap down Inertial Measurement Unit (IMU) and firewire camera rigidly attached to the end of a large robotic manipulator. Inertial vision data from the IMU and camera are recorded on a notebook computer for subsequent analysis. The manipulator, with a radial workspace of over 2 m, is used to simulate the motion of a moving airborne vehicle. Ground-truth measurements of the manipulator trajectory are recorded from the manipulator's controller directly.

For these experiments, data was collected from the sensors and robotic manipulator during motion, in real time. The collected data was then calibrated offline to align measurement frames and time sequences. The calibrated data was pre-processed to extract image features, discard outlier measurements and perform data format conversion.

As discussed in Chapter 2, other investigations of inertial vision systems have included experimental measurements. Several examples are given, including sensor packages attached to small scale helicopters (Corke 2004), ground vehicles (Mourikis and Roumeliotis 2007) and robotic manipulators (Huster and Rock 2003, Armesto et al. 2008). The distinction between this experiment series and others is the inclusion of ground-truth measurements against which estimates may be validated.

The primary contribution of this chapter is the production of a series of data sets of inertial and vision measurement together with ground-truth pose measurements for

a series of trajectories mimicking the behaviour of small-scale unmanned aircraft. Specifically, these data sets contain inertial measurements of angular velocity, linear acceleration and magnetic bearing, visual observations of static image features who location in the world frame is known, and ground-truth measurements of the position and orientation of the sensor package.

This chapter is arranged as follows. Sections 3.1, 3.2 and 3.3 describe the physical experimental system sensors and actuators, considering the Microstrain IMU, Sony Camera and ABB Robotic manipulator respectively. Section 3.4 describes the physical experimental environment, including lighting and image features used. Section 3.5 provides a description of the data logging systems developed for this series of experiments. Calibration of measurement frames and time sequences across difference sensors and recording systems is considered in Section 3.6. Lastly, Section 3.7 describes data pre-processing, including image feature extraction.

3.1 3DM-GX1 Inertial Measurement Unit

The MicroStrain 3DM-GX1^{TM}, pictured in Figure 3.1, is an IMU combining a three angular rate gyros, three orthogonal accelerometers and three orthogonal magnetometers. Retailing for US$1,500 in 2005, it is a commercial off-the-shelf unit with properties typical of Micro Electrical Mechanical System (MEMS) IMUs. By 2009, advances in technology and mass-production have reduced the price of similar sensor units to under US$600 (Douxchamps 2009, SparkFun Electronics 2009).

The 3DM-GX1 communicates with other devices via a serial communications channel. A single 3DM-GX1 can communicate with a host computer over RS-232 or multiple 3DM-GX1s may communicate with a single host computer using a shared RS-485 channel. In addition to the three sets of orthogonal sensors, the 3DM-GX1 contains an embedded microcontroller that can perform orientation calculations and temperature compensation on all sensors, together with hard and soft iron calibration. The 3DM-GX1 can provide compensated, calibrated vector measurements from all three sets of sensors at rates of up to 125 Hz. Alternately, the 3DM-GX1 can provide estimates of orientation using a quaternion, orientation matrix or Euler angle representation at rates of up to 100 Hz (Mic 2006c).

At operating temperature, the 3DM-GX1 provides performance typical of a MEMS IMU, with measurements corrupted by low magnitude noise and slowly time-varying

Figure 3.1: Microstrain 3DM-GX1

biases. An extract of the detailed specifications for the 3DM-GX1 is given in Table 3.1.

Angular Rate	Range (°/sec)	+/- 300
	Bias In-Run stability (°/sec)	0.1
	Angular random walk (°/$\sqrt{\text{hour}}$)	3.5
	Resolution (°/sec)	0.01
Acceleration	Range (g)	+/- 5
	Bias Short term stability (mg)	0.2
	Noise (mg/$\sqrt{\text{Hz}}$ rms)	0.4
	Scale Factor Error (%)	0.5
	Resolution (mg)	0.2
A/D converter	Resolution (bits)	16

Table 3.1: Extract of 3DM-GX1 Detailed Specifications (Mic 2006b).

For this experiment series, the 3DM-GX1 communicated with a notebook PC running Ubuntu Linux via a Dolphin FASTUSB09103 USB to serial adapter (Dolphin Peripherals 2002). Additional USB to serial adapter were tested but found to fail at the high data rates this IMU operates at.

3.2 Sony XCD X710-CR FireWire Camera

The Sony XCD-X710CR (Son 2003), pictured in Figure 3.2, is a high-resolution industrial-use digital video camera module. It contains a 1/3-inch progressive scan

Figure 3.2: Sony XCD 710-CR FireWire Camera

CCD, providing high-quality raw colour images at 30 frames per second with a maximum resolution of 1024 $\times$ 768 pixels. Retailing for US$1,266 in 2009, the XCD-710CR is a self contained, commercial off the shelf firewire camera.

The camera communicates with a host computer over FireWire 400, IEEE 1394-1995 (IEEE p1394 Working Group 1995), bus. The camera both communicates and powers itself using the 6 circuit alpha connector. For this experiment, the camera was connected to a notebook PC via an Aten FH-600 powered FireWire hub to convert the 4 circuit alpha connector to the 6 circuit alpha connected used by the camera.

The camera also features an external trigger circuit that may be used to synchronise shutter timing across multiple cameras or other devices. This connection was not used in this experiment.

3.3 ABB IRB 6600 175/2.55 Robotic Manipulator

The ABB IRB 6600 175/2.55 is a large 6 degree of freedom industrial robotic manipulator (ABB 2004a), pictured in Figure 3.3. With a reach of 2.55 m, a workspace depicted in Figure 3.4 and handling capacity of 175 Kg, this manipulator is used for a wide range of industrial tasks, including spot welding, materials handling and pre-machining. Its large reach and 6 axis design makes it ideal for precise imitation of flying vehicle trajectories.

The ABB IRB 6600 is controlled by an ABB IRC5 Controller (ABB 2004b) running Robotware 5.10 (ABB 2008). The IRC5 provides the facility to command the robot in real time using a Flex Pendant interface, or to pre-program robot behaviour in

Figure 3.3: ABB IRB 6600 175/2.55 robotic manipulator

RAPID. Additionally, the IRC5 is capable of running multiple simultaneous user tasks, allowing data collection to occur during real-time or pre-programmed robot motion.

A custom mount was constructed from aluminium to rigidly affix the IMU and camera to the tooltip of the IRB 6600. The mount consisted of two plates of aluminium welded together at 90°, onto which were mounted the camera and IMU. The entire assembly then bolted onto the tooltip of the IRB 6600. The dimensions were calculated so that the z-axes of the IMU and camera were colinear with each other and the centre of the robot tooltip, and that there was a 12 cm offset between the IMU center and camera focal point. The mount assembly is depicted in Figure 3.5.

3.4 Experimental Environment and Setup

This section describes the environment and physical setup used in these experiments. The environment was controlled to ensure accuracy and repeatability of measurements, including ground truth data.

These experiments were performed in the manufacturing laboratory of the Department of Engineering at The Australian National University. A visual target, containing distinct image features with know locations was constructed. Lighting was adjusted to provide optimum target visibility and avoid shadows and reflections.

The visual target used was pattern of circular dots at the vertices of a square, printed

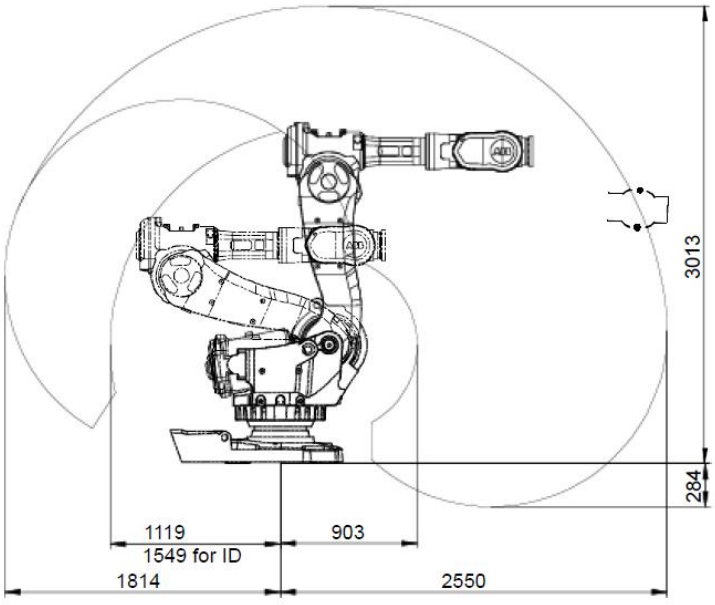

Figure 3.4: ABB IRB 6600 175/2.55 robotic manipulator workspace (ABB 2004a)

on a A0 paper and affixed to the ground. The target consisted of two square patterns of dots, one at the vertices of a square with side length 50 cm, the other at the vertices of a square with side length 10 cm. The dots on the outer square were 7.5 cm in diameter and those on the inner square were 5 cm in diameter. The dots on each square were numbered one to four, with the first dot marked by a ring surrounding it and numbering continuing clockwise. The visual target is depicted in Figure 3.6

The use of printed black circles on white paper provided high contrast features for which the boundaries may be computed using black-white segmentation and the centres computed using the center of mass of the image segments. Further, circular features retain their centre of mass after symmetric erosion and dilation effects that may occur due to camera motion and in image processing. Printing the target ensured high precision in both the placement and size of the image features.

The use of two set of four features provided two options of feature comparison, depending on the camera trajectory used. Identifying the outer four features provided a feature set more suited to robust estimation due to the greater angular separation between features. Contrariwise, the inner set of four features allowed for a greater range of camera motion whilst keeping the image feature in view.

Lighting was provided by ceiling mounted florescent tubes providing general il-

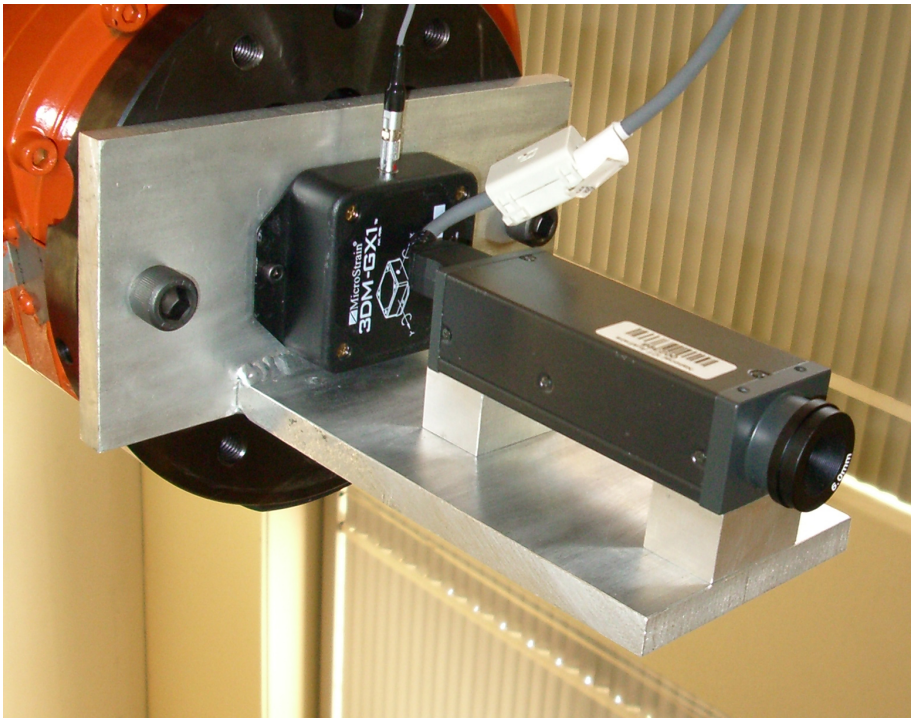

Figure 3.5: IMU and camera mount for ABB IRB 6600

lumination and two 500 W Halogen work lights directed at the visual target. This combination of lighting was found to provide good illumination of the visual target with low specularity and no shadows from equipment, including from the robotic manipulator.

The complete experiment setup, including lighting, visual target and surrounding environment is depicted in Figure 3.7.

3.5 Data Logging Software

For these experiments, data was collected from the sensors and robotic manipulator during motion, in real time. The collected data was then calibrated offline to align measurement frames and time sequences. This section describes the equipment and software used to record data during experiments.

These experiments used two discrete data collection systems to record IMU measurements, video frames and the true pose of the robot. Data from the IMU and camera was recorded on a notebook PC running Ubuntu Linux while robot pose data was

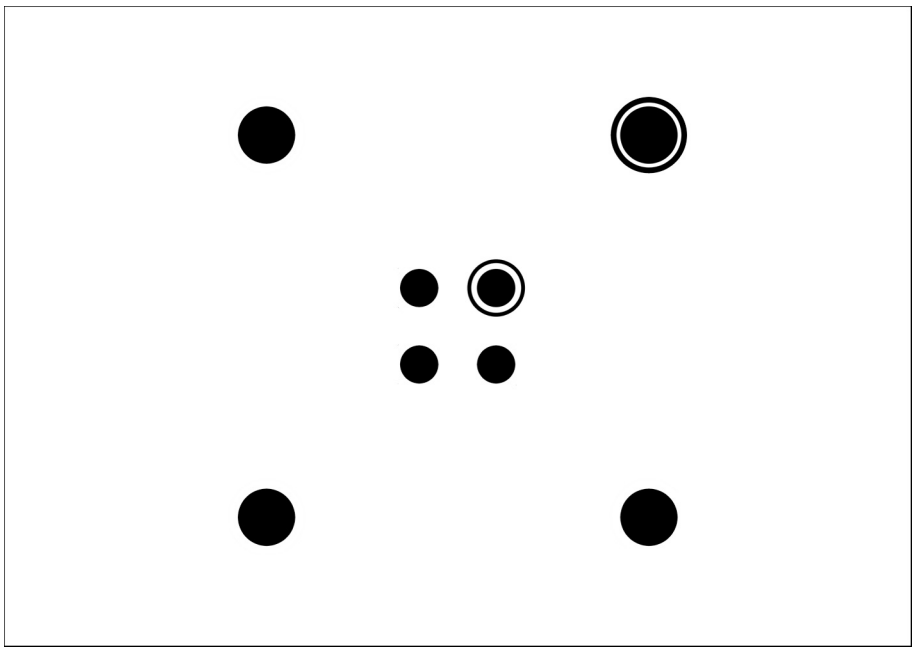

Figure 3.6: Visual feature target observed by camera. The target consists of two sets of four features, placed on the vertices of squares with side lengths 50 cm and 10 cm respectively. The first image feature in each square is marked by a double circle and numbering continues clockwise.

recorded directly on the IRC5 robot controller. Software libraries used in the data logging systems are listed in Table 3.2.

3.5.1 PC Data Logging System

The IMU and Camera data was recorded simultaneously by a single program running on notebook PC running Ubuntu Linux. The program used three concurrent threads, a control thread and one thread each for recording data from the IMU and camera. Received measurements are then recorded to disk together with a timestamp.

The data logging program makes use of several libraries to communicate with the IMU and camera. The IMU component uses the serial port control functions of the GNU C Library (glibc) to open the serial port and control the 3DM-GX1 IMU. The camera component uses libdc1394 and libraw1394 to open the FireWire communications channel and control the XCD-710CR camera. The camera component also makes use of libSDL to record camera frames as bitmap images and provide a real

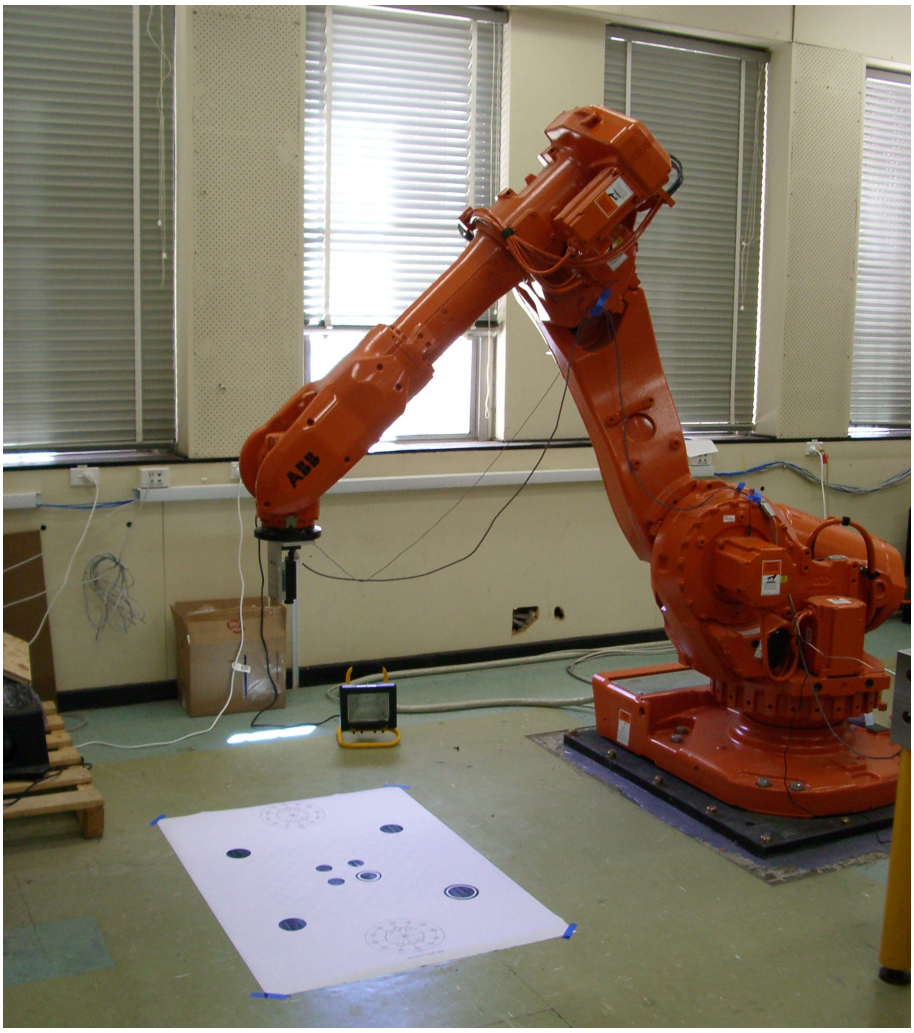

Figure 3.7: Experiment setup, including IRB 6600 with affixed camera and IMU, visual target, lighting, data capture system.

Subsystem	Library	Version
IMU	glibc nptl	2.7
Camera	libdc1394 libraw1394 libSDL glibc nptl	2.0.2 2.0.0 1.2 2.7
Robot	ABB Robotstudio ABB Robotware (with options 'Multitasking' and 'File and Serial Channel Handling')	5.10 5.10

Table 3.2: List of software libraries used by data logging system

time display of the video stream. Posix threads were used to allow capture from both sources to occur simultaneously.

3.5.2 Robot Data Logging System

A data logging system recording the true pose of the tooltip of the IRB 6600 robotic manipulator was implemented on the IRC5 controller, making use of the Robotware options of Multitasking and File and Serial Channel Handling. A second user task was created to run simultaneously with the pre-programmed motion task. The data logging task ran a RAPID program consisting of a polling loop operating at 40 Hz that retrieved the position and attitude of the end of the robot manipulator and recorded each measurement to a text file stored on the controller together with a time stamp.

3.6 Data Calibration

Recorded data was calibrated to align measurement frames and time sequences from different data logging systems. The measurement axes of the IMU, camera and robot, and the frame origins of the camera and robot were calibrated with respect to one

another for the experimental setup. Additionally, for each experiment, the time axes of the robot and IMU and camera data logging systems were calibrated with respect to one another.

This section describes the protocols used to calibrate measurements between sensors.

3.6.1 Measurement Axes and Frame Origins Calibration Protocols

The measurement axes of the IMU, camera and robot, together with the origins of the image feature and robot frames were calibrated with respect to one another to verify the experimental setup. The origin of the image feature frame was calibrated with respect to robot frame of reference using physical calibration marks on the image feature sheet. Intrinsic and extrinsic camera properties were calibrated with respect to the robot and image feature frames using the MATLAB camera calibration toolbox. The measurement axes of the accelerometers and gyroscopes of the IMU were calibrated with respect to the robot axes using a series of single axis excitation tests. Lastly, the IMU measurements were calibrated to take into account the physical offset between the IMU center and camera focal point.

The origin of the image feature frame was calibrated with respect to the robot frame of reference using calibration marks printed on the A0 sheet together with the image features. There were two calibration marks consisting of a schematic image of the robot tooltip, printed in very light grey so that they were visible to the human eye but indistinct to the vision sensor. The sheet was affixed to the ground and the robot tooltip manually moved into place against the printed calibration marks. The tooltip position at each calibration mark was recorded to an accuracy of 1 cm, due to coarseness in the robot manual control. Using the position of the two calibration marks, the transformation from an image feature frame origin, located in the center of image feature squares, to the robot frame, located at the base of the manipulator, was calculated.

Intrinsic and extrinsic camera properties were calibrated with respect to the robot and image feature frames using the MATLAB camera calibration toolbox (Bouguet 2008). The image feature sheet was replaced by another A0 print containing a checkerboard pattern, as prescribed in the documentation for the camera calibration toolbox. The location of checkerboard was calibrated with respect to the robot frame of refer-

ence using the same procedure as previously described for the image features. The camera was affixed to the robot and moved through a known path, observing the checkerboard from a variety of angles. Using the camera calibration toolbox, intrinsic camera properties, such as focal length and lens distortion, were estimated together with extrinsic camera properties, such as the camera position and attitude with respect to the checkerboard.

Internal alignment of the measurement axes of the IMU gyroscopes and accelerometers was tested by affixing the IMU to the robot and moving the robot through a series of single axis exciting paths. The IMU was affixed to the robot such that the natural orthogonal axes of the IMU housing coincided with the axes of robot tooltip. The robot then actuated along each of the x, y, z, roll, pitch and yaw axes in a sine wave of period 0.25 Hz and wavelength 40 cm or 0.4 radians. A sine wave was selected for its continuous, well defined first and second derivatives. Each axes calibration pattern was of 60 seconds, or 15 cycles, duration.

A regression line was computed from the data set corresponding to each axis, and the regression line compared with the axis of excitation. Analysis of the IMU axes calibration data indicated that the internal alignment of each sensor was within 1% of the expected axis direction. Consequently, no correction was made to the IMU data as a result of this calibration.

In the analysis of data from these experiments, I make the idealised assumption that the camera focal point and IMU center are co-located. As mentioned in Section 3.3, the mounting arrangements placed the IMU center 12 cm from the camera focal point, along a common z-axis. The effect of this displacement was to induce additional centripetal forces into the acceleration measurements of the IMU relative to the camera frame.

$$A_{\text{imu}} = A_{\text{cam}} + \Omega \times (\Omega \times P_{\text{imu}}) - \dot{\Omega} \times P_{\text{imu}} \tag{3.1}$$

where P_{imu} is the offset of the IMU from the center of rotation at the camera focal point.

These centripetal acceleration terms could be corrected for, using angular velocity and angular acceleration to obtain the acceleration at the camera focal point, represented in the body-fixed frame, however in practice it was found that they were insignificant in the trajectories used. Order of magnitude estimate for this experiment series established that the expected correction terms were several orders of magnitude smaller than the measured acceleration. Additionally, correction terms calculated us-

ing the measured angular velocity displayed high magnitude noise due to the $\Omega \times \Omega$ and $\dot{\Omega}$, calculated using a numerical derivative, terms in the correction. It was decided not to use correction for centripetal acceleration, instead using the raw acceleration measurements as if they taken at the camera focal point.

3.6.2 Time Calibration Protocol

A consequence of recording data from different sensors onto different systems was that the zero time was different for different recording systems due to unsynchronised clocks. That is, for data recorded on the notebook PC and robot controller, while each sequence has the same relative time between measurements, the time lines need to be aligned to a common starting point before they can be used.

Between recording systems, the absolute value of the clock may differ by as much as several seconds. In a networked environment, a common approach would be to synchronize the clocks of each computer system using a mechanism such as the Network Time Protocol (Burbank et al. 2008). In this case, the robot controller was not connected to other computers via a network, so a time calibration protocol was developed to inject identifiable signals into each measurement sequence via a known trajectory, against which their relative timing may be calibrated. This calibration protocol was performed at the commencement of data recording for each experiment.

The trajectory used for time calibration consisted of a sine wave in the x axis of the robot frame of reference, followed by two seconds of no motion, immediately prior to the experimental trajectory. Hence the calibration trajectory formed a prefix, appended to the start of the experimental trajectory. The sine used had a frequency of 0.25 Hz and a wavelength of 40 cm. The sine wave was selected for its well defined, continuous position, velocity and acceleration profiles. The two second pause ensures the calibration trajectory is distinct from the experiment trajectory.

From the calibration trajectory, the absolute timing of the measurement sequences was inferred. On the robot controller, the data logging task and the movement task were started simultaneously. Consequently, the first robot pose measurement was labelled as the absolute zero time point. As they were recorded by the same notebook PC system, camera and IMU measurements were mutually aligned. The were aligned to the robot time sequence by inferring the timing of the start and end of then sine wave in the calibration trajectory from the acceleration measurements.

The time point of the begining of the sine wave calibration sequence was detected

in the IMU data by smoothing the acceleration signal in the actuated direction and then searching for acceleration levels beyond a threshold. A zero-phase filter was used for the smoothing.

3.7 Data Pre-Processing

For these experiments, data was collected from the sensors and robotic manipulator during motion, in real time. The collected data was then calibrated offline to align measurement frames and time sequences. The calibrated data was pre-processed to extract image features, discard outlier measurements and perform data format conversion.

This section describes additional pre-processing of measurements, converting data from raw sensor values into quantities used by the observers described later in this thesis. Data was read from log files into MATLAB data structures. Robot pose measurements were converted from quaternion orientation and vector positions measurements into homogeneous transforms. Image features were labelled and extracted from camera measurements, and from feature sets the camera pose was estimated. IMU measurements were pre-filtered to discard extreme values indicative of erroneous data packets.

3.7.1 Robot Data Pre-Processing

Pose data logged from the robot controller was stored as a quaternion giving the tooltip orientation, and a three-vector giving the tooltip position. The raw data for each measurement was read into MATLAB and converted into a homogeneous transform 4×4 matrix.

3.7.2 IMU Data Pre-Processing

IMU data was pre-processed by reading it into a MATLAB data structure and filtering it to remove erroneous measurements and correct for scale and time-constant bias errors in the gyrometer measurements. Raw data from the IMU was contained in packets consisting of an accelerometer, a gyroscope and a magnetometer measurement, each a three-vector.

3.7.2.1 Erroneous Measurement Removal

Erroneous measurement were detected by calculating the norm of the vectorial measurement on each signal and rejecting those above a threshold. Causes of erroneous packets can include electrical faults and interference in the serial channel and vibration in the IMU mounting.

The three inertial data signals, the accelerometer, gyrometer and magnetomers were tested and based on a fault in any signal, the entire packet containing that measurement was discarded. Figures 3.8, 3.9 and 3.10 depict the raw acceleration measurements, a histogram of the acceleration measurement norms and final measurment sequence after discarded erroneous packets. Similar patterns are observered in the gyrometer and magnetomer measurement channels.

3.7.2.2 Gyrometer Scale and Constant-Bias Correction

Initial comparision of the Gyrometer measurements to theoretically predicted measurements indicated the presence of large scale error in the measurements, together with noticable constant biases. It was decided to correct the scale error in pre-processing and, as the process of scale correction required bias estimation, correct for large time-constant biases.

A windowed portion of the the actual and expected gyrometer measurements were low pass filtered and estimates of the scale factor and constant bias calculated using a least squares estiamte. Modeling the actual measurement process as $y_k = ax_k + b$, where y_k is the actual measurement, x_k is the expected measurement, a is a constant scale factor and b is constant bias, define $\hat{y}_k = \hat{a}x_k + \hat{b}$ were the hatted symbols are estimates of their unadored kin. These equations may be represented vectorially as

$$Y = XA \quad \text{where} \quad A = \begin{pmatrix} a \\ b \end{pmatrix}, \quad X = \begin{pmatrix} x_1 & 1 \\ \vdots & \vdots \\ x_n & 1 \end{pmatrix}, \quad Y = \begin{pmatrix} y_1 \\ \vdots \\ y_n \end{pmatrix} \tag{3.2}$$

and analogously $\hat{Y} = X\hat{A}$. Define the cost function $\phi = \sum_1^n (\hat{y}_k - y_k)^2 = (\hat{Y} - Y)^\top (\hat{Y} - Y)$. Setting $\frac{\mathbf{d}\phi}{\mathbf{d}\hat{A}} = 0$, one has $\hat{A} = (X^\top X)^{-1} X^\top Y$.

Using this estimate, of the scale factor and bias, the gyrometer measurements were corrected as part of the offline pre-processing. Output of this process is depicted in Figure 3.11. Note that this corrects for a time-constant estimate of the bias in the

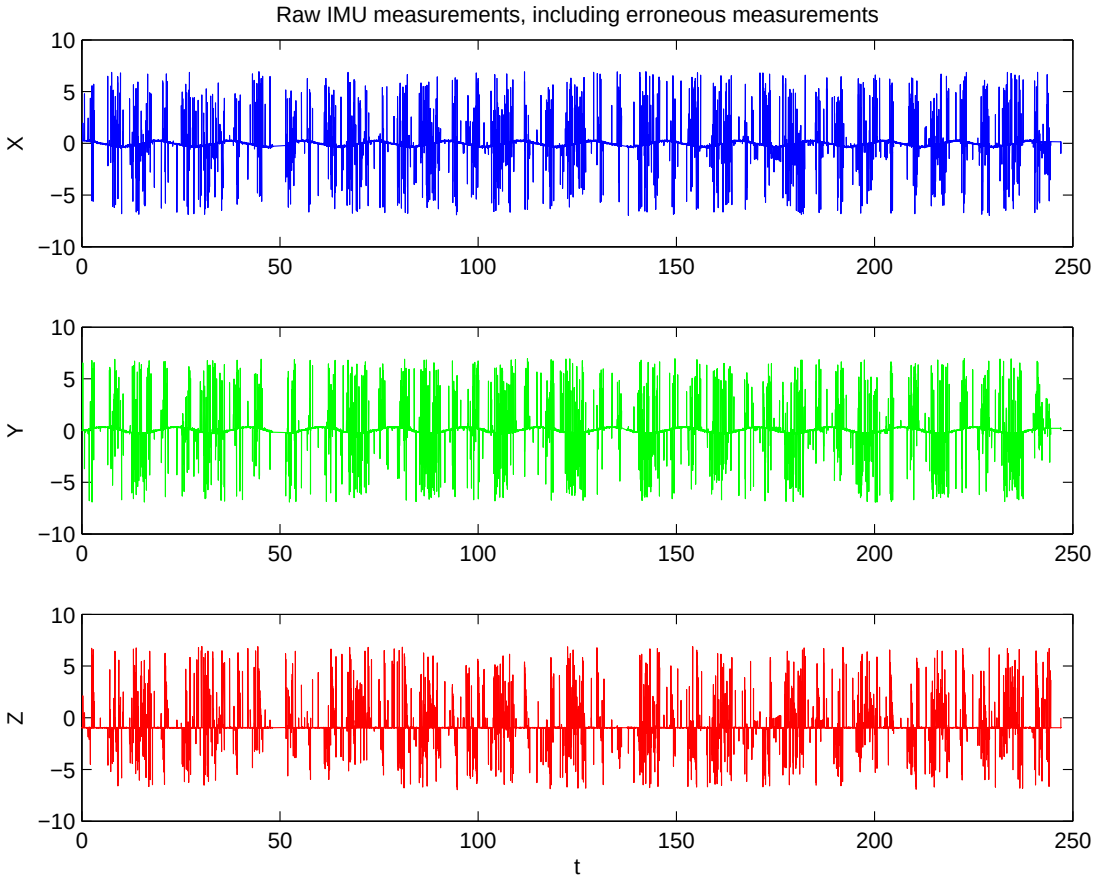

Figure 3.8: Raw acceleration measurements as received from IMU. Note the apparent superposition of high magnitude noise on the underlying signal with low magnitude gaussian noise. Similar patterns are observered in gyrometer and magnetometer signal channels.

gyrometer signal, but leaves a residual time-varying bias component which must be estimated online.

3.7.3 Camera Data Pre-Processing

Camera image data was pre-processed to identify, label and extract image features and calculate a pose estimate for the camera at each frame.

Image features were labelled, their coordinates extracted and correspondences between images specified using an assisted manual image feature identification program in the MATLAB environment. For the fist image in a sequence, the user was prompted to click on four image features, at the vertices of the squares described in Section 3.4,

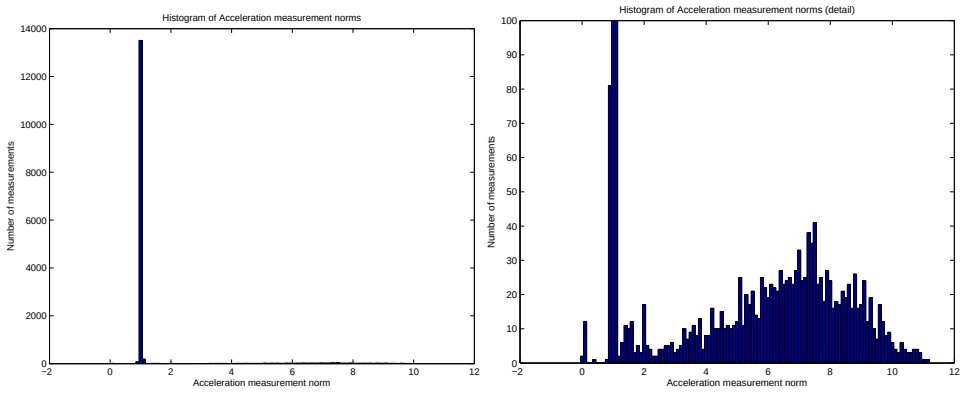

Figure 3.9: Histogram of norm of acceleration measurement vectors in raw IMU measurements.

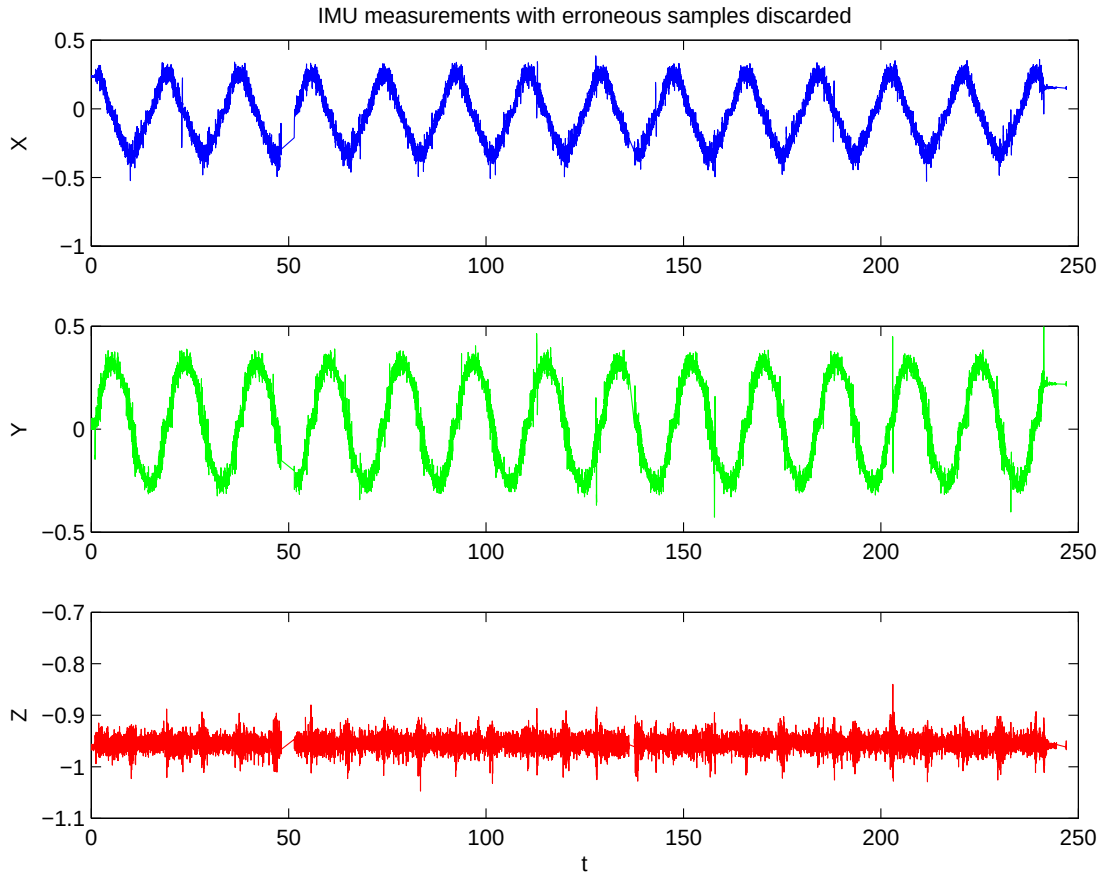

Figure 3.10: Acceleration measurements after discarding erroneous measurements

in order from 1 to 4. The image was thresholded to obtain a black and white im-

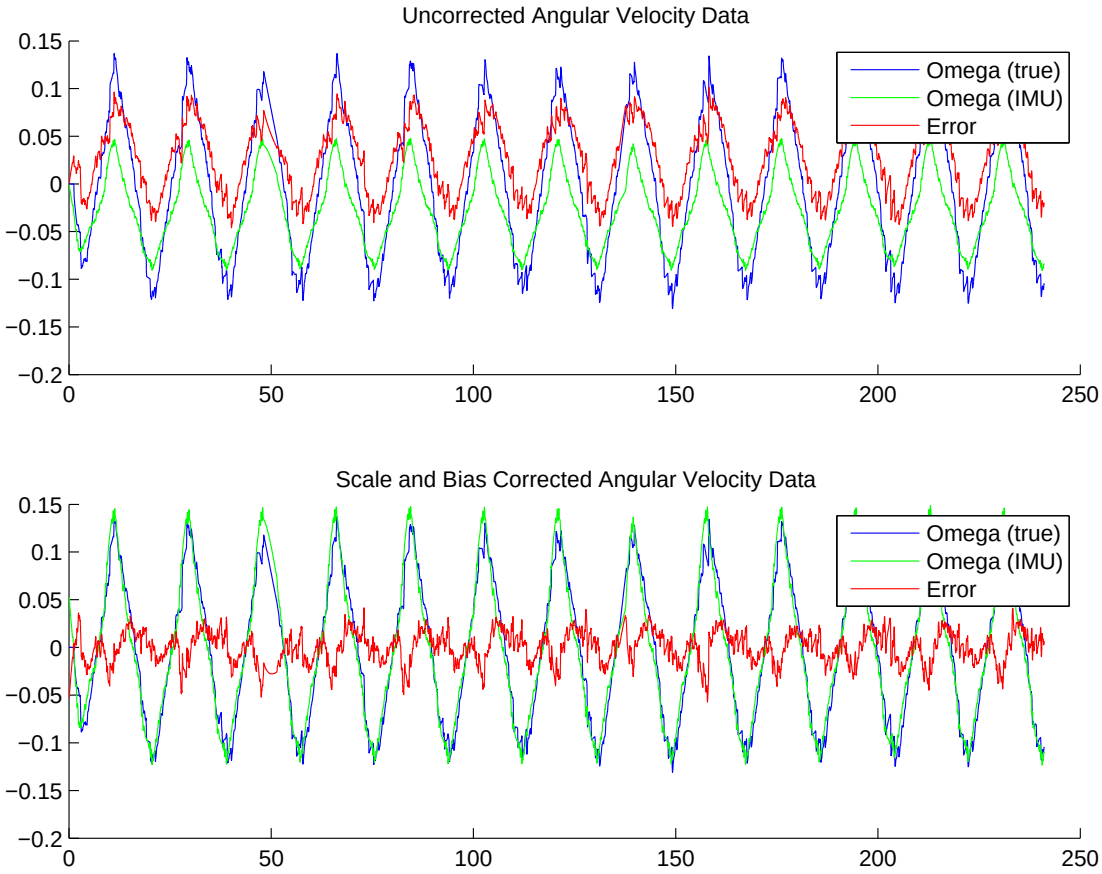

Figure 3.11: Uncorrected and Corrected low-pass filtered gyrometer measurements.

age and image feature edges smoothed using dilation and erosion, then the image was segmented. From the coordinates of the mouse clicks, black/white segment numbers for each image feature were identified. Final image coordinates for each image feature were determined by calculating the center of mass of their segment. Following a successfully labelled image, an attempt was made to process the next image automatically, taking the image coordinates of the image features in the last frame as the mouse click locations. If tracking was lost, indicated by multiple features having the same black/white segment or the wrong colour segment, processing was reinitialised using the frame on which tracking was lost as the first frame in the sequence, prompting the user to manually identify image features again.

This simple identification and tracking scheme proved robust at tracking the image features and excellent at detecting lost tracking for the experiments trajectories used; in particular for moderate camera movement between frames. It seldom produced false tracking positives, for example where image features tracks switched to

non-corresponding black/white segments. This is partially due to the design of the visual target, in Figure 3.6, where each feature is spatially distinct from its neighbours, and lighting conditions to avoid shadows. In the rare case of false tracking positives, tracking was manually reinitialised.

The image feature coordinates extracted from this process were two dimension coordinates in the image plane. From these, image feature coordinates on the unit sphere were calculated using the intrinsic camera parameters estimated in Section 3.6.1. Camera pose was estimated for each frame from its set of image features using the `compute_extrinsic` function of the MATLAB camera calibration toolbox (Bouguet 2008).

3.8 Chapter Summary

In this chapter a system and protocols for collection of experimental data from an inertial vision system, augmented with ground-truth reference measurements was presented.

For these experiments, data was collected from the sensors and robotic manipulator during motion, in real time. The collected data was then calibrated offline to align measurement frames and time sequences. The calibrated data was pre-processed to extract image features, discard erroneous measurements and perform data format conversion. The observers described later in this thesis were run offline on the data and compared to the measured ground truth data.

The contribution of this chapter has been the production of a series of data sets for inertial and visual sensor data together with ground-truth pose measurements.

The raw and pre-processed data sets from this experiment series are included on a DVD attachement to this thesis. Descriptions of the contents of the DVD, including data formats and experimentals paths are contained in Appendix A.

Chapter 4

Pose Observer Design on $\mathrm{SE}(3)$ by decomposition into Rotation and Translation

This chapter describes two approaches to designing a non-linear pose observer on the the special Euclidean group $\mathrm{SE}(3)$ of dimension four by exploiting the underlying $\mathrm{SO}(3) \times \mathbb{R}^3$ semi-direct product structure of the special Euclidean group $\mathrm{SE}(3)$ of dimension four to form observers for the attitude and position components separately. Two approaches are considered, each offering different insights into the problem.

The first approach considered is to pose separate cost functions on the attitude and position components of the state space and design two observers connected via a cascade of the attitude estimate into the position observer. The composite observer estimates pose and linear velocity together with gyrometer and accelerometer biases from vision measurements and inertial measurements of angular velocity and linear acceleration. In both the constituent attitude and position observer, the error is almost-globally asymptotically and locally exponentially convergent. The combined system is locally exponentially stable, exhibits a large basin of attraction and it is a straightforward process to tune the gains.

The second approach proposes a cost function directly on $\mathrm{SE}(3)$ and designs a single observer for simultaneous attitude and position estimation. A decomposition of the cost function in attitude and position components is identified and used to design observers for the rotational and translational components independently, yet maintains a structure admitting a Lyapunov stability argument on $\mathrm{SE}(3)$.

A series of observer are proposed using this second approach, with two principle observers arising from the same method applied to different error terms. Firstly, the

classical error arising the coordinate frame transformation between frame is investigated. Subsequent investigation involves an error term identified as invariant in the inertial frame. Crucially, the observers designed using the second error term offer significantly reduced coupling between measurements, including an elimination of vision measurements from feed-forward update terms, admitting a true multi-rate implementation of the observer.

The observers proposed using the second approach are posed on SE(3) from vision measurements and inertial measurements of angular and linear velocity. The observer proposed using this method maintain almost-global asymptotic and locally exponentially convergence, large basins of attraction and the straightforward tuning process.

Simulation and experimental results are given for both observers. Experimental results have been obtained using a 3DMG Inertial Measurement Unit (IMU) and a Philips webcam mounted on a small scale Vario Benzin-Acrobatic 23cc Helicopter.

The contributions of this chapter are

- An observer for pose, linear velocity and gyrometer and accelerometer biases from vision and inertial measurements.

- An observer for pose from vision and velocity measurement with Lyapunov stability argument based on a cost function on SE(3).

- Identification of an expression of the pose error in the inertial frame that eliminates coupling of error to motion of the body-fixed frame.

- An observer for pose from vision and velocity measurement with Lyapunov stability argument based on a cost function on SE(3) using this invariant error term, resulting in reduced measurement noise coupling.

- A practical adjustment to the previous observer to further reduce measurement noise coupling yet maintain exponential convergence properties.

Some material presented in Section 4.2 was originally presented in Cheviron et al. (2007). Some material from Sections 4.3, 4.4 and 4.5 was originally presented in Baldwin et al. (2007).

4.1 Problem Formulation and Measurement Model

4.1.1 Problem Formulation

Let $\mathcal{A}$ denote an inertial frame attached to the earth such that e_3 points vertically down. Let $\mathcal{B}$ denote a body-fixed frame attached to a vehicle of interest at the centre of mass. The origin of $\mathcal{B}$ expressed in $\mathcal{A}$ is given by the vector p, and that attitude of $\mathcal{B}$ expressed in $\mathcal{A}$ is given by the rotation matrix R.

I will use the convention that positions and vectors expressed in the inertial frame are denoted by lower case letters while quantities expressed in other frames are denoted by upper case letters. Thus, the position of the vehicle in the inertial frame is denote $p \in \mathcal{A}$ and $P \in \mathcal{B}$ is the position of the origin of the inertial frame in the body fixed frame.

The kinematics of $\mathcal{B}$ are given by

$$\dot{R} = R\Omega_\times, \tag{4.1a}$$

$$\dot{p} = v, \tag{4.1b}$$

where Ω is the angular velocity of $\mathcal{B}$ expressed in $\mathcal{B}$ and v is the linear velocity of $\mathcal{B}$ expressed in $\mathcal{A}$.$(\cdot)_\times$ is an operator taking a vector $\Omega \in \mathbb{R}^3$ to a skew-symmetric matrix

$$\Omega_\times = \begin{pmatrix} 0 & -\Omega_3 & \Omega_2 \\ \Omega_3 & 0 & -\Omega_1 \\ -\Omega_2 & \Omega_1 & 0 \end{pmatrix}. \tag{4.2}$$

The inverse of $(\cdot)_\times$ is given by the vex$(\cdot)$ operator, taking a skew-symmetric matrix to a vector $\in \mathbb{R}^3$.

The kinematics of linear velocity are given by

$$\dot{v} = a + ge_3, \tag{4.3}$$

where a is the net linear acceleration from sources other than gravity.

The pose of the body-fixed frame, (R, p), comprises both the attitude and position of $\mathcal{B}$ relative to $\mathcal{A}$. The pose can be interpreted as an element of SE(3), with the matrix representation

$$T = \begin{pmatrix} R & p \\ 0 & 1 \end{pmatrix} \in \mathbb{R}^{4\times 4}. \tag{4.4}$$

This format, commonly known as homogeneous coordinates identifies SE(3) as a subgroup of the general linear group GL(4) of dimension four with the group operation of concatenation of transforms identified with matrix multiplication.

The coordinates T of $\mathcal{B}$ relative to $\mathcal{A}$ may be interpreted as a coordinate transformation , $T : \mathcal{B} \to \mathcal{A}$

$$\begin{pmatrix} x \\ 1 \end{pmatrix} \mapsto T \begin{pmatrix} x \\ 1 \end{pmatrix} = \begin{pmatrix} Rx + p \\ 1 \end{pmatrix} \tag{4.5}$$

The kinematics of $T \in \mathrm{SE}(3)$ are

$$\dot{T} = T\Xi \tag{4.6}$$

where

$$\Xi = \begin{pmatrix} \Omega_\times & V \\ 0 & 0 \end{pmatrix} \in \mathfrak{se}(3). \tag{4.7}$$

and V is the linear velocity of the origin of $\mathcal{B}$ expressed in $\mathcal{B}$. That is,

$$V = R^\top v. \tag{4.8}$$

It is easily verified that equation (6.4) is a matrix representation of the kinematics equation (5.2).

The velocity Ξ is an element of the Lie Algebra $\mathfrak{se}(3)$ over SE(3) where $\mathfrak{se}(3)$ is identified with the subset of 4×4 matrices with an upper left skew-symmetric 3×3 block and bottom row zero. The correspondence of body-fixed frame velocities (Ω, V) to an element $\Xi \in \mathfrak{se}(3)$ is denoted by a wedge superscript

$$\Xi = (\Omega, V)^\wedge \tag{4.9}$$

Consider (Ω, V) as a single six-dimensional vector giving the system velocity of $\mathcal{B}$. We can then view $(\cdot,\cdot)^\wedge$ as an operator mapping between the $\mathbb{R}^6$ and $\mathfrak{se}(3)$ interpretations of the velocity of $\mathcal{B}$. Note that velocity vectors in $\mathfrak{se}(3)$ are associated with a frame of reference in which they are expressed. Thus, Ξ in equation (4.9) gives the velocity of the body-fixed frame $\mathcal{B}$ expressed in $\mathcal{B}$, as both Ω and V are expressed in $\mathcal{B}$.

As T gives the pose of $\mathcal{B}$ expressed in $\mathcal{A}$, T^{-1} gives the pose of $\mathcal{A}$ expressed in $\mathcal{B}$,

$$T^{-1} = \begin{pmatrix} R^\top & -R^\top p \\ 0 & 1 \end{pmatrix} = \begin{pmatrix} R^\top & P \\ 0 & 1 \end{pmatrix}. \tag{4.10}$$

where $P = -R^\top p$ is the position of the origin of $\mathcal{A}$ represented in $\mathcal{B}$. Note that P is a complementary quantity to p, equal in magnitude but being a vector in the opposite

direction, as opposed to being the same quantity represented in another frame, as is the case with v and V. The kinematics of T^{-1} are given by

$$\dot{T}^{-1} = -\Xi T^{-1} = -T^{-1}\,\mathrm{Ad}_T\,\Xi, \tag{4.11}$$

where $\mathrm{Ad}_T : \mathfrak{se}(3) \to \mathfrak{se}(3)$ is the Adjoint operator,

$$\mathrm{Ad}_T\,\Xi = T\Xi T^{-1}. \tag{4.12}$$

The adjoint by T, Ad_T, applied to Ξ maps the velocity of $\mathcal{B}$ relative to $\mathcal{A}$ expressed in $\mathcal{B}$ to the negative of the velocity of $\mathcal{A}$ relative to $\mathcal{B}$ expressed in $\mathcal{A}$. The rotational and linear velocities of $\mathcal{A}$ relative to $\mathcal{B}$ are then given by

$$\dot{R}^\top = -R^\top(R\Omega)_\times, \tag{4.13a}$$

$$\dot{P} = -V - \Omega_\times P. \tag{4.13b}$$

and the rate of change of velocity is given by

$$\dot{V} = A + gR^\top e_3 - \Omega_\times V, \tag{4.14}$$

where $A = R^\top a$. Note that the body-fixed fame expressions of linear velocity and acceleration are coupled to angular velocity.

Finally, I present some definitions that will be required in the sequel. Define an inner product and associated norm on the set of $\mathbb{R}^{n\times n}$ matrices.

$$\langle M, N\rangle := \frac{1}{2}\mathrm{tr}(M^\top N) \tag{4.15}$$

and

$$\|M\|_F^2 := \langle M, M\rangle = \frac{1}{2}\mathrm{tr}(M^\top M) \tag{4.16}$$

where $\|(\cdot)\|_F$ is the Frobenius norm.

Let $\mathbb{P}_a$ and $\mathbb{P}_s$ be projection operators decomposing a matrix $M \in \mathbb{R}^{n\times n}$ into an skew-symmetric component $\mathbb{P}_a(M)$ and a symmetric component $\mathbb{P}_s(M)$, given by

$$\mathbb{P}_a(M) = \frac{1}{2}(M - M^\top), \tag{4.17a}$$

$$\mathbb{P}_s(M) = \frac{1}{2}(M + M^\top). \tag{4.17b}$$

Further,

$$M = \mathbb{P}_a(M) + \mathbb{P}_s(M). \tag{4.18}$$

For any rotation matrix, one may obtain the angle-axis coordinates (θ, x) (e.g. Murray et al. 1993)

$$R = \exp(\theta\gamma_\times) = I + \sin(\theta)\gamma_\times + (1-\cos(\theta))\gamma_\times^2 \tag{4.19a}$$

$$\cos(\theta) = \frac{1}{2}(\mathrm{tr}(R) - 1) \tag{4.19b}$$

$$\gamma_\times = \frac{1}{\sin(\theta)}\mathbb{P}_a(R) \tag{4.19c}$$

where exp is the matrix exponential. Note that this gives and explicit form for the matrix exponential on the set of skew-symmetric matrices.

4.1.2 Measurement Model

We consider the vehicle of interest equipped with an inertial-vision sensor package; an IMU and a monocular camera, each affixed to the craft and taking measurements in the body-fixed frame.

The IMU operates at a high sampling frequency, taking measurements corrupted by low frequency noise in the form of measurement biases. Conversely, the camera takes measurements at a low sampling frequency, up to two orders of magnitude lower than the IMU, but the camera measurements are free of bias and hence stable at low frequencies. That is, the IMU provides high frequency measurements corrupted by low frequency noise and the camera provides low frequency measurements corrupted by high frequency noise. These complementary measurement characteristics suggest an approach similar to the linear system technique of complementary filtering, as discussed in Section 2.2.2.

The IMU provides measurements of angular velocity, Ω, and linear acceleration, A, in the body fixed frame, $\mathcal{B}$. In the observer considered in Section 4.2 it is a straightforward exercise to incorporate estimates of the slowly time varying IMU biases, b_Ω and b_A. Due to the coupling present in the observers in Section 4.3 this is no longer straightforward and in this Section I will consider bias free IMU measurements. In all cases, the IMU measurements are considered to be corrupted by zero-mean Gaussian noise processes n_Ω and n_A respectively.

Linear velocity, though not measured directly, can be estimated from linear acceleration and pose measurements as discussed in Section 2.2.3. For the observers presented in the latter part of this chapter, we will consider linear velocity as an inertial measurement corrupted by the zero-mean Gaussian noise process n_V and no bias.

Using the camera, we observe a constellation of landmarks whose position in the inertial frame is known. From each frame, the camera pose can be reconstructed from on the image coordinates of the observed landmarks. This is a well established result from Computer Vision known as the perspective-n-point problem. Section 3.7.3 describes the process used for calculating the pose for each frame in a video sequence. Using this process, we consider the camera as providing measurements of the camera pose, T^{-1}, expressed in the body-fixed frame. Equivalently, the measurement can be treated as being of T by matrix inverse. In this chapter, we make use of the components of T^{-1} as measurements of R, P. As discussed in Section 2.2.2, alternate sensors, such as Global Positioning System (GPS), may be substituted for a vision sensor under appropriate conditions.

The measurement model used is

$$R_y = \exp(n_R(t)_\times)R \tag{4.20a}$$

$$P_y = P + n_P(t) \tag{4.20b}$$

$$\Omega_y = \Omega + n_\Omega(t) + b_\Omega \tag{4.20c}$$

$$V_y = V + n_V(t) \tag{4.20d}$$

$$A_y = A + n_A(t) + b_A - gRe_3 \tag{4.20e}$$

where $n_{(\cdot)}(t)$ denotes a zero mean Gaussian noise process, $b_{(\cdot)}$ denotes a constant bias term, g is the magnitude of the gravity vector and e_3 is the basis vector pointing vertically down.

To provide context for the following theoretical developments, it is worth noting that commercial grade IMUs, such as the 3DM-GX1, supply inertial measurements at rates of up to 300 Hz. Further, with low frame rates and the additional overhead of calculating pose estimates, vision sensors provide measurements at rates of around 5 to 10 Hz.

4.2 Cascaded Pose Observer

In this section two non-linear observers are proposed which together form a pose observer via a cascade design. The first observer estimates the attitude and angular velocity measurement biases. The second observer estimates position, linear velocity and linear acceleration biases. Combined convergence is proven using adaptive control and back stepping analysis.

Define the error terms

$$\bar{R} = R^\top \hat{R}, \tag{4.21a}$$
$$P^\Delta = \hat{P} - P, \tag{4.21b}$$
$$V^\Delta = \hat{V} - V, \tag{4.21c}$$
$$\tilde{b}_\Omega = \hat{b}_\Omega - b_\Omega, \tag{4.21d}$$
$$\tilde{b}_A = \hat{b}_A - b_A. \tag{4.21e}$$

One has that $\bar{R}$ gives the orientation of the estimate relative to the body fixed frame and P^Δ gives the difference between the estimated and true locations of the origin of the inertial frame relative the vehicle. V^Δ give the difference between the estimated and true linear velocity relative to the estimated and true attitude, respectively. $\tilde{b}_\Omega$ and $\tilde{b}_A$ give the differences between the estimated and true biases on the gyroscopes and accelerometers, respectively.

4.2.1 Cascaded Pose Attitude Observer

In this section, a non-linear attitude observer is proposed for estimation of attitude and gyroscope bias using visual and gyroscope measurements.

Theorem 4.2.1 (Attitude and Gyroscope Bias Observer)**.** *Consider the system equation (6.2a) and* $\dot{b}_\Omega = 0$ *together with a bounded continuous driving term* Ω*. Let* $\Omega_y = \Omega + b_\Omega$ *be a noise-free, biased measurement of* Ω *and* $R_y^\top = R^\top$ *be a noise-free, unbiased measurement of* $R^\top$*.*

Define the observer

$$\dot{\hat{R}} = \hat{R}(\Omega_y - \hat{b}_\Omega + k_{P_\Omega}\xi_\Omega)_\times, \tag{4.22a}$$
$$\dot{\hat{b}}_\Omega = -k_{I_\Omega}\beta_\Omega, \tag{4.22b}$$
$$\xi_\Omega = -\operatorname{vex}(\mathbb{P}_a(\bar{R})), \tag{4.22c}$$
$$\beta_\Omega = -\operatorname{vex}(\mathbb{P}_a(\bar{R})), \tag{4.22d}$$

and recall the errors $\bar{R}$ *and* $\tilde{b}_\Omega$ *from equation (4.21a) and equation (4.21d) respectively.*

Then, for initial conditions

$$(\bar{R}(0), \tilde{b}_\Omega(0)) \notin \{(\bar{R}, \tilde{b}_\Omega) | \operatorname{tr}(\bar{R}) > -1 \text{ and } \tilde{b}_\Omega = 0\} \tag{4.23}$$

and choice of gains $k_{I_\Omega} > 0$ *and* $k_{P_\Omega} > 0$*, the error coordinates* $(\bar{R}, \tilde{b}_\Omega)$ *are almost-globally asymptotically and locally exponentially stable about* $(I, 0)$

Proof of Theorem 4.2.1. Recall the definition of $\bar{R}$ and $\tilde{b}_\Omega$ from equation (4.21a) and equation (4.21d). Setting $\Omega_y = \Omega + b_\Omega$, the error kinematics are

$$\dot{\bar{R}} = [\bar{R}, \Omega_\times] + \bar{R}(-\tilde{b}_\Omega + k_{P_\Omega}\xi_\Omega)_\times, \tag{4.24a}$$

$$\dot{\tilde{b}}_\Omega = -k_{I_\Omega}\beta_\Omega. \tag{4.24b}$$

Define the candidate Lyapunov function $\mathcal{V}$

$$\mathcal{V} = \frac{1}{2}\|I - \bar{R}\|^2 + \frac{1}{k_{I_\Omega}}\|\tilde{b}_\Omega\|^2. \tag{4.25}$$

Taking the time derivative of $\mathcal{V}$, one has

$$\begin{aligned}\dot{\mathcal{V}} &= -\left\langle I - \bar{R}, [\bar{R}, \Omega_\times] + \bar{R}(-\tilde{b}_\Omega + k_{P_\Omega}\xi_\Omega)_\times \right\rangle - 2\tilde{b}_\Omega^\top \beta_\Omega \\ &= -\left\langle \bar{R}^\top - I, (-\tilde{b}_\Omega + k_{P_\Omega}\xi_\Omega)_\times \right\rangle - \left\langle \tilde{b}_{\Omega_\times}, \beta_{\Omega_\times} \right\rangle\end{aligned} \tag{4.26}$$

using the fact that the trace of the matrix commutator is zero and the identity $2x^\top y = \mathrm{tr}(x_\times^\top y_\times) = \langle x_\times, y_\times \rangle$. Further, note that the matrix inner product with a skew-symmetric matrix in one entry acts only on the skew-symmetric portion of the matrix in the other entry. That is $\langle a_\times, M \rangle = \langle a_\times, \mathbb{P}_a(M) \rangle$. Hence

$$\begin{aligned}\dot{\mathcal{V}} &= -\left\langle \mathbb{P}_a(\bar{R})^\top, -\tilde{b}_{\Omega_\times} + k_{P_\Omega}\xi_{\Omega_\times} \right\rangle - \left\langle \tilde{b}_{\Omega_\times}, \beta_{\Omega_\times} \right\rangle, \\ &= k_{P_\Omega}\left\langle \mathbb{P}_a(\bar{R}), \xi_{\Omega_\times} \right\rangle - \left\langle \tilde{b}_{\Omega_\times}, \mathbb{P}_a(\bar{R}) + \beta_{\Omega_\times} \right\rangle.\end{aligned} \tag{4.27}$$

Substituting equation (4.22c) and equation (4.22d). Then equation (4.27) becomes

$$\begin{aligned}\dot{\mathcal{V}} &= k_{P_\Omega}\left\langle \mathbb{P}_a(\bar{R}), -\mathbb{P}_a(\bar{R}) \right\rangle - \left\langle \tilde{b}_{\Omega_\times}, \mathbb{P}_a(\bar{R}) - \mathbb{P}_a(\bar{R}) \right\rangle, \\ &= -k_{P_\Omega}\left\|\mathbb{P}_a(\bar{R})\right\|^2\end{aligned} \tag{4.28}$$

Applying Theorem 8.4 of (Khalil 2002), an application of Barbalat's Lemma, $\mathcal{V}$ is asymptotically convergent to an invariant set.

From the error dynamics, equation (4.24), the invariant sets of the error system are characterised by $(\mathbb{P}_a(\bar{R}) = 0, \tilde{b}_\Omega = 0)$. This yields two unconnected invariant sets: $S_1 = \{(\bar{R}, \tilde{b}_\Omega) | R = I, \tilde{b}_\Omega = 0\}$ and $S_2 = \{(\bar{R}, \tilde{b}_\Omega) | \mathrm{tr}(R) = -1, \tilde{b}_\Omega = 0\}$.

The set S_2 is an unstable set, as any open ball centred on $(\bar{R}_S, \tilde{b}_{\Omega_S}) \in S_2$ contains points $(\bar{R}, \tilde{b}_\Omega)$ such that $\mathcal{V}(\bar{R}, \tilde{b}_\Omega) < \mathcal{V}(\bar{R}_S, \tilde{b}_{\Omega_S})$. By monotonicity of $\mathcal{V}$, these points diverge from S_2 and must converge to S_1.

Hence, for almost all initial condition $(\bar{R}, \tilde{b}_\Omega) \notin S_2$, the error is asymptotically convergent to $(I, 0)$.

To prove local exponential convergence, consider a linearisation of the system about $(I,0)$. Let

$$\bar{R} = I + x_\times \tag{4.29a}$$
$$\tilde{b}_\Omega = -y \tag{4.29b}$$

where $x, y \in \mathbb{R}^3$. The kinematics of the linearisation are given by

$$\begin{aligned} \dot{x} &= [x_\times, \Omega_\times] + y_\times - k_{P_\Omega} x_\times, \\ &= -(k_{P_\Omega} I + \Omega_\times) x_\times + y_\times, \end{aligned} \tag{4.30a}$$
$$\dot{y} = -k_{I_\Omega} x_\times. \tag{4.30b}$$

Let $|\Omega_{\mathtt{max}}|$ denote the magnitude bound on Ω and choose

$$\begin{array}{rcl} & \alpha_2 & > 0 \\ & \alpha_1 & > \frac{\alpha_2(|\Omega_{\mathtt{max}}|^2 + k_{I_\Omega})}{k_{P_\Omega}} \\ \frac{\alpha_1 + k_{P_\Omega}\alpha_2}{k_{I_\Omega}} < & \alpha_3 & < \frac{\alpha_1 + k_{P_\Omega}\alpha_2}{k_{I_\Omega}} + \frac{|\Omega_{\mathtt{max}}|\alpha_2}{k_{I_\Omega}} \end{array} \tag{4.31}$$

Set M, N to be

$$M = \begin{pmatrix} \alpha_1 I & -\alpha_2 I \\ -\alpha_2 I & \alpha_3 \end{pmatrix}, \tag{4.32a}$$
$$N = \begin{pmatrix} \alpha_1 k_{P_\Omega} - \alpha_2 k_{I_\Omega} & -\alpha_2 |\Omega_{\mathtt{max}}| \\ -\alpha_2 |\Omega_{\mathtt{max}}| & \alpha_2 \end{pmatrix}. \tag{4.32b}$$

It is straightforward to verify that M and N are positive definite matrices. Further, consider the cost function $\mathcal{W} = \frac{1}{2} X^\top M X$, where $X = (x,y)^\top$. It is straightforward to verify

$$\frac{\mathbf{d}}{\mathbf{d}t}(X^\top M X) \leq -2 \begin{pmatrix} |x| & |y| \end{pmatrix} N \begin{pmatrix} |x| \\ |y| \end{pmatrix} \tag{4.33}$$

Hence the linearisation (x,y) is exponentially stable about $(0,0)$. Hence $(\bar{R}, \tilde{b}_\Omega)$ is locally exponentially stable about $(I,0)$. □

Remark 4.2.2. This theorem and its proof are derivatives of Theorem 4.2 in Mahony et al. (2008). This theorem is given as Proposition 4.2.3

Proposition 4.2.3 (Passive complementary filter with bias correction)**.** *Consider the rotation kinematics $\dot{R} = R\Omega_\times$ for a time-varying $R(t) \in \mathrm{SO}(3)$ and with measurements given by $R_y \approx R$, $\Omega_y \approx \Omega + b$. Let $(\hat{R}(t), \hat{b}(t))$ denote the solution of*

$$\dot{\hat{R}} = \hat{R}(\Omega_y - \hat{b} + k_P\omega)_\times, \qquad \hat{R}(0) = \hat{R}_0, \tag{4.34a}$$

$$\dot{\hat{b}} = -k_I\omega, \qquad \hat{b}(0) = \hat{b}_0 \tag{4.34b}$$

$$\omega = \mathrm{vex}(\mathbb{P}_a(\bar{R})), \qquad \bar{R} = \hat{R}^\top R_y. \tag{4.34c}$$

Define error variables $\bar{R} = \hat{R}^\top R$ and $\tilde{b} = b - \hat{b}$. Assume that $\Omega(t)$ is a bounded, absolutely continuous signal and that the pair of signals $(\Omega(t), \bar{R})$ are asymptotically independent. Define $\mathbb{U}_0 \in \mathrm{SO}(3) \times \mathbb{R}^3$ by

$$\mathbb{U}_0 = \left\{(\bar{R}, \tilde{b}) | \, \mathrm{tr}(\bar{R}) = -1, \tilde{b} = 0\right\} \tag{4.35}$$

Then:

i The set $\mathbb{U}_0$ is forward invariant and unstable with respect to the dynamic system equation (4.34).

ii The error $(\bar{R}(t), \tilde{b}(t))$ is locally exponentially stable to $(I, 0)$.

iii For almost all initial conditions $(\bar{R}_0, \tilde{b}_0) \notin \mathbb{U}_0$ the trajectory $(\hat{R}(t), \hat{b}(t))$ converges to the trajectory $(R(t), b)$

Remark 4.2.4. Note that for a system evolving on the special orthogonal group $\mathrm{SO}(3)$ of dimension four, global asymptotic stability is impossible due to topological constraints. The anti-podal equilibrium set $\{\bar{R} | \, \mathrm{tr}(\bar{R}) = -1\}$ are a consequence of the fact that the domain of attraction of a asymptotically stable equilibrium is homeomorphic to a Euclidean vector space (Bhatia and Szeg o 1970), while $\mathrm{SO}(3)$ is only locally diffeomorphic to $\mathbb{R}^3$. Consequently no system on $\mathrm{SO}(3)$ has an equilibrium that is globally asymptotically stable (Bhat and Bernstein 2000).

4.2.2 Cascaded Pose Position and Velocity Filter

In this section, I propose an observer for the linear time varying system of position, linear velocity and accelerometer biases in the body-fixed frame, using measurement of position, rotation and inertial measurements. I then prove that the cascade of the attitude observer presented in the previous section into the position observer to be proposed in stable.

The following results for input to state stability and linear parameter varying systems will be used in the stability proof of the position observer

Lemma 4.2.5. *Let* $\dot{x} = (A_0 + \phi(t))x$ *where* $A_0 \in \mathbb{R}^{n\times n}$ *is Hurwitz. If*

$$\max_t \|\phi(t)\|_2 \leq \frac{\sigma_{\mathtt{min}}(A_0)}{\sqrt{n}} \tag{4.36}$$

where $\sigma_{\mathtt{min}}(A_0)$ *is the smallest singular value of* A_0*. Then* x *is globally exponentially stable with equilibrium* $x = 0$*.*

Proof of Lemma 4.2.5. As A_0 is Hurwitz, then for any positive definite matrix $Q_0 \in \mathbb{R}^{n\times n}$ there exists a positive definite matrix $P_0 \in \mathbb{R}^{n\times n}$ such that $-Q_0 = P_0A_0 + A_0^\top P_0$. Taking the vec (Horn and Johnson 1994) of this relationship yields $-\mathrm{vec}(Q_0) = (A_0^\top \otimes I + I \otimes A_0^\top)\mathrm{vec}(P_0)$ where $\otimes$ is the Kronecker product. The spectrum of $(A_0^\top \otimes I + I \otimes A_0^\top)$ is the set $\{\lambda_i(A_0) + \lambda_j(A_0)\}$ for all $i,\ j$ (Helmke and Moore 1993).

Note $\|Z\|_F = \|\mathrm{vec}(Z)\|_2$, and $\|Z\|_2 \leq \|Z\|_F \leq \sqrt{\mathtt{rank}(Z)}\|Z\|$, where $\|\cdot\|_F$ is the Frobenius norm (Horn and Johnson 1985). Define $\sigma_{\mathtt{min}}(\cdot), \sigma_{\mathtt{max}}(\cdot) > 0$ as the minimum and maximum singular values of a matrix. One has

$$\sqrt{n}\|Q_0\|_2 \geq 2\sigma_{\mathtt{min}}(A_0)\|P_0\|_2 \tag{4.37}$$

and hence

$$\sigma_{\mathtt{max}}(P_0) = \|P_0\|_2 \leq \frac{\sqrt{n}\sigma_{\mathtt{max}}(Q_0)}{2\sigma_{\mathtt{min}}(A_0)}. \tag{4.38}$$

Define the energy function $\mathcal{L} = x^\top P_0 x$. Then

$$\begin{aligned} \dot{\mathcal{L}} &= -x^\top Q_0 x + x^\top [P_0, \phi(t)]x \\ &\leq -\|x\|^2\sigma_{\mathtt{min}}(Q_0) + 2\|x\|^2\sigma_{\mathtt{min}}(P_0)\|\phi(t)\|_2. \end{aligned} \tag{4.39}$$

Substituting equations 4.36 and 4.38, one sees that

$$\dot{\mathcal{L}} < 0 \tag{4.40}$$

Consequently $\mathcal{L}$ is a Lyapunov function and x is globally exponentially stable with equilibrium $x = 0$. □

Khalil (2002) Lemma 4.6 gives the following statement and its proof.

Proposition 4.2.6. *Suppose* $\mathrm{f}(t,x,u)$ *is continuously differentiable and globally Lipschitz in* (x,u)*, uniformly in* t*. If the unforced system* $\dot{x} = \mathrm{f}(t,x,0)$ *has a globally exponentially stable equilibrium point at the origin* $x = 0$*, then the system* $\dot{x} = \mathrm{f}(t,x,0)$ *is input-to-state-stable*

Using these results, one can prove the following theorem.

Theorem 4.2.7 (ISS Position Observer)**.** *Consider the system*

$$\dot{R} = R\Omega_\times \tag{4.41a}$$
$$\dot{P} = -V - \Omega_\times P \tag{4.41b}$$
$$\dot{V} = A - \Omega_\times V \tag{4.41c}$$
$$\dot{b}_A = 0 \tag{4.41d}$$

with continuous driving term $A(t)$ and bounded continuous driving term $\Omega(t)$ such that for all t, $\|\Omega(t)\|_2 \leq \beta$.

Let R_y, P_y, Ω_y and A_y be the noise free measurements

$$R_y = \exp(e^{-c_1 t} d_R(t))R \tag{4.42a}$$
$$P_y = P \tag{4.42b}$$
$$\Omega_y = \Omega + e^{-c_2 t} d_\Omega(t) \tag{4.42c}$$
$$A_y = A + b_A + gR^\top e_3. \tag{4.42d}$$

where $c_1, c_2 > 0$ and $d_{(\cdot)}(t)$ are continuous disturbance terms.

Consider the observer

$$\dot{\hat{P}} = -\hat{V} - \Omega_{y_\times}\hat{P} - k_1(\hat{P} - P_y), \tag{4.43a}$$
$$\dot{\hat{V}} = A_y - \hat{b}_A - gR_y^\top e_3 - \Omega_{y_\times}\hat{V} + k_2(\hat{P} - P_y), \tag{4.43b}$$
$$\dot{\hat{b}}_A = -k_3(\hat{P} - P_y). \tag{4.43c}$$

and the errors defined in equation (4.21).

Then, there exists a choice of gains k_1, k_2, k_3, such that the error system $(P^\Delta, V^\Delta, \tilde{b}_A)$ is exponentially stable with equilibrium $x' = 0$ and hence $(\hat{P}, \hat{V}, \hat{b}_A)$ are exponentially convergent to the true values (P, V, b_A).

Proof of Theorem 4.2.7. Recall the definition of the $(P^\Delta, V^\Delta, \tilde{b}_A)$ from equation (4.21). Set $R_y \equiv \exp(e^{-c_1 t} d_R(t))R$, $P_y \equiv P$, $\Omega_y \equiv \Omega + e^{-c_2 t} d_\Omega(t)$ and $A_y \equiv A + b_A + gR^\top e_3$. From equation (4.41) and equation (4.43) one has the error system kinematics

$$\dot{x} = (L + \phi(t))x + \Delta(t) \tag{4.44}$$

where $x = (P^{\Delta}, -V^{\Delta}, \tilde{b}_A)^{\top}$ and

$$L = \begin{pmatrix} -k_1 I & I & 0 \\ -k_2 I & 0 & I \\ -k_3 I & 0 & 0 \end{pmatrix}, \qquad \phi(t) = \begin{pmatrix} -\Omega_{\times}(t) & 0 & 0 \\ 0 & -\Omega_{\times}(t) & 0 \\ 0 & 0 & 0 \end{pmatrix},$$
$$\Delta(t) = \begin{pmatrix} -e^{-c_2 t} d_{\Omega(t)_{\times}} \hat{P} \\ e^{-c_2 t} d_{\Omega(t)_{\times}} \hat{V} - g(I - \exp(e^{-c_1 t} d_R(t)^{\top})) R^{\top} e_3 \\ 0 \end{pmatrix}, \tag{4.45}$$

The gains k_1, k_2, k_3 care chosen such that L is Hurwitz and additionally such that $\Omega(t)$ is bounded for all t such that

$$\|\phi(t)\|_2 = \|\Omega(t)\|_2 \leq \frac{\sigma_{\mathtt{min}}(L)}{3}. \tag{4.46}$$

It is straightforward to see that this is possible using pole placement arguments. By application of Lemma 4.2.5, one has that $\dot{x} = (A + \phi(t))x$ is globally exponentially stable. Then by Proposition 4.2.6, $\dot{x} = (A + \phi(t))x + u(t)$ is ISS for any Lipschitz continuous $u(t)$. Set $\Delta(t) \equiv u(t)$ and, as $\Delta(t)$ is exponentially decreasing to 0, x is globally exponentially stable. □

Combining the observers and stability results for the attitude and position observers from Theorems 4.2.1 and 4.2.7 respectively and choosing appropriate gains, one has that for initial conditions such that $(\bar{R}(0), \tilde{b}_{\Omega}(0)) \notin \{(\bar{R}, \tilde{b}_{\Omega}) | \operatorname{tr}(\bar{R}) > -1 \text{ and } \tilde{b}_{\Omega} = 0\}$ the estimate $(\hat{R}, \hat{P})$ is almost-globally asymptotically stable. Further, for initial attitude conditions within the bowl of locally exponential stability of the attitude observer, the estimate of $(\hat{R}, \hat{P})$ is exponentially stable.

4.2.3 Experimental Results

The attitude and position observers presented in equation (4.22) and equation (4.43) have been implemented in MATLAB and applied to experimental data obtained by Thibault Cheviron (Cheviron et al. 2007). The experimental platform consisted of a Microstrain 3DMG IMU and a Philips webcam mounted on a Vario Benzin-Acrobatic 23cc small scale helicopter, illustrated in Figure 4.1. Data capture rates were 50 Hz for the IMU and 10 Hz for the vision sensor.

The experiment consisted of a manual quasi-stationary (i.e. hover) flight over a visual target whose feature locations in the inertial frame are known. The experiment has been performed such that the target always lay in the field of view of the camera.

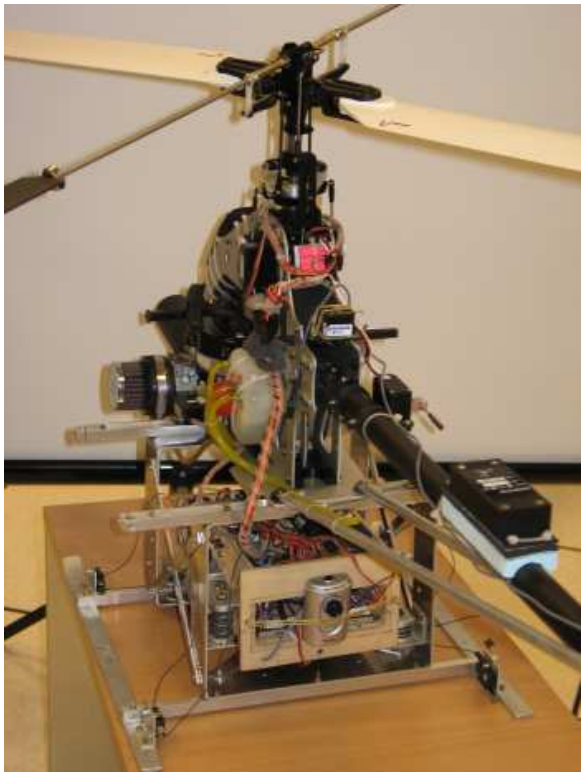

Figure 4.1: Experimental platform consisting of a Vario Benzin-Acrobatic 23cc helicopter, low-cost Philips webcam and Microstrain IMU

Camera calibration has been completed under static conditions prior to flight. From the calibration data, in addition to the intrinsic camera parameters, the extrinsic parameters of the orientation of the camera relative to the IMU have been estimated using a recursive least mean square algorithm. Using the extrinsic alignment matrix, data from the flight experiment has been pre-processed to align the camera and IMU frames of reference before the observer is run.

The gains k_{P_Ω} and k_{I_Ω} have been chosen to ensure satisfactory asymptotic stability of the linearised dynamics of the non-linear observer equation (4.22). The characteristic polynomial of this observer is $\Pi_1(s) = s^2 + k_{P_\Omega}s + k_{I_\Omega}$ and observer gains listed in Table 4.1 are chosen to correspond with a crossover frequency of 0.6 Hz and a damping factor of 0.8.

Analogously, the gain k_1, k_2 and k_3 have been chosen such that $k_1 = \mu + 2\nu$, $k_2 = 2\mu\nu + \nu^2$ and $k_3 = \mu\nu^2$, with $\mu = 0.01$ and $\nu = 10$ for the non-linear position and velocity observer such that the characteristic polynomial of the transient matrix L is

Gain	Value
k_{P_Ω}	15
k_{I_Ω}	$\frac{2}{225}$
k_1	20.01
k_2	10.2
k_3	1

Table 4.1: Observer gains used in flight experiment with $SO(3) \times \mathbb{R}^3$ observer.

$\Pi_2(s) = (s+\mu)(s+\nu)^2$.

The estimated helicopter orientation, depicted in blue, is contrasted with the industrial filter of the 3DMG IMU and vision measurements, depicted in green and red respectively, in Figure 4.2. Gyroscope bias estimates are shown in Figure 4.3.

The estimated helicopter position, depicted in blue, is contrasted with vision measurements, depicted in red, in Figure 4.4. Velocity and accelerometer bias are shown in Figures 4.5 and 4.6.

Excellent behaviour of both observer is seen, despite large errors in initial conditions, inertial sensor drive and occasional missing vision measurements. These figures demonstrate that accurate vision measurements allow successful estimates of unknown inertial biases.

4.3 Simultaneous Attitude and Position Filter Design

In this section, four non-linear observers are proposed using a cost function on SE(3) that decomposes into SO(3) and $\mathbb{R}^3$ components. This decomposition permits independent design of the rotation and translation components while admitting a whole-system Lyapunov stability argument on glsSE3.

The first observer estimates pose based on a cost function using the *coordinate frame transformation* between the true and estimated system as the error. The second observer identifies a simplification of the first observer based on identification of a passive dynamic. The third observer estimates pose based on a cost function using the *rigid body transformation* between the true and estimated systems represented in the body fixed frame as the error, further exploiting passive dynamics to simplify the observer and render it suitable for a multi-rate implementation. The final observer is a

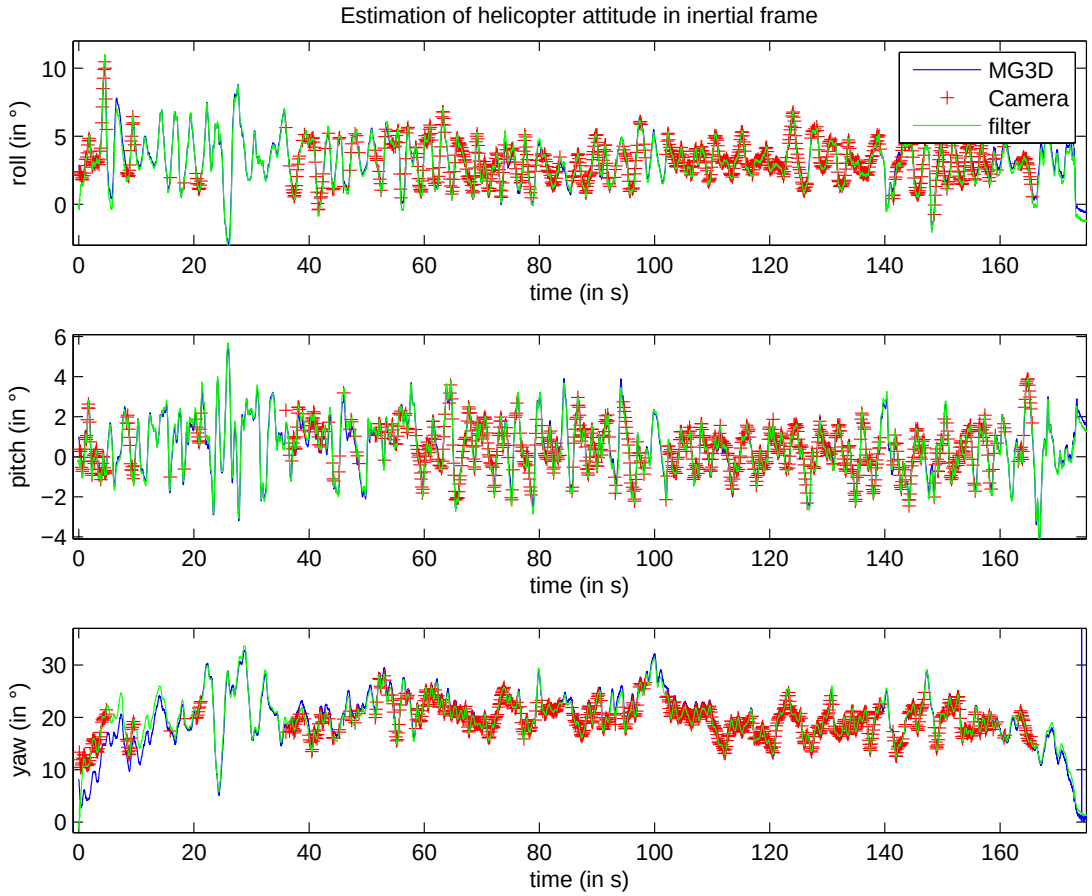

Figure 4.2: Estimate of helicopter attitude in the inertial frame produced by Cascaded Pose Observer using observer gains given in Table 4.1.

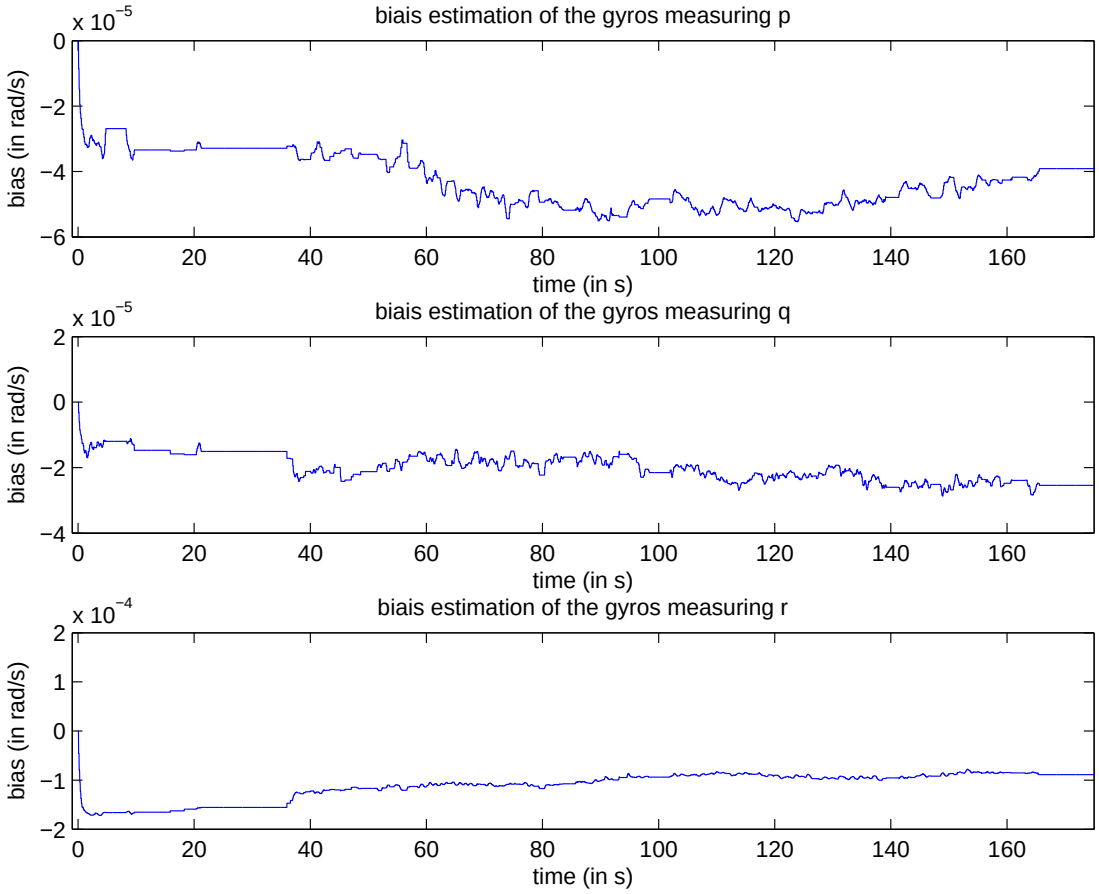

Figure 4.3: Estimate of gyroscope biases in the body-fixed frame produced by Cascaded Pose Observer using observer gains given in Table 4.1.

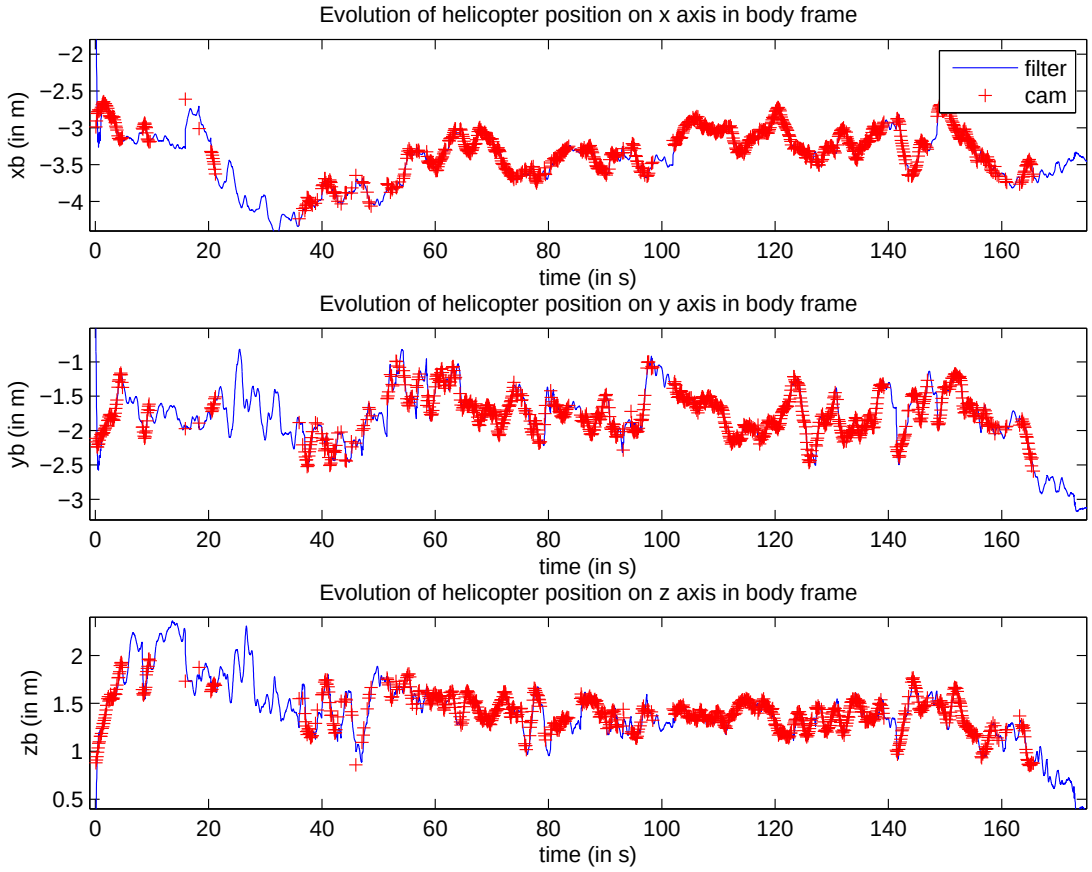

Figure 4.4: Estimate of helicopter position in the body-fixed frame produced by Cascaded Pose Observer using observer gains given in Table 4.1.

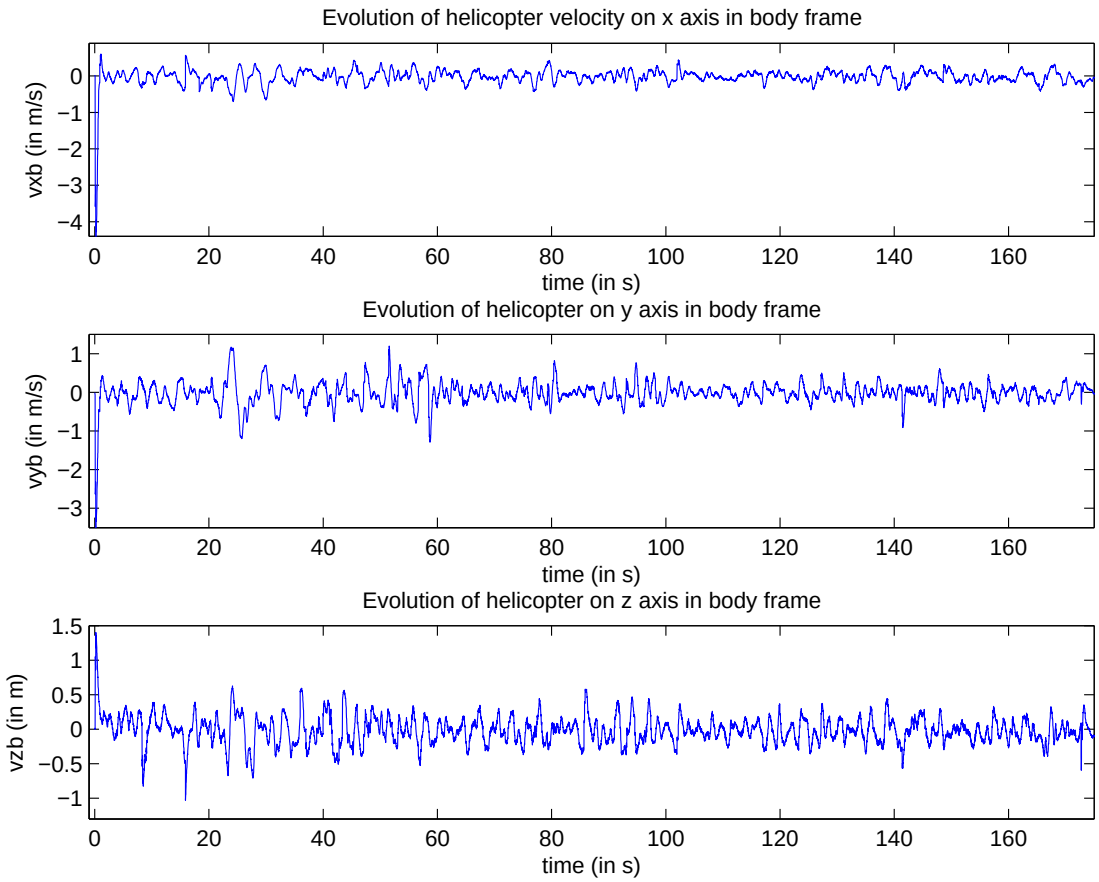

Figure 4.5: Estimate of helicopter velocity in the body-fixed frame produced by Cascaded Pose Observer using observer gains given in Table 4.1.

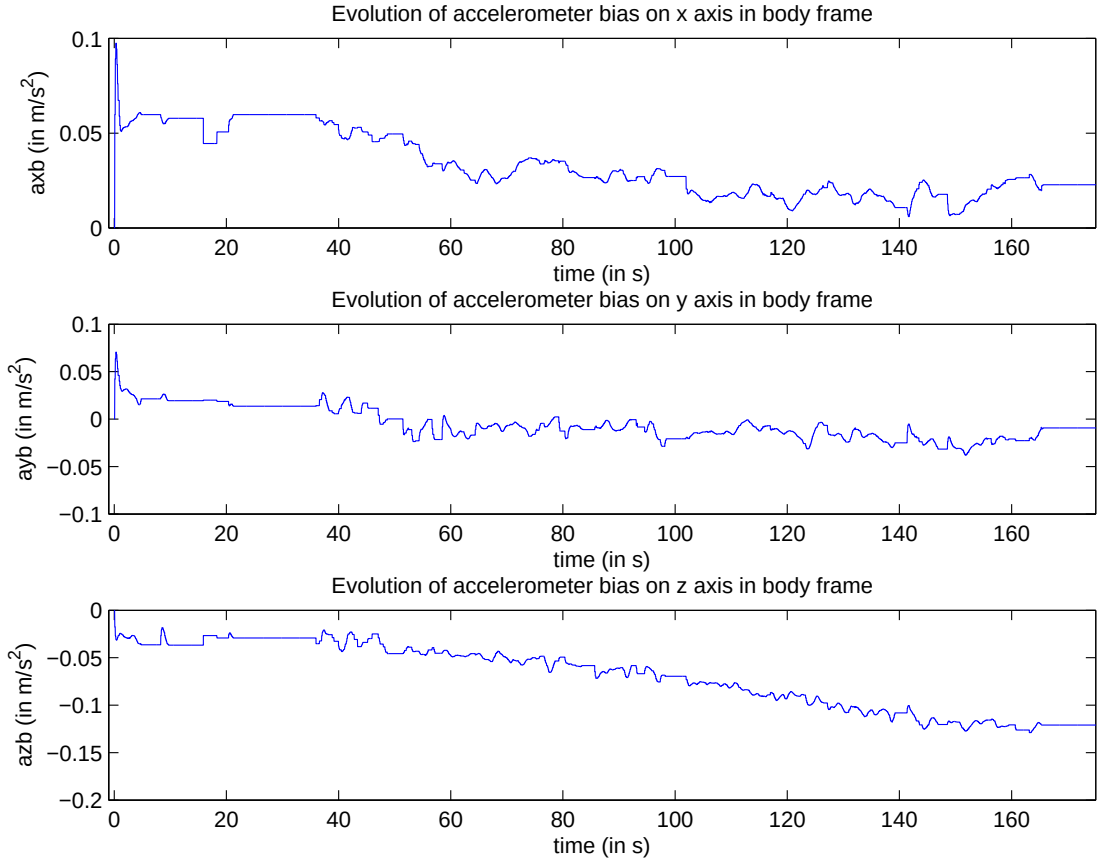

Figure 4.6: Estimate of accelerometer biases in the body-fixed frame produced by Cascaded Pose Observer using observer gains given in Table 4.1.

modification of the third observer, making use of exponential convergence properties to reduce coupling independent between measurement noise processes.

4.3.1 Coordinate Frame Transformation Error Observer

Define the error term

$$\bar{T} = T^{-1}\hat{T}. \tag{4.47}$$

$\bar{T}$ gives the *coordinate frame transformation* from $\mathcal{E}$ to $\mathcal{B}$. Note that $\bar{T}$ is the element of SE(3) corresponding to the independent rotation and position errors$\bar{R} = R^\top \hat{R}$, defined in equation (4.21a), and $\bar{p} = R^\top(\hat{p} - p)$. One has

$$\bar{T} = \begin{pmatrix} \bar{R} & \bar{p} \\ 0 & 1 \end{pmatrix} \tag{4.48}$$

and

$$\bar{T}^{-1} = \begin{pmatrix} \bar{R}^\top & \bar{P} \\ 0 & 1 \end{pmatrix}. \tag{4.49}$$

where

$$\bar{R} = R^\top \hat{R}, \tag{4.50a}$$
$$\bar{p} = R^\top(\hat{p} - p), \tag{4.50b}$$
$$\bar{P} = -\bar{R}^\top \bar{p} = \hat{P} - \bar{R}^\top P. \tag{4.50c}$$
$$\tag{4.50d}$$

Further, if $\bar{T} \to I$, then $\hat{T} \to T$, leading to the choice of positive definite cost function

$$\mathcal{V} = \frac{1}{2}\|I - \bar{T}\|_F^2 \tag{4.51}$$

Theorem 4.3.1 (Coordinate Frame Transformation Error Observer on SE(3))**.** *Consider the system defined in equation (6.4). Let $R_y^\top = R^\top$, $P_y = P$, $\Omega_y = \Omega$ and $V_y = V$ be measurements free of noise and bias.*

Define the observer

$$\dot{\hat{T}} = \hat{T}\hat{\Xi}, \tag{4.52a}$$
$$\hat{\Xi} = \left(\hat{\Omega}, \hat{V}\right)^{\wedge}, \tag{4.52b}$$
$$\hat{\Omega} = \mathrm{Ad}_{\hat{R}^{\top}R_y}\Omega_y + k_{P_\Omega}\xi_\Omega, \tag{4.52c}$$
$$\hat{V} = \hat{R}^{\top}R_y V_y + k_{P_p}\xi_V, \tag{4.52d}$$
$$\xi_\Omega = \mathrm{vex}(\mathbb{P}_a(\hat{R}^{\top}R_y)), \tag{4.52e}$$
$$\xi_V = \hat{P} - \hat{R}^{\top}R_y P_y. \tag{4.52f}$$

and recall the error $\bar{T} = T^{-1}\hat{T}$ from equation (4.47).

Then for all positive choice of gains k_{P_Ω} and k_{P_p}, and any initial condition

$$\bar{T}_0 \in \{\bar{T} | \bar{T} \in \mathrm{SE}(3), \mathrm{tr}(\bar{T}) \neq 0\} \tag{4.53}$$

the error $\bar{T}$ is almost-globally asymptotically convergent to I with locally exponential convergence. Hence $\hat{T} \to T$, $\hat{R} \to R$ and $\hat{p} \to p$ asymptotically and locally exponentially.

Proof of Theorem 4.3.1. This proof is set out as follows:

- Firstly, we define a cost function for the error in $\mathrm{SE}(3)$
- Secondly, we derive an identity that permits definition of independent cost functions on the rotational and translational error in terms of the overall cost function.
- Convergence of rotation and translation errors are then proven independently.
- Lastly, the initial conditions of the two error components are considered and the stable set on $\mathrm{SE}(3)$ derived.

Recall the cost function $\mathcal{V}$ from equation (4.51), expanding one has

$$\begin{aligned}
\mathcal{V} &= \frac{1}{2}\|I - \bar{T}\|_F^2 \\
&= \frac{1}{2}\mathrm{tr}\left((I-\bar{T})^{\top}(I-\bar{T})\right) \\
&= \frac{1}{2}\mathrm{tr}\left(I - \bar{T}^{\top} - \bar{T} + \bar{T}^{\top}\bar{T}\right) \\
&= \frac{1}{2}\mathrm{tr}\left(\begin{pmatrix} I & 0 \\ 0 & 1 \end{pmatrix} - \begin{pmatrix} \bar{R}^{\top} & 0 \\ \bar{p}^{\top} & 1 \end{pmatrix} - \begin{pmatrix} \bar{R} & \bar{p} \\ 0 & 1 \end{pmatrix} + \begin{pmatrix} I & \bar{R}^{\top}\bar{p} \\ \bar{p}^{\top}\bar{R} & 1 + \bar{p}^{\top}\bar{p} \end{pmatrix}\right) \\
&= \mathrm{tr}\,(I - \bar{R}) + \frac{1}{2}\|\bar{p}\|_2^2 \\
&= \mathcal{V}_R + \mathcal{V}_P
\end{aligned} \tag{4.54}$$

where $\mathcal{V}_R = \mathrm{tr}\,(I - \bar{R})$ and $\mathcal{V}_P = \frac{1}{2}\|\bar{p}\|_2^2$.

Recall the rotation error $\bar{R}$ from equation (4.50a). Setting $R_y \equiv R$ and $\Omega_y \equiv \Omega$, one has

$$\begin{aligned}\dot{\bar{R}} &= \bar{R}(\hat{\Omega} - \mathrm{Ad}_{\bar{R}^\top}\Omega)_\times \\ &= \bar{R}(\mathrm{Ad}_{\hat{R}^\top R}\Omega + k_{P_\Omega}\xi_\Omega - \mathrm{Ad}_{\bar{R}^\top}\Omega)_\times \\ &= k_{P_\Omega}\bar{R}\mathbb{P}_a(\bar{R})^\top\end{aligned} \tag{4.55}$$

Taking the time derivative of $\mathcal{V}_R$ and using the orthogonality of symmetric and skew-symmetric matrices, one has

$$\begin{aligned}\dot{\mathcal{V}}_R &= -\mathrm{tr}(\dot{\bar{R}}), \\ &= -k_{P_\Omega}\mathrm{tr}(\bar{R}\mathbb{P}_a(\bar{R})^\top), \\ &= -k_{P_\Omega}\mathrm{tr}(\mathbb{P}_s(\bar{R})\mathbb{P}_a(\bar{R})^\top + \mathbb{P}_a(\bar{R})\mathbb{P}_a(\bar{R})^\top), \\ &= -k_{P_\Omega}\mathrm{tr}(\mathbb{P}_a(\bar{R})^\top\mathbb{P}_a(\bar{R})), \\ &= -k_{P_\Omega}\|\mathbb{P}_a(\bar{R})\|_F^2.\end{aligned} \tag{4.56}$$

Let, $(\bar{\theta}, \bar{\gamma})$ denote the angle-axis coordinates of $\bar{R}$. From equation (4.19) one has

$$\bar{R} = \exp(\bar{\theta}, \bar{\gamma}_\times), \tag{4.57a}$$

$$\cos(\bar{\theta}) = \frac{1}{2}(\mathrm{tr}(\bar{R}) - 1), \tag{4.57b}$$

$$\bar{\gamma}_\times = \frac{1}{\sin(\bar{\theta})}\mathbb{P}_a(\bar{R}) \tag{4.57c}$$

The cost function $\mathcal{V}_R$ may be written as

$$\begin{aligned}\mathcal{V}_R &= \mathrm{tr}(I - \bar{R}), \\ &= 2(1 - \cos(\bar{\theta})), \\ &= 4\sin\left(\frac{\bar{\theta}}{2}\right)^2,\end{aligned} \tag{4.58}$$

using the identity $\cos(2\theta) = 1 - 2\sin(\theta)^2$.

Substituting $\sin(\bar{\theta})\bar{\gamma}_\times = \mathbb{P}_a(\bar{R})$ from equation (4.57c) into equation (4.56), one has

$$\begin{aligned}\dot{\mathcal{V}}_R &= -k_{P_\Omega}\|\mathbb{P}_a(\bar{R})\|_F^2 \\ &= -k_{P_\Omega}\sin(\bar{\theta})^2\|\bar{\gamma}_\times\|_F^2 \\ &= -k_{P_\Omega}\sin(\bar{\theta})^2 \\ &= -4k_{P_\Omega}\sin\left(\frac{\bar{\theta}}{2}\right)^2\cos\left(\frac{\bar{\theta}}{2}\right)^2 \\ &= -k_{P_\Omega}\cos\left(\frac{\bar{\theta}}{2}\right)^2\mathcal{V}_R\end{aligned} \tag{4.59}$$

using the identity $\sin(2\theta) = 2\sin(\theta)\cos(\theta)$.

Hence, for $\bar{\theta} \neq \pm\pi$ one has that $\mathcal{V}_R$ is decreasing to 0 and $\bar{R} \to I$. Moveover, in the neighbourhood of $R = I$, $\cos(\frac{\bar{\theta}}{2})$ is bounded away from zero and one has locally exponential stability.

Recall the translation error $\bar{P}$ from equation (4.50c). Setting $R_y \equiv R$, $\Omega_y \equiv \Omega$, $P_y \equiv P$ and $V_y \equiv V$, one has

$$\begin{aligned}\dot{\bar{P}} &= \frac{\mathbf{d}}{\mathbf{d}t}(\hat{R}^\top(p-\hat{p})) \\ &= -\hat{\Omega}_\times\bar{P} + \bar{R}^\top V - \hat{V} \\ &= -\hat{\Omega}_\times\bar{P} - k_{P_p}\bar{P}\end{aligned} \tag{4.60}$$

Noting $\mathcal{V}_P = \frac{1}{2}\|\bar{p}\|_2^2 = \frac{1}{2}\|\bar{P}\|_2^2$ and taking the time derivative of $\mathcal{V}_P$, one has

$$\begin{aligned}\dot{\mathcal{V}}_P &= \bar{P}^\top\dot{\bar{P}} \\ &= \bar{P}^\top(-\hat{\Omega}_\times\bar{P} - k_{P_p}\bar{P})\end{aligned} \tag{4.61}$$

Given that $x^T\Omega_\times x = 0$, one has

$$\begin{aligned}\mathcal{V}_P &= -k_{P_p}\bar{P}^\top\bar{P} \\ &= -k_{P_p}\|\bar{P}\|_2^2 \\ &= -2k_{P_p}\mathcal{V}_P\end{aligned} \tag{4.62}$$

Hence $\mathcal{V}_P$ is exponentially decreasing to 0 and $\bar{P} \to 0$ exponentially. Moreover, as both $\mathcal{V}_R$ and $\mathcal{V}_P$ are decreasing to 0, $\mathcal{V}$ is almost-globally asymptotically stable and locally exponentially stable.

The set of initial conditions for convergence of $\mathcal{V}$ is given by the intersection of the set of convergent initial conditions for $\mathcal{V}_R$ and $\mathcal{V}_P$. Noting that $\bar{\theta} = \pm\pi$ implies

$\cos(\bar{\theta}) = -1$ and hence $\mathrm{tr}(\bar{R}) = -1$, it is possible to express the convergent initial conditions in matrix form. As $\mathcal{V}_P$ is globally convergent given convergence of $\mathcal{V}_R$, and that $\mathrm{tr}(T) = \mathrm{tr}(R) + 1$ due to the structure of the matrix representation of $\mathfrak{se}(3)$, one has that

$$\bar{T}_0 \in \{\bar{T} | \bar{T} \in \mathrm{SE}(3), \mathrm{tr}(\bar{T}) \neq 0\} \tag{4.63}$$

□

Remark 4.3.2.
Note that by the same proof, replacing equation (4.52c) with

$$\hat{\Omega} = \Omega + k_{P_\Omega} \xi_\Omega \tag{4.64}$$

is also a convergent observer. In this case, equation (4.55) becomes $\dot{\bar{R}} = [\bar{R}, \Omega_\times] + k_{P_\Omega} \bar{R} \mathbb{P}_a(\bar{R})^\top$ and equation (4.56) becomes

$$\begin{aligned} \dot{\mathcal{V}}_R &= -\mathrm{tr}(\dot{\bar{R}}), \\ &= -k_{P_\Omega} \mathrm{tr}([\bar{R}, \Omega_\times] + \bar{R} \mathbb{P}_a(\bar{R})^\top), \\ &= -k_{P_\Omega} \| \mathbb{P}_a(\bar{R}) \|_F^2. \end{aligned} \tag{4.65}$$

as the trace of the matrix commutator is zero. This alternate observer makes use of the passivity of the error dynamics with respect to frame in which angular velocity measurement is treated. This passivity in the rotation is identified and discussed in detail in Mahony et al. (2008). The concept of passivity with respect to measurement frames is built up in the next section, where it is applied to the SE(3) system as a whole.

The observer defined in Theorem 4.3.1 suffers from coupling between measurement errors. The angular velocity estimate multiplies the measured angular velocity by with the measured rotation as part of an adjoint operation. This introduces additional high frequency noise into the direct integration component of the angular velocity estimate. Using equation (4.64) prevents this issue.

Remark 4.3.3.
Both the observer proposed in Theorem 4.3.1 and the observer proposed in the above remark are almost-globally asymptotically stable due to the topological constraints discussed in Remark 4.2.4 . The region of non-convergence for both comprises an unstable set of measure zero containing the anti-podal points to $I \in \mathrm{SO}(3)$. This is unavoidable due to the compact nature of SO(3), which forms a part of SE(3).

A weakness present in the observer of Theorem 4.3.1, and equally in the variant proposed in Remark 4.3.2, is the multiplication of the instantaneous rotation measurement with the linear velocity measurement in the feed-forward component of linear velocity estimate, in equation (4.52d).

In particular, the coupling prohibits proposing a multi-rate implementation for this observer. The inclusion of the low rate rotation measurement limits the rate at which $\hat{V}$ may be estimated and hence the observed run. Running the observers at a higher rate would require the input of some estimate for R, rather than a straight forward discretisation of the continuous time systems.

In both cases, the coupling of the high frequency stable inertial measurements with the low frequency stable vision measurements result in feed-forward terms corrupted by both high and low frequency noise.

4.4 Rigid Body Transformation Error Observer

The problems noted with the Coordinate Frame Transformation Error Observer stem from the choice of error $\bar{T} = T^{-1}\hat{T}$. Recalling the three interpretations of an element of $\mathrm{SE}(3)$, in Section 4.3.1 the error $\bar{T}$ was interpreted as the *coordinate frame transformation* taking a point expressed in $\mathcal{E}$ to a point expressed in $\mathcal{B}$.

Alternatively, the error $\bar{T}$ can be viewed as the coordinates of $\mathcal{E}$ expressed in $\mathcal{B}$. This directly associates $\bar{T}$ with the moving frame of reference $\mathcal{B}$. This causes an undesirable disturbance in the error dynamics when $\mathcal{B}$ changes, even when the motion is perfectly estimated and replicated in $\mathcal{E}$. That is, when $\mathcal{B}$ and $\mathcal{E}$ move but there is no change in the error magnitude. For example, when a translationally-static rigid body undergoes a rotation, the translational error $\bar{p}$ will change despite p and $\hat{p}$ remaining constant. Representing the error in the inertial frame eliminates this coupling and leads to a simpler estimator.

Analogous to the adjoint operator Ad_T, that changes the frame of reference associated with elements of $\mathfrak{se}(3)$, there is an inner-automorphism operator

$$\begin{aligned} I_T : \mathrm{SE}(3) &\to \mathrm{SE}(3), \quad T \in \mathrm{SE}(3) \\ I_T(Q) &:= TQT^{-1}, \end{aligned} \tag{4.66}$$

that acts to change the frame of reference associated with an element of the Lie-group $\mathrm{SE}(3)$. In particular, if $\bar{T}$ is associated with $\mathcal{B}$ and $T \in \mathrm{SE}(3)$ is the coordinates of $\mathcal{B}$ with respect to an inertial frame $\mathcal{A}$, then $I_T(\bar{T})$ is associated with the inertial frame $\mathcal{A}$.

Let

$$\tilde{T} := I_T(\bar{T}) = \hat{T}T^{-1} \tag{4.67}$$

denote the error $\bar{T}$ represented in the inertial frame of reference $\mathcal{A}$. One has

$$\tilde{T} = \begin{pmatrix} \tilde{R} & \tilde{p} \\ 0 & 1 \end{pmatrix} \tag{4.68}$$

and

$$\tilde{T}^{-1} = \begin{pmatrix} \tilde{R}^\top & \tilde{P} \\ 0 & 1 \end{pmatrix} \tag{4.69}$$

where

$$\tilde{R} = \hat{R}R^T, \tag{4.70a}$$
$$\tilde{p} = \hat{p} - \tilde{R}p, \tag{4.70b}$$
$$\tilde{P} = -\tilde{R}^\top \tilde{p} = R(\hat{P} - P). \tag{4.70c}$$
$$\tag{4.70d}$$

Importantly, note that $\tilde{T}$ does not have an interpretation as a coordinate frame transformation operator but still retains an interpretation as a rigid body transformation operator, taking an object from pose $\mathcal{E}$ to pose $\mathcal{B}$, represented in $\mathcal{A}$.

As with $\bar{T}$, when $\tilde{T} \to I$ then $\hat{T} \to T$ leading to the choice of positive definite cost function

$$\mathcal{V}(\tilde{T}) := \frac{1}{2}\|I - \tilde{T}\|_F^2. \tag{4.71}$$

Theorem 4.4.1 (Rigid Body Transformation Observer on SE(3))**.** *Consider the system defined in equation (6.4). Let $R_y^\top = R^\top$, $P_y = P$, $\Omega_y = \Omega$ and $V_y = V$ be measurements free of noise and bias.*

Define the observer

$$\dot{\hat{T}} = \hat{T}\hat{\Xi}, \tag{4.72a}$$
$$\hat{\Xi} = \left(\hat{\Omega}, \hat{V}\right)^\wedge, \tag{4.72b}$$
$$\hat{\Omega} = \Omega_y + k_{P_\Omega}\xi_\Omega, \tag{4.72c}$$
$$\hat{V} = V_y - (\hat{\Omega} - \Omega_y)_\times \hat{P} + k_{P_p}\xi_V, \tag{4.72d}$$
$$\xi_\Omega = \mathrm{vex}(\mathbb{P}_a(\hat{R}^\top R_y)), \tag{4.72e}$$
$$\xi_V = \hat{P} - P_y, \tag{4.72f}$$

and recall the error $\tilde{T} = \hat{T}T^{-1}$ *from equation (4.67)*

Then for all positive choice of gains k_{P_Ω} *and* k_{P_p}*, and any initial condition*

$$\tilde{T}_0 \in \left\{\tilde{T} | \tilde{T} \in \mathrm{SE}(3), \mathrm{tr}(\tilde{T}) \neq 0\right\} \tag{4.73}$$

the error $\tilde{T}$ *is almost-globally asymptotically convergent to I with locally exponential convergence. Hence* $\hat{T} \to T$*,* $\hat{R} \to R$ *and* $\hat{p} \to p$ *asymptotically and locally exponentially.*

Proof of Theorem 4.4.1. This proof follows similarly to that of Theorem 4.3.1.

- Firstly, we define a cost function on the error in $\mathrm{SE}(3)$
- Secondly, we derive an identity that permits definition of independent cost functions on the rotational and translational error in terms of the overall cost function.
- Convergence of rotation and translation errors are then proven independently.
- Lastly, the initial conditions of the two error components are considered and the stable set on $\mathrm{SE}(3)$ derived.

Recall the cost function $\mathcal{V}$ from equation (4.71) and making calculations analogous to equation (4.54), one has

$$\begin{aligned} \mathcal{V} &= \frac{1}{2}\|I - \tilde{T}\|_F^2 \\ &= \mathrm{tr}\left(I - \tilde{R}\right) + \frac{1}{2}\|\tilde{p}\|_2^2 \\ &= \mathcal{V}_R + \mathcal{V}_P \end{aligned} \tag{4.74}$$

where $\mathcal{V}_R = \mathrm{tr}\left(I - \tilde{R}\right)$ and $\mathcal{V}_P = \frac{1}{2}\|\tilde{p}\|_2^2$.

Recall the rotation error $\tilde{R}$ from equation (4.70a). Setting $R_y \equiv R$ and $\Omega_y \equiv \Omega$, one has

$$\begin{aligned} \dot{\tilde{R}} &= \tilde{R}\,\mathrm{Ad}_R(\hat{\Omega} - \Omega)_\times \\ &= k_{P_\Omega}\tilde{R}\,\mathrm{Ad}_R(\xi_\Omega)_\times \\ &= k_{P_\Omega}\tilde{R}\mathbb{P}_a(\tilde{R})^\top \end{aligned} \tag{4.75}$$

Taking the time derivative of $\mathcal{V}_R$ and using the orthogonality of symmetric and skew-symmetric matrices analogously to equation (4.56), one has

$$\begin{aligned} \dot{\mathcal{V}}_R &= -\mathrm{tr}(\dot{\tilde{R}}), \\ &= -k_{P_\Omega}\|\mathbb{P}_a(\tilde{R})\|_F^2. \end{aligned} \tag{4.76}$$

Again using an angle-axis formulation similar to equation (4.57c) and an argument identical to equation (4.58) and equation (4.59) one has $\dot{\mathcal{V}}_R = -k_{P_\Omega} \cos\left(\frac{\tilde{\theta}}{2}\right)^2 \mathcal{V}_R$. Hence, for $\tilde{\theta} \neq \pm\pi$ one has that $\mathcal{V}_R$ is decreasing to 0 and $\tilde{R} \to I$. Moveover, in the neighbourhood of $R = I$, $\cos(\frac{\tilde{\theta}}{2})$ is bounded away from zero and one has locally exponential stability.

Recall the translation error $\tilde{P}$ from equation (4.70c). Setting $R_y \equiv R$, $\Omega_y \equiv \Omega$, $P_y \equiv P$ and $V_y \equiv V$, one has

$$\begin{aligned} \dot{\tilde{P}} &= \frac{\mathbf{d}}{\mathbf{d}t}(R(\hat{P} - P)) \\ &= R(\Omega_\times(\hat{P} - P)) - \hat{\Omega}_\times \hat{P} - \hat{V} + \Omega_\times P + V) \\ &= -k_{P_p} \tilde{P} \end{aligned} \tag{4.77}$$

Noting $\mathcal{V}_P = \frac{1}{2}\|\tilde{p}\|_2^2 = \frac{1}{2}\|\tilde{P}\|_2^2$ and taking the time derivative of $\mathcal{V}_P$, one has

$$\begin{aligned} \dot{\mathcal{V}}_P &= \tilde{P}^\top \dot{\tilde{P}} \\ &= -k_{P_p} \tilde{P}^\top \tilde{P} \\ &= -2k_{P_p} \mathcal{V}_P \end{aligned} \tag{4.78}$$

Hence $\mathcal{V}_P$ is exponentially decreasing to 0 and $\tilde{P} \to 0$ exponentially. Moreover, as both $\mathcal{V}_R$ and $\mathcal{V}_P$ are decreasing to 0, $\mathcal{V}$ is almost-globally asymptotically stable and locally exponentially stable.

The set of initial conditions for convergence of $\mathcal{V}$ is given by the intersection of the set of convergent initial conditions for $\mathcal{V}_R$ and $\mathcal{V}_P$. As with Theorem 4.3.1 it is possible to express the convergent initial conditions in matrix form. Given $\mathcal{V}_P$ is globally convergent given convergence of $\mathcal{V}_R$, and one has that $\mathrm{tr}(T) = \mathrm{tr}(R) + 1$ due to the structure of the matrix representation of $\mathfrak{se}(3)$, one has

$$\tilde{T}_0 \in \left\{ \tilde{T} \,|\, \tilde{T} \in \mathrm{SE}(3), \mathrm{tr}(\tilde{T}) \neq 0 \right\} \tag{4.79}$$

□

The rigid body transformation observer does not suffer the problem of multiplicative measurement error coupling between high and low frequency stable measurements, identified with the coordinate frame transformation observer. The innovation and direct integration components of the estimate velocities contain no multiplications between measurements.

The rigid body transformation observer does however have additive coupling between inertial measurements in the direct integration component of the linear velocity estimate. However, as will be demonstrated in the next section, this term may be omitted and the result will still be an almost-globally asymptotically and locally exponentially stable observer.

4.5 Zero-Coupling Rigid Body Transformation Error Observer

Recall equation (4.72):

$$\hat{V} = V_y - (\hat{\Omega} - \Omega_y)_\times \hat{P} + k_{P_p}(\hat{P} - P_y) \tag{4.80}$$

The $(\hat{\Omega} - \Omega_y)_\times \hat{P}$ term will not exactly cancel with the $(\hat{\Omega} - \Omega)_\times \hat{P}$ term in the Lyapunov function due to the noise in the measurement Ω_y. While zero mean random noise will ensure that the expected value of the resulting filter has the desired properties, the cross term increases the high frequency noise in the position estimate. One may eliminate this source of estimation noise by discarding the problematic terms.

Corollary 4.5.1 (Zero-Coupling Rigid Body Transformation Error Observer)**.** *Consider the statement of Theorem 4.4.1 in which the observer system is almost-globally asymptotically and locally exponentially stable with equilibrium $\tilde{T} = I$.*

Assume that $P(t)$ is a bounded signal such that

$$\|P(t)\| \leq \|P_{\max}\|, \qquad \textit{for all } t. \tag{4.81}$$

Consider the modified observer with kinematics given in equation (4.72) with the substitution

$$\hat{V} = V_y + k_{P_p}\xi_V, \tag{4.82}$$

Then for the same initial conditions and choice of gains as in Theorem 4.4.1, the error $\tilde{T}$ is almost-globally asymptotically and locally exponentially stable. Hence $\hat{T} \to T$, $\hat{R} \to R$ and $\hat{p} \to p$ with locally exponential convergence.

Proof of Corollary 4.5.1. Recall the translation error $\tilde{P}$ from equation (4.70c). Setting $R_y \equiv R$, $\Omega_y \equiv \Omega$, $P_y \equiv P$, $V_y \equiv V$, $\hat{V} = V_y + k_{P_p}(\hat{P} - P)$, one has

$$\dot{\tilde{P}} = -k_{P_p}\tilde{P} - R(\hat{\Omega} - \Omega)_\times \hat{P} \tag{4.83}$$

Trivially, the system $\dot{\tilde{P}} = -k_{P_p}\tilde{P}$ is globally exponentially stable. Then, by Proposition 4.2.6 the system $\dot{\tilde{P}} = -k_{P_p}\tilde{P} + u(t)$ is ISS.

Let $u(t) = -R(\hat{\Omega} - \Omega)_\times \hat{P}$ be an exogenous input to the error system, which is exponentially decreasing as $\hat{R} \to R$ from Theorem 4.4.1. Then $\tilde{P}$ in equation (4.83) is ISS with an exponentially decreasing input when the rotation system is in the region of locally exponential convergence. Consequently, on the same region $\tilde{P}$ is locally exponentially stable with equilibrium $\tilde{P} = 0$.

Hence the modified observer system is almost-globally asymptotically and locally exponentially stable, with the same bowl of exponential convergence as the observer system of Theorem 4.4.1. □

The figures in Section 4.5.3 demonstrate that this modified form of $\hat{V}$ allows a temporary divergence in the position estimate, from the pseudo-input $u(t)$, while the system undergoes a transition to correct large orientation error. The selection of gains k_{P_Ω} and k_{P_p}, addressed in section 4.5.2, allows this deviation to be controlled to an extent.

4.5.1 Discrete Integration on SE(3) for Rigid Body Transformation Error Observer

A range of discrete time integration techniques can be used to create a discrete time implementation of the observers proposed in Sections 4.3, 4.4 and 4.5. In this section I will present several choices of discrete integration scheme applied to the Rigid Body Pose Error Observer presented in Section 4.4

The explicit, or forwards, Euler method is the simplest method of numerical integration. At each time step, the value of the differential equation is calculated using the value of the equation and its derivative at the previous time step. On SE(3) the forwards Euler integration step is given by

$$T(t+\tau) = \exp(\tau \mathrm{Ad}_{T(t)}\, \Xi(t))T(t) \tag{4.84}$$

where $\tau > 0$ is the integration time step and $\mathrm{Ad}_{T(t)}\, \Xi(t)$ is used as a tangent represented in the inertial frame. Note that there exist explicit forms of the matrix exponential on $\mathfrak{se}(3)$ (Park 1994) allowing direct implementation, albeit using sin and cos functions, rather than computationally expensive approximations used in the general case (e.g. Moler and Van Loan 2003).

Explicit Euler integration is known to be sensitive to high frequency noise, and may be corrupted by the IMU measurements in the velocity. An alternative is to use a higher order method such as the Runge-Kutta methods. A general second-order Runge-Kutta method, estimating the tangent at the midpoint of the time step, is given by

$$\begin{aligned} y_{t+\tau} &= y_t + \tau k_2 \\ k_2 &= \tau \mathrm{f}(t + \frac{1}{2}\tau, y_t + \frac{1}{2}k_1) \\ k_1 &= \tau \mathrm{f}(t, y_t). \end{aligned} \tag{4.85}$$

Applied to the observer presented in equation (4.72), one has

$$\begin{aligned} \hat{\Omega}(t) &= \Omega_y(t) + k_{P_\Omega} \operatorname{vex}(\mathbb{P}_a(\hat{R}^\top(t) R_y(t)) \\ \hat{V}(t) &= V_y(t) - (\hat{\Omega}(t) - \Omega_y(t))_\times \hat{P}(t) - k_{P_p}(\hat{P}(t) - P(t)) \\ \hat{\Xi}(t) &= (\hat{\Omega}(t), \hat{V}(t))^\wedge \\ \hat{T}(t + \frac{1}{2}\tau) &= \exp(\frac{1}{2}\hat{T}(t)\hat{\Xi}(t)\hat{T}^{-1}(t))\hat{T}(t) \\ \hat{\Omega}(t + \frac{1}{2}\tau) &= \Omega_y(t) + k_{P_\Omega} \operatorname{vex}(\mathbb{P}_a(\hat{R}^\top(t + \frac{1}{2}\tau) R_y(t)) \\ \hat{V}(t + \frac{1}{2}\tau) &= V_y(t) - (\hat{\Omega}(t + \frac{1}{2}\tau) - \Omega_y(t))_\times \hat{P}(t + \frac{1}{2}\tau) - k_{P_p}(\hat{P}(t + \frac{1}{2}\tau) - P(t)) \\ \hat{\Xi}(t + \frac{1}{2}\tau) &= \left(\hat{\Omega}(t + \frac{1}{2}\tau), \hat{V}(t + \frac{1}{2}\tau)\right)^\wedge \\ \hat{T}(t + \tau) &= \exp(\frac{1}{2}\hat{T}(t + \frac{1}{2}\tau)\hat{\Xi}(t + \frac{1}{2}\tau)\hat{T}^{-1}(t + \frac{1}{2}\tau))\hat{T}(t) \end{aligned} \tag{4.86}$$

It is also possible to apply symplectic integrator methods to this problem. Symplectic integrators are numerical integration techniques with the key property that they preserve symplectic invariants, in this case the group structure, while integrating the equation. Symplectic integrators were first proposed by (De Vogelaere 1956) in unpublished work and subsequently rediscovered by Ruth (1983) and Channell (1983). The introductions of Crouch and Grossman (1993), Channell and Scovel (1990) provide good historical reviews of symplectic integration. Park and Chung (2005) provides a review of symplectic integration techniques with relevance to $\mathrm{SE}(3)$.

Symplectic integration techniques were not used in this work as simple Euler and Runge-Kutta integration schemes were found to keep the solution on the Manifold under all well behaved operating conditions. That is, if the solution left the manifold, there were more serious problems than the choice integration scheme, such as an incorrect design choice leading to unbounded growth of the innovation term.

4.5.2 Gain selection

Corresponding to the analogy to linear complementary filters made in Section 4.1.2 for this family of observers, the values of gains k_{P_Ω} and k_{P_p} determine the crossover frequencies in the frequency response of the rotation and translation components of the state estimate, respectively. Specifically, the gains determine the crossover frequencies between the feed-forward components of estimates $\hat{\Omega}$ and $\hat{V}$, and the correction terms ξ_Ω and ξ_V.

Gain values corresponds to the crossover frequencies in radians per second. Gain values will typically be selected based on analysis of the sensors used, but will lie somewhere between zero and the Nyquist frequency of the sampling rate of the pose measurement. Values higher than the Nyquist frequency of the pose measurement may be used to aggressively counteract off-set errors occurring due to dropped frames or missing pose measurements when tracking moving targets.

Using the zero-coupling Rigid Body Transformation Error Observer of Section 4.5, it is observed that the rotation and translation errors are not individually strictly decreasing. The cost function permits a trade of error energy between the rotation and translation errors, causing the apparent divergence of the translation error in exchange for convergence of the rotation error under periods of high angular velocity. The ratio $\frac{k_{P_\Omega}}{k_{P_p}}$ determines the relative timing and magnitude of this divergence. A high ratio will delay the divergence and spread it over time. Conversely a low value may cause an immediate, sharp, spike.

4.5.3 Simulation Results

The observers presented in Theorem 4.3.1 and Theorem 4.4.1 has been implemented in MATLAB 7.1 as a discrete event simulation. The observers have been applied to simulations of static systems ($\Xi = 0$), with the initial values of true system, T, and estimate, $\hat{T}$, selected randomly such that

- The rotation, R, is initiated to a rotation of $\pi - 0.1$ around random axis selected uniformly.

- The position, p, is a selected from the cube $(-10..10, -10..10, -10..10)$ under a uniform random distribution.

Gain	**Value**
k_{P_Ω}: Orientation gain	1
k_{P_p}: Position gain	1

Table 4.2: Observer gains used in simulations depicted in Figures 4.7, 4.8, 4.9, 4.10, 4.7

The simulations have been run at 100 Hz, using synchronized velocity and pose measurements. White noise was added to measurements as per the measurement model detailed in Section 4.1.2. Gains used are given in Table 4.2.

Figure 4.7 depicts a typical result when all noise variances are set to zero.

In simulations using noisy measurements, convergence rates of the system were similar to the noiseless case for noise on the measurements R_y, P_y, V_y and Ω_y. Figure 4.8 depicts a simulation with even levels of noise on each measurement. The magnitude of the variance in the estimate, due to measurement noise, was small for noise in measurements R_y, P_y and V_y, but larger for comparative levels of noise in Ω_y. Figure 4.10 depicts a typical result with no angular velocity measurement noise, while Figure 4.9 depicts a typical result with only angular velocity measurement noise. Contrasting these figures with Figure 4.8 illustrates the impact of angular velocity measurement noise on estimator performance.

Figures 4.11 and 4.12 depict typical results for the Zero Coupling Rigid Body Transformation Error Observer of Section 4.5 in the absence of measurement noise. Note the position estimate no longer converges in a purely exponential fashion. Instead, convergence is slowed while the rate of angular convergence is high, an effect controlled by the ratio between gains k_{P_Ω} and k_{P_p} as discussed in Section 4.5.2.

4.5.4 Experimental Results

The Zero Coupling Rigid Body Transformation Error Observer presented in section observer presented in Section 4.5 has been implemented in MATLAB and applied to the experimental data obtained by Thibault Cheviron (Cheviron et al. 2007), described in Section 4.2.3. The experimental platform consisted of an IMU and webcam mounted on a small scale helicopter. Data capture rates were 50 Hz for the IMU and 10 Hz for the vision sensor. The experiment consisted of a manual quasi-stationary

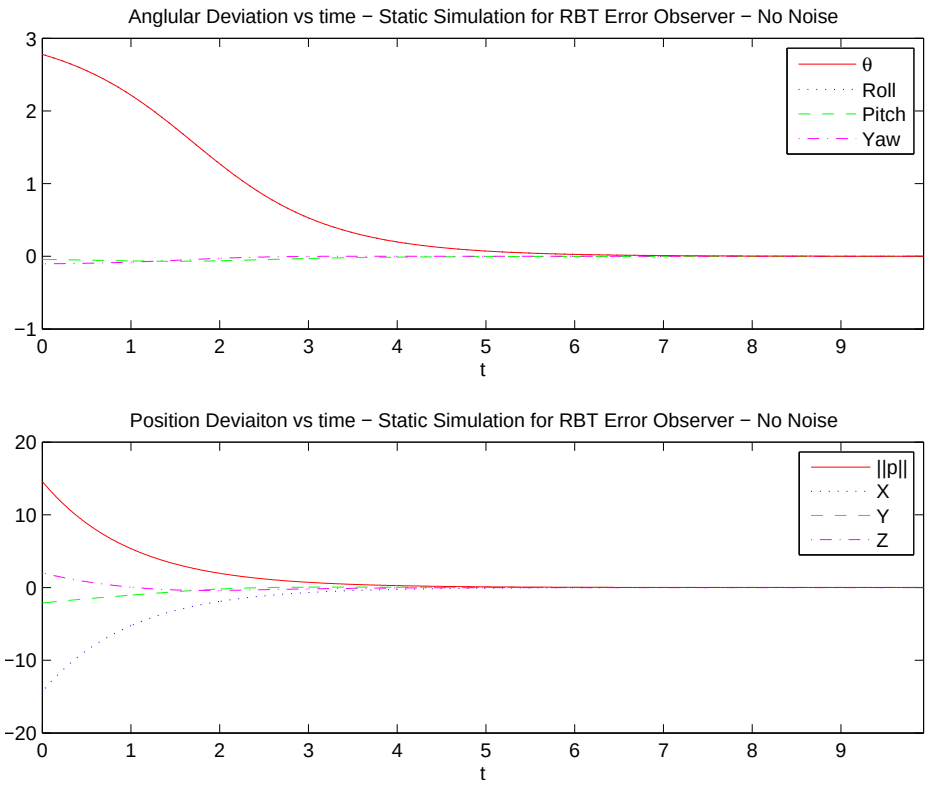

Figure 4.7: Simulation result showing attitude and position error in the inertial frame for Rigid Body Transformation Error Observer using observer gains given in Table 4.2. Static simulation with $\Xi = 0$, $T(0)$ and $\hat{T}(0)$ selected randomly and no sensor noise. Typical result from repeated testing.

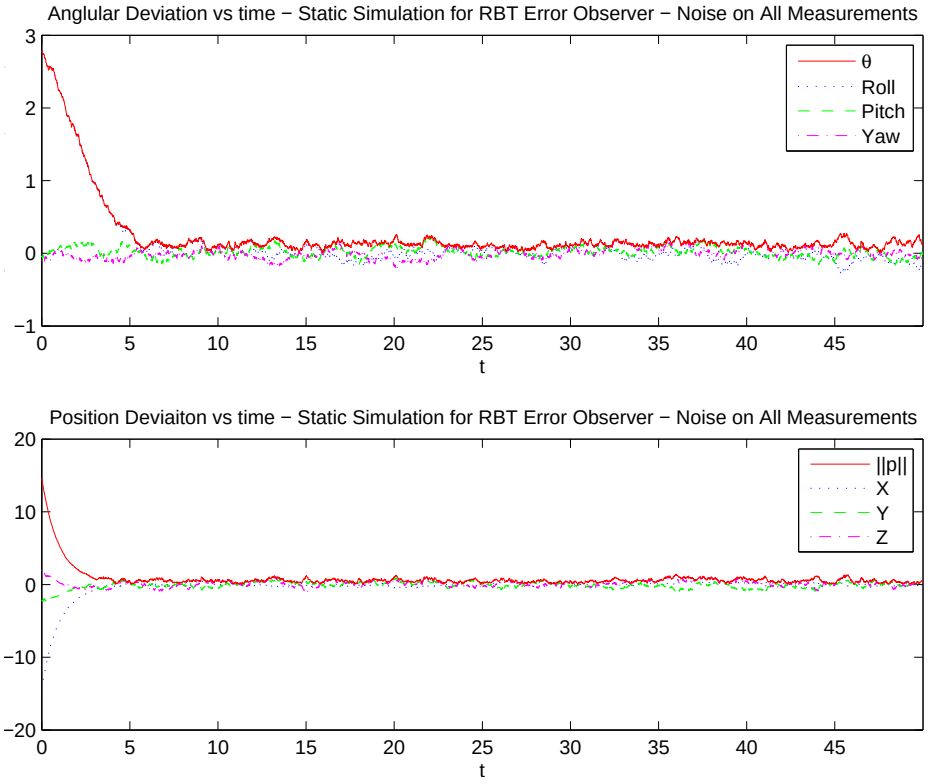

Figure 4.8: Simulation result showing attitude and position error in the inertial frame for Rigid Body Transformation Error Observer using observer gains given in Table 4.2. Static simulation with $\Xi = 0$, $T(0)$ and $\hat{T}(0)$ selected randomly and noise variances of 1.0 on all sensors. Typical result from repeated testing.

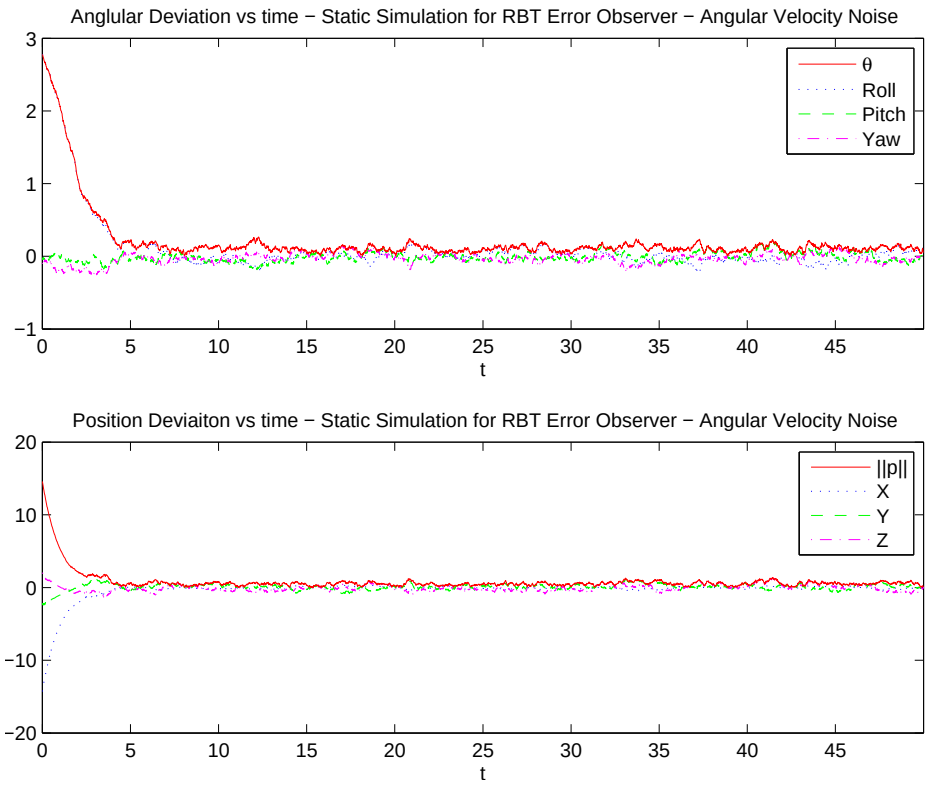

Figure 4.9: Simulation result showing attitude and position error in the inertial frame for Rigid Body Transformation Error Observer using observer gains given in Table 4.2. Static simulation with $\Xi = 0$, $T(0)$ and $\hat{T}(0)$ selected randomly and with noise variance of 1.0 on only the angular velocity sensor. Typical result from repeated testing.

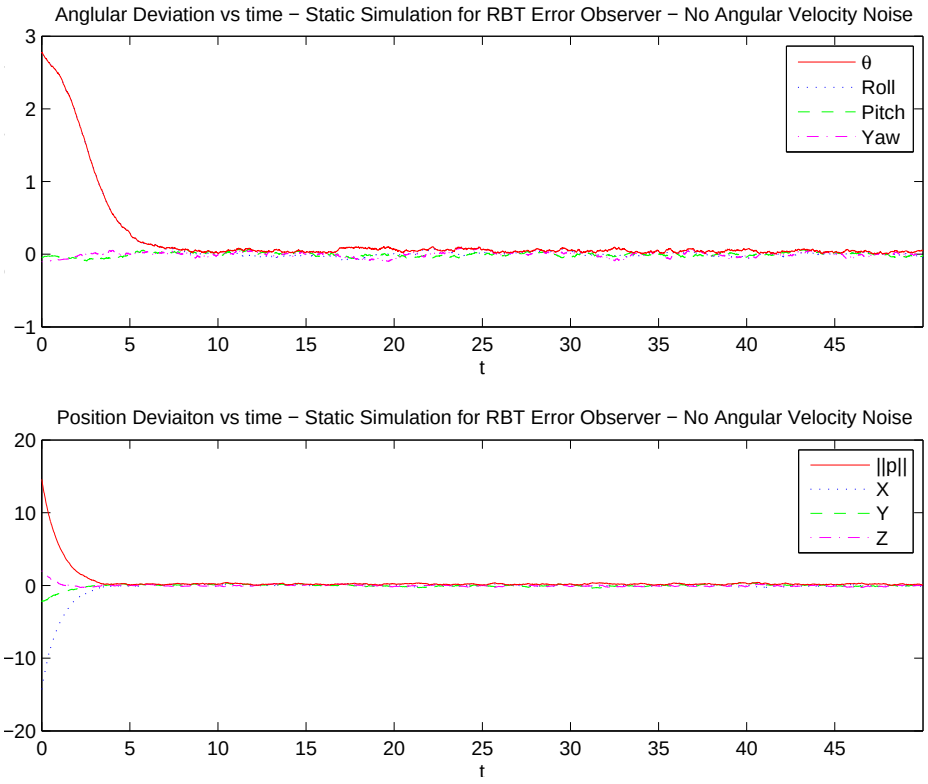

Figure 4.10: Simulation result showing attitude and position error in the inertial frame for Rigid Body Transformation Error Observer using observer gains given in Table 4.2. Static simulation with $\Xi = 0$, $T(0)$ and $\hat{T}(0)$ selected randomly and with noise variances of 1.0 on all sensors except the angular velocity sensor. Typical result from repeated testing.

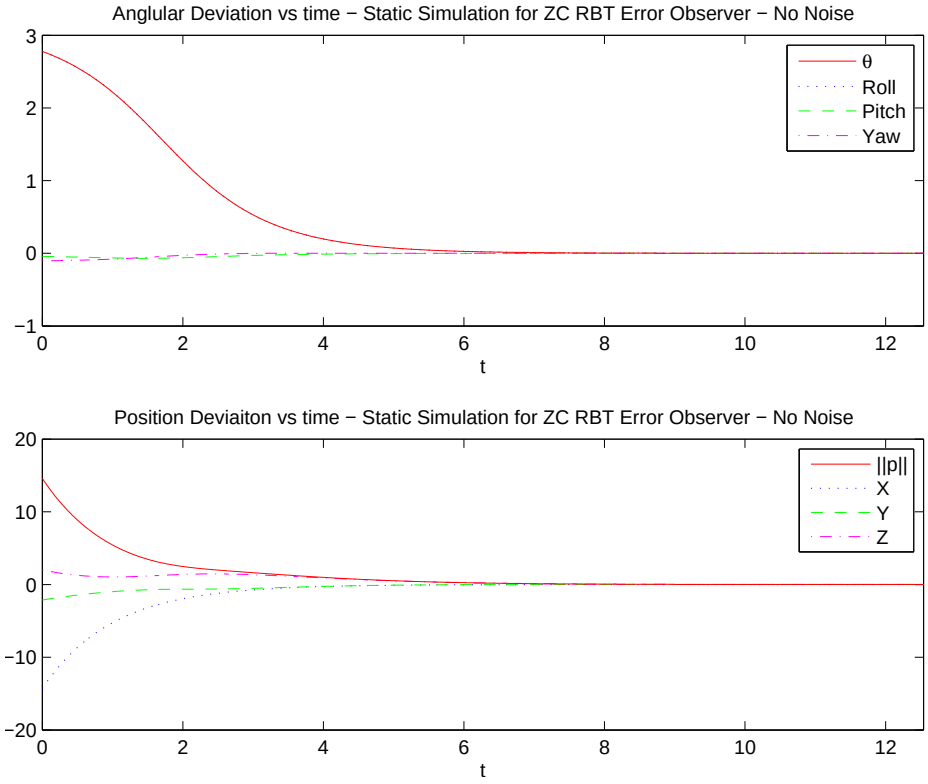

Figure 4.11: Simulation result showing attitude and position error in the inertial frame for Zero Coupling Rigid Body Transformation Error Observer using observer gains given in Table 4.2. Static simulation with $\Xi = 0$, $T(0)$ and $\hat{T}(0)$ selected randomly and no sensor noise. Typical result from repeated testing.

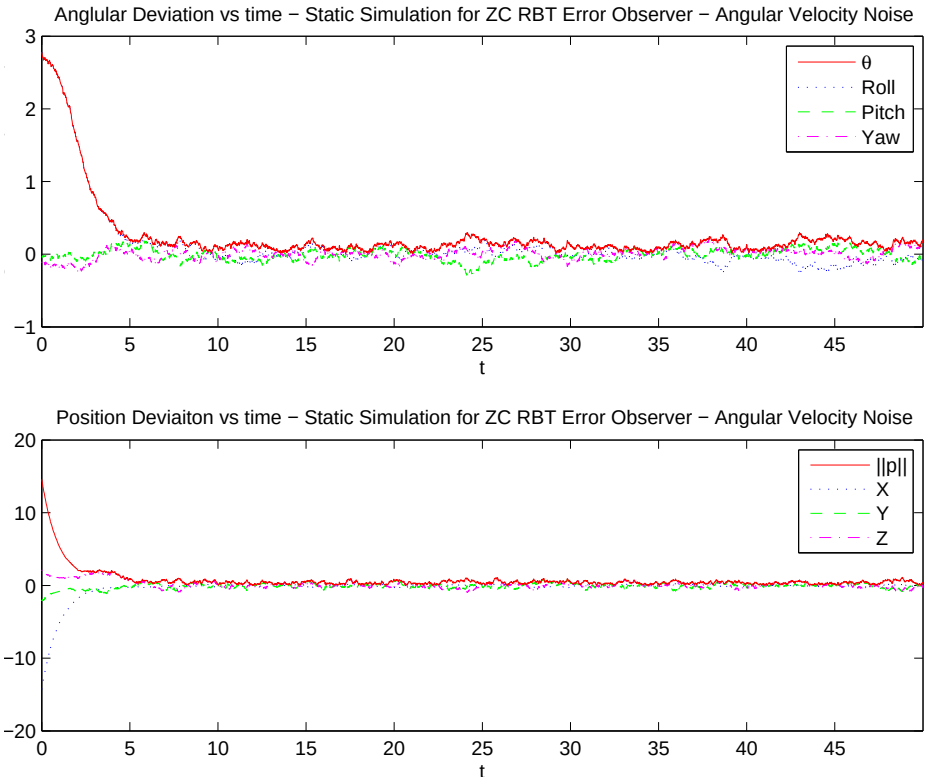

Figure 4.12: Simulation result showing attitude and position error in the inertial frame for Zero Coupling Rigid Body Transformation Error Observer using observer gains given in Table 4.2. Static simulation with $\Xi = 0$, $T(0)$ and $\hat{T}(0)$ selected randomly and with noise variance of 1.0 on only the angular velocity sensor. Typical result from repeated testing.

Gain	**Value**
k_{P_Ω}: Orientation gain	1
k_{P_p}: Position gain	5

Table 4.3: Observer gains used experimental results with Zero Coupling Rigid Body Transformation Error Observer

(i.e. hover) flight, such that no visual feature occlusion occurred. Data from the vision sensor and IMU were harmonised as in Section 4.2.3.

The observer was initialised with $\hat{T}(0) = I$ the gains given in Table 4.3. A pre-filter was used to estimate velocity from acceleration and pose measurements. No bias correction was performed on either the gyroscope measurements or velocity estimate.

The estimated helicopter attitude and position are depicted in figures 4.13 and 4.14. Again, the estimated pose is depicted in blue and contrasted with the camera measurements in red and, in the case of attitude, the industrial filter of the IMU in green.

These figures demonstrate the performance of the Zero Coupling Rigid Body Transformation Error Observer on real world data and in the presence of substantial initial value error.

4.6 Chapter Summary

In this chapter I have developed a series of observers for pose from inertial and vision measurements. The key approach was to exploit the underlying $\mathrm{SO}(3) \times \mathbb{R}^3$ semi-direct product structure of $\mathrm{SE}(3)$ to form observers for the attitude and position components separately.

The first pose observer proposed in Section 4.2, the Cascaded Pose Observer, tackles the problem by proposing a non-linear attitude observer and cascading this result into a non-linear position and velocity observer. Gyroscope and accelerometer biases are also estimated. The resulting system is locally exponentially convergent. Experimental results display good performance in the presence of measurement noise and inexact initial conditions.

In Section 4.3 a pair of observers are proposed which estimate orientation and position simultaneously. These observer are simple to design and tune, with a design analogous to linear complementary filters. The observer are almost-globally asymptotically

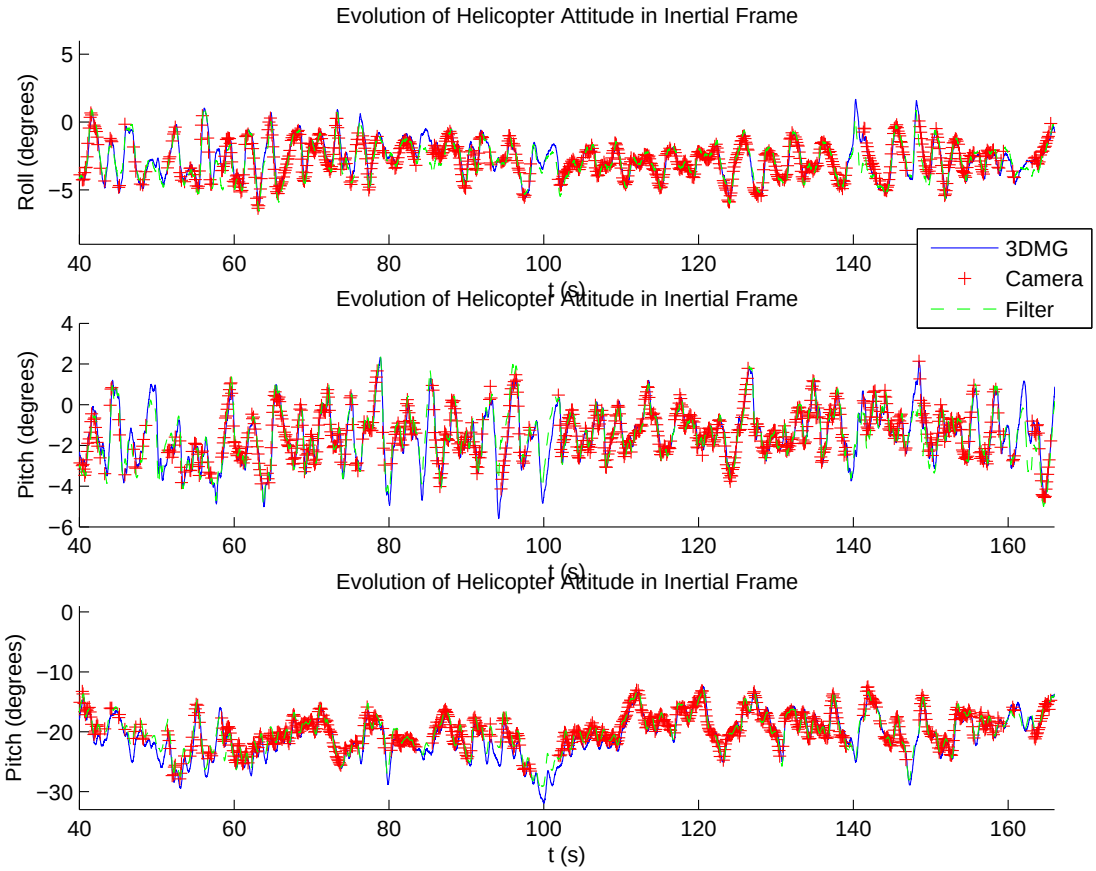

Figure 4.13: Estimate of helicopter attitude in the inertial frame produced by Zero Coupling Rigid Body Transformation Error Observer using observer gains given in Table 4.3.

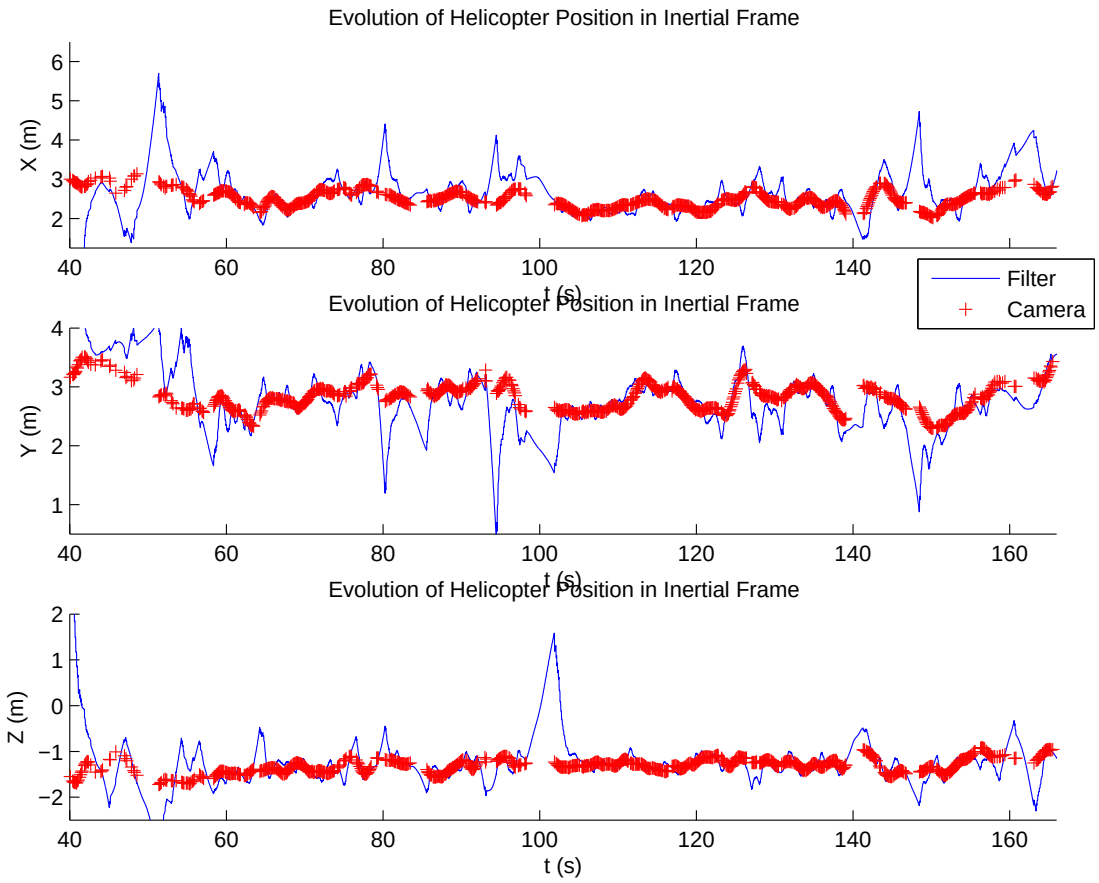

Figure 4.14: Estimate of helicopter position in the inertial frame produced by Zero Coupling Rigid Body Transformation Error Observer using observer gains given in Table 4.3.

and locally exponentially stable. In Section 4.4, the Rigid Body Transformation Error Observer is proposed, following from the identification of the *Rigid Body Transformation error*, $\tilde{T} = \hat{T}T^{-1}$; a representation of the state error in the inertial frame. This observer maintain the simplicity and almost-global asymptotic and locally exponential stability of the observers proposed in Section 4.3 but eliminates vision measurements from the feed-forward term, permitting a multi-rate implementation.

A final observer is proposed in Section 4.5, by using input-to-state stability properties to simplify the Rigid Body Transformation Error Observer by further eliminating coupling between measurements. The observer maintains the almost-globally asymptotic and locally exponential stability, straightforward tuning process and insensitivity to initial conditions of the prior observers, with the addition of a separation of measurement noise processes and excellent suitability for a multi-rate implementation.

A combination of simulation and experimental results demonstrate the performance of these observers. Simulations demonstrate the convergence properties and insensitivity to initial conditions. Experiments were performed using a scale helicopter demonstrate tracking performance on real world data.

Chapter 5

Observer Design on the Special Euclidean Group $\mathrm{SE}(3)$

This chapter describes the design of an observer for both pose and velocity measurement bias, with the pose observer evolving directly on the the special Euclidean group $\mathrm{SE}(3)$ of dimension four. Unlike in the previous chapter, the the special Euclidean group $\mathrm{SE}(3)$ of dimension four manifold is treated holistically with no decompositions used.

A twelve state non-linear observer is developed that estimates pose together with biases on angular and linear velocity measurements from measurements of pose and angular and linear velocity. The observer is almost-globally asymptotically and locally exponentially stable.

Of particular novelty in the design of the pose observer is the choice of and interpretation given to the pose error used. It is shown that the correct pose measurement error to use corresponds to the expression of the pose error as a rigid body transformation in the inertial frame. The design of the pose observer directly on $\mathrm{SE}(3)$ results in the identification of innovation terms on the Lie Algebra $\mathfrak{se}(3)$ over $\mathrm{SE}(3)$ and a state evolving on $\mathrm{SE}(3) \times \mathfrak{se}(3)$.

A key practical property of this pose observer is the separation in the state dynamics between the pose and velocity inputs. This separation permits an asynchronous multi-rate implementation, an architecture that is particularly appropriate in the situation where velocity measurements are available at a substantially higher rate than the pose measurements. This separation together with the Lyapunov stability argument posed directly on $\mathrm{SE}(3)$ permits the observer to be driven with velocity measurements obtained in the inertial frame, the body-fixed frame or a specific orthogonal combination of the two.

Simulation and experimental results are presented for the observer, demonstrating performance in tracking, bias estimation and in the presence of measurement noise. Experimental results have been obtained using data collected from the experimental platform described in Chapter A.1, using an inertial and vision sensor attached to a robotic manipulator. Comparison with ground-truth data demonstrates observer accuracy under experimental conditions.

The contributions of this chapter are

- Development of an observer for pose, and linear and angular velocity measurement biase estimates, designed directly on SE(3), with an almost-global asymptotic Lyapunov stability argument and locally exponential stability argument.
- Formal identification of analogous observers using orthogonal combinations of velocity measurements in both the inertial and body-fixed frames.
- An algorithm for implementation of this observer family using asynchronous measurements arriving at multiple rates.

The material presented in this chapter extends material first reported in Baldwin et al. (2008).

5.1 Problem Formulation

Let $\mathcal{A}$ again denote an inertial frame attached to the earth such that e_3 points vertically down. Let $\mathcal{B}$ denote a body-fixed frame attached to a vehicle of interest at the center of mass. The origin of $\mathcal{B}$ expressed in $\mathcal{A}$ is given by the vector p and the attitude of $\mathcal{B}$ expressed in $\mathcal{A}$ is given by the rotation matrix R.

The pose of the body-fixed frame, (R, p) comprises both the attitude and position of $\mathcal{B}$ relative to $\mathcal{A}$. The pose can be interpreted as an element of SE(3) with the matrix representation, commonly known as homogenous coordinates,

$$T = \begin{pmatrix} R & p \\ 0 & 1 \end{pmatrix}. \tag{5.1}$$

This representation identifies SE(3) as a subgroup of the general linear group GL(4) of dimension four with the group operation of concatenation of transforms identified with matrix multiplication.

The homogenous coordinate 4×4 matrix has the triple interpretation as the pose of $\mathcal{B}$ expressed in $\mathcal{A}$, as the *coordinate frame transformation* mapping objects expressed in $\mathcal{B}$ to objects expressed in $\mathcal{A}$, and as the *rigid body transformation* moving an object from the pose given by the attitude and position of $\mathcal{A}$ to the attitude and position of $\mathcal{B}$, expressed in $\mathcal{A}$.

As previously, we adopt the convention that positions and vectors expressed in the inertial frame are denoted by lower case letters, and quantities expressed in other frames are denoted by upper case letters.

The kinematics of $\mathcal{B}$ are given by

$$\dot{R} = R\Omega_\times, \tag{5.2a}$$

$$\dot{p} = v, \tag{5.2b}$$

where Ω denotes the angular velocity of the body-fixed frame, expressed in the body-fixed frame, and v denotes the linear velocity of the body-fixed frame expressed in the inertial frame. The operator $(\cdot)_\times$ takes the vector $\Omega \in \mathbb{R}^3$ to the skew-symmetric matrix

$$\Omega_\times = \begin{pmatrix} 0 & -\Omega_3 & \Omega_2 \\ \Omega_3 & 0 & -\Omega_1 \\ -\Omega_2 & \Omega_1 & 0 \end{pmatrix}. \tag{5.3}$$

Represented in $\mathrm{SE}(3)$, the kinematics of $\mathcal{B}$ are

$$\dot{T} = T\Xi \tag{5.4}$$

where $\Xi \in \mathfrak{se}(3)$ is the 6 dimensional velocity of $\mathcal{B}$ expressed in $\mathcal{B}$, and

$$\Xi = (\Omega, V)^\wedge, \tag{5.5}$$

with the wedge superscript denoting the correspondence between the body-fixed frame angular and linear velocities Ω and V to an element $\Xi \in \mathfrak{se}(3)$,

$$(\Omega, V)^\wedge = \begin{pmatrix} \Omega_\times & V \\ 0 & 0 \end{pmatrix}. \tag{5.6}$$

and V is the linear velocity of the origin of $\mathcal{B}$ expressed in $\mathcal{B}$. That is,

$$V = R^\top v. \tag{5.7}$$

It is easily verified that equation (6.4) is a matrix representation of the kinematics in equation (5.2).

Not that six-dimensional velocity vectors in $\mathfrak{se}(3)$, such as Ξ in equation (6.4) are associated with a frame of reference in which they are expressed. Thus Ξ gives the velocity of the body-fixed frame $\mathcal{B}$ expressed in $\mathcal{B}$.

The adjoint operator $\mathrm{Ad}_T : \mathfrak{se}(3) \to \mathfrak{se}(3)$ is defined, as in e.g. Murray et al. (1993), as

$$\mathrm{Ad}_T \, \Xi = T \Xi T^{-1}. \tag{5.8}$$

The adjoint by T, Ad_T, applied to Ξ acts to map the velocity of $\mathcal{B}$ relative to $\mathcal{A}$ expressed in $\mathcal{B}$ to the negative of the velocity of $\mathcal{A}$ relative to $\mathcal{B}$ expressed in $\mathcal{A}$. This is illustrated by calculating the kinematics of T^{-1}, the pose of $\mathcal{A}$ expressed in $\mathcal{B}$.

$$\dot{T}^{-1} = -\Xi T^{-1} = -T^{-1} \, \mathrm{Ad}_T \, \Xi. \tag{5.9}$$

For a connected Lie group, such as SE(3), a relation between the group and the Lie algebra of the group is given by the exponential map

$$\exp : \mathfrak{g} \to \mathrm{G}, \quad \sigma \mapsto \exp(\sigma). \tag{5.10}$$

The exponential map has the interpretation of mapping a direction and magnitude, given by the element of the Lie algebra, to an element of the Lie group. For example, mapping a velocity vector to the displacement obtained by moving with that velocity for unit time. For a matrix Lie group, the exponential map is given by the matrix exponential.

Finally, I present some definitions that will be required in the sequel. Define an inner product and associated norm on the set of $\mathbb{R}^{n \times n}$ matrices as

$$\langle M, N \rangle = \mathrm{tr}(M^\top N). \tag{5.11}$$

and

$$\|M\|_F^2 = \langle M, M \rangle = \mathrm{tr}(M^\top M) \tag{5.12}$$

where $\|(\cdot)\|_F$ is the standard Frobenius norm.

Let $\mathbb{P}_a$ and $\mathbb{P}_s$ be orthogonal projection operators with respect to the inner product equation (5.11), decomposing a matrix $M \in \mathbb{R}^{n \times n}$ into an anti-symmetric component $\mathbb{P}_a(M)$ and a symmetric component $\mathbb{P}_s(M)$. One has

$$\mathbb{P}_a(M) = \frac{1}{2}(M - M^\top), \tag{5.13a}$$

$$\mathbb{P}_s(M) = \frac{1}{2}(M + M^\top). \tag{5.13b}$$

Note that the anti-symmetric projection, $\mathbb{P}_a$, for $n = 3$ is also a projection from $\mathbb{R}^{3\times3}$ onto $\mathfrak{so}(3)$. An orthogonal projection $\mathbb{P}_{\mathfrak{se}(3)}$ from $\mathbb{R}^{4\times4}$ to $\mathfrak{se}(3)$ is defined by

$$\mathbb{P}_{\mathfrak{se}(3)}\left(\begin{bmatrix} A & B \\ C^T & D \end{bmatrix}\right) = \begin{bmatrix} \mathbb{P}_a(A) & B \\ 0 & 0 \end{bmatrix}, \tag{5.14}$$

where A is a 3×3 sub-matrix, B and C are 3×1 sub-matrices and D is a scalar.

5.1.1 Measurement Model

We again consider the vehicle of interest to be equipped with an inertial-vision sensor package; an Inertial Measurement Unit (IMU) and a monocular camera; both affixed to the craft and taking measurements in the body-fixed frame, $\mathcal{B}$. As throughout this thesis, the IMU operates at a measurement rate up to two orders of magnitude faster than the vision measurement rate. Additionally, the inertial measurements are corrupted by low frequency noise, while the vision measurements are stable at low frequencies and corrupted by high frequency noise. The complementary characteristics of these measurements will be exploited to form a high quality estimate.

In this chapter, we assume that measurements of the system velocity Ξ, including the angular and linear velocity components are available, such as from an IMU and linear velocity estimator as discussed in Section 2.2.3. The velocity measurements are assumed to be corrupted by slowly time-varying biases, b_Ω and b_V, and zero-mean Gaussian noise processes n_Ω and n_V. In particular, we assume the biases are sufficiently slowly varying that they may be treated as constant with respect to the time scale of observer convergence.

Using a vision sensor, we make observations of a constellation of static points whose position in the inertial frame is known. For each frame, from the observed image coordinates of three or more points, the pose of the camera can be reconstructed; a problem known as the perspective-n-point problem (Fischler and Bolles 1981). Using the procedure outlined in Section 3.7.3, Chapter A.1, employing the pose estimation algorithm of the `compute_extrinsic` function of the MATLAB camera calibration toolbox (Bouguet 2008). As discussed in Section 2.2.2, alternate sensors, such as Global Positioning System (GPS), may be substituted for a vision sensor under appropriate conditions.

Consequently in this chapter we treat the camera as providing bias-free measurements of T^{-1} at low rate, corrupted by zero-mean Gaussian noise process n_T, which

may be decomposed into orthogonal rotation and position noise processes n_Ω and n_p

One has the measurement model

$$\begin{aligned} T_y^{-1} &= \exp(n_T(t))T^{-1} && \text{(5.15a)} \\ &= \begin{pmatrix} R_y^\top & P_y \\ 0 & 1 \end{pmatrix} = \begin{pmatrix} \exp(n_R(t))R_y^\top & P_y(t)+n_p \\ 0 & 1 \end{pmatrix} \\ \Xi_y &= \Xi + n_\Xi(t) + b_\Xi && \text{(5.15b)} \\ &= (\Omega_y, V_y)^\wedge = (\Omega + n_\Omega(t) + b_\Omega, V + n_V(t) + b_V)^\wedge \end{aligned}$$

where $n_{(\cdot)}(t)$ denotes a zero-mean Gaussian noise process and $b_{(\cdot)}$ denotes a constant bias term.

To provide context for the following theoretical developments, it is worth noting that commercial grade IMUs, such as the 3DM-GX1, supply velocity measurements at rates of up to 300 Hz. With low frame rates and the additional overhead of calculating pose estimates, vision sensors provide measurements at rates of around 5 to 10 Hz.

5.2 Pose and Velocity Bias Observer on SE(3)

In this section, I describe an almost-globally asymptotically and locally exponentially convergent observer on SE(3) for estimation of pose and velocity measurement bias from measurements of pose and velocity. I identify an error pose which exhibits invariant to transformation of the body-fixed frame when such transformation is replicated in the estimation frame. Using this error, I define a Lyapunov function and prove almost-global asymptotic convergence to a critical set, the existence of a sole stable critical point and locally exponential convergence for this observer.

From the system kinematics in equation (6.4) and the assumption of time-constant sensor biases, one has the composite pose and bias system (T, b_Ξ)

$$\dot{T} = T\Xi \tag{5.16a}$$

$$\dot{b}_\Xi = 0 \tag{5.16b}$$

with $T \in \mathrm{SE}(3)$ and $b_\Xi \in \mathfrak{se}(3)$.

Consider the problem of estimating the pose and velocity sensor bias for a vehicle. Let $\hat{T}$ denote an estimate of T and the define the estimation frame $\mathcal{E}$ as the pose given

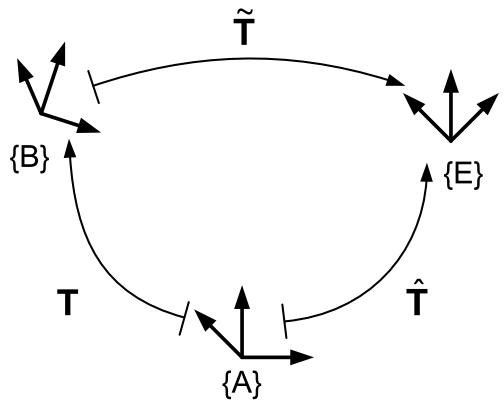

Figure 5.1: The rigid-body transformation from inertial frame, $\mathcal{A}$, to the body-fixed frame, $\mathcal{B}$, is represented by T and the transformation from $\mathcal{A}$ to the estimation frame, $\mathcal{E}$, is represented by $\hat{T}$. The transformation $\tilde{T}$, from the body fixed to estimation frames, expressed in $\mathcal{A}$, is then given by $\hat{T}T^{-1}$.

by $\hat{T}$ relative to the inertial frame $\mathcal{A}$. Then

$$\hat{T} = \begin{pmatrix} \hat{R} & \hat{p} \\ 0 & 1 \end{pmatrix} \tag{5.17}$$

where $\hat{R}$ is the rotation matrix giving the attitude of $\mathcal{E}$ in $\mathcal{A}$ and $\hat{p}$ is the origin of $\mathcal{E}$ expressed in $\mathcal{A}$.

The homogenous representation of T and $\hat{T}$ have the interpretation not only as the origin and attitude of $\mathcal{B}$ and $\mathcal{E}$ respectively, but also as the *rigid body transformation* moving an object an axes at the origin and identity attitude of $\mathcal{A}$ to the poses $\mathcal{B}$ and $\mathcal{E}$, respectively, expressed in $\mathcal{A}$. To obtain a well conditioned observer, we wish to also express an error term $\tilde{T}$ as a rigid body transformation moving an axes at the pose $\mathcal{B}$ to the pose $\mathcal{E}$, expressed in $\mathcal{A}$. To obtain this error, we apply the *coordinate frame transformation* from $\mathcal{A}$ to $\mathcal{B}$, T^{-1}, then apply the *rigid body transformation* from $\mathcal{B}$ to $\mathcal{E}$ expressed in $\mathcal{B}$, $T^{-1}\hat{T}$, and then apply the inverse *coordinate frame transformation*, from $\mathcal{B}$ to $\mathcal{A}$, T.

$$\tilde{T} = T(T^{-1}\hat{T})T^{-1} = \hat{T}T^{-1} \tag{5.18}$$

The relationship between T, $\hat{T}$ and $\tilde{T}$ is depicted in Figure 5.1. $\tilde{T}$ corresponds to the classical observer theory error $\tilde{x} = \hat{x} - x$; a vector from the true to the estimated system. Note that $\tilde{T}$ can only be interpreted as a rigid body transformation and does not have an interpretation as a coordinate frame transformation.

Theorem 5.2.1 (Pose and Velocity Measurement Bias Observer on $SE(3)$)**.** *Consider the system equation (5.16) and a bounded continuous solution $T(t)$ with bounded driving term $\Xi(t)$. Let $\Xi_y = \Xi + b_\Xi$ be a noise-free, biased measurement and $T_y^{-1} = T^{-1}$ be a measurement free of bias and noise.*

Define the observer

$$\dot{\hat{T}} = \hat{T}(\Xi_y - \hat{b}_\Xi + k_P \xi), \tag{5.19a}$$

$$\dot{\hat{b}}_\Xi = -k_I \beta, \tag{5.19b}$$

$$\xi = \mathrm{Ad}_{T_y^{-1}} \mathbb{P}_{\mathfrak{se}(3)}(\tilde{T}_y^{-1}), \tag{5.19c}$$

$$\beta = \mathbb{P}_{\mathfrak{se}(3)}(\mathrm{Ad}_{T_y^\top} \mathbb{P}_{\mathfrak{se}(3)}(\tilde{T}_y^{-1})); \tag{5.19d}$$

the errors

$$\tilde{T} = \hat{T} T^{-1}, \tag{5.20a}$$

$$\tilde{b}_\Xi = \hat{b}_\Xi - b_\Xi; \tag{5.20b}$$

and the set

$$U = \left\{ (\tilde{T}, \tilde{b}_\Xi) \in (\mathrm{SE}(3), \mathfrak{se}(3)) \mid \mathbb{P}_{\mathfrak{se}(3)}(\tilde{T}) = 0, \tilde{b}_\Xi = 0 \right\} \setminus \{(I,0)\}. \tag{5.21}$$

Then, for all positive choices of gains k_P, k_I, the error coordinates $(\tilde{T}, \tilde{b}_\Xi)$;

(i) converge to $U \cup \{(I,0)\}$ for all initial conditions,

(ii) are locally exponentially stable about $(I,0)$, and

(iii) in every neighbourhood of every point in U, there exists an initial condition $(\tilde{T}(0), \tilde{b}_\Xi(0))$ of an error trajectory converging to $(I,0)$. That is, the set U is unstable.

Proof of Theorem 5.2.1. This proof is set out as follows:

- Firstly, we will show global asymptotic convergence of the system to $U \cup \{(I,0)\}$ through application of Lyapunov's direct method and Barbalat's lemma.
- Secondly, we will show that in every neighbourhood of every point in the critical set, U, there is an initial condition $(\tilde{T}(0), \tilde{b}_\Xi(0))$ of an error trajectory converging to $(I,0)$ by application of a Lyapunov argument in a suitable representation.

- Thirdly, we compute a linearisation of a transformation of the error system and show that this linearisation is locally exponentially stable for the given exogenous signal $T(t)$, and hence all $T(t)$. This in turn is used to show locally exponential stability of the error system.

Recalling the definition of $\tilde{T}$ and $\tilde{b}_\Xi$, equation (5.20). Setting $\Xi_y \equiv \Xi + b_\Xi$, the pose deviation and bias error kinematics are

$$\dot{\tilde{T}} = \tilde{T}\,\mathrm{Ad}_T(k_P\xi - \tilde{b}_\Xi), \tag{5.22a}$$

$$\dot{\tilde{b}}_\Xi = -k_I\beta, \tag{5.22b}$$

Define a candidate Lyapunov function $\mathcal{L}$

$$\mathcal{L} \;= \tfrac{1}{2}\|I-\tilde{T}\|_F^2 + \tfrac{1}{2k_I}\|\tilde{b}_\Xi\|_F^2\,. \tag{5.23}$$

Taking the time derivative of $\mathcal{L}$ yields

$$\begin{aligned}\dot{\mathcal{L}} &= -\left\langle \dot{\tilde{T}}, I-\tilde{T}\right\rangle + \tfrac{1}{k_I}\left\langle \dot{\tilde{b}}_\Xi, \tilde{b}_\Xi\right\rangle \\ &= -\left\langle \tilde{T}\,\mathrm{Ad}_T(k_P\xi - \tilde{b}_\Xi), I-\tilde{T}\right\rangle - \left\langle \beta, \tilde{b}_\Xi\right\rangle \\ &= -k_P\left\langle \mathrm{Ad}_T(\xi), \tilde{T}^\top(I-\tilde{T})\right\rangle + \left\langle \tilde{b}_\Xi, \mathrm{Ad}_T^\top(\tilde{T}^\top(I-\tilde{T}))\right\rangle - \left\langle \beta, \tilde{b}_\Xi\right\rangle.\end{aligned} \tag{5.24}$$

Substituting ξ and β from equation (5.19c) and equation (5.19d), and setting $T_y^{-1} \equiv T^{-1}$ yields

$$\begin{aligned}\dot{\mathcal{L}} &= -k_P\left\langle \mathbb{P}_{\mathfrak{se}(3)}(\tilde{T}^{-1}), \tilde{T}^\top(I-\tilde{T})\right\rangle + \left\langle \mathrm{Ad}_T^\top(\tilde{T}^\top(I-\tilde{T})), \tilde{b}_\Xi\right\rangle \\ &\quad - \left\langle \mathbb{P}_{\mathfrak{se}(3)}(\mathrm{Ad}_{T^\top}\mathbb{P}_{\mathfrak{se}(3)}(\tilde{T}^{-1})), \tilde{b}_\Xi\right\rangle \\ &= -k_P\left\langle \mathbb{P}_{\mathfrak{se}(3)}(\tilde{T}^{-1}), \mathbb{P}_{\mathfrak{se}(3)}(\tilde{T}^\top(I-\tilde{T}))\right\rangle \\ &\quad + \left\langle \mathbb{P}_{\mathfrak{se}(3)}(\mathrm{Ad}_T^\top(\tilde{T}^\top(I-\tilde{T}))) - \mathbb{P}_{\mathfrak{se}(3)}(\mathrm{Ad}_{T^\top}\mathbb{P}_{\mathfrak{se}(3)}(\tilde{T}^{-1})), \tilde{b}_\Xi\right\rangle\end{aligned} \tag{5.25}$$

where in the last step, the fact that $\mathbb{P}_{\mathfrak{se}(3)}$ is an orthogonal projector is used. Further, the algebraic equalities

$$\mathbb{P}_{\mathfrak{se}(3)}(\tilde{T}^\top(I-\tilde{T})) = \mathbb{P}_{\mathfrak{se}(3)}(\tilde{T}^{-1}), \tag{5.26a}$$

$$\mathbb{P}_{\mathfrak{se}(3)}(\mathrm{Ad}_{T^\top}(\tilde{T}^\top(I-\tilde{T}))) = \mathbb{P}_{\mathfrak{se}(3)}(\mathrm{Ad}_{T^\top}\mathbb{P}_{\mathfrak{se}(3)}(\tilde{T}^{-1})), \tag{5.26b}$$

when substituted into $\dot{\mathcal{L}}$, yield

$$\dot{\mathcal{L}} = -k_P\,\|\mathbb{P}_{\mathfrak{se}(3)}(\tilde{T}^{-1})\|_F^2 \tag{5.27}$$

Consider the transformed variable $S = \tilde{T} - I$. Note that $\mathbb{P}_{\mathfrak{se}(3)}(\tilde{T}^{-1}) = \mathbb{P}_{\mathfrak{se}(3)}((S+I)^{-1})$. The right hand side of $(\dot{S}, \dot{\tilde{b}}_\Xi)$ is continuous in t, equal to 0 at $(S, \tilde{b}_\Xi) = 0$, locally Lipschitz in $(S, \tilde{b}_\Xi)$ and uniformly Lipschitz in t. In coordinates $(S, \tilde{b}_\Xi)$ it is easily seen that $\mathcal{L} = \frac{1}{2}\|S\|^2 + \frac{1}{2k_I}\|\tilde{b}_\Xi\|^2$ is radially unbounded, positive definite and has negative definite time derivative. Applying Theorem 8.4 of Khalil (2002), a special case of of Barbalat's lemma, one obtains $\lim_{t\to\infty} \dot{\mathcal{L}} = 0$.

From equation (5.27) one can see that $\dot{\mathcal{L}} = 0$ contains only the trajectories where $\mathbb{P}_{\mathfrak{se}(3)}(\tilde{T}^{-1}) = 0$. Direct calculations from equation (5.22a), identify the invariant set for $\mathbb{P}_{\mathfrak{se}(3)}(\tilde{T}^{-1}) = 0$ as

$$\left\{(\tilde{T}, \tilde{b}_\Xi) \in (\mathrm{SE}(3), \mathfrak{se}(3)) \mid \mathbb{P}_{\mathfrak{se}(3)}(\tilde{T}) = 0, \tilde{b_\Xi} = 0\right\}. \tag{5.28}$$

Hence for all initial conditions $(\tilde{T}, \tilde{B})$ is asymptotically convergent to $U \cup \{(I,0)\}$, proving claim (i).

Consider the angle-axis-position representation of an element of SE(3), (γ, θ, p), where γ and θ are the axis and angle of rotation of the attitude component of pose, and p is the position. Note that restricted to $\tilde{b}_\Xi = 0$ and $\tilde{p} = 0$, $\mathcal{L}$ reduces to $\mathcal{L} = 2(1 - \cos(\theta))$ by application of Rodrigues' rotation formula, see e.g. Murray et al. (1993). Moreover $\{\tilde{T} \in \mathrm{SE}(3) \mid \mathbb{P}_{\mathfrak{se}(3)}(\tilde{T}^{-1}) = 0\} \backslash \{I\}$ is characterised by $\theta = \pm\pi$. Hence, any open ball centred on $(\tilde{T}_U, \tilde{b}_{\Xi_U}) \in U$ contains points $(\tilde{T}, \tilde{b}_\Xi)$ for which $\theta \neq \pm\pi$, and thus$\mathcal{L}(\tilde{T}, \tilde{b}_\Xi) < \mathcal{L}(\tilde{T}_U, \tilde{b}_{\Xi_U})$. By monotonicity of $\mathcal{L}$, these points diverge from U and must converge to $(I,0)$, proving claim (iii).

To prove locally exponential stability, we use a linearisation of a system related to the error system $(\tilde{T}, \tilde{b}_\Xi)$. Let

$$\bar{R} = R^{-1}\tilde{R}R, \tag{5.29a}$$

$$\Delta P = = \hat{R}^{-1}\tilde{p} = \hat{P} - P. \tag{5.29b}$$

As $(\bar{R}, \Delta P, \tilde{b}_\xi) \to (I,0,0)$, then $(\tilde{T}, \tilde{B}) \to (I,0)$ with corresponding rate of convergence. A linearisation of $(\bar{R}, \Delta P, \tilde{B})$ about $(I,0,0)$ is given by $\bar{R} = I + x_{1\times}$, $\Delta P = x_3$, $\tilde{b}_\Xi = (-x_2, x_4)^\wedge$, where $x_1, x_2, x_3, x_4 \in \mathbb{R}^3$. The linearised dynamics are given by

$$\dot{x}_1 = -\Omega_\times x_1 - k_P x_1 + x_2, \tag{5.30a}$$

$$\dot{x}_2 = -k_I x_1 + \frac{k_I}{2} P_\times x_3, \tag{5.30b}$$

$$\dot{x}_3 = -\Omega_\times x_3 - k_P x_3 + P_\times x_2 + x_4, \tag{5.30c}$$

$$\dot{x}_4 = -k_I x_3. \tag{5.30d}$$

Consider a Lyapunov function given by

$$\mathcal{W} = \frac{\alpha_1}{2}\|x_1\|_2^2 - \alpha_2 x_1^\top x_2 + \frac{\alpha_3}{2}\|x_2\|_2^2 + \frac{\beta_1}{2}\|x_3\|_2^2 - \beta_2 x_3^\top x_4 + \frac{\beta_3}{2}\|x_4\|_2^2, \tag{5.31}$$

where α_1, α_2, α_3, β_1, β_2 and β_3 are positive constant chosen subject to algorithms given in Appendix B.

A principally mechanical proof then shows global exponential stability of the lienarisation and hence locally exponential stability of $(\bar{R}, \Delta P, \tilde{b}_\Xi)$, for all values of k_P and k_I, and all bounded continuous $T(t)$ and all bounded $\Xi(t)$.

The calculations and choice of constants α_1, α_2, α_3, β_1, β_2 and β_3 are omitted here for brevity. They are included, in full, in Appendix B.

It is easily verified that locally exponential stability of equation (5.29) implies locally exponential stability of $(\tilde{T}, \tilde{b}_\Xi)$ about $(I, 0)$, proving claim (ii).

□

Remark 5.2.2. Theorem 5.2.1 and its proof have the following consequences:

1. Since in every neighbourhood of every point in the critical set U there is an initial condition of an error trajectory leading to $(I, 0)$, we call U the unstable critical set for the error system. The set U is identified as the set with orientation errors of angle $\pm\pi$ and zero position and bias error. The geometry of U and $(I, 0)$ in the system is depicted in Figure 5.2.

2. Real world measurements can often contain low-magnitude zero-mean noise and time varying biases, as discussed in Section 5.1.1. The pose filter equation (5.19) is applicable to systems with these measurements as its locally exponential convergence properties act to dominate low-magnitude noise and an argument of time scale separation ensures tracking of time varying biases.

3. Note that the pose estimate dynamics, $\hat{\Xi} := \Xi_y - \hat{b}_\Xi + k_P \xi$, and its gain, k_P, may be decomposed into rotational and translational components. Setting $(\hat{\Omega}, \hat{V})^\wedge := \hat{\Xi}$, and letting k_{P_Ω} and k_{P_p} be the rotation and translational proportional gains, one has

$$\hat{\Omega}_\times = \Omega_{y_\times} - \hat{b}_{\Omega_\times} + k_{P_\Omega} \operatorname{Ad}_{R_y^{-1}} \left(\mathbb{P}_a(\tilde{R}_y^{-1}) \right), \tag{5.32a}$$

$$\hat{V} = V_y - \hat{b}_V - k_{P_p} \operatorname{Ad}_{R_y^{-1}} \left(\mathbb{P}_a(\tilde{R}_y^{-1}) \right) P_y + k_{P_p}(\hat{P} - P_y), \tag{5.32b}$$

where $\tilde{R}_y = \hat{R} R_y^{-1}$ is the error composed using the measured rotation available in a physical implementation.

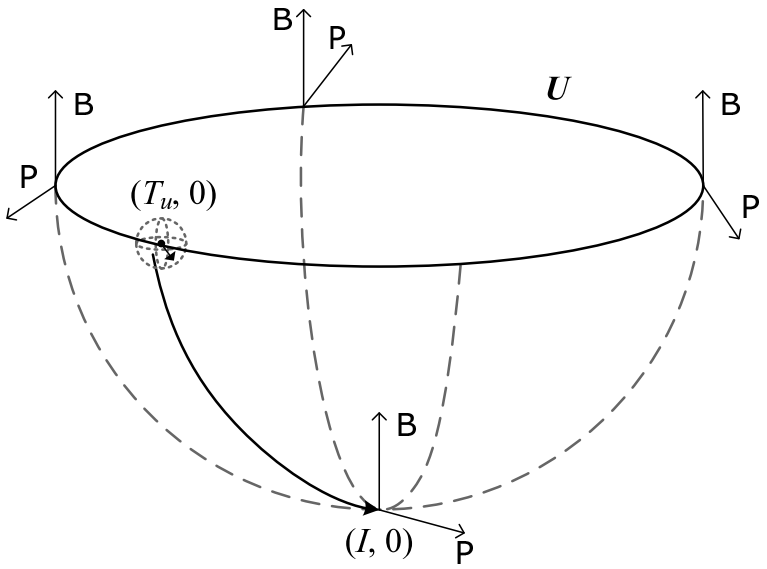

Figure 5.2: Sketch of the geometry of critical points of $\mathcal{L}$ on $\mathrm{SE}(3) \times \mathbb{R}^6$. On the half sphere representing $\mathrm{SO}(3)$ we represent the angle of rotation, θ, by vertical height in the bowl and the two dimensional axis of rotation by the angular position and heading on the bowl. The bias subspace, $b_\Xi = \mathbb{R}^6$ and the translational position subspace $p = \mathbb{R}^3$ are each attached at every point on the bowl, with p being attached in different directions around $\mathrm{SO}(3)$ according to the connection on $\mathrm{SE}(3)$. The critical sets $(I,0)$ and U form the base and rim of the $\mathrm{SO}(3)$ bowl respectively. Further, in every neighbourhood of every point $(T_U,0) \in U$, there is the initial conditions for a trajectory converging to $(I,0)$.

4. Similarly, the bias estimate kinematics, $\hat{b}_\Xi$, and gain, k_I, can be decomposed into angular and linear components. Setting $(\hat{b}_\Omega, \hat{b}_V)^\wedge := \hat{b}_\Xi$ and letting k_{I_Ω} and k_{I_p} be the rotation and translation bias gains, one has

$$\begin{aligned} \dot{\hat{b}}_{\Omega_\times} &= -k_{I_\Omega} \mathrm{Ad}_{R_y^{-1}} \mathbb{P}_a(\tilde{R}_y^{-1}) - k_{I_\Omega} \mathbb{P}_a(\hat{P} P_y^\top) \qquad (5.33a) \\ &= -k_{I_\Omega} \mathrm{Ad}_{R_y^{-1}} \mathbb{P}_a(\tilde{R}_y^{-1}) - k_{I_\Omega} \frac{1}{2}(P_y \times \hat{P})_\times, \\ \dot{\hat{b}}_V &= -k_{I_p}(\hat{P} - P_y). \qquad (5.33b) \end{aligned}$$

These equivalent disjoint terms may be used with independent positive gains k_{I_Ω} and k_{I_p}, to tune the angular and linear velocity bias estimate dynamics independently. For example, by setting a gain of $k_{I_p} = 0$, one may turn off linear velocity

bias estimation in the case where linear velocity is supplied by an unbiased estimator.

Excluding the addition of the bias terms, the filter dynamics expressed in equation (5.32a) and equation (5.32b) are similar to those proposed in equation (4.72) in Chapter 4 for the Rigid Body Transformation observer. The sole difference being the substitution of P_y for $\hat{P}$ in $\hat{V} = V_y - k_{P_p}(\hat{\Omega} - \Omega)\hat{P} + k_{P_p}(\hat{P} - P_y)$, resulting from strict adherence to the group structure. In the earlier work, I exploited the semi-direct product structure of SE(3) to design a filter, using the identity $\|I - T\|_F^2 = \|I - R\|_F^2 + \|P\|_2^2$, which permits partial exchange of quantities in the body-fixed and inertial frames in the cost function, yielding the alternate innovation term. Conversely, in this chapter, I perform observer design and analysis directly on SE(3).

Setting $k_{P_p} = 0$, $\hat{p}(0) = 0$, $k_{I_p} = 0$ and $\hat{b}_V = 0$, we obtain an orientation estimator on SO(3)

$$\dot{\hat{R}} = \hat{R}(\Omega_y - \hat{b}_\Omega + k_{P_\Omega}\mathbb{P}_a(\hat{R}^\top R_y))_\times, \tag{5.34a}$$

$$\dot{\hat{b}}_{\Omega_\times} = -k_{I_\Omega}\mathbb{P}_a(\hat{R}^\top R_y). \tag{5.34b}$$

This is the filter proposed in Equation (13) of Mahony et al. (2008). In Mahony et. al. the filter equation (5.34) was termed the passive complementary filter with bias correction, as a practical adjustment of their direct complementary filter. Both filters in Mahony et al. (2008) were analysed using a pose deviation measured as the *coordinate frame transformation* between the body-fixed and estimation frames. With Theorem 5.2.1, we have shown that the passive filter has an interpretation as the filter derived when measuring pose deviation as the *rigid-body transformation* between the body-fixed and estimation frame, represented in the inertial frame.

Note that the complementary filter may be depicted, analogously to linear systems, as a block diagram in Figure 5.3. This representation highlights the similarity to traditional proportional-integral design noted by Mahony et al. (2008). As discussed in Mahony et al. (2008) and presented in equation (5.34), the SO(3) sub-case is exactly a proportional integral controller with feedback term $\mathbb{P}_a(\hat{R}^\top R)$. In extending this metaphor to SE(3), we find that the pose and bias feedback terms, ξ and β are related but now depend on different non-linear adjoint transformations: $\mathrm{Ad}_{T^{-1}}$ and $\mathrm{Ad}_{T^\top}$.

Lastly, note that as with the Rigid Body Transformation Error Observer and Zero-Coupling Rigid Body Transformation Error Observer presented in Chapter 4, this observer again demonstrates a separation of measurement noise processes in the estimate

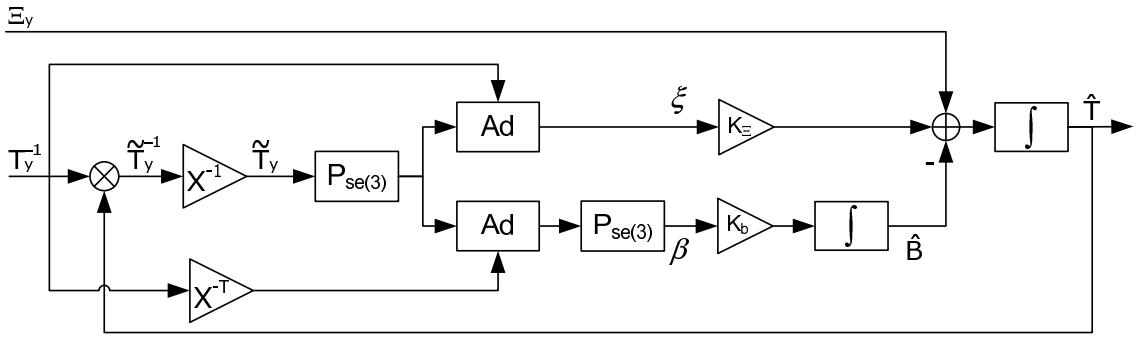

Figure 5.3: SE(3) Complementary Filter Block Diagram. Note the structure is analogous to classical proportional-integral control structures.

dynamics. Additionally, with two, or four, scalar gains to tune, the gain tuning process is straightforward.

5.2.1 Pose and Velocity Bias Observer for Partial Velocity Measurements in Mixed Frames

The following corollary extends the Theorem 5.2.1 to the case where the system velocity is measured using two or more measurement devices, with devices measuring velocity components in either the body-fixed or inertial frames. In particular, angular velocity is usually measurement in the body-fixed frame using an IMU. Linear velocity however can be difficult to obtain and may be measured in either the inertial or body-fixed frames. For example, a differential GPS system would provide inertial frame measurements of linear velocity, while a doppler laser system provied linear velocity in the body-fixed frame.

Consider the case where the system velocity Ξ is partially observable in each of two frames of reference, as ζ_A and ζ_B, where ζ_A is an observation in the inertial frame and ζ_B is an observation in the body-fixed frame. Let the velocity components observed in ζ_A and ζ_B be such that when transformed into a common frame of reference, they sum to give the total system velocity. That is

$$\Xi = \mathrm{Ad}_{T^{-1}}(\zeta_A) + \zeta_B. \tag{5.35}$$

Let $\mathbb{P}_A$ and $\mathbb{P}_B$ be two mutually-orthogonal projections of $\mathfrak{se}(3)$ conforming to one of three cases:

- $\mathbb{P}_A$ is the identity function and $\mathbb{P}_B$ the zero function,
- $\mathbb{P}_A$ is the zero function and $\mathbb{P}_B$ the identity function, or
- $\mathbb{P}_A$ preserves the linear velocity component and $\mathbb{P}_B$ preserves the angular velocity component.

Let ζ_A and ζ_B be related to the body-fixed frame velocity Ξ as

$$\begin{aligned} \zeta_A &= \mathrm{Ad}_T \, \mathbb{P}_A(\Xi), \\ \zeta_B &= \mathbb{P}_B(\Xi). \end{aligned} \tag{5.36}$$

Extending the measurement model introduced in Section 5.1.1, let measurements of ζ_A and ζ_B be given by

$$\begin{aligned} \zeta_{A_y} &= \mathrm{Ad}_T \, \mathbb{P}_A(\Xi) + n_{\zeta_A}(t) + b_{\zeta_A}, \\ \zeta_{B_y} &= \mathbb{P}_B(\Xi) + n_{\zeta_B}(t) + b_{\zeta_B} \end{aligned} \tag{5.37}$$

where $n_{(\cdot)}(t)$ is again a zero-mean Gaussian noise process and $b_{(\cdot)}$ denotes a constant bias term. Further, let n_{ζ_A}, b_{ζ_A}, n_{ζ_B} and b_{ζ_B} be restricted to projections of $\mathfrak{se}(3)$ corresponding to $\mathbb{P}_A$ and $\mathbb{P}_B$ respectively. That is, $\zeta_{B_y} = \mathbb{P}_B(\Xi_y)$.

Note that we now have one bias in the body-fixed frame, b_{ζ_B}, and one bias in the inertial frame, b_{ζ_A}, though these biases are on mutually orthogonal components of system velocity.

Corollary 5.2.3 (Pose and Velocity Measurement Bias Observer Driven By Velocity Measurements in Mixed Frames)**.** *Consider the system equation (5.16) and a bounded continuous solution $T(t)$ with bounded driving term $\Xi(t)$, with partial observations of $\Xi(t)$ as two mutually orthogonal components $\zeta_A(t)$, in the inertial frame, and $\zeta_B(t)$, in the body-fixed frame, as per equation (5.36). Let $\zeta_{A_y} = \zeta_A + b_{\zeta_A}$ and $\zeta_{B_y} = \zeta_B + b_{\zeta_B}$ be noise-free, biased measurements and $T_y^{-1} = T^{-1}$ be a measurement free of bias and noise.*

Define the observer

$$\dot{\hat{T}} = \mathrm{Ad}_{T_y^{-1}}(\zeta_{A_y} - \hat{b}_{\zeta_A})\hat{T} + \hat{T}(\zeta_{B_y} - \hat{b}_{\zeta_B}) + \hat{T}(k_P \xi), \tag{5.38a}$$

$$\dot{\hat{b}}_{\zeta_A} = -k_I \beta_A, \tag{5.38b}$$

$$\dot{\hat{b}}_{\zeta_B} = -k_I \beta_B, \tag{5.38c}$$

$$\beta_A = \mathbb{P}_A(\mathbb{P}_{\mathfrak{se}(3)}(\tilde{T}^{-1})), \tag{5.38d}$$

$$\beta_B = \mathbb{P}_B(\beta); \tag{5.38e}$$

and the errors

$$\tilde{b}_{\zeta_A} = \hat{b}_{\zeta_A} - b_{\zeta_A}, \tag{5.39a}$$
$$\tilde{b}_{\zeta_B} = \hat{b}_{\zeta_B} - b_{\zeta_B}; \tag{5.39b}$$

and the set

$$\begin{aligned} U = \big\{ (\tilde{T}, \tilde{b}_{\zeta_A}, \tilde{b}_{\zeta_B}) \in (\mathrm{SE}(3), \mathfrak{se}(3), \mathfrak{se}(3)) \mid \\ \mathbb{P}_{\mathfrak{se}(3)}(\tilde{T}) = 0, \tilde{b}_{\zeta_A} = 0, \tilde{b}_{\zeta_B} = 0 \big\} \setminus \{(I,0)\}. \end{aligned} \tag{5.40}$$

Let $\tilde{T}$, ξ and β be defined as in equation (5.20a), equation (5.19c) and equation (5.19d) respectively.

Then, for all positive choices of gains k_P, k_I, the error coordinates $(\tilde{T}, \tilde{b}_{\zeta_A}, \tilde{b}_{\zeta_B})$

(i) converge to $U \cup \{(I,0,0)\}$ for all initial conditions,

(ii) in every neighbourhood of every point in U, there exists an initial condition $(\tilde{T}(0), \tilde{b}_{\zeta_A}(0), \tilde{b}_{\zeta_B}(0))$ of an error trajectory converging to $(I,0,0)$. That is, the set U is unstable.

Proof of Corollary 5.2.3. Recall the definition of $\tilde{T}$, $\tilde{b}_{\zeta_A}$ and $\tilde{b}_{\zeta_B}$ from equation (5.20a) and equation (5.39). Setting $\zeta_{A_y} \equiv \zeta_A + b_{\zeta_A}$ and $\zeta_{B_y} \equiv \zeta_B + b_{\zeta_B}$, the pose deviation and bias error kinematics are

$$\dot{\tilde{T}} = \tilde{T}\,\mathrm{Ad}_T(k_P\xi - \mathrm{Ad}_{T^{-1}}(\tilde{b}_{\zeta_A}) - \tilde{b}_{\zeta_B}) \tag{5.41a}$$
$$\dot{\tilde{b}}_{\zeta_A} = -k_I \beta_A \tag{5.41b}$$
$$\dot{\tilde{b}}_{\zeta_B} = -k_I \beta_B \tag{5.41c}$$

Define the candidate Lyapunov function $\mathcal{W}$

$$\mathcal{W} = \tfrac{1}{2}\|I - \tilde{T}\|_F^2 + \tfrac{1}{2k_I}\|\tilde{b}_{\zeta_A}\|_F^2 + \tfrac{1}{2k_I}\|\tilde{b}_{\zeta_B}\|_F^2 \tag{5.42}$$

Taking the time derivative of $\mathcal{W}$ yields

$$\begin{aligned} \dot{\mathcal{W}} &= -\left\langle \mathrm{Ad}_T(k_P\xi - \mathrm{Ad}_{T^{-1}}(\tilde{b}_{\zeta_A}) - \tilde{b}_{\zeta_B}), \tilde{T}^\top(I - \tilde{T}) \right\rangle \\ &\quad - \left\langle \beta_A, \tilde{b}_{\zeta_A} \right\rangle - \left\langle \beta_B, \tilde{b}_{\zeta_A} \right\rangle \\ &= -k_P \left\langle \mathrm{Ad}_T\,\xi, \mathbb{P}_{\mathfrak{se}(3)}(\tilde{T}^\top(I - \tilde{T})) \right\rangle \\ &\quad + \left\langle \tilde{b}_{\zeta_A}, \mathbb{P}_A(\mathbb{P}_{\mathfrak{se}(3)}(\tilde{T}^\top(I - \tilde{T}))) - \beta_A \right\rangle \\ &\quad + \left\langle \tilde{b}_{\zeta_B}, \mathbb{P}_B(\mathbb{P}_{\mathfrak{se}(3)}(\mathrm{Ad}_{T^\top}(\tilde{T}^\top(I - \tilde{T})))) - \beta_B \right\rangle \\ &= -k_P \left\| \mathbb{P}_{\mathfrak{se}(3)}(\tilde{T}^1) \right\|_F^2 \end{aligned} \tag{5.43}$$

where in the last line we substitute for β_A, β_B and ξ from equation (5.38d), equation (5.38e) and equation (5.19c), using β from equation (5.19d) and employ the algebraic identities of equation (5.26).

From here, by an application of Barbalat's Lemma and unstable set argument analogous to those in the proof of Theorem 5.2.1, we prove claims (i) and (ii). □

Note that the estimate kinematics equation (5.38a) now explicitly couple the pose measurement T_y to velocity measurement ζ_{A_y}. This is required to retain the velocity invariance of error $\tilde{T}$, which is right invariant to synchronous velocity terms applied to T and $\hat{T}$. Alternative definitions of $\dot{\hat{T}}$, such as substituting $\hat{T}$ for T_y result break this property by driving T and $\hat{T}$ with different velocities due to coordinate frame transformation errors introduced in the approximation. However, in a practical application, an appropriate approximation of T_y at the sampling times of Ξ_y may yield acceptable results when used in feedback and under appropriate conditions. Such an approximation may include $\hat{T}$ for small initial condition errors or a zero-order hold of T_y for small sampling times.

The restriction of $\mathbb{P}_A$ and $\mathbb{P}_B$ to the three cases explicitly listed is necessary as these are the only three cases for which the corresponding measurement model, equation (5.37), admits a constant bias in both the body-fixed and inertial frames. Other orthogonal decompositions, such where $\mathbb{P}_A$ preserves the angular velocity component and $\mathbb{P}_B$ preserves the linear velocity component, result in measurement models that couple linear velocity, angular velocity and position in such a way as to not admit a physically realisable measurement model adhering to equation (5.35).

Further, from Corollary 5.2.3 further insight is gained into the innovation terms ξ and β. In particular, that ξ corresponds to an error vector in the inertial frame and β corresponds to an error vector in the body-fixed frame. Recall equation (5.43), one may alternately proceed

$$\begin{aligned}\dot{\mathcal{L}} &= -k_P \left\langle \mathrm{Ad}_T(\xi), \tilde{T}^\top (I - \tilde{T}) \right\rangle + \left\langle \tilde{b}_\Xi, \mathrm{Ad}_T^\top (\tilde{T}^\top (I - \tilde{T})) \right\rangle - \left\langle \beta, \tilde{b}_\Xi \right\rangle \\ &= -k_P \left\langle \xi, \mathbb{P}_{\mathfrak{se}(3)} (\mathrm{Ad}_T^\top (\tilde{T}^\top (I - \tilde{T}))) \right\rangle \\ &\quad + \left\langle \tilde{b}_\Xi, \mathbb{P}_{\mathfrak{se}(3)} (\mathrm{Ad}_T^\top (\tilde{T}^\top (I - \tilde{T}))) - \beta \right\rangle\end{aligned} \tag{5.44}$$

From which point setting $\xi \equiv \beta$ and substituting β from equation (5.19d) with the identities equation (5.26), one has

$$\dot{\mathcal{L}} = -k_P \|\beta\|_F^2 \tag{5.45}$$

and the Barbalat argument for almost-global asymptotic stability continues as prior. Similarly for $\dot{\mathcal{W}}$ in equation (5.43).

With the inclusion of an inertial frame bias in the model for Corollary 5.2.3, it is clear from the corresponding innovation term β_A that $\mathbb{P}_{\mathfrak{se}(3)}(\tilde{T}^{-1})$ is an error vector on the Lie algebra in the direction of the geodesic from $\tilde{T}$ to I. This corresponds to the many familiar examples from linear systems where bias correction is accomplished by integrating the error vector $-(\hat{x}-x)$.

Further, the innovations ξ and β are two methods of transforming this vector into a vector from $\hat{T}$ to T, which can then be used to drive the estimation frame dynamics of $\hat{T}$. From equation (5.32) and equation (5.33), the difference between ξ and β is in the how the coupling of the rotation and translation components induced by the semi-direct product structure of SE(3) is represented.

5.3 Observer Implementation

In this section, I identify solutions to problems that can appear when implementing the pose filter in a digital microprocessor with real-world sensor measurements. As described in Section 5.1.1, the pose and velocity sensors operate at different measurement rates which we seek to exploit in order to obtain a high-quality pose estimate at the maximum possible update rate. This is addressed using a multi-rate implementation of the pose and bias observer, exploiting the logical separation between the velocity and pose measurement terms in the estimate dynamics. Additionally, the discretisation of the continuous time equations was found to be numerically unstable under certain avoidable conditions. Causes of numerical instability are identified and solutions provided. For clarity, observer algorithm based on these design choices is sketched.

5.3.1 Multi-rate Implementation

Section 5.1.1 describes a sensor suite containing two sensors, an velocity sensor and a pose sensor, operating at different rates; the velocity sensor at up to 300 Hz and the pose sensor at 5 Hz. Further, the measurements may not arrive at regular time intervals, especially in the case of corrupt packets or dropped frames.

Examining the form of Equation (5.19) it is easy to decompose the bias and pose estimate dynamics into two integration terms, one each for pose and velocity measure-

ments, that can be applied when the corresponding measurement arrives. One has

$$\begin{aligned}
\Xi_y \text{ measured:} &\begin{cases} \dot{\hat{T}} &= \hat{T}\Xi_y \\ \dot{\hat{b}}_\Xi &= 0, \end{cases} \\
T_y \text{ measured:} &\begin{cases} \dot{\hat{T}} &= \hat{T} k_P \operatorname{Ad}_{T_y^{-1}} \mathbb{P}_{\mathfrak{se}(3)}(\tilde{T}_y^{-1}) \\ \dot{\hat{b}}_\Xi &= -k_I \mathbb{P}_{\mathfrak{se}(3)}(\operatorname{Ad}_{T_y^\top} \mathbb{P}_{\mathfrak{se}(3)}(\tilde{T}_y^{-1})). \end{cases}
\end{aligned} \tag{5.46}$$

For each integration case, one maintains a calculated integration time step, t_δ, containing the time difference between measurements from the same sensor. The integration step then proceeds with, for example, the standard euler integration

$$\begin{aligned}
\hat{T}(t_k) &= \hat{T}(t_{k-1}) \exp(t_\delta \dot{\hat{T}}(t_{k-1})) \\
\hat{b}_\Xi(t_k) &= \hat{b}_\Xi(t_{k-1}) + t_\delta \dot{\hat{b}}_\Xi(t_{k-1})
\end{aligned} \tag{5.47}$$

The idea here is that we essentially run a direct integration of the velocity measurements and use the pose measurements as a correction term that is applied as an impulse immediately when available. Other alternatives, such as a zero-order hold with regular integration at a smaller time step, decrease the accuracy of the correction effect of the pose measurement integration by partially applying it when the system and estimate have already changed. Hence, the delayed portion of the pose measurement correction term will be in the wrong frame of reference when integrated.

It is also possible to extend this separation further to separate angular and linear velocity components provided the integration time step for each is sufficiently small. The size of the time step becomes important in this case as in the explicit form of the matrix exponential on $\mathfrak{se}(3)$ (Park 1994), the translation in the exponential result is dependent on both the linear and angular velocity components. However, for sufficiently fast measurement rates, such as in the order of 100 Hz, this further separation should result in acceptable performance when in combination with pose measurement feedback.

5.3.2 Discretisation

Discrete implementation of the continuous time equations resulted in numerical instability due to two sources when using simple backwards Euler integration on experimental data with velocity measurements at 63 Hz and pose measurements at up to 30 Hz.

Firstly, when implementing the multi-rate integration scheme described in the previous section, it was found that following a large number of sequential pose measurements were dropped, the system over-corrected when a new measurement was received. This was due to dynamic integration time step, t_δ, calculated as the difference between to the arrival time of the previous and new measurement. Applying an upper bound, of three to five times the expected inter-measurement time, to t_δ used in integration prevented this disturbance.

Secondly, the angular velocity bias estimate update, equation (5.33a), is proportional to the magnitude of the translational distance from the origin of the inertial frame to the body-fixed and estimate frames.

$$\dot{\hat{b}}_\Omega \propto (P \times \hat{P}) \tag{5.48}$$

While asymptotically 0, at large displacements the term equation (5.48) becomes stiff, numerically destabilising the filter. It has been verified in simulations that the numerical instability is due to the product of the displacement magnitude and integration time step. Decreasing either numerically stabilises the filter. In simulations and experiments, I have avoided the regions of numerical instability by restricting translational movement. Equivalently, pre-conditioning may be used to rescale translational movement.

5.3.3 Observer Algorithm

An example implementation of the observer, equation (5.19), is depicted in Algorithm 1. This example includes the asynchronous multi-rate and numerical stability concepts described in the previous two sections.

5.4 Simulation Results

The observer equation (5.19) has been implemented in MATLAB 2007b as a discrete event simulation. Simulated velocity and pose sensor measurement have been generated with noise added as per the measurement model described in Section 5.1.1. The simulation used velocity measurements at 100 Hz and pose measurements at 5 Hz with synchronized measurement clocks.

Algorithm 1 Asynchronous Multi-rate Implementation

$\hat{T}(0) \leftarrow\!\shortmid I_{4\times 4}$
$\hat{b}_{\Xi}(0) \leftarrow\!\shortmid 0_{4\times 4}$

$t_{\texttt{last\_}\Xi} \leftarrow\!\shortmid 0$
$t_{\texttt{last\_}T} \leftarrow\!\shortmid 0$
$t_{\texttt{last\_estimate}} \leftarrow\!\shortmid 0$
$t_{\delta_T}^{\texttt{max}} \leftarrow\!\shortmid$ external constant
repeat
  wait for measurement available
  if velocity measurement available **then**
    $t_{\delta_\Xi} \leftarrow\!\shortmid t - t_{\texttt{last\_}\Xi}$
    $\Xi_y(t) \leftarrow\!\shortmid$ Sensor Data
    $\hat{\Xi}(t) = \Xi_y(t) - \hat{b}_{\Xi}(t_{\texttt{last\_}T})$
    $\hat{T}(t) \leftarrow\!\shortmid \hat{T}(t_{\texttt{last\_estimate}}) \exp(t_{\delta_\Xi}\hat{\Xi}(t))$
    $t_{\texttt{last\_estimate}} \leftarrow\!\shortmid t$
    $t_{\texttt{last\_}\Xi} \leftarrow\!\shortmid t$
  else if pose measurement available **then**
    $t_{\delta_T} \leftarrow\!\shortmid \max(t - t_{\texttt{last\_}T}, t_{\delta_T}^{\texttt{max}})$
    $T_y(t) \leftarrow\!\shortmid$ Sensor Data
    $\xi(t) \leftarrow\!\shortmid \mathrm{Ad}_{T_y^{-1}(t)} \mathbb{P}_{\mathfrak{se}(3)} \left((\hat{T}(t_{\texttt{last\_estimate}}) T_y^{-1}(t))^{-1} \right)$
    $\beta(t) \leftarrow\!\shortmid \mathbb{P}_{\mathfrak{se}(3)} \left(\mathrm{Ad}_{T_y^{\top}(t)} \mathbb{P}_{\mathfrak{se}(3)} \left((\hat{T}(t_{\texttt{last\_estimate}}) T_y^{-1}(t))^{-1} \right) \right)$
    $\hat{T}(t) \leftarrow\!\shortmid \hat{T}(t_{\texttt{last\_estimate}}) \exp(t_{\delta_T} k_P \xi(t))$
    $\hat{b}_{\Xi}(t) \leftarrow\!\shortmid \hat{b}_{\Xi}(t_{\texttt{last\_}T}) - t_{\delta_T} k_I \beta(t)$
    $t_{\texttt{last\_estimate}} \leftarrow\!\shortmid t$
    $t_{\texttt{last\_}T} \leftarrow\!\shortmid t$
  end if
until end of data

Gain	**Value**
k_{P_Ω}: Orientation proportional gain	1
k_{I_Ω}: Orientation integral gain	1
k_{P_p}: Position proportional gain	0.1
k_{I_p}: Position integral gain	0.1

Table 5.1: Observer gains used in simulations depicted in Figures 5.4, 5.5 and 5.6.

Gain	**Value**
n_R: Orientation measurement noise variance	0.001
n_P: Translation measurement noise variance	0.001
n_Ω: Angular velocity measurement noise variance	0.1
n_V: Linear velocity measurement noise variance	0.1
b_Ω: Constant angular velocity measurement bias	0.1
b_V: Constant linear velocity measurement bias	0.25

Table 5.2: Artificial noise and bias figures applied to measurements in simulations depicted in Figures 5.4, 5.5 and 5.6.

$$
\begin{aligned}
r &= 0.2 \ \text{m} & \begin{pmatrix} x(t) \\ y(t) \end{pmatrix} &= \begin{pmatrix} \cos(\omega t) & -\sin(\omega t) \\ \sin(\omega t) & \cos(\omega t) \end{pmatrix} \begin{pmatrix} r \\ 0 \end{pmatrix} + \begin{pmatrix} x_0 - r \\ y_0 \end{pmatrix} \\
t_f &= 120 \ \text{s} & z(t) &= z_0 + \tfrac{\delta_z}{t_f} t \\
x_0 &= 0.2 \ \text{m} & & \\
y_0 &= 0 \ \text{m} & & \\
z_0 &= -0.7 \ \text{m} & \phi(t) &= \tfrac{\pi}{2} + \omega t \\
\delta_z &= 0.2 \ \text{m} & \theta(t) &= \arctan(\tfrac{\dot{z}(0)}{\dot{x}(0)}) = \arctan(\tfrac{\delta_z}{t_f r}) \\
\omega &= \tfrac{4\pi}{t_f} \ \text{rad}\,\text{s}^{-1} & \psi(t) &= 2\theta(t)
\end{aligned}
$$

$$
T(t) = \begin{pmatrix} & & x(t) \\ R_{\psi(t)} R_{\theta(t)} R_{\phi(t)} & & y(t) \\ & & z(t) \\ 0 & & 1 \end{pmatrix} \tag{5.49}
$$

Figures 5.4, 5.5 and 5.6 depict the pose and bias estimate convergence for body descending along a trim trajectory from above an observed target, described in equa-

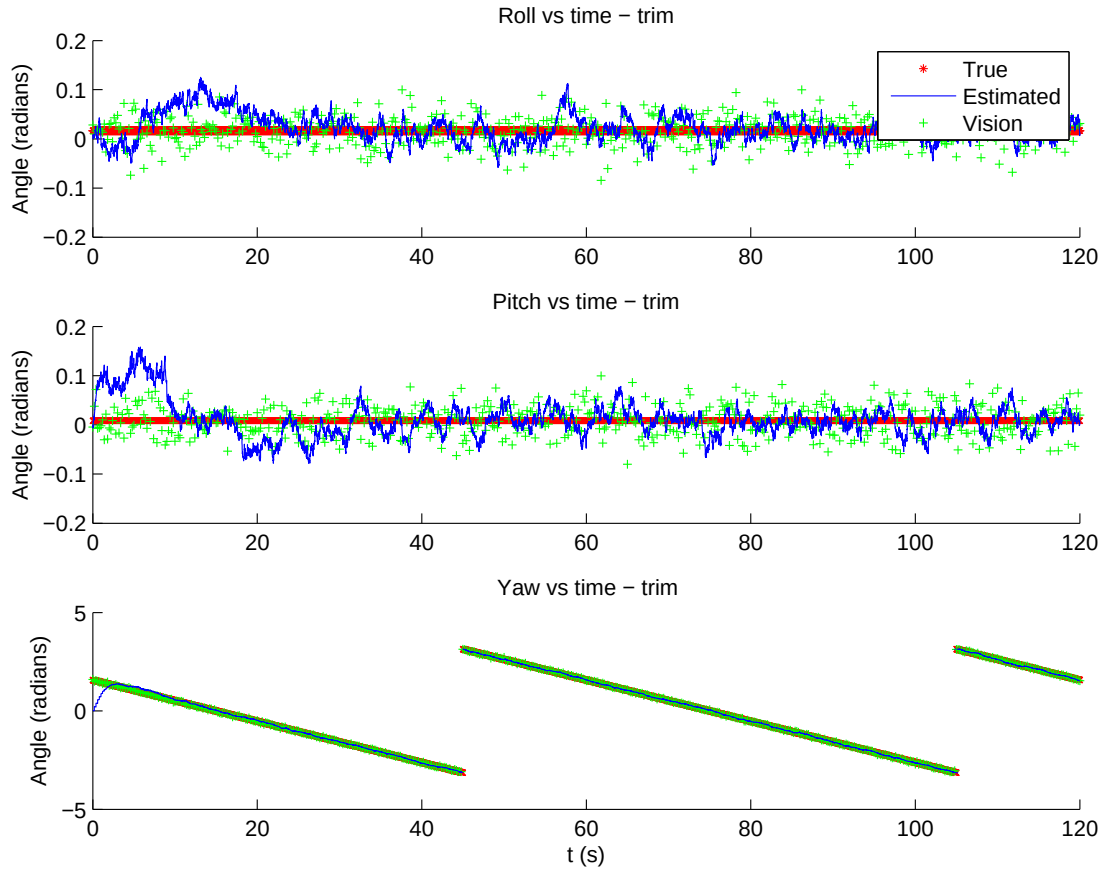

Figure 5.4: Simulation results for orientation component of pose estimate using simulated measurements along a trim trajectory specified by equation (5.49), with observer gains as per Table 5.1 and initial conditions $\hat{T}(0) = I$ and $\hat{b}_{\Xi} = 0$. Artificial measurement noise was added according to Table 5.2. The true pose is indicated by red marks and the visual pose measurements by green marks. Note that while the vision measurements are coincidental with the true pose, they are at a lower rate of 5 Hz. The estimated pose is indicated by the blue path.

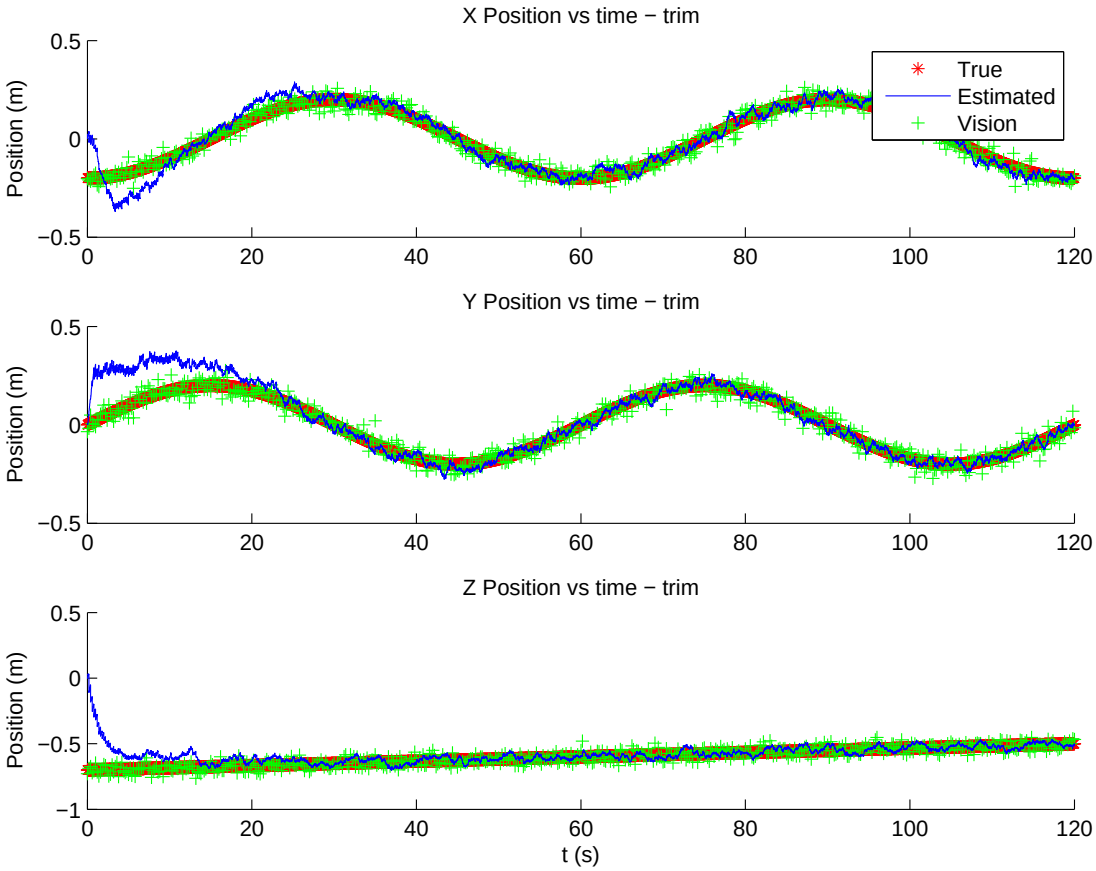

Figure 5.5: Simulation results for position component of pose estimate using simulated measurements along a trim trajectory specified by equation (5.49), with observer gains as per Table 5.1 and initial conditions $\hat{T}(0) = I$ and $\hat{b}_{\Xi} = 0$. Artificial measurement noise was added according to Table 5.2. The true pose is indicated by red marks and the visual pose measurements by green marks. Note that while the vision measurements are coincidental with the true pose, they are at a lower rate of 5 Hz. The estimated pose is indicated by the blue path.

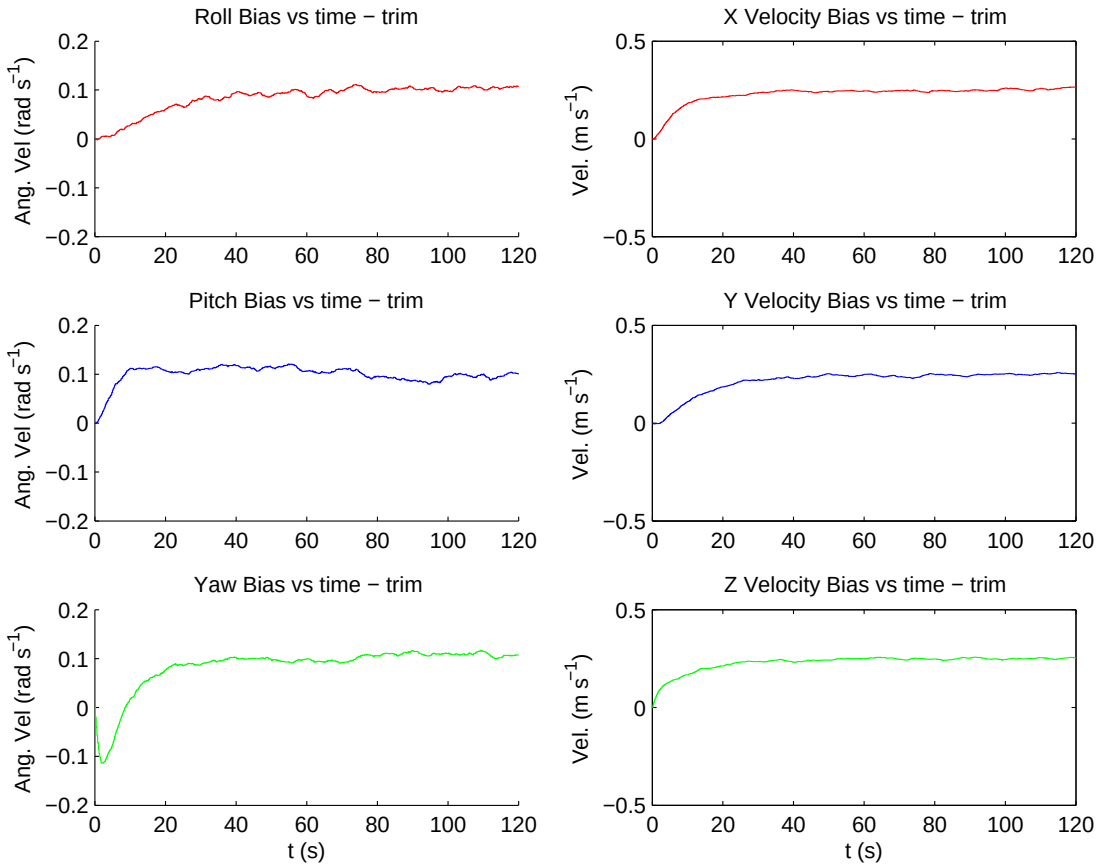

Figure 5.6: Simulation results for velocity bias estimates using simulated measurements along a trim trajectory specified by equation (5.49), with observer gains as per Table 5.1 and initial conditions $\hat{T}(0) = I$ and $\hat{b}_{\Xi} = 0$. Artificial measurement noise was added according to Table 5.2.

Gain	**Value**
k_{P_Ω}: Orientation proportional gain	1
k_{I_Ω}: Orientation integral gain	1
k_{P_p}: Position proportional gain	0.1
k_{I_p}: Position integral gain	0.1

Table 5.3: Observer gains used in experiments depicted in Figures 5.7, 5.8 and 5.9.

tion (5.49), where the position is given by (x, y, z) and the orientation by a yaw about the z axis of ϕ, followed by a pitch about the y axis of θ and roll about the x axis of ψ. Observer gains used are listed in Table 5.1 and measurement noise in Tables 5.2.

Note the initial conditions for the simulation estimates were $\hat{T} = I$ and $\hat{b}_\Xi = 0$. In the estimate, we see rapid convergence over this substantial initial condition error in both position and orientation.

5.5 Experimental Results

Experiments have been conducted using the apparatus and methods described in Chapter A.1, consisting of an inertial and vision sensor attached to a large robotic manipulator. Using the robotic manipulator, the sensor package has been moved through a path and both sensor data and ground-truth measurements of the manipulator configuration recorded. Using the recorded data pose has been estimated offline, after the experiment, using the observer specified in Theorem 5.2.1.

Vision measurement were recorded at 30 Hz, with regular patches of dropped frames. Inertial measurements of angular velocity in the body-fixed frame were recorded at a modal rate of 63 Hz, containing some time varying bias components. In the absence of an available linear velocity sensor, linear velocity in the body-fixed frame was estimated using a numerical derivative of the recorded ground-truth pose measurements. The linear velocity estimate was calculated at the same time points as the angular velocity measurements and, as a numerical derivative contains no bias component but substantial process noise.

Figures 5.7, 5.8 and 5.9 depict estimation results from sensor data collected while driving the robot through a circular path of 1 m diameter with the sensor package oriented to point at a spot on the ground at the center of the path.

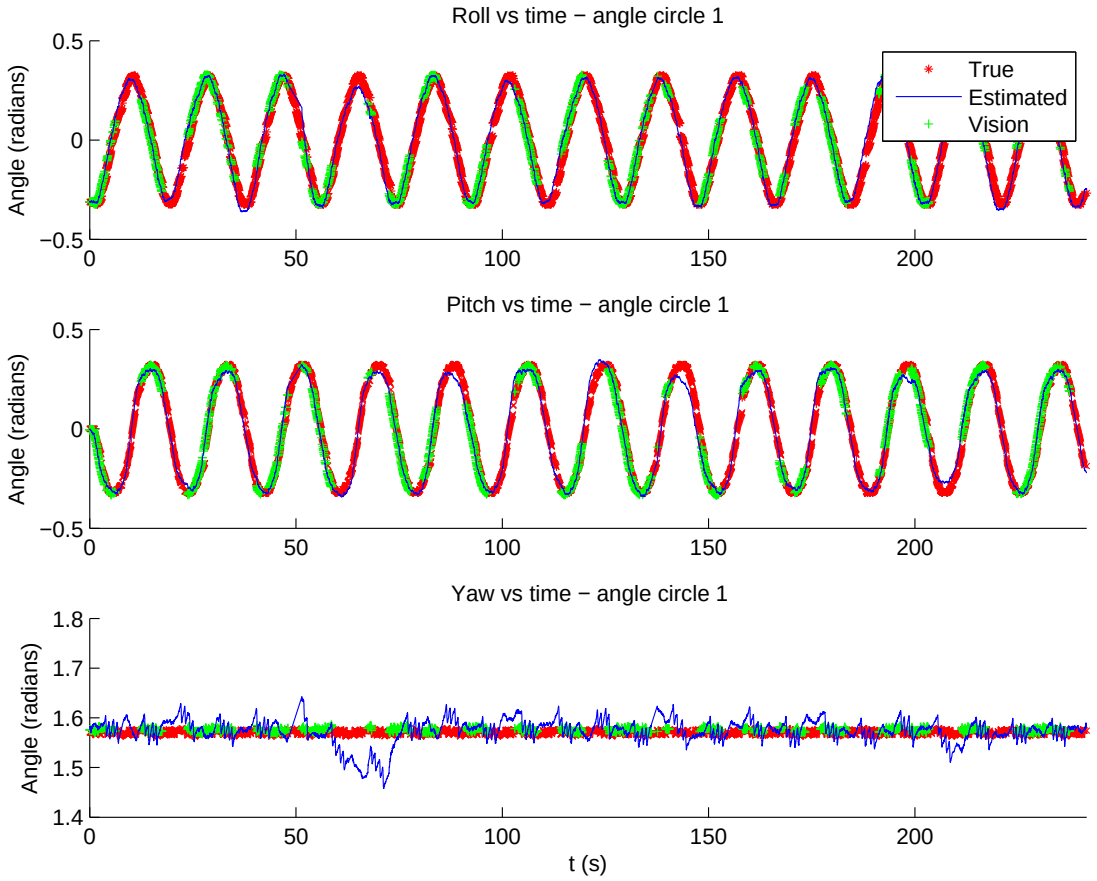

Figure 5.7: Experimental results for orientation component of pose estimate using inertial and visual measurements from sensors attached to a robotic manipulator moved through a circular path. Observer gains used are given in Table 5.3 and initial conditions were $\hat{T}(0) = T_y(0)$, $\hat{b}_\Xi = 0$. The estimated pose is indicated by the blue path and visual pose measurements by green marks. The ground truth measurements of the actual path recorded by the robot are indicated by the red marks.

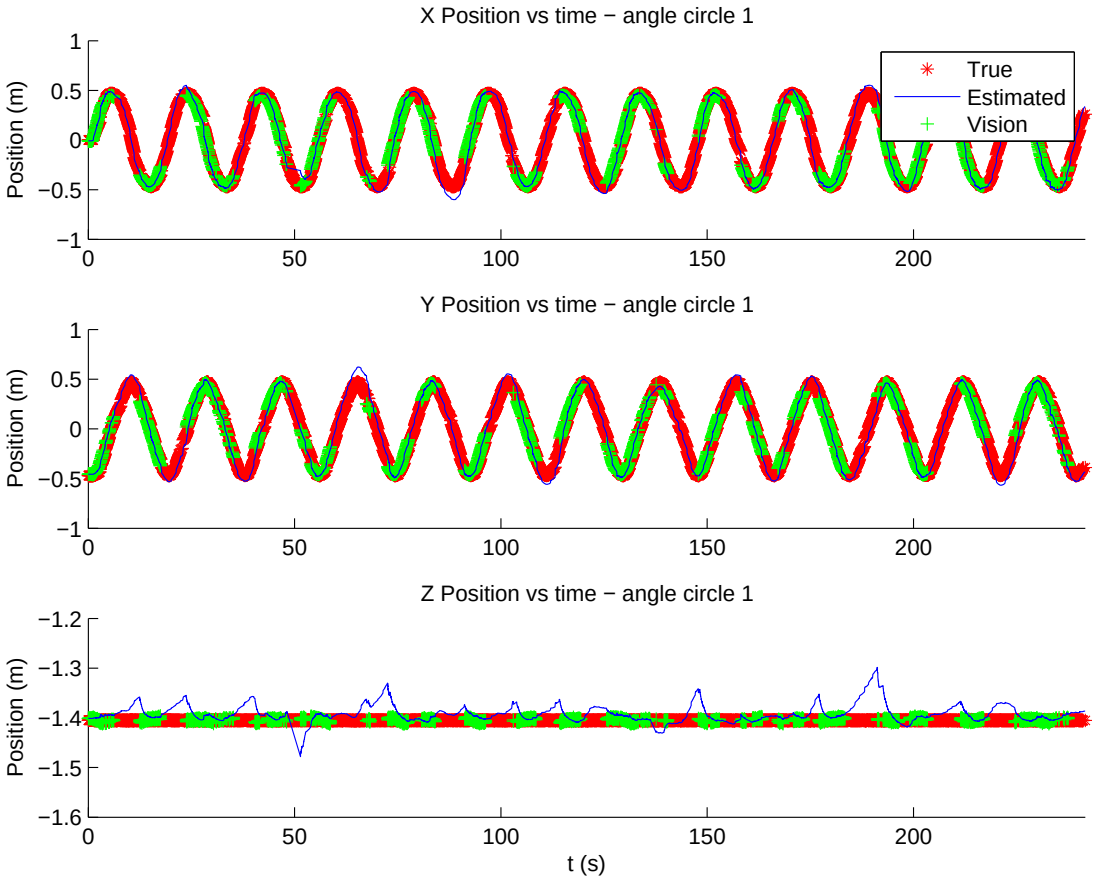

Figure 5.8: Experimental results for position component of pose estimate using inertial and visual measurements from sensors attached to a robotic manipulator moved through a circular path. Observer gains used are given in Table 5.3 and initial conditions were $\hat{T}(0) = T_y(0)$, $\hat{b}_\Xi = 0$. The estimated pose is indicated by the blue path and visual pose measurements by green marks. The ground truth measurements of the actual path recorded by the robot are indicated by the red marks.

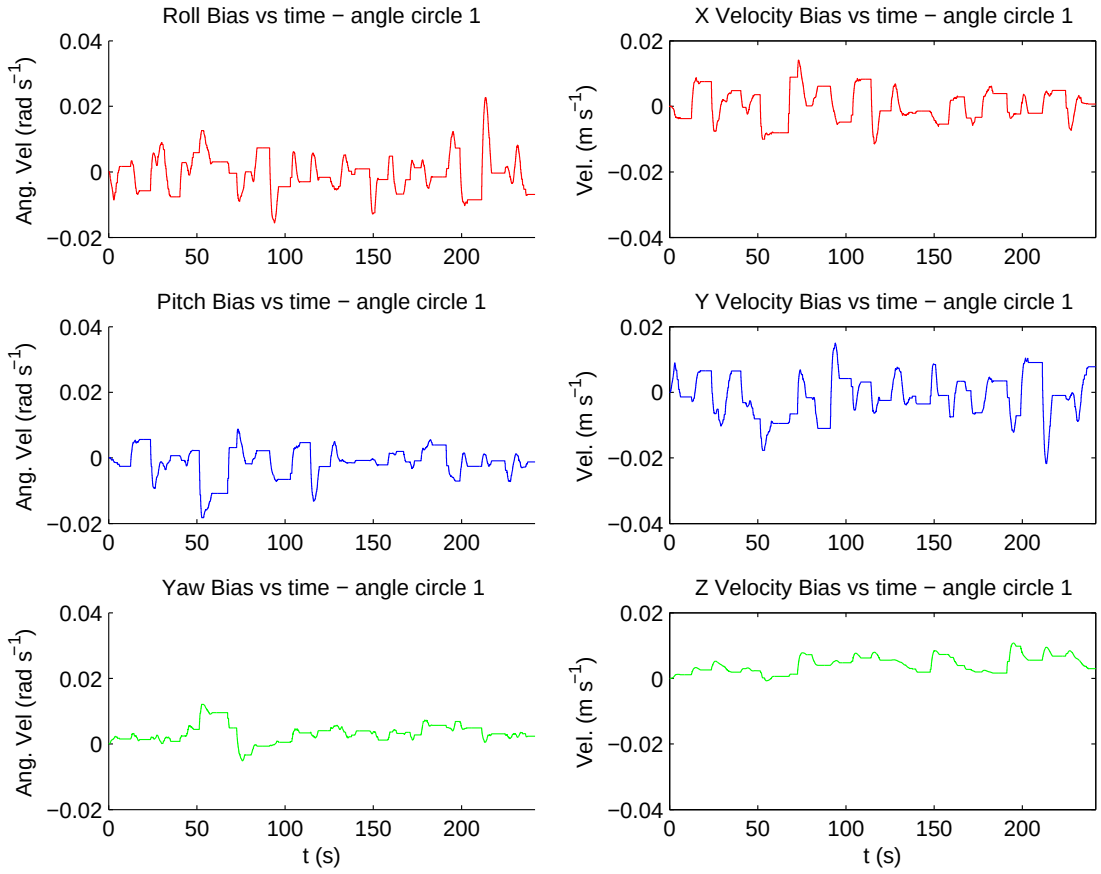

Figure 5.9: Experimental results for velocity bias estimates using inertial and visual measurements from sensors attached to a robotic manipulator moved through a circular path. Observer gains used are given in Table 5.3 and initial conditions were $\hat{T}(0) = T_y(0)$, $\hat{b}_\Xi = 0$.

Figures 5.7 and 5.8 depict the ground-truth pose, the timing and accuracy of vision pose measurements and the estimated pose. Figure 5.9 depicts the angular and linear velocity bias estimates. Note that the orientation and position pose components track the true pose well over the full 4 minute period, even with significant blocks of dropped frames. Additionally, in the unactuated z position axis the observer tracks the pose measurements well despite a 10 cm estimation error between the results of the measurement process and the true position.

5.6 Chapter Summary

In this chapter, I have developed a twelve state observer for pose and velocity measurement bias. The observer evolves directly on SE(3) from measurements of pose and angular and linear velocity. Almost-global asymptotic and locally-exponential stability of the observer was proven. This observer also exhibits a straightforward gain tuning process and separation of measurement noise processes.

In the process of designing this observer, a right invariant pose error metric was identified, with an interpretation as the state error represented as a rigid body transformation expressed in the inertial frame.

The observer structure and its relationship to other position and orientation estimators was discussed. A related observer and the necessary conditions for pose estimation using mixed velocity measurements in both the inertial and body-fixed frames was identified.

A scheme for an asynchronous multi-rate discrete implementation of the pose observer was discussed together with resulting sources of numerical instability.

Simulation and experimental results were shown to demonstrate the convergence properties in the presence of noise and insensitivity to initial conditions of this observer.

Chapter 6

Observer Design from Direct Vision Measurements of Feature Bearing

This chapter presents a pose observer evolving on the special Euclidean group $\mathrm{SE}(3)$ of dimension four from velocity measurements and measurements of the bearing of landmarks of known location. In contrast to previous chapters, this corresponds to using the location of features on a spherical camera image directly rather than using pose reconstructed from the image features. That is, instead of designing an observer taking trajectories in $\mathrm{SE}(3)$ and $\mathfrak{se}(3)$ to an estimate on $\mathrm{SE}(3)$, an observer is designed to take trajectories on $(\mathbb{S}^2)^n$ and $\mathfrak{se}(3)$ to an estimate on $\mathrm{SE}(3)$, where n is the number of landmarks tracked.

The use of bearing-only vision measurements directly brings considerable benefits and problems. By eliminating the use of a pose reconstruction algorithm from the vision post-processing the computational requirements for the whole observer system are significantly reduced. However, the complexity of the observer convergence proof is significantly increased and only local stability is proven due to the projective nature of bearing measurements.

As with work presented in the prior chapters, the observer presented in this chapter maintains the key properties of separating measurement noise processs in estimate dynamics and is suitable for an asynchronous multi-rate implementation.

Simulation and experimental results are presented for the observer, demonstrating performance in the presence of measurement noise. To apply the observer to experimental data, an extension is postulated adding velocity measurement bias estimation as an integral of the pose correction innovation term, based on insight gained in Chapters 4 and 5. Experimental results have been obtained using data collected from the apparatus and methods described in Chapter A.1, using an inertial and visual sensor

attached to a robotic manipulator. Comparison with ground-truth data demonstrates observer accuracy under experimental conditions.

The contributions of this chapter are

- An observer for pose designed directly on $\mathrm{SE}(3)$ from measurements of bearing to known landmarks on $(\mathbb{S}^2)^n$ and velocity on $\mathfrak{se}(3)$, with a local asymptotic Lyapunov stability argument.
- Experimental demonstration of the landmark bearing pose observer augmented with a velocity bias estimate that is naturally defined by analogy to prior work.

This chapter is based upon material published in Baldwin et al. (2009).

6.1 Problem Description

Let $\mathcal{A}$ again denote an inertial frame attached to the earth such that e_3 points vertically down. Let $\mathcal{B}$ denote a body-fixed frame attached to a vehicle of interest at the center of mass. The origin of $\mathcal{B}$ expressed in $\mathcal{A}$ is given by the vector p, and the attitude of $\mathcal{B}$ expressed in $\mathcal{A}$ is given by the rotation matrix R.

The element of $\mathrm{SE}(3)$

$$T = \begin{pmatrix} R & p \\ 0 & 1 \end{pmatrix} \tag{6.1}$$

has the triple interpretation as the pose of $\mathcal{B}$ expressed in $\mathcal{A}$, as the *coordinate frame transformation* mapping objects expressed in $\mathcal{B}$ to objects expressed in $\mathcal{A}$, and as the *rigid body transformation* moving an object from the pose given by the attitude and position of $\mathcal{A}$ to the attitude and position of $\mathcal{B}$, expressed in $\mathcal{A}$.

As previously, we adopt the convention that positions and vectors expressed in the inertial frame are denoted by lower case letters, and quantities expressed in other frames are denoted by upper case letters.

The kinematics of $\mathcal{B}$ are given by

$$\dot{R} = R\Omega_\times, \tag{6.2a}$$

$$\dot{p} = v, \tag{6.2b}$$

where Ω denotes the angular velocity of the body-fixed frame, expressed in the body-fixed frame, and v denotes the linear velocity of the body-fixed frame expressed in the

inertial frame. $(\cdot)_\times$ is an operator taking the vector $\Omega \in \mathbb{R}^3$ to the skew-symmetric matrix

$$\Omega_\times = \begin{pmatrix} 0 & -\Omega_3 & \Omega_2 \\ \Omega_3 & 0 & -\Omega_1 \\ -\Omega_2 & \Omega_1 & 0 \end{pmatrix}. \tag{6.3}$$

Represented in SE(3), the kinematics of $\mathcal{B}$ are

$$\dot{T} = T\Xi \tag{6.4}$$

where

$$\Xi = (\Omega, V)^\wedge \tag{6.5}$$

and

$$(\Omega, V)^\wedge = \begin{pmatrix} \Omega_\times & V \\ 0 & 0 \end{pmatrix}. \tag{6.6}$$

Let $P = -R^\top p$, the position of the origin of $\mathcal{A}$ expressed in $\mathcal{B}$, then $\dot{P} = -\Omega_\times P - V$ where $V = R^\top v$, the velocity of $\mathcal{B}$ expressed in $\mathcal{B}$. $\Xi \in \mathfrak{se}(3)$ is a representation of the 6 dimensional velocity of $\mathcal{B}$ expressed in $\mathcal{B}$. The wedge operator, $(\cdot,\cdot)^\wedge$, maps between the $\mathbb{R}^6$ and $\mathfrak{se}(3)$ interpretations of the system velocity.

Consider an ensemble of three or more landmark points $\{z_i\} \in \mathcal{A}$ that are stationary in the inertial frame and distributed in space such that they are non-colinear. This arrangement is depicted in Figure 6.1. Let $\mathbf{Y}_i = T^{-1}\mathbf{z}_i$, the position of the i-th landmark expressed in $\mathcal{B}$, where bold face denotes the homogeneous coordinate representation of a point,

$$\mathbf{Y} = \begin{pmatrix} Y \\ 1 \end{pmatrix}. \tag{6.7}$$

As the z_i are stationary in the inertial frame, $\dot{z}_i = 0$ and

$$\dot{Y}_i = -\Omega_\times Y_i - V \tag{6.8}$$

or

$$\dot{\mathbf{Y}}_i = -\Xi \mathbf{Y}_i. \tag{6.9}$$

Let π_a and $\pi_a^\perp$ denote the projection matrices onto the subspace spanned by $a \in \mathbb{R}^n$ and the subspace perpendicular to the span of a, respectively, such that $I = \pi_a + \pi_a^\perp$.

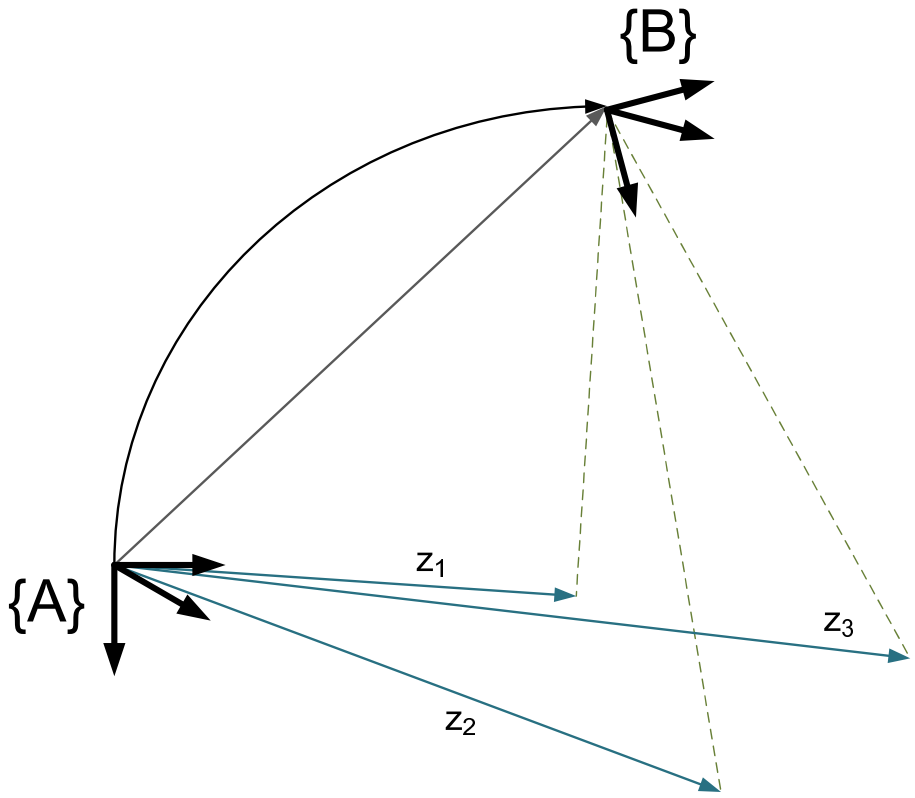

Figure 6.1: The true system state, T, contains the rotation and translation from the origin of the inertial frame, $\mathcal{A}$, to the origin of the body fixed frame, $\mathcal{B}$. The landmarks have location z_i in the inertial frame and are observed from the body fixed frame.

One has

$$\pi_a = \frac{1}{\|a\|^2} aa^\top, \tag{6.10a}$$

$$\pi_a^\perp = \frac{1}{\|a\|^2}(I - aa^\top) \tag{6.10b}$$

where $\|\cdot\|$ is the standard Euclidean norm.

The bearing of the i-th landmark from the origin of $\mathcal{B}$, expressed in $\mathcal{B}$, is then given by the unit vector $X_i \in \mathbb{S}^2$,

$$X_i = \frac{Y_i}{\|Y_i\|}, \tag{6.11}$$

with dynamics

$$\dot{X}_i = -\Omega_\times X_i - \frac{1}{\|Y_i\|}\pi_{X_i}^\perp V. \tag{6.12}$$

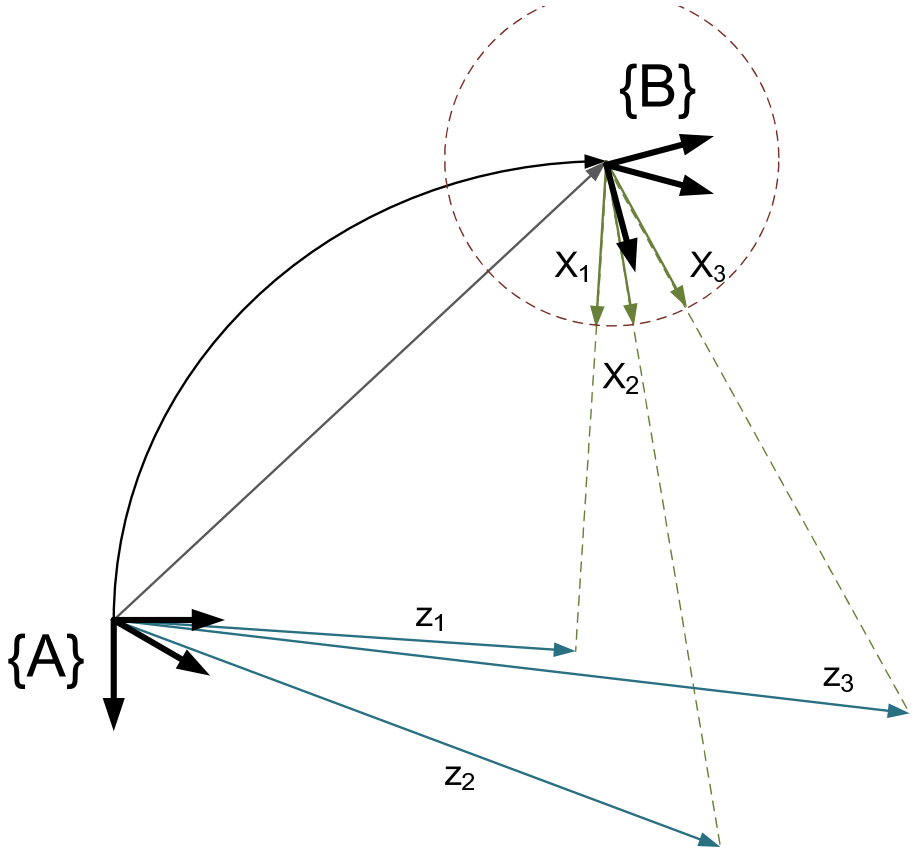

Figure 6.2: The true system state, T, contains the rotation and translation from the origin of the inertial frame, $\mathcal{A}$, to the origin of the body fixed frame, $\mathcal{B}$. The landmarks have location z_i in the inertial frame and are observed from the body-fixed frame as bearings X_i, represented on the unit sphere.

6.1.1 Measurement Model

We again consider the vehicle of interest to be equipped with an inertial-vision sensor package; an Inertial Measurement Unit (IMU) and a monocular camera; both affixed to the craft and taking measurements in the body-fixed frame, $\mathcal{B}$. As throughout this thesis, the IMU operates at a measurement rate up to two orders of magnitude faster than the vision measurement rate. Additionally, the inertial measurements are corrupted by low frequency noise, while the vision measurements are stable at low frequencies and corrupted by high frequency noise. We again use the complementary characteristics of these measurements to form a high quality estimate.

In this chapter, we assume that measurements of the system velocity Ξ, including

the angular and linear velocity components, are available, such as from an IMU and linear velocity estimator as discussed in Section 2.2.3. The inertial measurements are assumed to be free of bias and corrupted by a zero-mean noise process n_Ξ.

From the vision sensor we use measurements of the bearing of known landmarks, X_i, represented as unit vectors on the unit sphere $\mathbb{S}^2$. These measurements are corrupted by a zero-mean noise process, n_{X_i}, on the tangent plane to the measurement.

Let Ξ_y and X_{y_i} denote measurements of system velocity and bearing of the i-th landmark. The measurement model is then

$$\Xi_y = \Xi + n_\Xi, \tag{6.13a}$$

$$X_{y_i} = \frac{X_i + n_{X_i}}{\|X_i + n_{X_i}\|}. \tag{6.13b}$$

6.1.2 Estimation Model and Error Terms

Let $\hat{T}$ denote an estimate of T and define the estimation frame $\mathcal{E}$ as the pose given by $\hat{T}$ relative to the inertial frame. Then

$$\hat{T} = \begin{pmatrix} \hat{R} & \hat{p} \\ 0 & 1 \end{pmatrix} \tag{6.14}$$

where $\hat{p}$ is the origin of $\mathcal{E}$ expressed in $\mathcal{A}$ and $\hat{R}$ is the rotation matrix giving the attitude of $\mathcal{E}$ expressed in $\mathcal{A}$.

Given an ensemble of landmarks $\{z_i\}$ whose position is known in the inertial frame, one may express the location and bearing of these landmarks relative to the estimated frame $\mathcal{E}$ as

$$\hat{\mathbf{Y}}_i = \hat{T}^{-1}\mathbf{z}_i, \tag{6.15a}$$

$$\hat{X}_i = \frac{\hat{Y}_i}{\|\hat{Y}_i\|}. \tag{6.15b}$$

$\hat{X}_i$ is then an estimate of the measurement X_{y_i}.

As discussed previously in Section 5.2, a right invariant error pose on $\mathrm{SE}(3)$ is given by

$$\tilde{T} = \hat{T}T^{-1}, \tag{6.16}$$

where $\tilde{T}$ has the interpretation as the *rigid body transformation* from $\mathcal{B}$ to $\mathcal{E}$, expressed in $\mathcal{A}$. Further, recall the error metric used in Chapters 4 and 5 of

$$\|(I - \tilde{T})\|^2. \tag{6.17}$$

measuring the difference between the target and actual error transformations.

The difference between the estimated and actual position of the landmarks relative to the vehicle, $\hat{Y}_i$ and Y_i respectively, is an error term that respects the invariance properties of $\tilde{T}$. Let Y_i^Δ denote the difference between $\hat{Y}_i$ and Y_i, then

$$\begin{aligned} \mathbf{Y}_i^\Delta &= \hat{\mathbf{Y}}_i - \mathbf{Y}_i \\ &= (\hat{T} - T)\mathbf{z}_i \\ &= (I - \tilde{T}^{-1})\hat{T}\mathbf{z}_i \\ &= (I - \tilde{T}^{-1})\hat{\mathbf{Y}}_i, \end{aligned} \tag{6.18}$$

or the difference between the inverse of the error and the identity applied to $\hat{Y}_i$. This has the interpretation as the difference between the images of I and $\tilde{T}^{-1}$ applied to $\hat{Y}_i$. This difference is projection of the matrix errror $I - \tilde{T}$, along the vector $\hat{Y}_i$. For non-colinear $\{z_i\}$, the ensemble $\sum_{i=1}^n \|Y_i^\Delta\|^2$ contains projections of the error across a complete basis for $\mathbb{R}^3$, and is equal to zero only for $\tilde{T} = I$.

Similarly, the difference between the estimated and actual bearing of the landmarks relative to the vehicle, $\hat{X}_i$ and X_i, is also an error term that respect the invariance properties of $\tilde{T}$. Let X_i^Δ denote the difference between $\hat{X}_i$ and X_i, then

$$\begin{aligned} \mathbf{X}_i^\Delta &= \hat{\mathbf{X}}_i - \mathbf{X}_i \\ &= \left(\frac{1}{\|\hat{Y}_i\|}\hat{T} - \frac{1}{\|Y_i\|}T\right)\mathbf{z}_i \\ &= \left(\frac{1}{\|\hat{Y}_i\|}\hat{T} - \frac{1}{\|Y_i\|}T\right)\mathbf{z}_i \\ &= \left(I - \frac{\|\hat{Y}_i\|}{\|Y_i\|}\tilde{T}^{-1}\right)\frac{1}{\|\hat{Y}_i\|}\hat{T}\mathbf{z}_i \\ &= \left(I - \frac{\|\hat{Y}_i\|}{\|Y_i\|}\tilde{T}^{-1}\right)\hat{\mathbf{X}}_i. \end{aligned} \tag{6.19}$$

When $\|\hat{Y}_i\| \approx \|Y_i\|$, X_i^Δ again gives a projection of the error along the direction $\hat{Y}_i$. Hence, $\{X_i^\Delta\}$ provides complete information about the error locally around $\tilde{T} = I$ for non-colinear $\{z_i\}$.

6.2 Observer Design

In this section I defined a non-linear observer for pose on $\mathfrak{se}(3)$ from inertial measurements and bearing-only vision measurements. Firstly, I give a series of assumptions about the behaviour of the system being estimated. I establish a necessary and sufficient condition for convergence of the pose estimate and then present the observer and prove it meets this condition with local asymptotic convergence. I present the observer for time case with exact measurements and then, using the stability of the error system to argue validity for the case of noisy measurements. Finally, I identify conditions that would provide almost-global convergence.

6.2.1 System Assumptions

Consider a vehicle equipped with an inertial vision sensor package together with a set of landmarks at fixed points in the environment. As detailed in Section 6.1, let $\{z_i\}$ denote the location of the landmarks expressed in the inertial frame, $\mathcal{A}$. Assume that the landmarks are arranged such that there exists a separating hyperplane between the region containing the landmarks and the region in which the vehicle operates. Such a situation arises naturally when, for example, the vehicle operates in the air above landmarks distributed across the ground.

Further, assume that the trajectory of the vehicle is bounded away from the landmark points for all time. That is there exists an $\varepsilon \in \mathbb{R}$ such that for all t and all landmarks z_i

$$\|Y_i(t)\| > \varepsilon > 0. \tag{6.20}$$

Recall the measurement model described in Section 6.1.1, with the IMU providing measurements of the system velocity, Ξ, and the vision sensor providing measurements of the bearing of landmarks, X_i. Consider that the locations $\{z_i\}$ are known and that the correspondence between landmarks in different visual images can be solved.

6.2.2 Landmark Bearing Pose Observer

I now define a non-linear observer and prove local asymptotic convergence by a non-linear Lyapunov analysis. Firstly, I establish that convergence of the estimated visual measurements is a necessary and sufficient condition to ensure convergence of the system pose estimate. I then define an observer evolving on $\mathrm{SE}(3)$ from measurements

on $\mathbb{S}^2$ and $\mathfrak{se}(3)$. Using Lyapunov arguments on the embedding space and a local linearisation, I then prove local asymptotic convergence of the observer for the case of exact measurements. Using this convergence result, I argue for the validity of the observer to the case of noisy measurements. Lastly, I identify conditions that would provide almost-global convergence.

Lemma 6.2.1. *Consider the system equation (6.4) and constellation of landmarks* $\{z_i\}$*. For a set of three or more non-colinear landmarks* $\{z_i\}$ *then* $\hat{X}_i = X_i$ *for all* i *if and only if* $\hat{T}T^{-1} = I$*.*

Proof of Lemma 6.2.1. Consider the stabiliser group for a single landmark bearing measurement, X_i. It consists of translation along and rotation about the axis in direction X_i,

$$G_{X_i} = \left\{ T \,\middle|\, T = \begin{pmatrix} \exp(\alpha X_i) & \beta X_i \\ 0 & 1 \end{pmatrix} \quad \alpha, \beta \in \mathbb{R} \right\}. \tag{6.21}$$

Noting that

$$\hat{X}_i = \frac{\|Y_i\|}{\|\hat{Y}_i\|} \tilde{T} X_i, \tag{6.22}$$

then for any $\tilde{T} \neq I$, as the z_i are non-colinear at least one of the X_i will lie such that $\hat{X}_i \neq \alpha X_i$ for some $\alpha \in \mathbb{R}$. Hence, for a set $\{X_i\}$ derived from a set $\{z_i\}$ of three or more non-colinear elements, the intersection of the stabiliser groups contains only the identity element,

$$\bigcap_{i=1}^{n} G_{X_i} = \{I\}. \tag{6.23}$$

□

Theorem 6.2.2 (Landmark Bearing Pose Observer)**.** *Consider the system equation (6.4) and constellation of landmarks* $\{z_i\}$ *such that at least three landmarks are non-colinear, together with a bounded piecewise continuous driving term* Ξ *and trajectory* T *such that, for all* i *and for all* t*,* $\|Y_i(t)\| > \varepsilon > 0$*. Let* $X_{y_i} = X_i$ *and* $\Xi_y = \Xi$ *be measurements free of bias and noise.*

Define the observer

$$\dot{\hat{T}} = \hat{T}(\Xi_y + \xi) \tag{6.24a}$$

$$\xi = (\xi_\Omega, \xi_V)^\wedge \tag{6.24b}$$

$$\xi_\Omega = -k_{P_\Omega} \sum_{i=1}^{n} \hat{X}_i \times X_{y_i} \tag{6.24c}$$

$$\xi_v = -k_{P_p} \sum_{i=1}^{n} \frac{\pi_{\hat{X}_i}^\perp X_{y_i}}{\|\hat{Y}_i\|}, \tag{6.24d}$$

and recall the error $\tilde{T} = \hat{T}T^{-1}$ from equation (6.16).

Then there exists $k_{P_p} > 0$ such that for all choices of $k_{P_\Omega} > 0$, $\tilde{T}$ is locally asymptotically stable about I.

Proof of Theorem 6.2.2. Recall the definition of $\hat{X}_i$ from equation (6.15b). It is straightforward to verify that

$$\dot{\hat{X}} = -(\Omega + \xi_\Omega) \times \hat{X}_i - \frac{\pi_{\hat{X}_i}^\perp (V + \xi_V)}{\|\hat{Y}_i\|} \tag{6.25}$$

Consider the per-feature error $X_i^\Delta := \hat{X}_i - X_i$. One has

$$\begin{aligned} \dot{X}_i^\Delta = &- \Omega \times X_i^\Delta - \xi_\Omega \times \hat{X}_i \\ &- \left(\frac{\pi_{\hat{X}_i}^\perp}{\|\hat{Y}_i\|} - \frac{\pi_{X_i}^\perp}{\|Y_i\|} \right) V - \frac{\pi_{\hat{X}_i}^\perp \xi_V}{\|\hat{Y}_i\|}. \end{aligned} \tag{6.26}$$

Define the positive definite cost function

$$\begin{aligned} &\mathcal{V} : (\mathbb{R}^3)^n \to \mathbb{R} \\ &\mathcal{V} = \sum_{i=1}^{n} \frac{1}{2} \left\| X_i^\Delta \right\|^2. \end{aligned} \tag{6.27}$$

Then

$$\begin{aligned} \dot{\mathcal{V}} = &- \sum_{i=1}^{n} \left\langle \hat{X}_i \times X_i^\Delta, \xi_\Omega \right\rangle - \sum_{i=1}^{n} \left\langle X_i^\Delta, \frac{\pi_{\hat{X}_i}^\perp \xi_V}{\|\hat{Y}_i\|} \right\rangle \\ &- \sum_{i=1}^{n} \left\langle X_i^\Delta, \left(\frac{\pi_{\hat{X}_i}^\perp}{\|\hat{Y}_i\|} - \frac{\pi_{X_i}^\perp}{\|Y_i\|} \right) V \right\rangle \\ = &\left\langle \sum_{i=1}^{n} \hat{X}_i \times X_i, \xi_\Omega \right\rangle + \left\langle \sum_{i=1}^{n} \frac{\pi_{\hat{X}_i}^\perp X_i}{\|\hat{Y}_i\|}, \xi_V \right\rangle \\ &+ \left\langle \sum_{i=1}^{n} \frac{\pi_{\hat{X}_i}^\perp X_i}{\|\hat{Y}_i\|} + \frac{\pi_{X_i}^\perp \hat{X}_i}{\|Y_i\|}, V \right\rangle. \end{aligned} \tag{6.28}$$

Substituting ξ_Ω and ξ_V from equation (6.24c) and equation (6.24d) and setting $\Omega_y \equiv \Omega$, $V_y \equiv V$, and $X_{y_i} \equiv X_i$. One has

$$\begin{aligned}\dot{\mathcal{V}} = \quad & -k_{P_\Omega} \left\| \sum_{i=1}^{n} \hat{X}_i \times X_i \right\|^2 - k_{P_p} \left\| \sum_{i=1}^{n} \frac{\pi_{\hat{X}_i}^{\perp} X_i}{\|\hat{Y}_i\|} \right\|^2 \\ & + \left\langle \sum_{i=1}^{n} \frac{\pi_{\hat{X}_i}^{\perp} X_i}{\|\hat{Y}_i\|} + \frac{\pi_{\hat{X}_i}^{\perp} \hat{X}_i}{\|Y_i\|}, V \right\rangle .\end{aligned} \tag{6.29}$$

The proof continues by considering a given trajectory $T(t)$ and considering a local analysis around the associated constant error trajectory $\tilde{T}(t) \equiv I$. Consider the first order local approximation $\hat{X}_i = X_i + \alpha_i$, $\|\hat{Y}_i\| = \|Y_i\| + \beta_i$, where $\alpha_i \in T_{X_i}\mathbb{S}^2$ and $\beta_i \in \mathbb{R}$ are small perturbations induced by small variations in $\tilde{T}$, and $T_{X_i}\mathbb{S}^2$ denotes the tangent plane to $\mathbb{S}^2$ at point X_i. One has that $\alpha_i^\top X_i = 0$. Hence

$$\begin{aligned} \pi_{\hat{X}_i}^{\perp} X_i &= -\alpha_i \\ \pi_{X_i}^{\perp} \hat{X}_i &= \alpha_i \\ \frac{\pi_{\hat{X}_i}^{\perp} X_i}{\|\hat{Y}_i\|} + \frac{\pi_{X_i}^{\perp} \hat{X}_i}{\|Y_i\|} &= \frac{\beta_i \alpha_i}{\|Y_i\|(\|Y_i\| + \beta_i)} \end{aligned}$$

Then

$$\mathcal{V} = \sum_{i=1}^{n} \frac{1}{2} \|\alpha_i\|^2 \tag{6.31a}$$

$$\begin{aligned}\dot{\mathcal{V}} = & -k_{P_\Omega} \left\| \sum_{i=1}^{n} \alpha_i \times X_i \right\|^2 - k_{P_p} \left\| \sum_{i=1}^{n} \frac{\alpha_i}{\|Y_i\| + \beta_i} \right\|^2 \\ & + \left\langle \sum_{i=1}^{n} \frac{\beta_i \alpha_i}{\|Y_i\|(\|Y_i\| + \beta_i)}, V \right\rangle \\ \leq & -k_{P_\Omega} \left\| \sum_{i=1}^{n} \alpha_i \times X_i \right\|^2 - k_{P_p} \left\| \sum_{i=1}^{n} \frac{\alpha_i}{\|Y_i\| + \beta_i} \right\|^2 \\ & + \left\| \sum_{i=1}^{n} \frac{\beta_i \alpha_i}{\|Y_i\|(\|Y_i\| + \beta_i)} \right\| V_{\max}\end{aligned} \tag{6.31b}$$

In the limit α_i and β_i are images of a perturbation $\tilde{\eta} \in T_I \mathrm{SE}(3) \cong \mathfrak{se}(3)$. Note that for $\tilde{T} = I$, then $\hat{X}_i = X_i$ and $\|\hat{Y}_i\| = \|Y_i\|$. That is, to first order α_i and β_i are the differentials of the mappings

$$g_i : \tilde{T} \mapsto \|\hat{Y}_i\|, \tag{6.32a}$$

$$h_i : \tilde{T} \mapsto \hat{X}_i. \tag{6.32b}$$

The derivatives of equation (6.32) around $\tilde{T} = I$ are

$$Dg_i(t)\langle\tilde{\eta}\rangle|_{\tilde{T}=I} = (z_i - p)^\top(\tilde{\Omega} \times z_i + \tilde{V}), \tag{6.33a}$$

$$Dh_i(t)\langle\tilde{\eta}\rangle|_{\tilde{T}=I} = -\pi_{X_i}^\perp \frac{R^\top(\tilde{\Omega} \times z_i + \tilde{V})}{\|z_i - p\|}. \tag{6.33b}$$

Where $\tilde{\eta} = \left(\tilde{\Omega}, \tilde{V}\right)^\wedge \in \mathfrak{se}(3)$ and $\tilde{V} = \hat{V} - V$.

As $\|Y_i\| > \varepsilon > 0$, choose $\tilde{\eta}$ such that $\forall i$, $\beta_i < \frac{\varepsilon}{2}$. Then

$$\begin{aligned} \left\| \sum_{i=1}^{n} \frac{\alpha_i}{\|Y_i\| + \beta_i} \right\|^2 &\leq \left\| \sum_{i=1}^{n} \frac{2\alpha_i}{\varepsilon} \right\|^2, \\ &= 4\tilde{\eta}^\top M^\top M \tilde{\eta} \quad \text{where } M = \sum_{i=1}^{n} \frac{Dh_i}{\varepsilon}, \end{aligned} \tag{6.34}$$

and

$$\begin{aligned} \left\| \sum_{i=1}^{n} \frac{\beta_i}{\|Y_i\|} \frac{\alpha_i}{\|Y_i\| + \beta_i} \right\| &\leq \left\| \sum_{i=1}^{n} \frac{\alpha_i}{\varepsilon} \right\|, \\ &= \sqrt{\tilde{\eta}^\top M^\top M \tilde{\eta}} \end{aligned} \tag{6.35}$$

Observe that the null space of $Dh_i\langle\tilde{\eta}\rangle|_{\tilde{T}=I}$ is given by $R^\top(\tilde{\Omega} \times z_i + \tilde{V}) = \gamma X_i$, $\gamma \in \mathbb{R}$. Then M is full rank as the $\{z_i\}$ are non-colinear. Hence $M^\top M$ is a positive definite matrix with non-zero minimum eigenvalue λ^2.

One has

$$\dot{\mathcal{V}} \leq -k_{P_\Omega} \left\| \sum_{i=1}^{n} \alpha_i \times X_i \right\|^2 - (4k_{P_p}\lambda^2 - \lambda V_{\max})\|\tilde{\eta}\|^2$$

Then, choosing k_{P_p} such that

$$k_{P_p} \geq \frac{V_{\max}}{4\lambda}, \tag{6.36}$$

$\mathcal{V}$ is negative definite. Applying Theorem 8.4 of (Khalil 2002) the local system linearisation is stable and $\hat{X}_i - X_i \to 0$ $\forall i$ locally. Further, by Lemma 6.2.1, $\tilde{T} \to I$ locally. □

Remark 6.2.3. On Theorem 6.2.2, note:

1. Similar to the arguments previously presented in Chapters, while this proof is for the case of error system convergence from exact measurements, the observer is applicable to the case of measurements corrupted by zero-mean noise process. The local convergence properties ensure that following any perturbation $\tilde{T} = I$ due to measurement noise, the system will converge back to $\tilde{T} = I$.

2. The requirement $\forall i \ \|Y_i\| > \varepsilon > 0$ is not a constraint in a practical situation as the set of landmarks $\{z_i\}$ may be modified online to dynamically remove any landmarks the vehicle moves close to and return them when the vehicle moves away.

3. This observer is low in complexity for both implementation and tuning. Excluding the matrix exponential in the time update (which may be approximated), the innovation terms are composed entirely from vector-scalar and vector-vector operations, eliminating computationally costly matrix operations. Additionally, to tune the observer, only two scalar gains, k_{P_Ω} and k_{P_p}, need to be considered.

4. The cross term, containing the linear velocity, V, in $\dot{\mathcal{V}}$ equation (6.28) is unavoidable when working with projective measurements. Each summand corresponds to the difference between components of linear velocity perpendicular to the actual and estimated i-th bearing, scaled by the inverse of the actual or estimated distance to the landmark. As the actual landmark distance, $\|Y_i\|$ is not a measured quantity, the resulting error term can not be cancelled by a clever choice of innovation term. In the analogous system with non-projective measurements Y_i, these terms cancel and the observer admits an almost-global stability proof.

   I believe that understanding the bounds of this cross term is critical to proving global observer properties. In particular, the existence of a uniform bound between this cross term and the translation error innovation, i.e.

$$\left\| \sum_{i=1}^{n} \frac{\pi^{\perp}_{\hat{X}_i} X_i}{\|\hat{Y}_i\|} + \frac{\pi^{\perp}_{\hat{X}_i} \hat{X}_i}{\|Y_i\|} \right\| \leq c \left\| \sum_{i=1}^{n} \frac{\pi^{\perp}_{\hat{X}_i} X_i}{\|\hat{Y}_i\|} \right\| \tag{6.37}$$

   would permit a simple almost-global stability proof for this observer. However, the existance of such bound is not known.

6.3 Simulation Results

The observer equation (6.24) has been implemented in MATLAB 2007b as a discrete event simulation. Simulated velocity and feature bearing measurements have been generated with noise added as per the measurement model detailed in Section 6.1.1. The simulation used velocity measurements at 100 Hz and feature bearing measurements at 20 Hz with synchronized measurement clocks. Simulations used a feature

Gain	**Value**
k_{P_Ω}: Orientation gain	5
k_{P_p}: Position gain	10

Table 6.1: Observer gains used in simulations depicted in Figures 6.3, 6.4, 6.5 and 6.6.

Gain	**Value**
n_X: Bearing measurement noise variance	0.01
n_Ω: Angular velocity measurement noise variance	0.1
n_V: Linear velocity measurement noise variance	0.1

Table 6.2: Artificial noise figures applied to measurements in simulations depicted in Figures 6.3, 6.4, 6.5 and 6.6.

constellation of $\{(1,1,0),\ (1,-1,0),\ (-1,-1,0),\ (-1,1,0)\}$ with features never occluded by camera position or orientation.

$$
\begin{array}{rcl@{\qquad}rcl}
r & = & 0.5\text{ m} & \begin{pmatrix} x(t) \\ y(t) \end{pmatrix} & = & \begin{pmatrix} \cos(\omega t) & -\sin(\omega t) \\ \sin(\omega t) & \cos(\omega t) \end{pmatrix} \begin{pmatrix} r \\ 0 \end{pmatrix} + \begin{pmatrix} x_0 - r \\ y_0 \end{pmatrix} \\
t_f & = & 240\text{ s} & & & \\
x_0 & = & -0.5\text{ m} & z(t) & = & z_0 + \frac{\delta_z}{t_f} t \\
y_0 & = & 0\text{ m} & & & \\
z_0 & = & -1.5\text{ m} & \phi(t) & = & \frac{\pi}{2} + \omega t \\
\delta_z & = & 0.5\text{ m} & \theta(t) & = & \arctan(\frac{\dot{z}(0)}{\dot{x}(0)}) = \arctan(\frac{\delta_z}{t_f r}) \\
\omega & = & \frac{2\pi}{t_f}\text{rad s}^{-1} & \psi(t) & = & 2\theta(t)
\end{array}
$$

$$
T(t) = \begin{pmatrix} & & x(t) \\ R_{\psi(t)} R_{\theta(t)} R_{\phi(t)} & & y(t) \\ & & z(t) \\ 0 & & 1 \end{pmatrix} \tag{6.38}
$$

Figures 6.3 and 6.3 depict the pose estimate for a body descending along a trim trajectory from above the observed feature constellation using an observer initialised with $\hat{T}(0) = I$. The trim trajectory is described in equation (6.38). Observer gains used in simulations are given in Table 6.1. For reference, the results of a pose reconstruction from each frame of simulated landmark bearing measurements, calculated as described

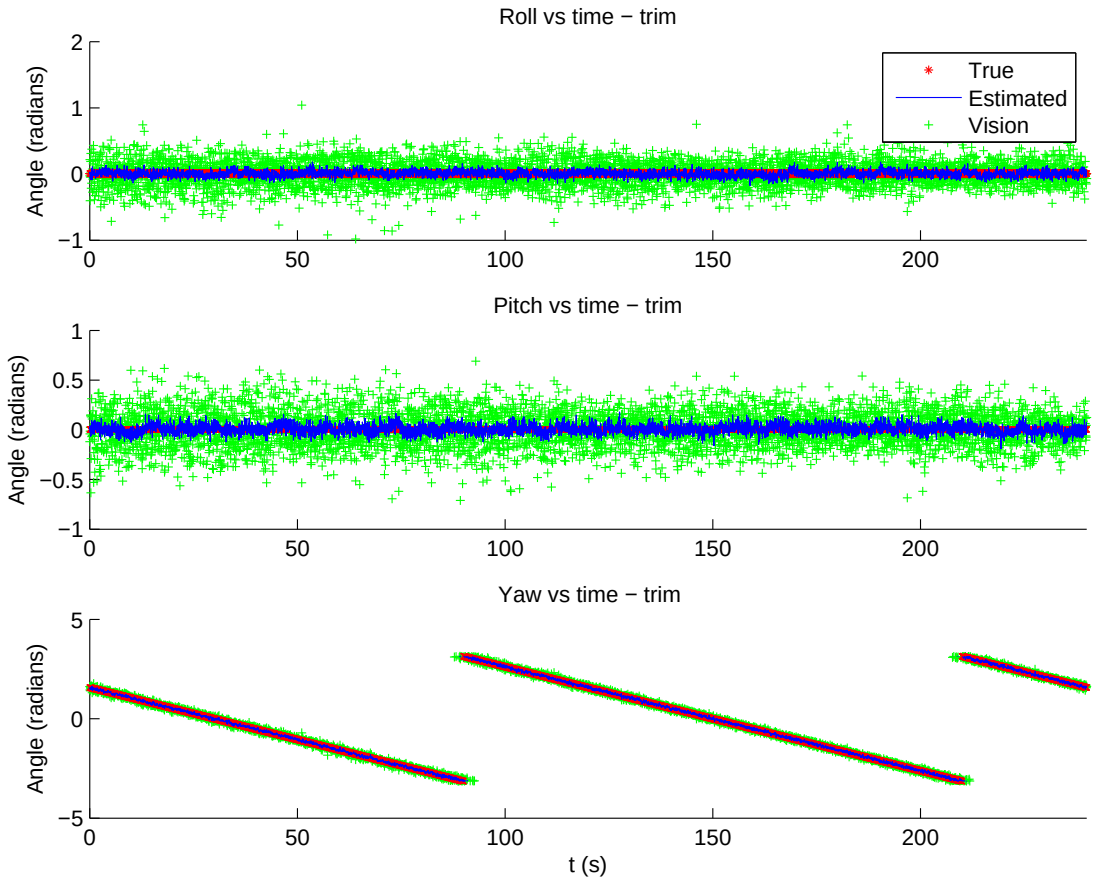

Figure 6.3: Simulation results for orientation component of pose estimate using simulated measurements along a trim trajectory specified by equation (6.38), with observer gains as per Table 6.1 and initial conditions $\hat{T}(0) = I$. Artificial measurement noise was added according to Table 6.2. The true pose is indicated by red marks and the visual pose measurements by green marks. Note that while the vision measurements are coincidental with the true pose, they are at a lower rate of 20 Hz. The estimated pose is indicated by the blue path.

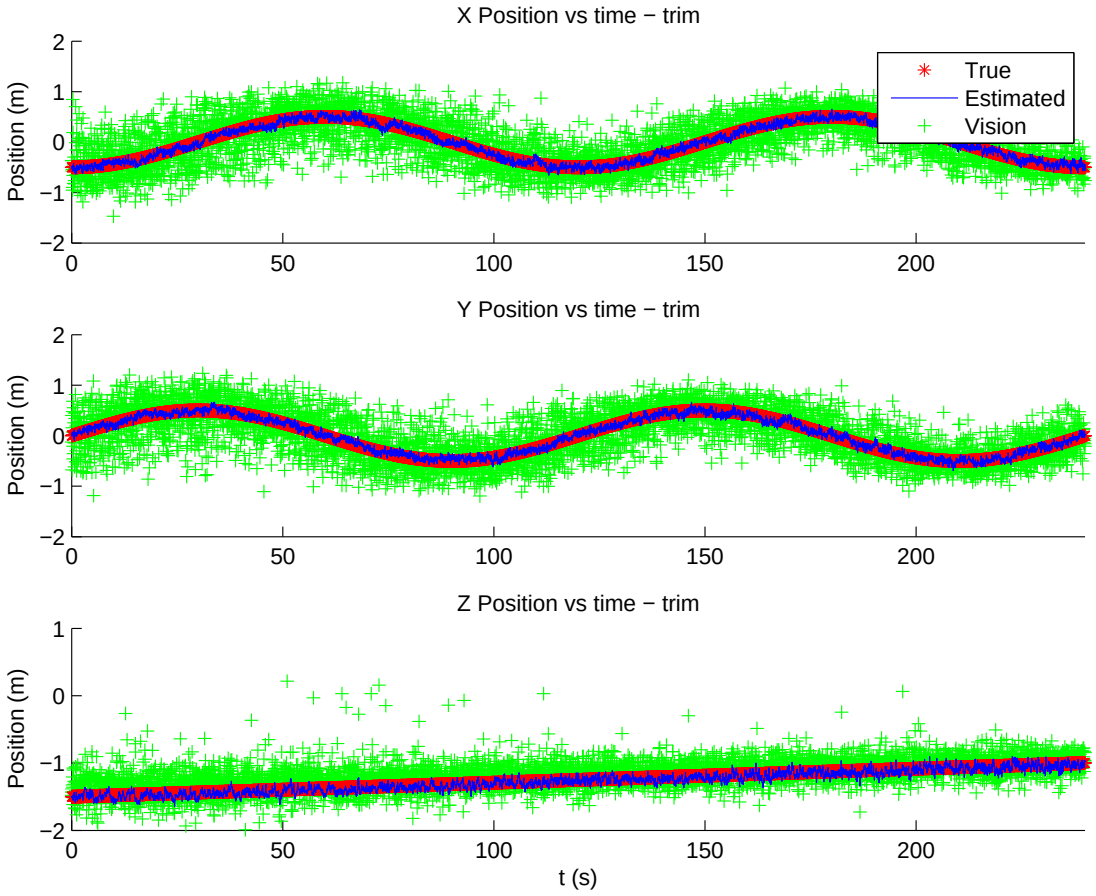

Figure 6.4: Simulation results for position component of pose estimate using simulated measurements along a trim trajectory specified by equation (6.38), with observer gains as per Table 6.1 and initial conditions $\hat{T}(0) = I$. Artificial measurement noise was added according to Table 6.2. The true pose is indicated by red marks and the visual pose measurements by green marks. Note that while the vision measurements are coincidental with the true pose, they are at a lower rate of 20 Hz. The estimated pose is indicated by the blue path.

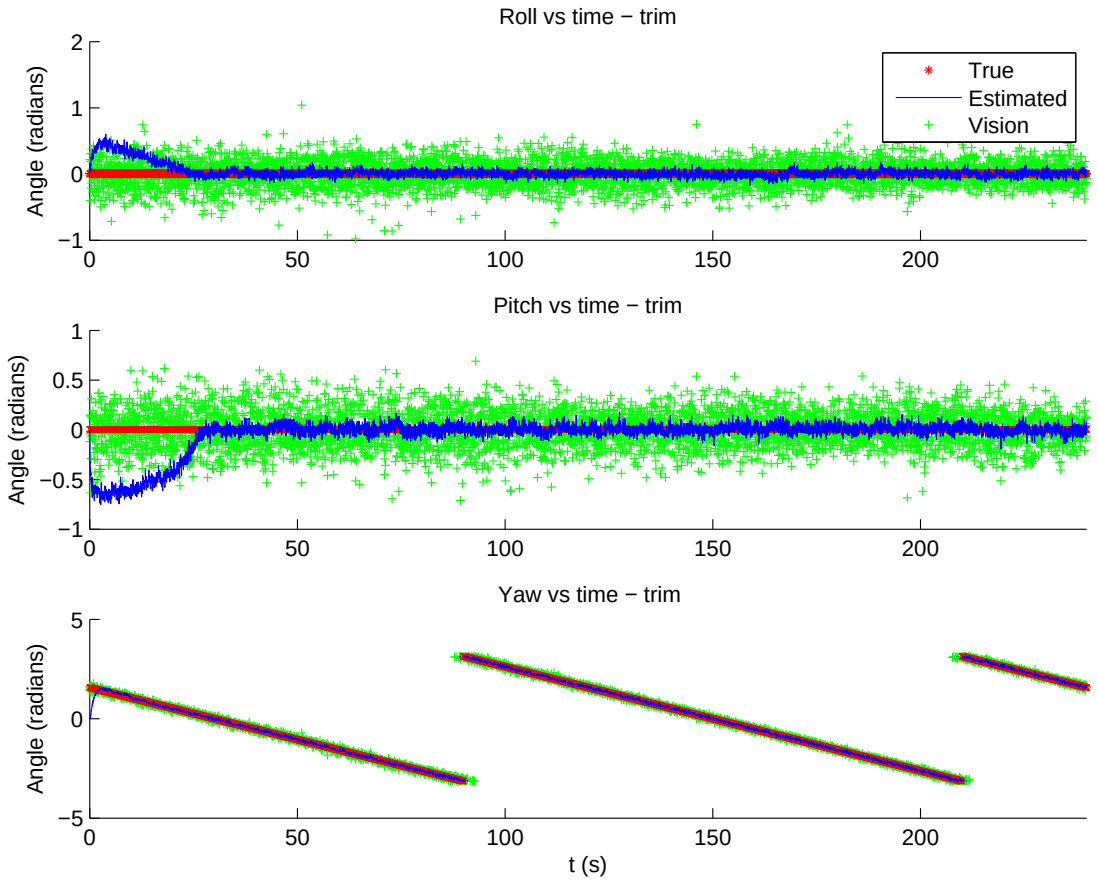

Figure 6.5: Simulation results for orientation component of pose estimate for large initial condition error, using simulated measurements along a trim trajectory specified by equation (6.38), with observer gains as per Table 6.1 and initial conditions given in equation (6.39). Artificial measurement noise was added according to Table 6.2. The true pose is indicated by red marks and the visual pose measurements by green marks. Note that while the vision measurements are coincidental with the true pose, they are at a lower rate of 20 Hz. The estimated pose is indicated by the blue path.

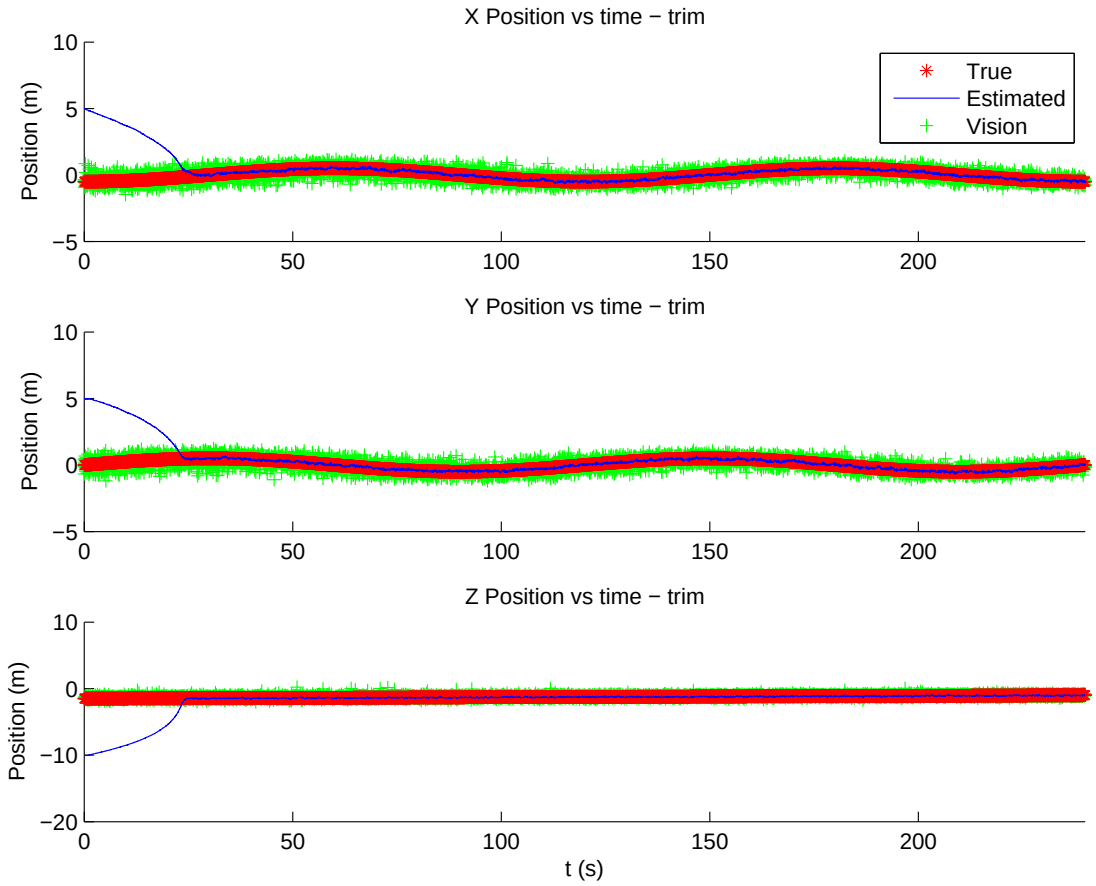

Figure 6.6: Simulation results for position component of pose estimate for large initial condition error, using simulated measurements along a trim trajectory specified by equation (6.38), with observer gains as per Table 6.1 and initial conditions given in equation (6.39). Artificial measurement noise was added according to Table 6.2. The true pose is indicated by red marks and the visual pose measurements by green marks. Note that while the vision measurements are coincidental with the true pose, they are at a lower rate of 20 Hz. The estimated pose is indicated by the blue path.

in Section 3.7.3, are plotted as vision measurements.

Tuning observer gains was found to be easy, with changes in gains resulting in good performance for values between $0.001 \leq k_{P_\Omega} \leq 10$ and $0.01 \leq k_{P_p} \leq 10$, with gain choice governed by the tradeoff between convergence rate and overshoot due to discrete time implementation.

Figures 6.5 and 6.5 depict the pose estimate for a body descending along the same trim trajectory, this time with an observer initialised 'far' from the true system state as given by equation (6.39). Note that using the same gains the observer remains convergent.

$$\hat{T}(0) = \begin{pmatrix} 1 & 0 & 0 & 5 \\ 0 & 1 & 0 & 5 \\ 0 & 0 & 1 & -10 \\ 0 & 0 & 0 & 1 \end{pmatrix} \tag{6.39}$$

The depicted results are typical of those obtained from repeated experiments using random noise, varied initial conditions and trajectories.

6.4 Experimental Results

Experiments have been conducted using the apparatus and methods described in Chapter A.1, consisting of an inertial and vision sensor attached to a large robotic manipulator. Using the robotic manipulator, the sensor package has been moved through a path and both sensor data and ground-truth measurements of the manipulator configuration recorded. Using the recorded data pose has been estimated offline, after the experiment, using the observer specified in Theorem 6.2.2.

Vision measurement were recorded at 30 Hz, with regular patches of dropped frames. Inertial measurements of angular velocity in the body-fixed frame were recorded at a modal rate of 63 Hz, containing some time varying bias components. In the absence of an available linear velocity sensor, linear velocity in the body-fixed frame was estimated using a numerical derivative of the recorded ground-truth pose measurements. The linear velocity estimate was calculated at the same time points as the angular velocity measurements and, as a numerical derivative contains no bias component but substantial process noise.

As discussed in Section 3.7.2 and demonstrated in the results of Section 5.5, the experimental angular velocity measurements included a slowly time varying bias com-

Gain	**Value**
k_{P_Ω}: Orientation proportional gain	5
k_{I_Ω}: Orientation integral gain	0.25
k_{P_p}: Position proportional gain	10
k_{I_p}: Position integral gain	0.25

Table 6.3: Observer gains used in experiments depicted in Figures 6.7, 6.8 and 6.9.

ponent. Consequently, for stable pose estimation from experimental measurements it was also necessary to maintain an estimate of the velocoity measurement biases. Using insight from the results of Theorems 4.2.1 and 5.2.1, I postulate the observer

$$\dot{\hat{T}} = \hat{T}(\Xi_y - \hat{b}_\Xi + \xi), \tag{6.40a}$$

$$\dot{\hat{b}}_\Xi = -k_I \beta, \tag{6.40b}$$

$$\xi = \left(k_{P_\Omega}\xi_\Omega, k_{P_p}\xi_V\right)^\wedge, \tag{6.40c}$$

$$\beta = \left(k_{I_\Omega}\xi_\Omega, k_{I_p}\xi_V\right)^\wedge, \tag{6.40d}$$

$$\xi_\Omega = -\sum_{i=1}^{n} \hat{X}_i \times X_{y_i}, \tag{6.40e}$$

$$\xi_v = -\sum_{i=1}^{n} \frac{\pi_{\hat{X}_i}^\perp X_{y_i}}{\|\hat{Y}_i\|}. \tag{6.40f}$$

That is, adding a bias estimate defined as the integral of the pose correction innovation with an independent gain.

Figures 6.7, 6.8 and 6.9 depict estimation results from sensor data collected while driving the robot through a circular path of 1 m diameter with the sensor package oriented to point at a spot on the ground at the center of the path. For reference, the results of a pose reconstruction from each frame of landmark bearing measurements, calculated as described in Section 3.7.3, are plotted as vision measurements.

Figures 6.7 and 6.8 depict the ground-truth pose, the timing and accuracy of vision pose measurements and the estimated pose. Figure 6.9 depicts the angular and linear velocity bias estimates. Note that again the orientation and position pose components track the true pose well over the full 4 minute period, even with significant blocks of dropped frames, with initial drift from misestimated biases corrected as the experiment proceeds.

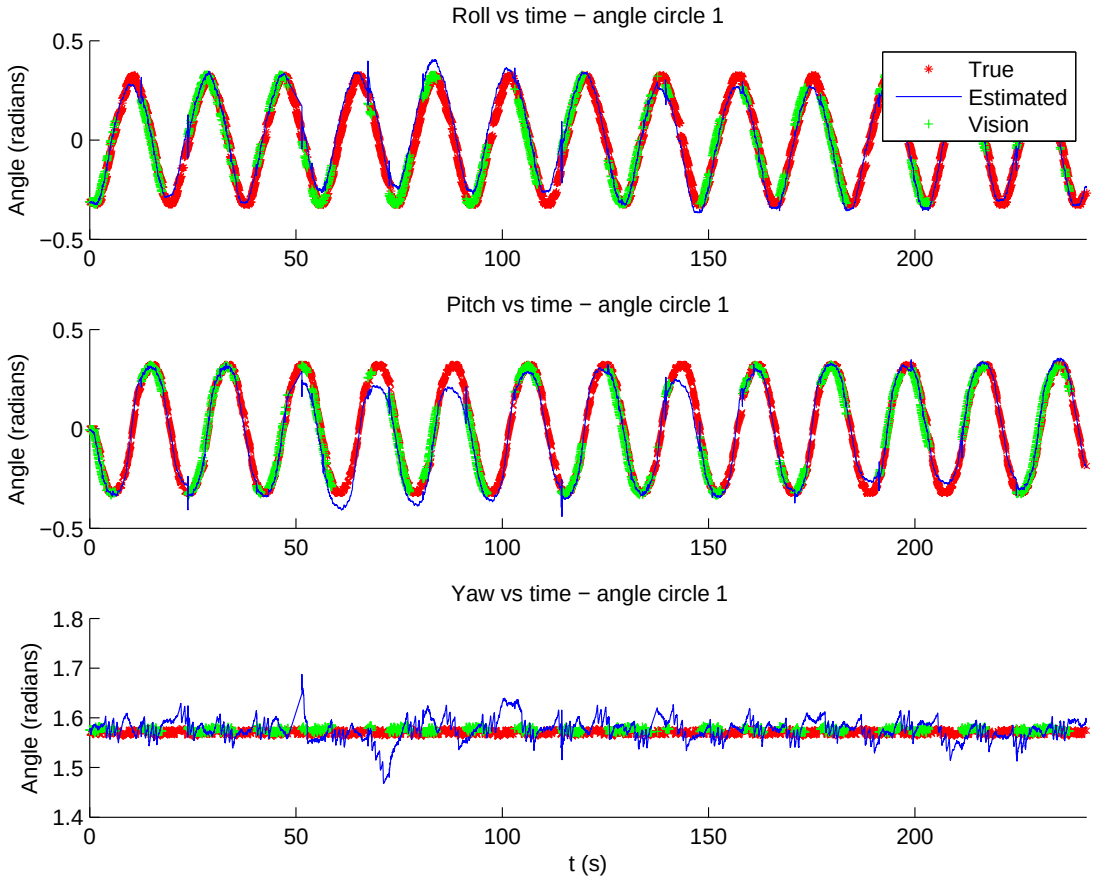

Figure 6.7: Experimental results for orientation component of pose estimate using inertial and visual measurements from sensors attached to a robotic manipulator moved through a circular path. Observer gains used are given in Table 6.3 and initial conditions were $\hat{T}(0) = T_y(0)$, $\hat{b}_\Xi = 0$. The estimated pose is indicated by the blue path and visual pose measurements by green marks. The ground truth measurements of the actual path recorded by the robot are indicated by the red marks.

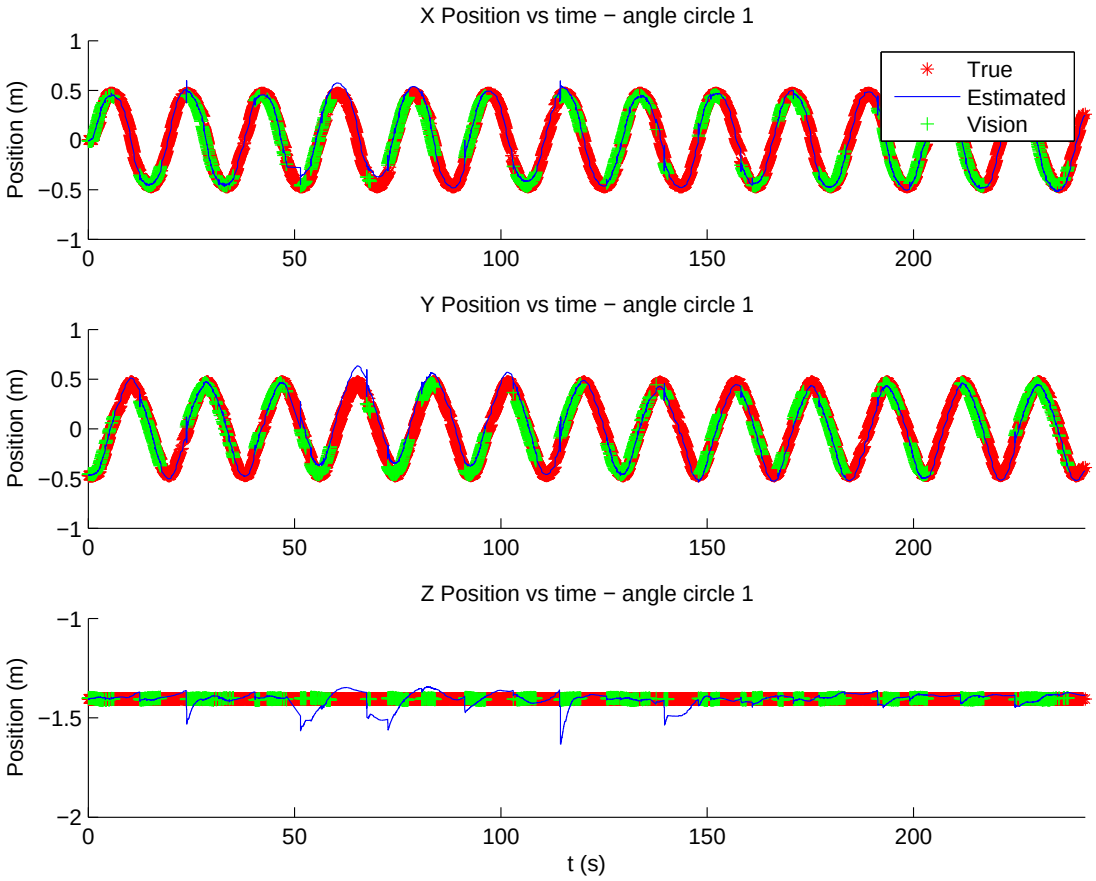

Figure 6.8: Experimental results for position component of pose estimate using inertial and visual measurements from sensors attached to a robotic manipulator moved through a circular path. Observer gains used are given in Table 6.3 and initial conditions were $\hat{T}(0) = T_y(0)$, $\hat{b}_\Xi = 0$. The estimated pose is indicated by the blue path and visual pose measurements by green marks. The ground truth measurements of the actual path recorded by the robot are indicated by the red marks.

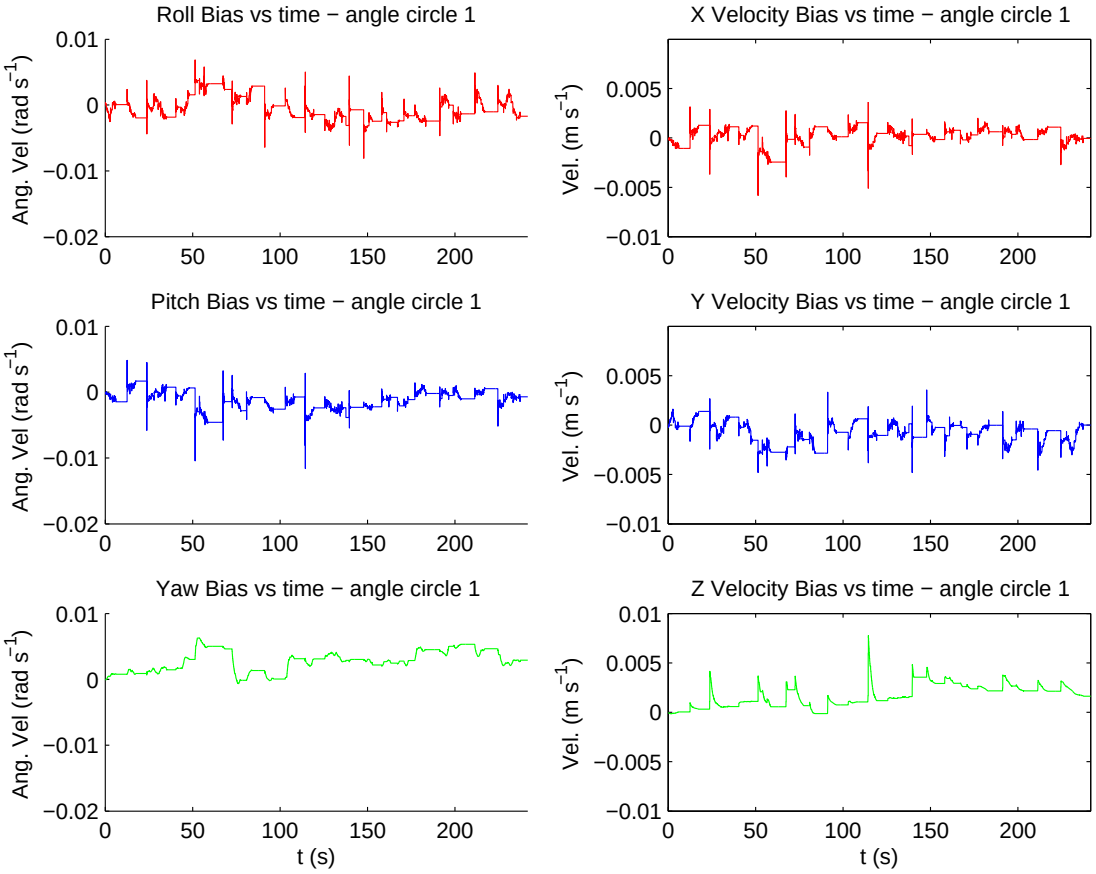

Figure 6.9: Experimental results for velocity bias estimates using inertial and visual measurements from sensors attached to a robotic manipulator moved through a circular path. Observer gains used are given in Table 6.3 and initial conditions were $\hat{T}(0) = T_y(0)$, $\hat{b}_\Xi = 0$.

6.5 Chapter Summary

In this chapter I have developed an observer for pose from measurements directly from an inertial-vision sensor suite. The observer evolves directly on $\mathrm{SE}(3)$ from measurements on $(\mathbb{S}^2)^n \times \mathfrak{se}(3)$ of bearing to known landmarks and angular and linear velocity. Local asymptotic stability of the observer is proven and arguments given in support of global observer properties. The observer is computationally simple, with innovations composed from vector-vector and vector-scalar operations, is suitable for multi-rate implementation, and exhibits a straightforward gain tuning process and a separation of measurement noise processs.

Simulations and experimental results demonstrate the convergence properties of the observer in the presences of substantial measurement noise. In particular, simulations demonstrate the wide basin of attraction in which the observer is stable. Experimental results include postulation and demonstration of an additional velocity measurement bias estimate based on insight gained work presented in earlier chapters.

Chapter 7

Conclusions

In this thesis I have reported on the development and analysis of a series of estimators for attitude and position from a combination of inertial and vision sensor measurements by use of non-linear observers evolving on the special Euclidean group $\mathrm{SE}(3)$ of dimension four.

A range of sensor models and observer designs were investigated, including:

- A cascaded pose observer design using independently designed observer for attitude and position to combine unbiased measurements of pose from vision with biased inertial measurements of angular velocity and linear acceleration. The resulting system was proven almost-globally asymptotically and locally exponentially stable.

- Designing a pose observer for simultaneous estimation of attitude and position using a single Lyapunov argument that decomposes into separately analysable attitude and position components. This investigation lead to the identification of the *Rigid Body Transformation error,* $\tilde{T} = \hat{T}T^{-1}$ as a right invariant error term, representing the state error in the inertial frame. Again, these observers were proven to be almost-globally asymptotically and locally exponentially stable.

- Development of an observer for both pose and velocity measurement biases, with design and the argument for almost-global stability posed directly on $\mathrm{SE}(3)$. Again, almost-global asymptotic and locally exponential stability were proven. Additionally, the case where velocity is partially measured in multiple frames of reference with independent bias process was considered.

- Substitution of vision measurements of pose with vision measurements of bearing to known landmarks, from which pose was calculated in the prior cases. In this case, pose was estimated from a combination of velocity measurements

and landmark bearing measurements with the observer again evolving on $\mathrm{SE}(3)$. Locally asymptotic stability was proven.

In addition to the theoretical development, simulation and experimental results are presented demonstrating performance in the presence of measurement noise and biases, and large initial condition errors. Experimental results presented include ground truth data for performance evaluation.

The observers developed in this research have achieved the goals of robustness, insensitivity to initial conditions, capacity for multi-rate implementation, straightforward tuning processes and have the backing of formal mathematical stability proofs.

The techniques developed in this thesis demonstrate the utility and effectiveness of using non-linear observers to fuse high frequency inertial measurements with low frequency vision measurements to obtain high quality, high rate estimates of attitude and position.

Bibliography

Product Specification - Articulated Robot IRB6600. ABB, 3hac 023933-001 edition, 2004a.

Product Specification - Controller IRC5 with FlexPendant. ABB, 3hac021785-001 edition, 2004b.

Product Specification - Controller Software IRC5. ABB, 2008.

R. Abdursul, H. Inaba, and B. K. Ghosh. Nonlinear observers for perspective time-invariant linear systems. *Automatica*, 40(3):481–490, March 2004.

P.-A. Absil, K. Hüper, and R. Sepulchre. Optimization on manifolds. In *46th IEEE Conference on Decision and Control,*, New Orleans, LA, 2007. URL `http://www.inma.ucl.ac.be/~absil/oom/cdc07/`.

P.-A. Absil, R. Mahony, and R. Sepulchre. *Optimization Algorithms on Matrix Manifolds*. Princeton University Press, Princeton, NJ, 2008.

N. Aghannan and P. Rouchon. On invariant asymptotic observer. In *Proceedings of the 41st IEEE Conference on Decision and Control*, Las Vega, NV, December 2002.

N. Aghannan and P. Rouchon. An intrinsic observer for a class of lagrangian systems. *IEEE Transactions on Automatic Control*, 48(6):936–945, 2003.

A. Aguiar and J. Hespanha. State estimation for systems with implicit outputs for the integration of vision and inertial sensors. In *Proceedings of the 44th IEEE Conference on Decision and Control and 2005 European Control Conference CDC-ECC '05.*, pages 621–626, 12–15 Dec. 2005.

A. Aguiar and J. Hespanha. Minimum-energy state estimation for systems with perspective outputs. *IEEE Transactions on Automatic Control*, 51(2):226–241, Feb. 2006. doi: 10.1109/TAC.2005.861686.

D. J. Allerton and H. Jia. A review of multisensor fusion methodologies for aircraft navigation systems. *Journal of Navigation*, 58(3):405–417, 2005.

A. Alocer, P. Oliveira, A. Pascoal, and J. Xavier. Estimation of attitude and position from range only measurements using geometric descent optimization on the special euclidean group. In *9th International Conference on Information Fusion*, Florence Italy, July 2006a.

A. Alocer, P. Oliveira, A. Pascoal, and J. Xavier. Maximum likelihood attitude and position estimation from pseudo-range measurements using geometric descent optimization. In *Proceedings of the IEEE Conference on Decision and Control*, San Diego, CA, December 2006b.

O. Amidi. *An Autonomous Vision-Guided Helicopter*. PhD thesis, Robotics Institute, Carnegie Mellon University, 1996.

O. Amidi, T. Kanade, and R. Miller. *Robust Vision for Vision-Based Control of Motion*, chapter 15, Vision-based autonomous helicopter research at Carnegie Mellon robotics institute (1991-1998), pages 221–232. IEEE press and SPIE Optical Engineering press, New York, USA, 1999.

B. D. Anderson and J. B. Moore. *Optimal Filtering*. Prentice-Hall, Englewood Cliffs, N.J, 1979.

L. Armesto, S. Chroust, M. Vincze, and J. Tornero. Multi-rate fusion with vision and inertial sensors. In *Proceedings of the IEEE International Conference on Robotics & Automation*, New Orleans, LA, April 2004.

L. Armesto, J. Tornero, and M. Vincze. Fast ego-motion estimation with multi-rate fusion of interial and vision. *International Journal of Robotics Research*, 26(6): 577–289, 2007. doi: 10.1177/0278364907079283.

L. Armesto, J. Tornero, and M. Vincze. On multi-rate fusion for non-linear sampled-data systems: Application to a 6D tracking system. *Robotics and Autonomous Systems*, 56(8):706–715, August 2008. doi: 10.1016/j.robot.2007.11.009.

D. Auroux and S. Bonnabel. Symmetry-preserving nudging: theory and application to a shallow water model. *submitted*, 2008.

E. Bachmann, I. Duman, U. Usta, R. McGhee, X. Yun, and M. Zyda. Orientation tracking for humans and robots using inertial sensors. In *Proceedings of the 1999 IEEE International Symposium on Computational Intelligence in Robotics and Automation*, pages 187–194, 8-9 Nov. 1999. doi: 10.1109/CIRA.1999.810047.

T. Bailey and H. Durrant-Whyte. Simultaneous localisation and mapping (SLAM): Part ii state of the art. *Robotics and Automation Magazine*, 13(3):108–117, September 2006. doi: 10.1109/MRA.2006.1678144.

G. Baldwin, R. Mahony, J. Trumpf, T. Hamel, and T. Cheviron. Complementary filter design on the special euclidean group SE(3). In *Proceedings of the European Control Conference 2007*, Kos, Greece, July 2007.

G. Baldwin, R. Mahony, J. Trumpf, and T. Hamel. Complementary filtering on the Special Euclidean group. *Submitted to IEEE Transactions on Robotics*, 2008. Pending Review.

G. Baldwin, R. Mahony, and J. Trumpf. A nonlinear observer for 6 dof pose estimation from inertial and bearing measurements. In *Proceedings of the 2009 IEEE International Conference on Robotics and Automation (ICRA '09)*, pages 2237–2242, Kobe, Japan, May 2009.

B. Barshan and H. Durrant-Whyte. Inertial navigation systems for mobile robots. *IEEE Transactions on Robotics and Automation*, 11(3):328–342, June 1995. doi: 10.1109/70.388775.

P. Batista, C. Silvestre, and P. Oliveira. Observer design for a class of kinematic systems. In *Proceedings of the 46th IEEE Conference on Decision and Control*, New Orleans, LA, USA, December 12-14 2007. The IEEE.

K. Bekris, M. Glick, and L. Kavraki. Evaluation of algorithms for bearing-only slam. In *Proceedings of the IEEE International Conference on Robotics and Automation*, pages 1937–1943, 2006.

S. P. Bhat and D. S. Bernstein. A topological obstruction to continuous global stabilization of rotational motion and the unwinding phenomenon. *Systems & Control Letters*, 39(1):63–70, January 2000.

N. P. Bhatia and G. P. Szeg o. *Stability Theory of Dynamical Systems*. Springer, Berlin, 1970.

S. Bonnabel. Left-invariant extended Kalman filter and attitude estimation. In *Proceedings of the 46th IEEE Conference on Decision and Control*, pages 1027–1032, 2007. doi: 10.1109/CDC.2007.4434662.

S. Bonnabel and P. Rouchon. *Control and Observer Design for Nonlinear Finite and Infinite Dimensional Systems*, chapter On Invariant Observers. Springer-Verlag, 2005.

S. Bonnabel and P. Rouchon. Inertial navigation and filtering : A comparison between luenberger observers and Kalman filter on a particular example. Technical report, Centre Automatique et Systemes, Ecole des Mines de Paris, 2006. In French.

S. Bonnabel, P. Martin, and P. Rouchon. Groupe de lie et observateur non-linéaire. In *Conference Internationale Francophone d'Automatique*, Bordeaux, France, June 2006a. In French.

S. Bonnabel, P. Martin, and P. Rouchon. A non-linear sysmmetry-preserving observer for velocity-aided inertial navigation. In *Proceedings of the IEEE American Control Conference*, pages 2910–2914, June 2006b.

S. Bonnabel, P. Martin, and P. Rouchon. Symmetry-preserving observers. *IEEE Transactions on Automatic Control*, 53(11):2514–2526, December 2008.

S. Bonnabel, P. Martin, and P. Rouchon. Non-linear symmetry preserving observers on lie groups. *IEEE Transactions on Automatic Control*, 54(7):1709–1713, July 2009a.

S. Bonnabel, M. Mirrahimi, and P. Rouchon. Observer-based hamiltonian indentification for quantum systems. *Automatica*, 45(5):1101–1358, May 2009b.

W. M. Boothby. *An Introduction to Differentiable Manifolds and Riemannian Geometry*. Academic Press, 2002.

J.-Y. Bouguet. Camera calibration toolbox for matlab, June 2008. Accessed 24 March 2009.

R. G. Brown. Integrated navication systems and Kalman filtering: A perspective. *Journal of the Institute of Navigation*, 19(4):255–362, 1972.

R. G. Brown and P. Y. C. Hwang. *Introduction to Random Signals and Applied Kalman Fitlering*. Wiley Publishing, New York, 2nd edition, 1992.

F. Bullo and A. D. Lewis. *Geometric Control of Mechanical Systems*. Springer, 2005.

J. Burbank, W. Kasch, J. Martin, and D. Mills. Network time protocol version 4 protocol and algorithms specification, September 2008. URL `http://www.ietf.org/internet-drafts/draft-ietf-ntp-ntpv4-proto-11.txt`. Accessed 24 March 2009.

Business Wire. Honeywell part of industry team awarded $126 million air force contract; will supply inertial measurement unit for joint direct attack munition program, 1995. URL `http://www.thefreelibrary.com/HONEYWELL+PART+OF+INDUSTRY+TEAM+AWARDED+{\$}126+MILLION+AIR+FORCE...-a017769846`. Accessed 12 September 2009.

G. Buskey, J. Roberts, P. Corke, P. Ridley, and G. Wyeth. Sensing and control for a small-size helicopter. In B. Siciliano and P. Dario, editors, *Experimental Robotics VIII*, volume 5. Springer-Verlag, 2003.

P. J. Channell. Symplectic integration algorithms. Technical Report Internal Report AT-5:ATN-83-9, Los Alamos National Laboratory, 1983.

P. J. Channell and C. Scovel. Symplectic integration of hamiltonian systems. *Nonlinearity*, 3:231–259, 1990.

X. Chen and H. Kano. A new state observer for perspective systems. *IEEE Transactions on Automatic Control*, 47(4):658–663, 2002. doi: 10.1109/9.995045.

Y. Cheng and J. L. Crassidis. Particle filtering for sequential spacecraft attitude estimation. In *AIAA Guidance, Navigation, and Control Conference and Exhibit*, number AIAA-2004-5337, Providence, RI, August 2004.

T. Cheviron, T. Hamel, R. Mahony, and G. Baldwin. Robust nonlinear fusion of inertial and visual data for position, velocity and attitude estimation of UAV. In *Proceedings of the 2007 IEEE International Conference on Robotics and Automation*, pages 2010–2016, Roma, Italy, April 2007.

P. D. Christofies and N. El-Farra. *Control of Nonlinear and Hybrid Process Systems*. Springer-Verlag, Berlin Heidelberg, 2005.

P. Corke. An inertial and visual sensing system for a small autonomous helicopter. *Journal of Robotic Systems*, 21(2):43–51, February 2004. doi: 10.1002/rob.10127.

P. Corke, J. Dias, M. Vincze, and J. Lobo. Integration of vision and inertial sensors. In *Proceedings of the IEEE International Conference on Robotics and Automation, ICRA '05*, number W-M04, Barcellona, Spain, April 2005. Full day Workshop.

P. I. Corke. *High-Performance Visual Closed-Loop Robot Control*. A thesis submitted in total fulfillment of the requirements for the degree of doctor of philosophy, Department of Mechanical and Manufacturing Engineering, University of Melbourne, July 1994.

L. W. Couch. *Digital and Analog Communication Systems*. Prentice Hall, 2001.

J. J. Craig. *Introduction to Robotics*. Addison Wesley, second edition, 1989.

J. L. Crassidis, F. L. Markley, and Y. Cheng. Nonlinear attitude filtering methods. *Journal of Guidance, Control,and Dynamics*, 30(1):12–28, January 2007.

P. E. Crouch and R. Grossman. Numerical integration of ordinary differential equations on manifolds. *Journal of Nonlinear Science*, 3:1–33, 1993.

R. Cunha, C. Silvestre, J. Hespanha, and A. Aguiar. Vision-based control for rigid body stabilization. In *Proceedings of the 46th IEEE Conference on Decision and Control*, pages 2345–2350, 12–14 Dec. 2007. doi: 10.1109/CDC.2007.4434472.

R. Cunha, C. Silvestre, and J. a. Hespanha. Output-feedback control for stabilization on se(3). *Systems & Control Letters*, 57(12):1013–1022, December 2008. doi: 10.1016/j.sysconle.2008.06.008.

F. Daum and J. Huang. Curse of dimensionality and particle filters. In *Proceedings of the IEEE Aerospace Conference*, volume 4, pages 1979–1993, 2003.

De Vogelaere. Methods of integration which preserve the contact transformation property of the hamiltonian equations. Technical Report Report 4, Department of Mathematics, University of Notre Dame, 1956.

D. DeMenthon and L. S. Davis. Exact and approximate solutions of the perspective-three-point problem. *IEEE Transactions on Pattern Analysis and Machine Intelligence*, 14(11):1100–1105, November 1992.

D. DeMenthon, P. David, and H. Samet. SoftPOSIT: An algorithm for registration of 3D models to noisy perspective images combining softassign and POSIT. Technical Report CAR-TR-969, CS-TR-4257, Center for Automation Research Technical Report, May 2001.

J. Dias and J. Lobo. Tutorial on integration of vision and inertial sensors. In *Robotics: Science and Systems Conference*, Zurich, Switzerland, June 2008.

Dolphin Peripherals. Pc input solutions - usb to serial converter, 2002. URL `http://www.dolphinfast.com/products/9103.html`. Accessed 23 March 2009.

A. Doucet, J. F. G. de Freitas, and N. J. Gordon, editors. *Sequential Monte Carlo Methods in Practice*. Springer-Verlag, 2001.

D. Douxchamps. A small list of imu / ins / inu, February 2009. URL `http://damien.douxchamps.net/research/imu/`. Accessed 23 March 2009.

H. Durrant-Whyte and T. Bailey. Simultaneous localisation and mapping (SLAM): Part i the essential algorithms. *Robotics and Automation Magazine*, 13(2):99–110, June 2006. doi: 10.1109/MRA.2006.1638022.

Federation of American Scientists. Joint direct attack munition (JDAM) GBU-31, May 2008. URL `http://www.fas.org/man/dod-101/sys/smart/jdam.htm`. Accessed 11 September 2009.

M. A. Fischler and R. C. Bolles. Random sample consensus: a paradigm for model fitting with applications to image analysis and automated cartography. *Communications of the ACM*, 24(6):381–395, June 1981.

B. Ghosh, M. Jankovic, and Y. Wu. Some problems in perspective system theory and its application to machine vision. In *Proceedings of the lEEE/RSJ International Conference on Intelligent Robots and Systems*, volume 1, pages 139–146, July 7–10 1992.

B. K. Ghosh, M. Jankovic, and Y. T. Wu. Perspective problems in system theory and its application to machine vision. *Journal of Mathematical Systems, Estimation and Control*, 4(1):3–38, 1994.

GlobalSecurity.org. Joint direct attack munition (JDAM), November 2006. URL http://www.globalsecurity.org/military/systems/munitions/jdam-specs.htm. Accessed 11 September 2009.

N. Guenard, T. Hamel, and R. Mahony. A practical visual servo control for an unmanned aerial vehicle. *IEEE Transactions on Robotics*, 24(2):331–340, 2008. ISSN 1552-3098. doi: 10.1109/TRO.2008.916666.

F. Gustafsson, F. Gunnarsson, N. Bergman, U. Forssell, J. Jansson, R. Karlsson, and P.-J. Nordlund. Particle filters for positioning, navigation, and tracking. *IEEE Transactions on Signal Processing*, 50(2):425–437, Feb. 2002. doi: 10.1109/78.978396.

T. Hamel and R. Mahony. Attitude estimation on SO(3) based on direct inertial measurements. In *Proceedings of the 2006 IEEE International Conference on Robotics and Automation (ICRA '06)*, pages 2170–2175, Orlando, FL, April 2006.

R. Hartley and A. Zisserman. *Multiple View Geometry in Computer Vision*. Cambridge University Press, second edition, March 2004.

U. Helmke and J. Moore. *Optimization and Dynamical Systems*. Springer-Verlag, 1993.

J. Hespanha. State estimation and control for systems with perspective outputs. In *Proceedings of the 41st IEEE Conference on Decision and Control*, volume 2, pages 2208–2213, 10–13 Dec. 2002.

Honeywell. Hg1700 inertial measurement unit, June 2006. URL http://www51.honeywell.com/aero/common/documents/myaerospacecatalog-documents/Missiles-Munitions/HG1700_Inertial_Measurement_Unit.pdf. Accessed 12 September 2009.

R. Horaud, B. Conio, O. Leboulleux, and B. Lacolle. An analytical solution for the perspective 4-point problem. *Computer Vision, Graphics and Image Processing*, 47: 33–44, 1989.

R. A. Horn and C. R. Johnson. *Matrix Analysis*. Cambridge University Press, 1985.

R. A. Horn and C. R. Johnson. *Topics in Matrix Analysis*. Cambridge University Press, 1994.

A. Huster and S. M. Rock. Relative position estimation for intervention-capable AUVs by fusing vision and inertial measurements. In *Proceedings of the 12th International Symposium on Unmanned Untethered Submersible Technology*, Durham, NH, August 2001.

A. Huster and S. M. Rock. Relative position sensing by fusing monocular vision and inertial rate sensors. In *Proceedings of the 11th International Conference on Advanced Robotics*, volume 3, pages 1562–1567, Coimbra, Portugal, July 2003. IEEE.

A. Huster, E. W. Frew, and S. M. Rock. Relative position estimation for AUVs by fusing bearing and inertial rate sensor measurements. In *Proceedings of the Oceans 2002 Conference*, pages 1857–1864, Biloxi, MS, October 2002.

IEEE p1394 Working Group. 1394-1995 IEEE standard for a high peformance serial bus - firewire, January 1995.

M. Jankovic and B. K. Ghosh. Visually guided ranging from observations of points, lines and curves via an identifier based nonlinear observer. *Systems & Control Letters*, 25(1):63–73, 1995. doi: doi:10.1016/0167-6911(94)00053-X.

E. S. Jones, A. Vedaldi, and S. Soatto. Inertial structure from motion with autocalibration. In *Workshop on Dynamical Vision*, October 2007.

S. Julier and J. Uhlmann. A new extension of the Kalman filter to nonlinear systems. In *International Symposium on Aerospace/Defense Sensing, Simuation and Controls*, Orlando, FL, 1997.

S. Julier and J. Uhlmann. Reduced sigma point filters for the propagation of means and covariance through nonlinear transformations. In *Proceedings of the IEEE American Control Conference*, pages 887–892, Anchorage AK, USA, 2002a. IEEE.

S. Julier and J. Uhlmann. The scaled unscented transformation. In *Proceedings of the IEEE American Control Conference*, pages 4555–4559, Anchorage AK, USA, 2002b. IEEE.

S. J. Julier, J. K. Uhlmann, and H. F. Durrant-Whyte. A new approach for filtering nonlinear systems. In *Proceedings of the IEEE American Control Conference*, pages 1628–1632 vol.3, Seattle, Washington, June 1995.

T. Kailath, A. H. Sayed, and B. Hassibi. *Linear Estimation*. Prentice Hall, Inc., 2000.

R. E. Kalman. A new approach to linear filtering and prediction problems. *Transactions of the ASME–Journal of Basic Engineering*, 82(Series D):35–45, 1960.

R. E. Kalman and R. Bucy. New results in linear filtering and prediction theory. *Transactions of the ASME–Journal of Basic Engineering*, 83(1):95–108, March 1961.

H. K. Khalil. *Nonlinear Systems*. Prentice Hall, Inc., third edition, 2002.

S.-G. Kim, J. L. Crassidis, Y. Cheng, and A. M. Fosbury. Kalman filtering for relative spacecraft attitude and position estimation. *Journal of Guidance, Control and Dynamics*, 30(1):133–143, 2007.

X. Kong. INS algorithm using quaternion model for low cost IMU. *Robotics and Autonomous Systems*, 46(4):221–246, April 2004. doi: doi:10.1016/j.robot.2004.02.001.

F. Le Bras, R. Mahony, T. Hamel, and P. Binetti. Adaptive filtering and image based visual servo control of a ducted fan flying robot. In *Proceedings of the 45th IEEE Conference on Decision and Control*, pages 1751–1757, 2006. doi: 10.1109/CDC.2006.376767.

E. Lefferts, F. Markley, and M. Shuster. Kalman filtering for spacecraft attitude estimation. *AIAA Journal of Guidance, Control and Dynamics*, 5(6):417–429, September 1982.

D. MacKay. *Information Theory, Inference, and Learning Algorithms*. Cambridge University Press, 2003.

R. Mahony, T. Hamel, and J.-M. Pflimlin. Complementary filter design on the special orthogonal group SO(3). In *Proceedings of the IEEE Conference on Decision and Control*, Seville, Spain, December 2005.

R. Mahony, T. Hamel, and J.-M. Pflimlin. Non-linear complementary filters on the special orthogonal group. *IEEE Transactions on Automatic Control*, 53(5):1203–1218, July 2008.

J. L. Marins, X. Yun, E. R. Bachmann, R. B. McGhee, and M. J. Zyda. An extended Kalman filter for quaternion-based orientation estimation using marg sensors. In

Proceedings of the 2001 IEEE/RSJ International Conference on Intelligent Robots and Systems, Maui, Hawaii, October 2001.

P. Martin and E. Salaün. Invariant observers for attitude and heading estimation from low-cost inertial and magnetic sensors. In *Proceedings of the 46th IEEE Conference on Decision and Control*, New Orleans, LA, December 12-14 2007. The IEEE.

P. Martin and E. Salaün. Design and implementation of a low-cost attitude and heading nonlinear estimator. In *Proceedings of the 5th International Conference on Informatics in Control, Automation and Robotics*, Funchal, Madeira, Portugal, 2008a.

P. Martin and E. Salaün. Design and implementation of a low-cost aided attitude and heading reference system. In *Proceedings of AIAA Guidance, Navigation and Control Conference and Exhibit*, Honolulu, Hawaii, August 2008b.

P. Martin and E. Salaün. An invariant observer for earth-velocity-aided attitude heading reference systems. In *Proceedings of the 17th World Congress of The International Federation of Automatic Control*, Seoul, Korea, July 2008c.

P. Martin and E. Salaün. A general symmetry-preserving observer for aided attitude heading reference systems. In *Proceedings of the 47th IEEE Conference on Decision and Control*, pages 2294–2301, 2008d. doi: 10.1109/CDC.2008.4739372.

P. Martin, P. Rouchon, and J. Rudolph. Invariant tracking. *ESAIM: Control Optimisation and Calculus of Variations*, 10:1–13, January 2004. doi: 10.1051/cocv:2003037.

A. Matveev, X. Hu, R. Frezza, and H. Rehbinder. Observers for systems with implicit output. *IEEE Transactions on Automatic Control*, 45(1):168–173, 2000.

Z. Meng, C. Fan, G. Zhang, and Z. You. A brief survey of the deterministic solution for satellite attitude estimation. In *Seventh International Symposium on Instrumentation and Control Technology: Optoelectronic Technology and Instruments, Control Theory and Automation, and Space Exploration*, volume 7129, page 712928. SPIE, 2008. doi: 10.1117/12.807456.

3DM-G & 3DM-GX1Gyro Enhanced Orientation Sensor FAQs. Microstrain, Inc., April 2004.

3DM-GX1 Data Communications Protocol. Microstrain, Inc., 3.1.01 edition, March 2006a.

3DM-GX1 Detailed Specifications. Microstrain, Inc., 2006b.

3DM-GX1 Fastest Data Output Rates. Microstrain, Inc., 2006c.

C. Moler and C. Van Loan. Nineteen dubious ways to compute the exponential of a matrix, twenty-five years later. *SIAM Review*, 45(1):3 – 46, 2003.

A. Mourikis, N. Trawny, S. Roumeliotis, A. Johnson, and L. Matthies. Vision-aided inertial navigation for precise planetary landing: Analysis and experiments. In *Proceedings of Robotics: Science and Systems*, Atlanta, GA, USA, June 2007.

A. I. Mourikis and S. I. Roumeliotis. A multi-state constraint Kalman filter for vision-aided inertial navigation. In *Proceedings of the IEEE International Conference on Robotics and Automation*, pages 3565–3572, 10-14 April 2007. doi: 10.1109/ROBOT.2007.364024.

R. M. Murray, Z. Li, and S. S. Sastry. *A Mathematical Introduction to Robotic Manipulation*. CRC Press, 2000 Corporate Blvd., N.W., Boca Raton, Florida 33431, 1993.

M. Niculescu. Sensor fusion algorithms for unmanned air vehicles. In *Proceedings of the IEEE International Conference on Information Decision and Control*, volume 65-70, Feb 2002.

Novatel. Oemv-2, 2009. URL `http://www.novatel.com/Documents/Papers/OEMV2.pdf`. Accessed 13 September 2009.

M.-S. Oh. Monte carlo integration vis importance sampling: Dimensionality effect and an adaptive algorithm. *Contemporary Mathematics*, 115:165–187, 1991.

P. J. Olver. *Equivalence, Invariants and Symmetry*. Cambridge University Press, 1995.

Y. Oshman and A. Carmi. Estimating attitude from vector observations using a genetic algorithm-embedded quaternion particle filter. In *AIAA Guidance, Nagication and Control Conference*, Providence, RI, August 2004a.

Y. Oshman and A. Carmi. Spacecraft attitude estimation from vector observations using a fast particle filter. In *Proceedings of 14th AAS/AIAA Space Flight Mechanics Conference*, Maui, Hawaii, February 2004b. (Paper No. AAS 04-141).

M. Pachter and A. Porter. Bearings-only measurements for ins aiding: the three-dimensional case. In *Proceedings of the IEEE American Control Conference*, volume 6, pages 5363–5368 vol.6, 2004.

F. Park. Computational aspects of the product-of-exponentials formula for robot kinematics. *IEEE Transactions on Automatic Control*, 39(3):643–647, March 1994. doi: 10.1109/9.280779.

J. Park and W.-K. Chung. Geometric integration on euclidean group with application to articulated multibody systems. *IEEE Transactions on Robotics*, 21(5):850–863, 2005. ISSN 1552-3098. doi: 10.1109/TRO.2005.852253.

A. M. Pascoal, I. Kaminer, and P. Oliveira. Navigation system design using time-varying complementary filters. *IEEE Transactions on Aerospace and Electronic Systems*, 36(4):1099–1114, October 2000. doi: 10.1109/7.892661.

J. W. Polderman and J. C. Willems. *Introduction to Mathematical Systems Theory: A Behavioural Approach*. Springer Verlag, New York, 1998.

P. Pounds. *Design, Construction and Control of a Large Quadrotor Micro Air Vehicle*. PhD thesis, The Australian National University, 2008.

P. Pounds. Personal Communciation, September 2009.

J. G. Proakis and M. Salehi. *Communication Systems Engineering*. Prentice Hall, 2001.

H. Rehbinder and B. K. Ghosh. Pose estimation using line-based dynamic vision and inertial sensors. *IEEE Transactions on Automatic Control*, 48(2):186–199, 2003.

J. Roberts, P. Corke, and G. Buskey. Low-cost flight control system for a small autonomous helicopter. In *vProceedings of the Australasian Conference on Robotics and Automation*, Auckland, New-Zealand, 2002.

N. Rouche, P. Habets, and M. Laloy. *Stability Theory by Liapunov's Direct Method*. Springer-Verlag, 1977.

R. D. Ruth. A canonical integration technique. *IEEE Transactions on Nuclear Science*, 30:2669–2671, 1983.

S. Salcudean. A globally convergent angular velocity observer for rigid body motion. *IEEE Transactions on Automatic Control*, 36(12):1493–1497, December 1991.

A. K. Sanyal, T. Lee, M. Leok, and N. H. McClamroch. Global optimal attitude estimation using uncertainty ellipsoids. *Systems & Control Letters*, 57(3):236–245, March 2008.

S. Saripalli, J. Roberts, P. Corke, and G. Buskey. A tale of two helicopters. In *Proceedings of the IEEE/RSJ Intertnational Conference on Intelligent Robots and Systems*, pages 805–810, Las Vegas, NV, October 2003.

A. Sarlette, S. Bonnabel, and R. Sepulchre. Coordinated motion design on lie groups. *Accepted for publication in IEEE Transactions on Automatic Control*, 2008a.

A. Sarlette, S. Bonnabel, and R. Sepulchre. Coordination on lie groups. In *Proceedints of the 47th IEEE Conference on Decision and Control*, Cancun, Mexico, 2008b.

R. Sepulchre, M. Janković, and P. Kokotović. *Constructive Nonlinear Control*. Springer, Great Britain, 1997.

M. D. Shuster and S. D. Oh. Three-axis attitude determination from vector observations. *Journal of Guidance and Control*, 4(1):70–77, January-February 1981.

J.-J. Slotine and W. Lie. *Applied Nonlinear Control*. Prentice Hall, 1991.

P. J. Sloyan. The bargain basement bomb. *Long Island Newsday*, page 23, November 14 1999. URL `http://www.fas.org/man/dod-101/sys/smart/docs/e19991115bargain.htm`. Accessed 11 September 2009.

S. Soatto, R. Frezza, and P. Perona. Motion estimation via dynamic vision. *IEEE Transactions on Automatic Control*, 41(3), 1996. doi: 10.1109/9.486640.

E. Sontag. Smooth stabilization implies coprime factorization. *IEEE Transactions on Automatic Control*, 34(4):435–443, April 1989. doi: 10.1109/9.28018.

E. D. Sontag and Y. Wang. On characterizations of the input-to-state stability property. *Systems & Control Letters*, 24(5):351–359, April 1995. doi: 10.1016/0167-6911(94)00050-6.

Digital Video Camera Module Technical Manual. Sony Corporation, a-bs3-100-13 (1) edition, 2003.

SparkFun Electronics. Sparkfun electronics - imu 6 degrees of freedom - v4 with bluetooth® capability, 2009. URL `http://www.sparkfun.com/commerce/product\_info.php?products\_id=8454`. Accessed 23 March 2009.

J. Thienel and R. Sanner. A coupled nonlinear spacecraft attitude controller/observer with an unknown constant gyro bias. In *Proceedings of the 40th IEEE Conference on Decision and Control*, volume 4, pages 3441–3446vol.4, 4-7 Dec. 2001. doi: 10.1109/.2001.980390.

J. Thienel and R. M. Sanner. A coupled nonlinear spacecraft attitude controller and observer with an unknown constant gyro bias and gyro noise. *IEEE Transactions on Automatic Control*, 48(11):2011 – 2015, Nov. 2003. doi: 10.1109/TAC.2003.819289.

J. K. Thienel. *Nonlinear observer/Controller designs for spacecraft attitude control systems with uncalibrated gyros*. PhD thesis, Faculty of the Graduate School of the University of Maryland, Department of Aerospace Engineering, 2004.

J. K. Thienel and R. M. Sanner. Hubble space telescope angular velocity estimation during the robotic servicing mission. *Journal of Guidance, Control and Dynamics*, 30:29–34, January-February 2007.

D. H. Titterton and J. L. Weston. *Strapdown Inertial Navigation Technology*. The Institution of Electrical Engineers and The American Institute of Aeronautics, London, UK and Reston, Virginia, USA, 2004.

N. Trawny, A. I. Mourikis, S. I. Roumeliotis, A. E. Johnson, and J. F. Montgomery. Vision-aided inertial navigation for pin-point landing using observations of mapped landmarks. *Journal of Field Robotics*, 24(5):357–378, May 2007.

R. van der Merwe, N. de Feitas, A. Doucet, and E. Wan. The unscented particle filter. In *Advanced in Neural Information Processing Systems 13*, Vancouver, BC, November 2000.

J. Vasconcelos, R. Cunha, C. Silvestre, and P. Oliveira. Landmark based nonlinear observer for rigid body attitude and position estimation. In *Proceedings of the 46th IEEE Conference on Decision and Control*, New Orleans, LA, USA, December 2007.

J. Vasconcelos, C. Silvestre, and P. Oliveira. A nonlinear observer for rigid body attitude estimation using vector observations. In *Proceedings of the 17th World Congress The International Federation of Automatic Control*, Seoul, Korea, July 2008.

J. F. Vasconcelos, R. Cunha, C. Silvestre, and P. Oliveira. Stability of a nonlinear attitude observer on SO(3) with nonideal angular velocity measurements. In *Proceedings of the European Control Conference 2009*, Budapest, Hungary, August 2009.

P. Vernaza and D. D. Lee. Rao-blackwellized particle filtering for 6-dof estimation of attitude and position via gps and inertial sensors. In *Proceedings of the IEEE International Conference on Robotics and Automation*, Orlando, Florida, May 2006.

B. Vik and T. Fossen. A nonlinear observer for GPS and INS integration. In *Proceedings of the 40th IEEE Conference on Decision and Control*, Orlando, Florida, December 2001.

M. Vincze, J. Dias, P. Corke, S. Chroust, and J. Lobo. Integration of vision and inertial sensors. In *Proceedings of the 11th International Conference on Advanced Robotics, ICAR '03*, Coimbra, Portugal, July 2003. half day Workshop.

G. Wahba. Problem 65-1, a least squares estimate of spacecraft attitude. *SIAM Review*, 7(3):409, July 1965.

E. A. Wan and R. van der Merwe. The unscented Kalman filter for nonlinear estimation. In *Proceedings of Symposium 2000 on Adaptive Systems for Signal Processing, Communication and Control*, Lake Louise, Alberta, Canada, October 2000. IEEE.

L. Wiess. *Dynamic Visual Servo Control of Robots: An Adaptive Image-Based Approach*. PhD thesis, Carnegie-Mellon University, 1984.

Y. Wu, D. Hu, W. Meiping, X. Hu, and T. Wu. Observability analysis of rotation estimation by fusing inertial and line-based visual information:a revisit. *Automatica*, 42:1809 – 1812, July 2006. doi: doi:10.1016/j.automatica.2006.05.005.

W.-H. Zhu and T. Lamarche. Velocity estimation by using position and acceleration sensors. *IEEE Transaction on Industrial Electronics*, 54(5):2706–2715, Oct. 2007. doi: 10.1109/TIE.2007.899936.

Appendix A

Data Structure Descriptions for Attached Data Sets

A DVD attachment to this thesis contains an electronic copy of this thesis and all figures contained within, raw and pre-processed experimental data sets and the MATLAB code used to produce the simulation and experimental results presented in this thesis. Please refer to the readme document in the root directory of the DVD file system for the location of specific items on the DVD.

A.1 Experimental Paths

Four experimental data sets were obtained using the methods and equipment described in Chapter . The programmed paths for the robotic manipulator in each are

- `Angle_Circle_1`: Circular path of 1 m diameter, centered above the optical target, with camera axis pointed towards the center of the optical target
- `Angle_Fig8_1`: Figure 8 shape of 1 m size on the long axis, centered above the optical target, with camera axis pointed towards the center of the optical target.
- `Angle_Clover_1`: Continuous four-leaved-clover shape, fitted within a 1 m $\times$ 1 m square, with vertical movement added, centered above the optical target, with camera axis pointed towards the center of the optical target.
- `Halfangle_Circle_1`: Circular path of 1 m diameter, centered above the optical target, with camera axis pointed halfway between vertically down and towards the center of the optical target

Additionally, calibration data was obtained for each of the six IMU axes and camera calibration data.

A.2 Raw Data Data Structures

The raw outputs from each sensor are recorded in text files using a structured output.

IMU data packets are stored over five lines, representing an instantaneous vector packet Mic (2006a). The first line contains the time in seconds from the Unix epoch, and microseconds. The second through fourth lines contain the components of the magnetometer, accelerometer and gyrometer measurements respectively. The last line contains the tick count from the IMU and the packet checksum. For example:

```
1231910139 66420
M: (  1.470,  1.471,  0.061 )
A: ( -5.991,  1.588, -3.324 )
R: ( -5.027,  0.930, -5.953 )
T: 57630                Check: -1530
```

Camera frames are recorded as a bitmap file (later converted to jpeg) and single line in a log file. Each log file line contains, in order, the time in seconds from the Unix epoch, and the time component in microseconds, the frame number and the path and filename for the recorded image. For example:

```
1231910139 123632: frame    1  - images/frame1.bmp
```

Pose data recorded on the robot controller is stored as a single line in a pose log file. Each line contains, in order, the time in hours, minutes and seconds, the 3-vector giving the position of the tooltip in mm, the unit quaternion giving the attitude of the tooltip, and a 4-vector giving coordinates representing the robot configuration (e.g. elbow up, elbow down). For example:

```
06:29:08 [ 42.0084 -1161.5 1529.46 ]
[ 0.111617 0.700829 -0.696231 0.107902 ] [ -1 -1 -2 0 ]
```

A.3 MATLAB Data Structures

When loaded into MATLAB, data is arranged in structure containing multiple matrices such that the last dimension of each matrix is of the same size and represents a discrete time index. For example `T.T(:, :, k)` is the pose measurement at time `T.t(k)`.

Four main data structures are used, `Tf`, `T`, `Xi`, `IMU` and `vis`, containing data for the programmed path, the recorded path, the calculated velocity (angular and linear), the inertial measurement unit and the camera measurements.

Within these structures, for fully pre-processed data, specific fields include:

- `Tf` Programmed ('forward') path. Due to the robot controller, does not always correspond to actual path `T`.
  - `Tf.t` - $1 \times k$: Time from experiment t_0.
  - `Tf.T` - $4 \times 4 \times k$: Pose $\in \mathrm{SE}(3)$ of Camera focal point.
- `T` Pose recorded from robot at approximately 40 Hz
  - `T.t` - $1 \times k$: Time from experiment t_0.
  - `T.T` - $4 \times 4 \times k$: Pose $\in \mathrm{SE}(3)$ of camera focal point.
- `IMU` IMU Measurements
  - `IMU.t` - $1 \times k$: Time from experiment t_0.
  - `IMU.tick` - $k \times 1$: 3DM-GX1 data packet tick field.
  - `IMU.Omega` - $3 \times k$: 3DM-GX1 instantaneous angular rate measurement, rotated into camera frame.
  - `IMU.A` - $3 \times k$: 3DM-GX1 instantaneous acceleration measurement, rotated into camera frame with gravity cancelled using `T`.
  - `IMU.M` - $3 \times k$: 3DM-GX1 instantaneous magnetic field measurement.
- `vis` Video capture at approximately 30Hz
  - `vis.t` - $1 \times k$: T Time from experiment t_0.
  - `vis.frame` - $1 \times k$: Frame number.
  - `vis.filename` - $1 \times k$: Cell array containing filename of image file for each frame.

  - `vis.inner` - 1×1: Flag indicating feature constellation used. 1 for the smaller 'inner' set and 0 for the larger 'outer' set.
  - `vis.f` - $2 \times n \times k$: Pixel coordinates of identified image features.
  - `vis.X` - $3 \times n \times k$: Bearing $\in \mathbb{S}^2$ calculated from `f`.
  - `vis.T` - $4 \times 4 \times k$: Pose $\in \mathrm{SE}(3)$, reconstructed from features `f` using *modernPosit*.
  - `vis.T_inv` - $4 \times 4 \times k$: Inverse of `vis.T`.

- `Xi` System velocity as elements of $\mathfrak{se}(3)$, computed from numerical derivative of measured pose (`T`).
  - `Xi.t` - $1 \times k$: Time from experiment t_0
  - `Xi.Xi` - $4 \times 4 \times k$: Velocity $\in \mathfrak{se}(3)$.

The inner and outer feature constellations referred to by `vis.inner` have common centre and the following dimensions. The inner visual target consists of four points in a square with 10 cm sides. The points are at (in order clockwise) $\{(5,5)$, $(5,-5)$, $(-5,-5)$, $(-5,5)\}$ cm. The outer visual target is four points in a square with 50 cm sides. The points are at (in order clockwise) $\{(25,25)$, $(25,-25)$, $(-25,-25)$, $(-25,25)\}$ cm.

Appendix B

Full Proof of Theorem 5.2.1, Chapter 5, Claim (ii): Linearisation of $(\tilde{T}, \tilde{b}_{\Xi})$

In this appendix, I present a full proof of the linearisation argument for locally-exponential stability for Theorem 5.2.1 of Chapter 5, for all values of k_P and k_I, and all bounded continuous $T(t)$ and all bounded $\Xi(t)$. This long and largely mechanical proof was ommitted from the main body of the thesis for brevity and continued narative, but is presented here for completeness.

Previously, in Proof 5.2, I have show global asymptotic convergence of the system $(\tilde{T}, \tilde{b}_{\Xi})$ to the union of the set U and$(I, 0)$. I then demonstrate that U is an unstable set leaving a sole stable equilibrium point.

In this part of the proof, I show that about $(I, 0)$ the system is locally-exponentially convergent by algebraic analysis a matrix Lyapunov argument posed on a linearisation.

Proof. Expanding the matrix representation of $(\tilde{T}, \tilde{b}_{\Xi})$ one obtains

$$(\tilde{T}, \tilde{b}_{\Xi}) = \left(\begin{pmatrix} \tilde{R} & \tilde{p} \\ 0 & 1 \end{pmatrix}, \begin{pmatrix} \tilde{b}_{\Omega_\times} & \tilde{b}_V \\ 0 & 0 \end{pmatrix} \right) \tag{B.1}$$

and the corresponding component-wise system

$$\left(\tilde{R}, \tilde{p}, \tilde{b}_{\Omega_\times}, \tilde{b}_V\right) \tag{B.2}$$

Consider the linearly related system equation (B.3a), equation (B.3b)[1] and equa-

[1] A restatement of Equation (5.29a)

tion (B.3c)[2].

$$\left(\bar{R}, \Delta P, \tilde{b}_{\Omega_\times}, \tilde{b}_V\right) \tag{B.3a}$$

$$\text{where} \qquad \bar{R} = \mathrm{Ad}_R^{-1}\, \tilde{R} \tag{B.3b}$$

$$\text{and} \qquad \Delta P = -\hat{R}^{-1}\tilde{p} = \hat{P} - P \tag{B.3c}$$

By linearity one has

$$\begin{aligned} \left(\bar{R}, \Delta P, \tilde{b}_{\Omega_\times}, \tilde{b}_V\right) &\to (I, 0, 0, 0) \\ \Rightarrow \left(\tilde{R}, \tilde{p}, \tilde{b}_{\Omega_\times}, \tilde{b}_V\right) &\to (I, 0, 0, 0) \\ \Rightarrow \left(\tilde{T}, \tilde{b}_{\Xi}\right) &\to (I, 0) \end{aligned}$$

A linearisation of $\left(\bar{R}, \Delta P, \tilde{b}_{\Omega_\times}, \tilde{b}_V\right)$ about $(I, 0, 0, 0)$ is given by

$$\bar{R} \simeq I + x_{1_\times} \qquad (\text{note: } x_1 \simeq \mathrm{vex}(\mathbb{P}_a(\bar{R}))) \tag{B.4a}$$

$$\Delta P \simeq x_3 \tag{B.4b}$$

$$\tilde{b}_\Omega \simeq -x_2 \tag{B.4c}$$

$$\tilde{b}_V \simeq x_4 \tag{B.4d}$$

The linearised dynamics are given by equation (B.5a)[3], equation (B.5b)[4], equation (B.5c)[5] and equation (B.5d)[6],

$$\dot{x}_1 = -\Omega_\times x_1 - k_P x_1 + x_2, \tag{B.5a}$$

$$\dot{x}_2 = -k_I x_1 + \frac{k_I}{2} P_\times x_3, \tag{B.5b}$$

$$\dot{x}_3 = -\Omega_\times x_3 - k_P x_3 + P_\times x_2 + x_4, \tag{B.5c}$$

$$\dot{x}_4 = -k_I x_3. \tag{B.5d}$$

Consider a Lyapunov function given by equation (B.6)[7]

$$\mathcal{W} = \frac{\alpha_1}{2}\|x_1\|_2^2 - \alpha_2 x_1^\top x_2 + \frac{\alpha_3}{2}\|x_2\|_2^2 + \frac{\beta_1}{2}\|x_3\|_2^2 - \beta_2 x_3^\top x_4 + \frac{\beta_3}{2}\|x_4\|_2^2, \tag{B.6}$$

where α_1, α_2, α_3, β_1, β_2 and β_3 are each > 0.

[2] A restatement of Equation (5.29b)
[3] A restatement of Equation (5.30a)
[4] A restatement of Equation (5.30b)
[5] A restatement of Equation (5.30c)
[6] A restatement of Equation (5.30d)
[7] A restatement of Equation (5.31)

$\mathcal{W}$ is positive definite for choices of α_1, α_2, α_3, β_1, β_2, β_3 such that

$$\alpha_2^2 < \alpha_1\alpha_2 \tag{A}$$

$$\text{and} \quad \beta_2^2 < \beta_2\beta_3 \tag{B}$$

The time derivative of $\mathcal{W}$ is

$$\begin{aligned}\dot{\mathcal{W}} = &-x_1^\top(\alpha_1 k_P - \alpha_2 k_I)x_1 + x_1^\top(\alpha_1 I + \alpha_2 k_P I - \alpha_2\Omega_\times - \alpha_3 k_I I)x_2 - \alpha_2 x_2^\top x_2 \\ &- x_3^\top(\beta_1 k_P - \beta_2 k_I)x_3 + x_3^\top(\beta_1 I + \beta_2 k_P I - \beta_2\Omega_\times - \beta_3 k_I I)x_4 - \beta_2 x_4^\top x_4 \\ &- \frac{1}{2}\alpha_2 k_I x_1^\top P_\times x_3 \\ &+ (\frac{1}{2}\alpha_3 k_i - \beta_1)x_2^\top P_\times x_3 \\ &+ \beta_2 x_2^\top P_\times x_4\end{aligned} \tag{B.7}$$

Taking scalar bounds, one obtains

$$\dot{\mathcal{W}} \leq -x^\top Q x \tag{B.8a}$$

$$\text{where} \quad x = \begin{pmatrix} \|x_1\| \\ \|x_2\| \\ \|x_3\| \\ \|x_4\| \end{pmatrix} \tag{B.8b}$$

$$Q = \begin{pmatrix} a_1 & -\frac{b}{2} & -\frac{c}{2} & 0 \\ -\frac{b}{2} & a_2 & -\frac{d}{2} & -\frac{e}{2} \\ -\frac{c}{2} & -\frac{d}{2} & a_3 & -\frac{f}{2} \\ 0 & -\frac{e}{2} & -\frac{f}{2} & a_4 \end{pmatrix} \tag{B.8c}$$

$$\begin{aligned} a_1 &= \alpha_1 k_P - \alpha_2 k_I & b &= \alpha_1 + \alpha_2(k_P + |\Omega_{\max}|) - \alpha_3 k_I \\ a_2 &= \alpha_2 & c &= \tfrac{1}{2}\alpha_2 k_I |P_{\max}| \\ \text{and} \quad a_3 &= \beta_1 k_P - \beta_2 k_I & d &= (\tfrac{1}{2}\alpha_3 k_I - \beta_1)|P_{\max}| \\ a_4 &= \beta_2 & e &= \beta_2 |P_{\max}| \\ & & f &= \beta_1 + \beta_2(k_P + |\Omega_{\max}|) - \beta_3 k_I \end{aligned}$$

where $|P_{\max}|$ and $|\Omega_{\max}|$ denote the maximum values attained by the bounded exogenous signals $P(t)$ and $\Omega(t)$.

Ensuring $\dot{\mathcal{W}}$ is negative definite is equivalent to ensuring Q is a positive definite matrix. This is equivalent to the determinants of all leading principal minors being

positive

$$|Q_{1\times1}| > 0 \tag{C}$$
$$|Q_{2\times2}| > 0 \tag{D}$$
$$|Q_{3\times3}| > 0 \tag{E}$$
$$|Q_{4\times4}| > 0 \tag{F}$$

Where $Q_{n\times n}$ is the leading principal minor of size n of Q (i.e. the upper left $n \times n$ block of Q.)

Choosing

$$\beta_1 = \frac{1}{2}\alpha_3 k_I, \tag{i}$$
$$\alpha_3 = \frac{1}{k_I}(\alpha_1 + \alpha_2(k_P + |\Omega_{\max}|)), \tag{ii}$$
$$\text{and} \quad \beta_3 = \frac{1}{k_I}(\beta_1 + \beta_2(k_P + |\Omega_{\max}|)), \tag{iii}$$

sets b, d and $f = 0$, leaving

$$Q = \begin{pmatrix} a_1 & 0 & -\frac{c}{2} & 0 \\ 0 & a_2 & 0 & -\frac{e}{2} \\ -\frac{c}{2} & 0 & a_3 & 0 \\ 0 & -\frac{e}{2} & 0 & a_4 \end{pmatrix} \tag{B.9}$$

Choosing

$$\alpha_1 = q\frac{k_I}{k_P}\alpha_2, \qquad q > 1 \tag{iv}$$

ensures conditions equation (C) and equation (D):

$$|Q_{1\times1}| = a_1 = (q-1)k_I\alpha_2 \tag{B.10a}$$
$$|Q_{2\times2}| = a_1 a_2 = (q-1)k_I\alpha_2^2 \tag{B.10b}$$

Substituting equation (i), equation (ii), equation (iii) and equation (iv) into Q equa-

tion (B.8c) yields

$$Q = \begin{pmatrix} a_1 & 0 & -\frac{c}{2} & 0 \\ 0 & a_2 & 0 & -\frac{e}{2} \\ -\frac{c}{2} & 0 & a_3 & 0 \\ 0 & -\frac{e}{2} & 0 & a_4 \end{pmatrix} \tag{B.11}$$

$$\begin{aligned} a_1 &= (q-1)k_I\alpha_2 & b &= 0 \\ a_2 &= \alpha_2 & c &= \tfrac{1}{2}\alpha_2 k_I |P_{\max}| \\ a_3 &= \tfrac{1}{2}(qk_I + k_P^2 + k_P|\Omega_{\max}|)\alpha_2 - \beta_2 k_I & d &= 0 \\ a_4 &= \beta_2 & e &= \beta_2 |P_{\max}| \\ & & f &= 0 \end{aligned}$$

Note that $|Q_{3\times3}|$ and $|Q_{4\times4}|$ factorise as

$$|Q_{3\times3}| = a_1a_2a_3 - \frac{1}{4}a_2c^2 = a_2(a_1a_3 - \frac{1}{4}c^2) \tag{B.12a}$$

$$\begin{aligned} |Q_{4\times4}| &= a_1a_2a_3a_4 - \frac{1}{4}a_2c^2a_4 - \frac{1}{4}a_1a_3e^2 + \frac{1}{16}e^2c^2 \\ &= (a_2a_4 - \frac{1}{4}e^2)(a_1a_3 - \frac{1}{4}c^2) \end{aligned} \tag{B.12b}$$

Hence conditions equation (E) and equation (F) can be satisfied by ensuring

$$a_2 > 0 \tag{B.13a}$$

$$(a_2a_4 - \frac{1}{4}e^2) > 0 \tag{B.13b}$$

$$(a_1a_3 - \frac{1}{4}c^2) > 0 \tag{B.13c}$$

As $a_2 = \alpha_2$, equation (B.13a) is trivially satisfied by the prior requirement all α_i and β_i are positive.

Choosing

$$\alpha_2 = \frac{1}{4}\gamma\beta_2|P_{\max}|^2, \qquad \gamma > 0 \tag{v}$$

and substituting into equation (B.13b) yields

$$\begin{aligned} a_2a_4 - \frac{1}{4}e^2 &= \alpha_2\beta_2 - \frac{1}{4}\beta_2^2|P_{\max}|^2 \\ &= (\gamma-1)\frac{1}{4}\beta_2^2|P_{\max}|^2 > 0 \end{aligned} \tag{B.14}$$

Substituting equation (v) into a_1, a_3 and $\frac{1}{4}c^2$, equation (B.11),

$$a_1 = \frac{1}{4}(q-1)\gamma k_I |P_{\max}|^2 \beta_2 \tag{B.15a}$$

$$a_3 = \left(\frac{1}{8}\gamma |P_{\max}|^2 (q k_I + k_P^2 + k_P |\Omega_{\max}|) - k_I\right)\beta_2 \tag{B.15b}$$

$$\frac{1}{4}c^2 = \frac{1}{256}\gamma^2 k_I^2 |P_{\max}|^6 \beta_2^2 \tag{B.15c}$$

Noting the common factor β_2^2 in $(a_1 a_3 - \frac{1}{4}c^2)$ one finds $(a_1 a_3 - \frac{1}{4}c^2)/\beta_2^2$ is a positive quadratic in q, so that equation (B.13c), and hence equation (E) and equation (F), may be satisfied by selecting q sufficiently large.

From equation (B.13c) one has

$$\begin{aligned} 0 < \frac{a_1 a_3 - \frac{1}{4}c^2}{\beta_2^2} =& \frac{1}{32}\gamma^2 |P_{\max}|^4 k_I q^2 + \frac{1}{4}\gamma |P_{\max}|^2 k_I \\ &+ \left(\frac{1}{32}\gamma^2 |P_{\max}|^4 k_I (k_P^2 + k_P |\Omega_{\max}| - k_I) - \frac{1}{4}\gamma |P_{\max}|^2 k_I\right) q \\ &- \frac{1}{32}\gamma^2 |P_{\max}|^4 k_I (k_P^2 + k_P |\Omega_{\max}| + \frac{1}{8}|P_{\max}|^2 k_I) \end{aligned} \tag{B.16}$$

Direct calculations show equation (B.16) holds for

$$\begin{aligned} q >& \frac{4}{\gamma |P_{\max}|^2} + \frac{k_I - k_P^2 - k_P |\Omega_{\max}|}{2k_I} \\ &+ \sqrt{\frac{|P_{\max}|^2}{8} + \left(\frac{k_P^2 + k_P |\Omega_{\max}| + k_I}{2k_I} - \frac{4}{\gamma |P_{\max}|^2}\right)^2} \end{aligned} \tag{vi}$$

satisfies equation (B.16). Hence, selecting a $q > 1$ such that equation (vi) is satisfied, together with choices equation (i), equation (ii), equation (iii), equation (iv) and equation (v) satisfies equation (C), equation (D), equation (E) and equation (F). Hence Q is positive definite and $\dot{\mathcal{W}}$ negative definite.

It remains to show $\mathcal{W}$ is positive definite for choices equation (i) to equation (vi). That is, that equation (A) and equation (B) are satisfied.

Substituting equation (i), equation (ii), equation (iii), equation (iv), equation (v) and equation (vi) into equation (A)

$$\begin{aligned} \alpha_2^2 <& \alpha_1 \alpha_3 \\ \alpha_2^2 <& \frac{q(q k_I + k_P^2 + k_P |\Omega_{\max}|)\alpha_2^2}{k_P^2} \\ 1 <& \frac{k_I}{k_P} q^2 + \left(1 + \frac{|\Omega_{\max}|}{k_p}\right) q \end{aligned} \tag{B.17}$$

or

$$q > \frac{k_P}{2k_I}\left(-(k_P+|\Omega_{\max}|)+\sqrt{(k_P+|\Omega_{\max}|)^2+4k_I}\right) \tag{vii}$$

Substituting equation (i), equation (ii), equation (iii), equation (iv), equation (v) and equation (vi) into equation (B)

$$\begin{aligned}
\beta_2^2 <& \beta_1\beta_3 \\
\beta_2^2 <& \gamma|P_{\max}|^2(qk_I+k_P^2+k_P|\Omega_{\max}|)\beta_2^2. \\
& \frac{\left(8k_P^2+8k_P|\Omega_{\max}|+\gamma|P_{\max}|^2(qk_I+k_P^2+k_P|\Omega_{\max}|)\right)}{64k_P^2k_I} \\
1 <& \frac{\gamma^2|P_{\max}|^4k_I}{64k_P^2}\left(q+\frac{k_P(8+|P_{\max}|^2k_I)(k_P+|\Omega_{\max}|)}{\gamma|P_{\max}|^2k_I}\right). \\
& \left(q+\frac{k_P(k_P+|\Omega_{\max}|)}{k_I}\right)
\end{aligned} \tag{B.18}$$

or

$$\begin{aligned}
q > & -\frac{k_P(k_P+|\Omega_{\max}|)}{k_I}\left(1+\frac{4}{\gamma|P_{\max}|^2}\right) \\
& +\frac{4k_P}{\gamma|P_{\max}|^2k_I}\sqrt{(k_P+|\Omega_{\max}|)^2+4k_I}
\end{aligned} \tag{viii}$$

Thus, selecting a $q > 1$ such that lower bounds equation (vi), equation (vii) and equation (viii) are satisfied together with choices equation (i), equation (ii), equation (iii), equation (iv) and equation (v) ensures conditions equation (A) and equation (B), and hence $\mathcal{W}$ is positive definite.

As $\mathcal{W}$ is positive definite and $\dot{\mathcal{W}}$ is negative definite, $\mathcal{W}$ is a Lyapunov function for the system (x_1,x_2,x_3,x_4) and hence (x_1,x_2,x_3,x_4) is exponentially stable.

Hence, for all choice of gains

$$k_P > 0, \quad k_I > 0$$

and all bounded exogenous signals

$$|P(t)| \leq |P_{\max}| \qquad\qquad |\Omega(t)| \leq |\Omega_{\max}|$$

the system $(\bar{R},\Delta P,\tilde{b}_{\Omega_\times},\tilde{b}_V)$ is locally exponentially stable about $(I,0,0,0)$ and hence $(\tilde{T},\tilde{b}_\Xi)$ is locally exponentially stable about $(I,0)$.

□

Remark B.0.1. Choices for Lyapunov function constants α_1, α_2, α_3, β_1, β_2, β_3, q and γ may be made as follows:

1. Select arbitrary

$$\begin{aligned} \gamma &> 1 \\ \beta_2 &> 0 \\ \text{and} \quad \delta &> 1 \end{aligned}$$

2. From equation (iv), equation (vi), equation (vii) and equation (viii), set

$$q = \delta \max \left(\begin{array}{l} 1, \\ \dfrac{4}{\gamma |P_{\max}|^2} + \dfrac{k_I - k_P^2 - k_P |\Omega_{\max}|}{2k_I} \\ \quad + \sqrt{\dfrac{|P_{\max}|^2}{8} + \left(\dfrac{k_P^2 + k_P |\Omega_{\max}| + k_I}{2k_I} - \dfrac{4}{\gamma |P_{\max}|^2} \right)^2}, \\ \dfrac{k_P}{2k_I} \left(-(k_P + |\Omega_{\max}|) + \sqrt{(k_P + |\Omega_{\max}|)^2 + 4k_I} \right), \\ -\dfrac{k_P (k_P + |\Omega_{\max}|)}{k_I} \left(1 + \dfrac{4}{\gamma |P_{\max}|^2} \right) \\ \quad + \dfrac{4k_P}{\gamma |P_{\max}|^2 k_I} \sqrt{(k_P + |\Omega_{\max}|)^2 + 4k_I} \end{array} \right)$$

3. From equation (v), set

$$\alpha_2 = \frac{1}{4} \gamma \beta_2 |P_{\max}|^2$$

4. From equation (iv), set

$$\alpha_1 = q \frac{k_I}{k_P} \alpha_2$$

5. From equation (ii), set

$$\alpha_3 = \frac{1}{k_I} \left(\alpha_1 + \alpha_2 (k_P + |\Omega_{\max}|) \right)$$

6. From equation (i), set

$$\beta_1 = \frac{1}{2} \alpha_3 k_I$$

7. From equation (iii), set

$$\beta_3 = \frac{1}{k_I} \left(\beta_1 + \beta_2 (k_P + |\Omega_{\max}|) \right)$$

Appendix C

Observer for Linear Velocity and its Interconnection with Pose Observers

Much of the work presented in this thesis considers the estimation of pose from vision measurements and measurements of both angular and linear velocity. As discussed in Section 2.2.3, angular velocity is easily measured using widely available intrinsic sensors, but there does not exist a cheap, simple, intrinsic sensor for linear velocity. In the absence of a specific sensor, it is possible to estimate linear velocity using measurements from accelerometers, which are cheap and widely available.

Observers for linear velocity have been considered by many authors relating to a range of sensor types and models (e.g. Pascoal et al. 2000, Zhu and Lamarche 2007), in addition to the application of Kalman filter techniques (e.g. Titterton and Weston 2004). In this appendix, I present an example observer designed to facilitate a multi-rate implementation using inertial and vision sensors, consistent with work presented in the main body of this thesis.

C.1 Linear Velocity Estimation

Assume that linear acceleration is measured in the body-fixed frame as $A_y = A + b_A$, where b_A is a constant bias term. Depending on the frame in which they are represented, the kinematics of linear velocity require estimation or measurement of either attitude, R_y or angular velocity, Ω_y.

For the inertial vision systems considered in this thesis, it is desired that a measurement of linear velocity be available at a high rate, equal to the inertial measurement rate of A_y and Ω_y. Given true dynamics $\dot{v} = RA$, one can not construct a high rate estimator for linear velocity in the inertial frame without either estimating R or measuring

R_y at high rate. However, estimation of linear velocity in the body-fixed frame requires accurate measurement of Ω, including correction of measurement biases.

Consider the following estimator for linear velocity and accelerometer and gyrometer measurement biases.

Theorem C.1.1 (Linear Velocity Observer)**.** *Consider the linear velocity and bias system*

$$\dot{V} = A - \Omega_\times V, \tag{C.1a}$$
$$\dot{b}_A = 0, \tag{C.1b}$$
$$\dot{b}_\Omega = 0, \tag{C.1c}$$

with bounded driving terms $\Omega(t)$ and $A(t)$, such that $V(t)$ is bounded. Let $\Omega_y = \Omega + b_\Omega$, $A_y = A + b_A$ and $V_y = V$ be noise free measurements.

Consider the observer

$$\dot{\hat{V}} = A_y - \hat{b}_A - (\Omega_y - \hat{b}_\Omega)_\times \hat{V} - k_V(\hat{V} - V_y), \tag{C.2a}$$
$$\dot{\hat{b}}_A = k_A(\hat{V} - V_y), \tag{C.2b}$$
$$\dot{\hat{b}}_\Omega = k_\Omega(\hat{V} \times V_y), \tag{C.2c}$$

and the errors

$$V^\Delta = \hat{V} - V, \tag{C.3a}$$
$$\tilde{b}_A = \hat{b}_A - b_A, \tag{C.3b}$$
$$\tilde{b}_\Omega = \hat{b}_\Omega - b_\Omega. \tag{C.3c}$$

Then, for any positive choice of gains k_V, k_A and k_Ω, the error system $(V^\Delta, \tilde{b}_A, \tilde{b}_\Omega)$ is globally asymptotically to $(0,0,0)$ and hence $\hat{V}$, $\hat{b}_A$, and $\hat{b}_\Omega$ are globally asymptotically to their true values.

Proof of Theorem C.1.1. Recall the definition of V^Δ, $\tilde{b}_A$ and $\tilde{b}_\Omega$ from equation (C.2). Set $\Omega_y \equiv \Omega + b_\Omega$, $A_y \equiv A + b_A$ and $V_y \equiv V$. One has

$$\dot{V}^\Delta = -\tilde{b}_A - \tilde{b}_{\Omega_\times}\hat{V} - \Omega_\times V^\Delta - k_V V^\Delta, \tag{C.4a}$$
$$\dot{\tilde{b}}_A = k_A V^\Delta, \tag{C.4b}$$
$$\dot{\tilde{b}}_\Omega = k_\Omega(\hat{V} \times V_y). \tag{C.4c}$$

Let

$$\mathcal{L} = \frac{1}{2}\|V^{\Delta}\|^2 + \frac{1}{2k_A}\|\tilde{b}_A\|^2 + \frac{1}{2k_\Omega}\|\tilde{b}_\Omega\|^2 \tag{C.5}$$

and one has

$$\dot{\mathcal{L}} = -k_V {V^{\Delta}}^{\top} V^{\Delta} - {V^{\Delta}}^{\top} \Omega_{\times} V^{\Delta} + {V^{\Delta}}^{\top} \tilde{b}_{\Omega_{\times}} \hat{V} + \tilde{b}_{\Omega}^{\top}(\hat{V} \times V). \tag{C.6}$$

Recalling that $x^{\top}(y \times x) = 0$ and $x^{\top}(y \times z) = y^{\top}(z \times x)$, one has

$$\dot{\mathcal{L}} = -k_V \|V^{\Delta}\|^2. \tag{C.7}$$

Noting that the dynamics of $x = (V^{\Delta}, \tilde{b}_A, \tilde{b}_\Omega)$ can be written

$$\dot{x} = \begin{pmatrix} -(k_V + \Omega_{\times}) & -I & V_{\times} \\ k_A I & 0 & 0 \\ k_\Omega V_{\times} & 0 & 0 \end{pmatrix} x - \begin{pmatrix} V^{\Delta} \times \tilde{b}_\Omega \\ 0 \\ 0 \end{pmatrix}, \tag{C.8}$$

one has $\dot{x} = \mathrm{f}(t,x)$ where $\mathrm{f}(t,x)$ is continuous in t and locally Lipschitz in x, uniformly in t, and that $\mathrm{f}(t,0)$ is uniformly bounded for all t. Choose the energy function $V = \mathcal{L}$ and note that V is radially unbounded, continuous, positive definite, a function only of x and $\dot{V}$ is continuous and negative semi-definite. Then by application of Theorem 8.4 from Khalil (2002), x is globally asymptotically stable.

Hence $\hat{V}$, $\hat{b}_A$, and $\hat{b}_\Omega$ are asymptotically convergent V, b_A and b_Ω respectively. □

Note that for convergence of the gyrometer bias estimate $\hat{b}_\Omega$, a persistence of excitation in V is required such that $V(t)$ is not excitation along a single direction. That is, that $\{V(t)\}$ over all t spans $\mathbb{R}^2$. Practically, this is not likely to be an issue in the type of systems considered in this thesis.

Further, if the gyrometer measurements are bias free then when turning off the gyrometer bias estimate the system is trivially globally exponentially convergent.

C.2 Cascading Linear Velocity Estimates into Pose Estimators

Interconnection of estimation systems is a well studied area (e.g. Sepulchre et al. 1997), including the application of results from input-to-state stability (Sontag 1989, Sontag and Wang 1995) to the cascade of one estimator to the inputs of another, and the creation of feedback cycles connecting the outputs an estimator to its inputs.

As applied earlier in this thesis, in Chapter 4, Section 4.2, the following conditions hold:

- For the system $\dot{x} = \mathrm{f}(t,x,u)$ which satisfies certain continuity conditions (e.g. Lemma 4.6, Khalil 2002), if $\mathrm{f}(t,x,0)$ is exponentially stable, then x is input-to-state stable. If $\mathrm{f}(t,x,0)$ is locally asymptotically stable, then x locally input-to-state stable (Christofies and El-Farra 2005).
- If $\dot{z} = g(t,z)$ is (locally) asymptotically stable then (x,z) for $\dot{x} = \mathrm{f}(t,x,z)$ is (locally) asymptotically stable (Sepulchre et al. 1997).
- If $\dot{z} = g(t,z)$ is exponentially stable then (x,z) for $\dot{x} = \mathrm{f}(t,x,z)$ is exponentially stable.

Hence, for asymptotic stability of a pose estimate whose inputs include a linear velocity estimation such as from the observer posed in Theorem C.1.1, it is sufficient for the pose observer to be locally asymptotically stable.